Life Histories of Juvenile Woolly Mammoths from Siberia: Stable Isotope and Elemental Analyses of Tooth Dentin

by

Adam Nicholas Rountrey

A dissertation submitted in partial fulfillment
of the requirements for the degree of
Doctor of Philosophy
(Geology)
in The University of Michigan
2009

Doctoral Committee:

Professor Daniel C. Fisher, Chair
Professor Philip D. Gingerich
Professor Kyger C. Lohmann
Associate Professor Daniel J. Chiego Jr.

2009

Acknowledgements

I am most grateful to my advisor, Daniel C. Fisher, for his encouragement, dedication, and passion for all things dental and proboscidean. I thank him for his willingness to hear, discuss, and help develop many fledgling ideas over the years. I would also like to thank my other committee members, Philip D. Gingerich, Kyger C. Lohmann, and Daniel J. Chiego Jr., for their thoughtful criticisms, encouragement, and assistance in technical aspects of this work.

This research would not have been possible without access to the elephant and mammoth specimens. Robert Allen , Gennady Boeskorov and Pyotr Lazarev (Mammoth Museum, Institute of Applied Ecology of the North, Yakutia, Russian Federation), Bernard Buigues (International Mammoth Committee, Saint Mandé, France), Sergey Grishin (Shemanovsky Museum, Yamalo-Nenets Autonomous Okrug, Russian Federation), Gary Haynes (University of Nevada, Reno), Dick Mol (Natural History Museum Rotterdam, The Netherlands), Alexei Tikhonov (Zoological Institute, Russian Academy of Sciences, Saint Petersburg, Russian Federation), and Sergey Vartanyan (Geographical Institute, Saint Petersburg State University, Russian Federation) donated, collected, or facilitated access to specimens.

I thank David Fox, Lora Wingate, James Gleason, and Ted Huston for my education in the arts of isotopic and elemental analysis. I would also like to express my gratitude to Robyn Burnham for providing me with lab space, Shanan Peters for

introducing me to R, and Scott Beld for assistance with specimen preparation, thin section production, growth increment analysis, and photography.

This work benefitted from my discussions with Aaron Wood, Kathlyn Smith, Ross Secord, Miriam Zelditch, Paul Koch, William Sanders, Bruce Wilkinson, Tom Eiting, and Ryan Bebej. I would also like to thank Devapriya Chattopadhyay, Michael D'Emic, Brady Foreman, Takehito (Ike) Ikejiri, G. Alexander Janevski, Megan Ortega, John Whitlock, and Iyad Zalmout for their support and friendship.

Funding was provided through grants or fellowships from the Geological Society of America, the Scott Turner Endowment (University of Michigan, Department of Geological Sciences), the Rackham Graduate School (University of Michigan), the National Geographic Society (Expeditions Council 0394-08 to D. Fisher, and Committee for Research and Exploration 8503-08 to D. Fisher), and the National Science Foundation (EAR-0545095 to D. Fisher).

Lastly, I would like to thank my loving wife, Melanie, for offering constant support over the past six years, my parents for encouraging me to pursue my interests, and my son, River, for keeping me sane at times when research became consuming.

Table of Contents

List of Figures

List of Tables

Chapter 1

Introduction

Woolly mammoths captivate and intrigue us. Why? Is it simply, as may be the case for dinosaurs, their large size? Perhaps, but I think the interest in mammoths is due, in part, to a feeling of connection with these animals. It fires the imagination knowing that humans once lived alongside such extraordinary animals, hunted them, and left paintings and engravings that provide a sense of how they perceived them.

There may also be a sense that something once a common human experience– observing and, perhaps, interacting with mammoths– has been lost. Press interviews with paleontologists and geneticists involved in the study of mammoths often conclude with questions about the likelihood of producing a living mammoth through cloning. Clearly, there is a desire to recreate a lost experience.

The circumstances surrounding the extinction of mammoths are also a topic of public interest and scientific debate. This may be partly because of the connection mentioned above, but the suggestion that humans may have played a role in mammoth extinction makes this all the more intriguing and dramatic. Drama aside, understanding the cause of the extinction and the impacts it may have had on humans and other organisms is a topic worthy of investigation.

I do not attempt, in this dissertation, to resolve the cause or causes of mammoth extinction, and extinction itself receives little attention in these chapters. Nor is my work related to attempts to produce a living mammoth. However, I do have as a primary goal, regaining that which appears lost. My research is centered around expanding our knowledge of the life histories and paleobiology of woolly mammoths in northern Siberia. Indeed, relatively little is known about how arctic mammoths lived. A comment made recently by a prominent and knowledgeable colleague sums up the issue, "…but what were they doing up there?"

Apart from cave art and engravings, we have no observational information about living mammoths. However, the fact that mammoths possessed evergrowing tusks means that a record (actually two duplicate records) of each mammoth's life was produced. We have only to understand the system of recording to gain knowledge of mammoth paleobiology.

The tusks of mammoths are highly-modified, evergrowing, second incisors (Luckett, 1996). In modern African elephants, the tusk begins mineralization before birth (Raubenheimer, 2000), and accretion of dentin continues through life. Thus, it would seem that virtually the entire life of an elephant or mammoth would be recorded in its tusks. However, the tusks are subject to abrasion and breakage that usually results in a loss of the portion of the tusk that formed during early life. This normally makes study of the first few years of life in adult elephant or mammoth tusks impossible. In order to study this period, the tusks of individuals that died young, before breakage or abrasion removed the earliest-formed dentin, must be analyzed.

In the following chapters, juvenile tusks are used to investigate the first years of life in a modern African elephant (*Loxodonta africana*) and in a set of Siberian woolly mammoths (*Mammuthus primigenius*). The aim is to increase our understanding of early life history in mammoths.

Tusks record aspects of nutritional status, diet, reproductive status, and climate. They record these in several ways. Dentin, the mineralized tissue that makes up the bulk of a tusk consists of an organic matrix (collagen) and a mineral fraction, which is nominally hydroxyapatite ($Ca_{10}[PO_4]_6[OH]_2$). Dentin grows by accretion, and is marked by a hierarchically arranged system of temporally periodic growth lines demarcating growth increments. First-order increments are annual, second-order increments (in elephants and mammoths) represent sets of around seven days (Fisher, 2001; Fisher pers. comm.), and third-order increments are daily. These growth increments aid in using tusks for reconstruction of life histories in three ways: (1) the thickness of a growth increment is related to the nutritional status of the animal during the time in which the increment was formed (Fisher, 1996); (2) counts of growth increments can be used to determine the age of an animal at death; and (3) the increments allow samples taken for compositional analyses to be tied to specific times in an animal's life (e.g., Koch et al., 1989; Fisher and Fox, 2003).

The isotopic compositions of the mineral and organic fractions of dentin vary in response to environmental and physiological factors. These factors include diet (Koch, 1989 unpublished dissertation), nutritional stress (Fisher and Fox, 2003), and climate (Fox et al., 2007). Serial samples, with temporal control provided by growth

increments, enable changes in diet, nutritional status, and climate to be tracked through an animal's life.

The elemental composition of bone has been used to determine aspects of paleodiet (reviewed by Klepinger, 1984), but essentially no studies have examined patterns in elemental concentrations in dentin with sufficient temporal resolution and coverage to identify seasonal patterns that might be linked to physiological or environmental factors. Therefore, in addition to analyzing the isotopic composition of serial samples of tusk dentin ($\delta^{13}C$ and $\delta^{15}N$ of collagen, $\delta^{13}C$ and $\delta^{18}O$ of substituted CO_3 in hydroxyapatite), I have determined the ratios of Mg, P, Mn, Fe, Cu, Zn, Sr, Ba, and Pb to Ca in the same or similar samples. This allows variation in isotopic composition to be used as a reference for any variation observed in elemental ratios.

Much of this work is exploratory in nature, seeking only to document what patterns might be present in juvenile tusks. However, there are specific applications to a larger, ongoing study of the life histories of adult mammoths from Siberia. The larger study is an attempt to identify causative factors in the extinction of woolly mammoths in northern Asia by studying changes in life history parameters such as maturation age and interbirth interval. If climate/vegetation changes were driving extinction, maturation age and interbirth interval might increase, while if human hunting were driving extinction, the opposite would be expected (Fisher, 1996). By analyzing tusks from many individuals dating before and up to the time of the mainland extinction, trends in these life history parameters might be observed that would support one hypothesis over the other.

In addition to increasing our knowledge about how mammoths lived, which may have implications for understanding their extinction, the analysis of juvenile tusks is important to the study of mammoth extinction for two reasons. First, by determining the age at death for juveniles, a tusk size-age relationship can be determined that would aid in estimating the number of years of dentin growth missing from the tusks of adults. This would allow more accurate estimates of maturation age. Second, weaning age, as determined through analyses of $\delta^{15}N$ in dentin growth layers, is itself a parameter that has been observed to change (increase) under stressful conditions (reduced resource availability) (York et al., 2008). Therefore, documenting any trends in weaning age up to the time of extinction may also provide evidence to support or refute hypotheses about the cause of extinction.

Chapter 2 is an investigation of the effects of various chemical pretreatment techniques on the $\delta^{13}C$ and $\delta^{18}O$ of structural CO_3 in tusk dentin. Workers currently use a variety of pretreatment processes that can have different effects on the determined $\delta^{13}C$ and $\delta^{18}O$ values. While there have been several studies on the effects of pretreatment, I focus on determining the effects of each stage in typical pretreatment procedures in an attempt to clarify the mechanisms through which differences in final values arise. Additionally, I examine the effects on a well-homogenized sample of modern elephant dentin, eliminating the possible confounding factor of the presence of secondary carbonate (i.e. carbonate added during postmortem exposure or burial) in the dentin. The result of this study is a preferred procedure for pretreatment of modern dentin samples. I also propose a modification of this procedure for use when

sample size is limited. In addition, I note an unexpected effect on $\delta^{18}O$ due to the presence of organic material in samples analyzed on a Kiel carbonate device.

In Chapter3, I report on the analysis of the tusk of a juvenile African elephant with a constrained date of death from a known geographic region. This provides reference elemental ratios for the study of juvenile mammoth tusks and also documents the correlation of tusk compositional measures to weather data. As part of this work, I developed methods for high-resolution compositional sampling of dentin in which growth increments are difficult to see in thick slabs. As this is typically the case for mammoth dentin, development of this technique was necessary to enable precise sampling of specific intervals of time in mammoth tusks. Compositional data series were cross-correlated with each other and with weather data series from a nearby station. Several compositional variables are correlated with weather data and fit with expectations based on known feeding patterns for elephants in this area.

Chapter 4, is an analysis of five juvenile mammoth tusks from Siberia. Compositional patterns consistent with decreasing milk intake are observed as well as seasonal patterns in $\delta^{13}C_{collagen}$. One apparently weaned individual exhibited patterns of variation in $\delta^{13}C_{collagen}$ and $\delta^{15}N_{collagen}$ not observed in any other juvenile tusk suggesting that this pattern may not occur in nursing mammoths. Elemental ratios indicate various amounts of diagenetic alteration, but in some individuals, seasonal patterns in elemental ratios are also identified. The tusk of one individual contains a neonatal line marking the time of birth. From this, a compositional marker is proposed for identification of the time of birth in dentin. A preliminary equation for determining

age based on tusk size is also presented. Weaning ages for these individuals cannot be determined as there is insufficient post-weaning growth present to differentiate between nursing and fully weaned phases.

Chapter 5 is a detailed analysis of an individual mammoth calf. The specimen, a remarkably well-preserved, mummified body, is the most complete mammoth ever discovered. No permanent tusk was present, so compositional sampling was carried out on the deciduous tusk and the dP^2 (deciduous premolar). Sampling of the dP^2 required development of a new sampling technique, which is described. Tissue samples and gut contents were also collected for analysis. Remnants of milk and vegetation were found in the intestine, and the isotopic compositions of these materials are reported. A neonatal line is present in the dP^2, and counts of growth increments reveal that the calf died at an age of about 31 days, implying that most of the compositional samples from this individual represent the prenatal period.

I conclude in Chapter 6 by summarizing the findings of this work, suggesting areas for further research, and attempting to answer, to some degree, the question of what juvenile mammoths were "doing up there."

References

Fisher, D.C., 2001. Season of Death, Growth Rates, and Life History of North American Mammoths. In: West, D. (Ed.), Proceedings of the International Conference on Mammoth Site Studies, Publications in Anthropology 22. University of Kansas, Lawrence, pp. 121–135.

Fisher, D.C., 1996. Extinction of proboscideans in North America. In: Shoshani, J., Tassy, P. (Eds.), The Proboscidea: Evolution and Paleoecology of Elephants and Their Relatives. Oxford University Press, Oxford, pp. 296–315.

Fisher, D.C., Fox, D.L., 2003. Season of death and terminal growth histories of Hiscock mastodons. In: Laub, R.S. (Ed.), The Hiscock Site: Late Pleistocene and Holocene Paleoecology and Archaeology of Western New York State, Bulletin of the Buffalo Society of Natural Sciences, 37, pp. 83–101.

Klepinger, L.L., 1984. Nutritional assessment from bone. Annual Review of Anthropology 13, 75–96.

Koch, P.L., 1989. Paleobiology of late Pleistocene mastodonts and mammoths from southern Michigan and western New York. Unpublished doctoral dissertation, University of Michigan.

Koch, P.L., Fisher, D.C., Dettman, D., 1989. Oxygen isotope variation in the tusks of extinct proboscideans: A measure of season of death and seasonality. Geology 17, 515–519.

Lister, A., Bahn, P., 2007. Mammoths: Giants of the ice age. University of California Press, Berkeley, 192 pp.

Luckett, W.P., 1996. Ontogenetic evidence for incisor homologies in proboscideans. In: Shoshani, J., Tassy, P. (Eds.), The Proboscidea: Evolution and Paleoecology of Elephants and Their Relatives. Oxford University Press, Oxford, pp. 26–31.

Raubenheimer, E.J., 2000. Development of the tush and tusk and tusklessness in the African elephant (*Loxodonta Africana*). Koedoe 43(2), 57–64.

York, A.E., Thomason, J.R., Sinclair, E.H., Hobson, K.A., 2008. Stable carbon and nitrogen isotope values in teeth of Stellar sea lions: age of weaning and the impact of the 1975–1976 regime shift in the North Pacific Ocean. Canadian Journal of Zoology 86, 33–44.

Chapter 2

The effects of pretreatment method on the $\delta^{13}C$ and $\delta^{18}O$ of carbonate in modern dentin

Introduction

The occurrence of carbonate (CO_3) in the mineral fraction of bone and teeth has been exploited in many studies for carbon and oxygen isotope analyses (e.g., Koch et al. 1989; Cerling et al., 1997; Wright and Schwarcz, 1998). This mineral fraction is nominally hydroxyapatite ($Ca_{10}[PO_4]_6[OH]_2$), with substitutions occurring at the Ca, PO_4, and OH sites. CO_3 substitutes in the crystal lattice in the PO_4 position (commonly referred to as type B) and in the OH position (commonly referred to as type A) (Beshah et al., 1990). CO_2 evolved from this CO_3 by acidification can be analyzed on an isotope ratio mass spectrometer (IRMS) allowing for determination of $\delta^{13}C$ and $\delta^{18}O$.

Workers have used a variety of pretreatment methods in attempts to determine the primary carbonate $\delta^{18}O$ and $\delta^{13}C$ values of dentin or bone, which are subject to both addition of exogenous minerals, and exchange. Comparisons of isotope values among studies are problematic because different pretreatment methods have different effects on dentin or bone with respect to the removal of

contaminants and alteration of the isotopic composition of the carbonate. Furthermore, it is not clear which method is most suitable for modern samples in which contamination is minimal.

In this study, we test the effects of a variety of pretreatment techniques in an attempt to identify a preferred procedure for routine work on modern, well-preserved dentin, as well as a modification of the procedure for use in sample-limited cases such as when attempting to analyze serial samples from a small tooth.

Previous Work

Although a variety of pretreatment methods has been used in isotope studies of structural carbonate in hydroxyapatite, most involve two steps: (1) a step intended to remove organic material, and (2) a step to remove non-structural carbonate. Removal of organic material has long been standard practice in isotope analyses of carbonates (e.g., Urey et al. 1951). Furthermore, the presence of exogenous, non-structural carbonate in hydroxyapatite, such as that introduced by pore waters, was also recognized as a potential problem that could lead to isotopic compositions representing mixtures of the primary and exogenous carbonate (e.g., Haynes, 1968).

In early applied work on the analysis of carbonate in hydroxyapatite, Deniro and Epstein (1978) showed that differences in the $\delta^{13}C$ of animal diets are reflected in the $\delta^{13}C$ of the carbonate fraction of bone. However, they warned that using this technique to determine the diets of fossil organisms might be inappropriate, as the carbonate in bone is known to undergo exchange with groundwater and/or

atmospheric CO_2. In addition to the problems caused by exchange, fossil mineralized tissues can also be contaminated with exogenous calcium carbonate. However, Haynes (1968) found that treating bone with acetic acid preferentially removed calcium carbonate with little effect on hydroxyapatite. Carbonate ^{14}C dates determined after acetic acid treatment were more similar to expected dates based on correlations or collagen ^{14}C dates than carbonate ^{14}C dates determined without this pretreatment (Haynes, 1968). Sullivan and Krueger (1983) argued that the exchange of C in structural carbonate is less than 10 % and, while this may have a marked effect on ^{14}C dates, it has little effect on $\delta^{13}C$. Thus, they suggested that acetic acid-pretreated apatite could indeed be used for paleodietary studies.

Further expanding tests of the validity of $\delta^{13}C$ in structural carbonate, Krueger (1991) exposed recent archaeological bone to ^{13}C-spiked synthetic groundwater for up to 550 days and found that treatment with acetic acid was effective at removing most carbonate of diagenetic origin. However, Zazzo et al. (2004) found that acetic acid treatment only removed 12 to 54 % of isotopic shifts due to contamination in fresh bone exposed to microbially active soil. The efficacy of the treatment was related to the concentration of dissolved inorganic carbon (DIC) present in experimental solutions (lower DIC led to reduced efficacy). At high experimental DIC concentrations much of the alteration was apparently due to the presence of adsorbed carbonate or secondary precipitated carbonate, while at low DIC concentrations the alteration was attributed to exchange or precipitation of secondary phosphate (Zazzo et al., 2004). They attribute the difference in efficacy of the treatment observed by Krueger (1991)

to Krueger's (1991) use of archaeological bone, which may have larger crystallite size, and an experimental solution in which DIC was relatively high (Zazzo et al. 2004).

Lee-Thorp and van der Merwe (1991) conducted experiments with several pretreatment techniques. In their study, variation in the acetic acid treatment time was the main variable of interest, but different concentrations of acetic acid were also tested. They found that treatment of modern bone with sodium hypochlorite (NaOCl) followed by acetic acid treatment altered $\delta^{13}C$, CO_2 yield, CO_3/PO_4 IR absorbance ratios, and sometimes mineralogy, compared to treatment with NaOCl alone. Shifts in $\delta^{13}C$ were toward more negative values. They attributed the reduced CO_2 yields and decreased absorbance ratios in acid-treated samples to the removal of adsorbed carbonate. However, they noted that explaining the change in $\delta^{13}C$ is difficult. Lee-Thorp and van der Merwe (1991) proposed that surficial exchange with atmospheric CO_2 might account for the apparent difference in isotopic composition of adsorbed versus structural carbonate, but this hypothesis was not tested.

Garvie-Lok et al. (2004) studied the effect of different acetic acid concentrations and treatment times on sample yields and the isotopic composition of bone (only results for fresh bone are discussed below). In this study, all samples were treated with 2 % NaOCl prior to acid treatment. As also observed by Koch et al. (1997), Garvie-Lok et al. (2004) noted depletion in ^{13}C and enrichment in ^{18}O following 0.1 M acetic acid or 1.0 M acetic acid, with the effect of 1.0 M acetic acid being greater. After 24 hours of 0.1 M acetic acid treatment, $\delta^{13}C$ was 0.9 ‰ lower, and $\delta^{18}O$ was 0.7 ‰ higher than the NaOCl-treated control. After 24 hours of 1.0 M acetic acid treatment, $\delta^{13}C$ was 1.6 ‰

lower, and $\delta^{18}O$ was 4.2 ‰ higher than the NaOCl-treated control. Much of the alteration appeared to occur during the first 4 to 12 hours of the acid treatment.

The removal of organics seems an appropriate step as it is possible that volatile organics might produce interference during the analysis, but it is difficult to find references that discuss possible interferences of organic matter with the measurement of isotope ratios in acid-evolved CO_2 from hydroxyapatite. Nonetheless, organic removal is common practice. In some of the earliest work in this area, Urey et al. (1951) heated calcium carbonate samples in helium for 15 minutes at 475 ^{o}C to remove organics. Lowenstam and Epstein (1957) used Clorox to digest algae and free carbonate crystals for analysis, but they noted that some samples appeared to have been altered by the treatment (e.g., for *Halimeda* sp. $\delta^{18}O$ was enriched 0.4 ‰ and $\delta^{13}C$ depleted 0.4 ‰). DeNiro and Epstein (1978), following Lowenstam and Epstein (1957), used commercial Clorox (NaOCl) to remove organic matter from shell and bone.

Koch (1989, unpublished dissertation) tested the effects of the use of NaOCl and 30 % H_2O_2 to remove organic material on $\delta^{18}O$ and $\delta^{13}C$ of tusk dentin (and human enamel). Treatment with H_2O_2 for one day caused shifts of around +1 ‰ in $\delta^{18}O$ compared to untreated dentin samples and resulted in an increase in the range of $\delta^{13}C$ values. NaOCl treatment led to larger shifts relative to untreated samples. Furthermore, he observed contamination at mass 47 in samples treated with NaOCl, but not in untreated or H_2O_2-treated samples. Thus, Koch (1989, unpublished dissertation) concluded that treatment with H_2O_2 was preferable.

In one of the few studies to focus on the effect of NaOCl on isotope values in dentin, Zazzo et al. (2006) examined the alterations caused by NaOCl treatment of serial samples of dentin from steers with known shifts from C_3 to C_4 diets. In this study, the effect of NaOCl on $\delta^{13}C$ values appeared to depend on the $\delta^{13}C$ of the sample. For untreated samples with $\delta^{13}C$ around -12 ‰ (C_3 diet), NaOCl treatment led to more enriched $\delta^{13}C$ values (~ +1.8 ‰). Untreated samples with $\delta^{13}C$ around -3 ‰ (C_4 diet) treated with NaOCl, showed more depleted $\delta^{13}C$ values (~ -2.0 ‰).

There may be an explanation for the pattern observed by Zazzo et al. (2006) without calling on a $\delta^{13}C$-dependent effect. The crystal structure and composition of dentin is known to exhibit changes associated with increasing crystallite maturity including trends toward lower substitution rates of CO_3 for PO_4 and increased crystallite size (Zioupos and Rogers, 2006). In these samples, both expected $\delta^{13}C$ and crystallite maturity are correlated with time, and it is possible that crystallite maturity is, in some way, responsible for the observed pattern in NaOCl effect. The authors attribute the alteration to either exchange of bicarbonate produced during the NaOCl treatment with carbonate in hydroxyapatite, or adsorption of this bicarbonate on the hydroxyapatite crystals. Ultimately Zazzo et al. (2006) used values from untreated samples in their primary research aim.

Koch et al. (1997) conducted what is probably the most complete experiment on the effects of pretreatment on mineralized tissues. As part of this study, modern enamel and bone were analyzed untreated, treated with 2 % NaOCl alone, treated with 30 % H_2O_2 alone, treated with 2 % NaOCl followed by 0.1 M acetic acid, treated

with 2 % NaOCl followed by 1.0 M acetic acid, and treated with 2 % NaOCl followed by 1 M acetic acid-calcium acetate buffer. They found that the effects of NaOCl and H_2O_2 on enamel isotope composition were similar and not significant. However, NaOCl increased the variation and altered mean values in bone (particularly $\delta^{18}O$, which was on average 1.49 ‰ higher in samples treated with NaOCl). H_2O_2 treatment of bone was not assessed. All acetic acid treatments, which followed NaOCl treatment, produced enriched $\delta^{18}O$ values and depleted $\delta^{13}C$ values for enamel relative to untreated samples of enamel. They note that acetic acid-calcium acetate buffer had the minimal effect (on average, +0.53 ‰ $\delta^{18}O$ and – 0.11‰ $\delta^{13}C$ versus NaOCl treatment alone) , while 1 M acetic acid had the greatest effect (on average, +1.57 ‰ $\delta^{18}O$ and -0.27 ‰ $\delta^{13}C$). The pattern was the same in bone, yet the differences were more pronounced.

That several studies mentioned above observed changes in the δ values of modern mineralized tissue with no diagenetic carbonate shows that the issues of sample pretreatment are complex. While it is desirable to remove diagenetic carbonate from fossil samples by acid treatment, what causes the shifts in modern materials, and how should they be treated?

Koch et al. (1997) proposed three possible mechanisms to account for the observed changes in isotopic composition of modern mineralized tissues subjected to pretreatment: 1) recrystallization of hydroxyapatite to brushite in acid solutions with oxygen from the treatment solution being incorporated, 2) the presence of minerals of different solubilities and different isotopic compositions in the mineralized tissues, 3)

differing isotopic compositions of CO_3 in the PO_4 site versus the OH site. However, they note that hypothesis (1) cannot account for differences in carbon isotope composition, and that, regarding hypothesis (2), it is difficult to account for the differences in isotopic composition of the fractions of differing solubility. Thus, they provisionally prefer hypothesis three and suggest that it be tested. The preferred treatment, based on Koch et al. (1997), is treatment with either NaOCl or H_2O_2, followed by treatment with 1 M acetic acid-calcium acetate buffer.

Another possibility is that the second hypothesis of Koch et al. (1997) is correct, and that the fraction with higher solubility represents a fraction highly susceptible to exchange. Neuman and Mulryan (1967) suggested that 40 % of CO_3 in synthetic carbonated hydroxyapatites was present as exchangeable bicarbonate. Poyart et al. (1975) showed that 30% of CO_3 in bone was apparently bicarbonate. Furthermore, loss of 15% of total CO_2 (i.e. half of the bicarbonate pool) was observed when bones were heated to constant weight, and this (presumably bicarbonate) fraction was shown to be subject to rapid exchange (with $^{14}CO_2$) (Poyart et al., 1975b). Neuman and Mulryan (1967) also observed loss of about 50 % of exchanged CO_3 when bones were heated. Others have mentioned a highly exchangeable, hydrated layer on hydroxyapatite crystallites, which, upon drying, yields partly hydrated "non-apatitic environments" (Cazalbou et al., 2004; Rey et al., 2007). Jiang et al. (2007) attribute changes in dentin mineral, including relative loss of carbonate and increased crystallinity after H_2O_2 treatment to dissolution of this layer. These studies show the importance of this exchangeable fraction of fresh bone and dentin, and suggest that

analysis of modern materials may present problems that differ from those encountered with fossil material.

In an effort to further expand our knowledge of the effects of different pretreatments on modern dentin, in this study we analyze $\delta^{18}O$ and $\delta^{13}C$ on a well-homogenized, finely-powdered sample of modern elephant dentin subjected to the following treatments: (1) no treatment, (2) 3 % NaOCl, (3) 30 % H_2O_2, (4) 1 M acetic acid-calcium acetate buffer (AACA), (5) 3 % NaOCl followed by AACA, (6) 30 % H_2O_2 followed by AACA. These treatments are similar to those tested by Koch et al. (1997) on enamel and bone, but are intended to compliment that data set. We accept the recommendation to use AACA rather than 1.0 M or 0.1 M acetic acid, and do not test the effects of these. Our study differs from that of Koch et al. (1997) in that we test the effects of treatments on dentin rather than enamel or bone. Furthermore, Koch et al. (1997) tested the effect of H_2O_2 only on enamel, and did not test the effect of H_2O_2 followed by AACA, or the effect of AACA alone.

We also produce a larger number of replicate analyses for most treatments, test the effect of sealed versus open treatment vessels, measure pH during treatment, and determine the carbonate content of all samples. The concentration of our NaOCl solution is 3 % rather than the 2% used by Koch et al. (1997). Values appearing in the literature are typically between 1.5 and 3% (e.g., Lee-Thorp et al., 1989; Garvie-Lok et al., 2004; Zazzo et al., 2004), and we arbitrarily chose to use 3 %. All treatments or individual steps in multi-step treatments were conducted over 24-hours (± 30 min.)

Methods and Materials

The dentin used in the study came from the tusk of a juvenile African elephant that died in 1983 at the Shabi Shabi seep in Hwange National Park, Zimbabwe. The tusk was collected within one year of the animal's death. As part of another study (this dissertation, Chapter 3), the tusk was cut longitudinally, and then transversely into segments. Dentin for this study was milled from one of these segments using a dental drill and a 1 mm-diameter diamond bit. To ensure minimal contamination, the polished longitudinal cut surface of this segment was milled and discarded prior to sample collection. Sample dentin was milled only from areas at least 2 mm away from the dentin-cementum junction and the tusk axis. The resultant powder was put through a 150-µm sieve to remove larger particles. Subsequent sieving of a subsample revealed that most particles were less than 63 µm in diameter.

10-mg subsamples were weighed into 1.5 mL centrifuge tubes, freeze-dried, reweighed, and then subjected to treatments. 10-mg subsamples were separately subjected to each treatment to allow assessment of replicability.

Untreated

1-mg samples of the freeze-dried powder were loaded into stainless steel cups, heated to 200^{o}C under vacuum for 1 hour to remove volatiles, and then loaded into Kiel vessels for isotope analysis.

NaOCl

0.8 mL of 3 % NaOCl was added to each 10-mg subsample and tubes were left for 24 hours at room temperature. The caps on tubes were open during the 24 hours on all but one subsample. After 24 hours, the tubes were agitated then centrifuged at 6000 rpm for 5 minutes on an Eppendorf 5414 microcentrifuge. The supernatant was pipetted off, and 1 mL ultrapure water was added to each tube. The tubes were agitated and centrifuged again, and the supernatant was pipetted off. This rinse procedure was repeated for a total of 5 rinses. Following the final rinse, samples were freeze-dried and weighed. 1-mg samples from each tube were weighed into stainless steel cups, heated to 200°C under vacuum for one hour, and loaded into Kiel vessels.

H_2O_2

0.8 mL of 30 % H_2O_2 was added to each 10-mg subsample, and tubes were left for 24 hours. The caps on tubes were open during the 24 hours on all but one subsample. Following this, the rinsing and drying procedure was identical to that used for NaOCl.

AACA

0.8 mL of AACA was added to each 10-mg subsample, and the samples were left for 24 hours (again all caps except one were left open). Following this, the rinsing and drying procedure was identical to that used for NaOCl.

NaOCl + AACA

Samples were processed as described for NaOCl above, but following freeze-drying and weighing, 0.8 mL of AACA was added to each tube and the samples were left for 24 hours. The cap on one tube was closed during this time. After 24 hours, samples were rinsed, freeze-dried, and weighed as described above, then loaded into boats, heated under vacuum, and loaded into Kiel vessels.

H_2O_2 + AACA

After 1-mg samples for H_2O_2-only were removed for analysis, the remaining material was treated with AACA as described for NaOCl + AACA. As less than 10 mg of sample was present, 0.08 mL of AACA was added per mg of sample in order to keep the ratio of sample mass to treatment solution volume identical.

pH Measurements

Additional samples (i.e. not those used for later isotope analysis) were treated with H_2O_2, NaOCl, and AACA to allow measurement of pH during the 24-hour treatment period. Measurements were made with a Mettler SevenGo pro SG8 pH meter and Ross Ultra electrode.

Isotope Analysis

Samples were measured in two runs on a Finnegan Kiel-IV coupled to a Thermo MAT 253 stable isotope mass spectrometer housed in the Department of Geological Sciences at the University of Michigan. Samples of the international carbonate

standard NBS 19 were analyzed in each run to control for differences between runs or drift within runs. In addition, samples in each treatment group were spaced throughout the runs to minimize any apparent differences among treatments that might be caused by drift. Dentin samples were reacted with 4 drops of 100 % H_3PO_4 at ~77°C for 15 minutes, as is standard laboratory practice for hyroxyapatite samples, and the resulting CO_2 was analyzed for $\delta^{18}O$ and $\delta^{13}C$. CO_3 content in samples was calculated using the TCO_2 (initial pressure) reported by the mass spectrometer. The relationship between TCO_2 and actual CO_3 content in samples was calibrated using microbalance-weighed samples of NBS 19 analyzed in run 1.

Results

Stable Isotopes

Table 2.1 shows $\delta^{18}O$ and $\delta^{13}C$ for samples and standards. Mean values for NBS 19 standards are statistically identically between the two runs, and the standard deviations are low (for $\delta^{18}O$, 0.07 ‰; for $\delta^{13}C$, 0.02 ‰). Regressions (least squares) of $\delta^{18}O$ and $\delta^{13}C$ on time show no significant drift in either run (Table 2.2).

Pairwise Bonferroni-corrected Cramér tests (Baringhaus and Franz, 2004, Franz, 2006) were conducted to identify significant differences between treatment groups. This is a multivariate, nonparametric, two-sample test with a null hypothesis that two sample sets have the same distribution. $\delta^{13}C$ and $\delta^{18}O$ were the dependent variables. The Bonferroni-corrected p-values are shown in Table 2.3. Most treatments differ significantly ($p < 0.05$) from each other. However, due to the high variance in AACA

$\delta^{18}O$, AACA is only significantly different from NaOCl. H_2O_2-treated samples do not differ significantly from H_2O_2-AACA-treated samples (Table 2.3).

Untreated samples had a mean $\delta^{18}O$ of 2.37 ‰ (s.d. = 0.21) and a mean $\delta^{13}C$ of -13.06 ‰ (s.d. = 0.02). Treatment with NaOCl alone or NaOCl-AACA led to less positive $\delta^{18}O$ values (1.12 ± 0.19 ‰ and 2.04 ± 0.08 respectively), while treatment with H_2O_2 alone or H_2O_2-AACA led to more positive $\delta^{18}O$ values (3.01 ± 0.03 ‰ and 3.13 ± 0.08 ‰). Treatment with AACA alone had little effect on mean $\delta^{18}O$ (2.34 ± 0.47 ‰), though variation increased. For $\delta^{13}C$, treatment with NaOCl alone led to a less negative mean value of -12.36 ± 0.03 ‰, while H_2O_2, AACA, NaOCl-AACA, and H_2O_2-AACA led to more negative values (-13.36 ± 0.05 ‰, -13.48 ± 0.05 ‰, -13.32 ± 0.05 ‰, and -13.47 ± 0.05 ‰ respectively). Figure 2.1 shows the relationships among mean values.

Those treatments conducted with tube caps closed, in two cases, yielded δ values markedly different (i.e. outside of the 3 σ range) from the same treatments conducted with the caps open (Table 2.1, Fig. 2.1). The $\delta^{13}C$ for NaOCl treatment with the cap on was -13.26 ‰, which is 0.9 ‰ more negative than the same treatment conducted with the cap open. In the other case, the $\delta^{18}O$ for H_2O_2 treatment with the cap on was 3.30 ‰, which is 0.29 ‰ more positive than the same treatment with the caps left open.

One of the unexpected results that was apparent only because samples of each treatment were spread throughout the analytical runs, was that some δ values show a strong dependence on time spent in the Kiel before analysis. Table 2.2 shows the p-

values for least squares regressions of $\delta^{18}O$ or $\delta^{13}C$ on time calculated using the "lm" function in R (R Development Core Team, 2008). In four cases, the regressions are significant (p-value < 0.05). To show the possible impact of this dependence on time, we have calculated the expected offset that would occur with replicate samples in the same run separated by 24 hours (Table 2.4), which is several hours less than the duration of a full hydroxyapatite run on the Kiel-IV/MAT 253 using the methods of this study. While the offsets in $\delta^{13}C$ that occur with H_2O_2-treated samples and H_2O_2-AACA-treated samples are relatively minor (0.11‰ and 0.12 ‰ respectively), the offsets in $\delta^{18}O$ for untreated (-0.57 ‰) and AACA (-1.32 ‰) are substantial.

Sample Loss

All centrifuge tubes were weighed prior to use, and samples were weighed after each relevant step in the process. Table 2.5 shows the percent of initial dry sample lost in each treatment. As expected, samples losses were greatest in the two step pretreatments, with NaOCl-AACA causing 56.9 % loss, and H_2O_2-AACA causing 50.9 % loss . Of the single step processes, AACA produced the least sample loss (31.7 %), while NaOCl led to the greatest loss (36.4 %).

When caps were left in place during pretreatment, loss was greater (more than 3σ) in NaOCl, AACA, and NaOCl-AACA, but slightly (still outside 3σ) less in H_2O_2 (Table 2.5). Capping had no effect on H_2O_2-AACA.

Sample CO_3 Content

Table 2.1 shows the calculated μmol CO_3 in each sample along with the adjusted weight percent CO_3 (also Fig. 2.2). The adjusted value accounts for sample losses during pretreatment. Because 1 mg of sample was weighed out for analysis of all samples, but some treatment samples, for example, had lost organic material, the expected CO_3 yields from 1 mg samples from different treatment groups are different. To correct for this, the percent sample loss for each treatment was used to calculate the mass of untreated dentin that was represented in 1 mg of a treated sample.

As expected, the absolute yield of CO_2 was higher in treatments that removed organics (Table 2.1). The lowest absolute yields occurred in the untreated and AACA-treated samples (Table 2.1).

The weight percent CO_3 for untreated samples was 2.83 ± 0.05 % (Table 2.1). The value for untreated samples is higher than adjusted values for all treatments, with the exception of NaOCl (Fig. 2.2), implying that all treatments except NaOCl removed some carbonate from the samples. The greatest effect is observed in the H_2O_2-AACA treatment, in which samples had an average adjusted weight percent CO_3 of 1.66 ± 0.05 %.

pH

The NaOCl solution stayed basic during treatment, but pH dropped from 10 to 8 over the course of the 24 hours (Table 2.6), with the majority of change occurring in the first 30 minutes. The H_2O_2 solution stayed acidic during treatment, with pH changing from 4.9 to 5.5 during the 24-hour treatment (Table 2.6). In this case, the

majority of the change occurred in the first hour. The pH of the AACA solution (4.6) did not change during treatment (Table 2.6). When caps were left in place, the NaOCl solution became slightly acidic (pH = 6.5) by the end of treatment, and H_2O_2 also ended slightly more acidic at 5.1.

Discussion

Analyzing untreated samples simplifies the processing of samples, maximizes sample retention, and may seem reasonable for modern materials that are expected to contain no diagenetic carbonate (e.g., Munro 2008). However, the presence of a highly exchangeable "non-apatitic environment" (Cazalbou et al., 2004; Rey et al., 2007) and/or adsorbed bicarbonate (Poyart et al. 1975), suggests that some pretreatment is necessary. A portion of the rapidly exchangeable fraction is thermolabile and can be removed by heating, but this does not result in complete removal of the rapidly exchangeable carbonate (Poyart et al., 1975b). Thus, some additional pretreatment seems necessary.

It was noted that $\delta^{18}O$ of untreated samples was dependent upon time spent in the Kiel before analysis, with those samples analyzed later in a run showing depletion in ^{18}O (Table 2.1, Table 2.4). This pattern also holds for samples treated with AACA alone (Table 2.1, Table 2.4). As these two treatment groups contain the only samples in which organics were not removed, it is hypothesized that the presence of organics is related to this phenomenon. The pattern is difficult to explain, but must be attributable to a change in the samples that occurs in the Kiel, as standards and other

samples do not show this "drift." Several samples of NBS 19 were run in vessels that contained dentin collagen (mineral removed with 0.5 M HCl) to test the effect of the presence of organics, but the trend toward depleted $\delta^{18}O$ did not occur (although $\delta^{18}O$ was about 0.1‰ higher in these samples than in pure NBS 19 samples- this is within 2σ). This rules out any direct time-dependent interference of organics and implies that the collagen present in untreated and AACA-treated samples must somehow interact with the hydroxyapatite to progressively change the isotopic composition. Regardless of the mechanism by which it occurs, which deserves further study, the observation that $\delta^{18}O$ changes with time in the Kiel suggests that samples should not be analyzed without first removing the organic components.

Treatment with AACA alone does not remove the time dependent effect in $\delta^{18}O$ (Table 2.2), and it leads to a shift toward more negative $\delta^{13}C$ as compared with untreated samples (Fig. 2.1). This shift is likely due to removal of carbonate in a higher-solubility pool as the corrected weight percent CO_3 is lower in these samples than in untreated samples (1.92 % versus 2.83 % in untreated samples) (Table 2.1). While removal of a more soluble mineral fraction by AAVA may be desirable, the presence of the time-dependent $\delta^{18}O$ effect in samples treated in this way, suggests that treatment with AACA alone is insufficient.

The greatest offsets from untreated samples occurred in those samples treated with NaOCl alone (Fig. 2.1). NaOCl-treated samples are depleted in ^{18}O and enriched in ^{13}C compared to all other treatment groups. This differs from the data reported in Koch et al. (1997) which show enrichment in ^{18}O and an increase in variation in $\delta^{13}C$ for

bone samples treated with NaOCl (no change in enamel samples). The NaOCl-treated samples also show a slight increase in corrected weight percent CO_3 over untreated samples (Fig. 2.2). As the solution remained basic during treatment, and abundant CO_2 was produced due to oxidation of organics, it is inferred that either carbonate was precipitated during treatment or bicarbonate was adsorbed on crystal surfaces as suggested by Zazzo (2006).

Alternatively, the removal of organics from the samples may have increased the susceptible crystallite surface area leading to higher CO_2 yields. The low organic content (and associated lowerCO_2 production during oxidation) of enamel samples may account for the similar δ values before and after NaOCl treatment of enamel observed by Koch et al. (1997). Sakae et al. (1988) observed that, when dentin powders were treated with 10 % NaOCl for 30 minutes, changes in the crystallinity of dentin crystals, loss of Mg, and formation of calcite occurred. These observations, the observations of Zazzo (2006) indicating possible $\delta^{13}C$ dependence of the NaOCl effect on dentin, and the offsets in δ values compared with all other treatments, suggest that treatment with NaOCl alone is not advisable.

Treatment with AACA following NaOCl treatment appears to somewhat reverse the effects of NaOCl treatment. NaOCl-AACA samples are depleted in ^{13}C and enriched in ^{18}O compared to NaOCl-treated samples (Fig. 2.1). AACA treatment has been shown to remove calcite from mixtures of calcite and enamel (Koch et al., 1997). If much of the isotopic offset in NaOCl-treated samples versus untreated samples is due to the presence of precipitated calcite in the NaOCl-treated samples, treatment with AACA

should remove this. This would result in δ values closer to treatments such as AACA alone. Indeed, the $\delta^{13}C$ of NaOCl-AACA-treated samples falls between those of untreated and AACA-treated samples, but $\delta^{18}O$ is depleted relative to untreated and (most) AACA-treated samples (Fig. 2.1).

H_2O_2-treated samples were depleted in ^{13}C and enriched in ^{18}O relative to untreated samples (Fig 2.1). The corrected weight percent CO_3 was less than that of untreated samples (Fig. 2.2). The reduction in weight percent CO_3, and the shift toward more negative $\delta^{13}C$, as occurred in AACA treatment, may be attributable to loss of carbonate in a more soluble pool as the H_2O_2 solution remained acidic during treatment. Similarly, the low pH, would have prevented the precipitation of calcite that may have occurred coincident with the oxidation of organics in NaOCl solution.

Kawamoto and Tsujimoto (2003) tested the effect of H_2O_2 treatment on dentin, and found that the X-ray diffraction pattern of dentin was unchanged by treatment with 30 % H_2O_2, and that the Ca content of dentin samples remained similar from 1 to 10 days (end of treatment) in the treatment. They argued that the inorganic fraction of dentin is not damaged by H_2O_2 treatment. However, Jiang et al. (2007) observed decreased carbonate and increased crystallinity of dentin exposed to H_2O_2. This suggests that the inorganic fraction of dentin was altered by H_2O_2. They attribute the alteration to dissolution of the "non-apatitic environments." If this hypothesis is correct, the loss of carbonate observed in this study may be due to loss of carbonate in this exchangeable fraction.

H_2O_2-AACA-treated samples have similar $\delta^{13}C$ and $\delta^{18}O$ to H_2O_2-treated samples, with $\delta^{18}O$ slightly more positive and $\delta^{13}C$ slightly more negative in the H_2O_2-AACA group (Fig. 2.1). The effect of AACA on H_2O_2-treated samples is similar to the effect of AACA on NaOCl-treated samples, but the magnitude of the resultant shift is about eight times less (in both $\delta^{13}C$ and $\delta^{18}O$). Presumably, the calcite or bicarbonate produced in the NaOCl treatment is not produced or is not precipitated/adsorbed in the H_2O_2 treatment; thus the shift is expected to be less. In addition, the acidity of H_2O_2 may be sufficient to remove some of the high-solubility pool that is presumably removed by AACA alone. This would explain the reduced effect of AACA on samples treated with H_2O_2.

Open Versus Closed Tubes

Sample loss was greater in NaOCl and AACA (and NaOCl-AACA) when caps were left in place during reactions. As the pH at the end of treatment was higher in the NaOCl-treated sample with the cap in place, the greater sample loss in this case may result from the prevention/reduction of calcite precipitation or bicarbonate adsorption. The $\delta^{13}C$ of this NaOCl sample was 1 ‰ more negative than those samples processed with caps open, and similar to that of the NaOCl-AACA-treated samples (Fig. 2.1). However, $\delta^{18}O$ was similar to NaOCl-treated samples with the caps removed (Fig. 2.1). Thus, capping the tube, which lowered pH, seems to have affected only $\delta^{13}C$. This is an interesting occurrence that highlights the need for researchers to provide details regarding this aspect of methodology when reporting results.

Although sample loss was greater in AACA treatment conducted with the cap closed (Table 2.5), $\delta^{13}C$ and $\delta^{18}O$ do not differ from samples treated with caps open. Furthermore, when a closed-cap NaOCl-treated sample was subjected to AACA treatment (also with the cap closed), $\delta^{13}C$ and $\delta^{18}O$ are within 2σ of samples treated with the caps open during both phases of the treatment. The fact that NaOCl-treated samples with quite different $\delta^{13}C$ (i.e. open versus closed cap) are essentially identical after AACA treatment implies that the carbon of consequence in NaOCl-treated samples is in a higher-solubility fraction.

H_2O_2 treatment with the cap closed led to less sample loss than treatment with the cap open (Table 2.5), and enrichment in ^{18}O (Fig. 2.1). This treatment remained slightly more acidic than those with open caps; thus the reduction in sample loss is probably not attributable to decreased dissolution of a high solubility fraction. The change in $\delta^{18}O$ suggests again that noting the details of methodology is important when reporting results.

AACA treatment of a capped H_2O_2-treated sample produced a $\delta^{18}O$ value within 2σ of open-cap H_2O_2-AACA-treated samples.

Weight % CO_3

The carbonate content of all samples was less than expected based on previous work reported by LeGeros (1991), who suggested dentin was 5.7% CO_3. However, Posner and Tannenbaum (1984) suggest 3 to 4 %. The slightly lower numbers

reported here for untreated samples may be due to loss of some bicarbonate during the roasting (200 ^{o}C under vacuum) of the samples.

Conclusions

The goals of this study were to identify a preferred pretreatment for modern and well-preserved fossil dentin. Other than minimizing unnecessary sample loss, the criteria upon which a decision of preference should be made are not necessarily clear. Although observing the differences in δ values in different treatment groups versus untreated samples seems reasonable, the untreated samples do not represent a "true" value. As Neuman and Mulryan (1967) have shown, 40 % of bone (and presumably dentin) CO_3 occurs in a rapidly exchanging pool. As this fraction is subject to rapid exchange, it seems that inclusion of CO_2 evolved from this fraction in the analyzed CO_2 is not desirable. Thus, a preferred treatment should minimize inclusion of this fraction in the sample. As it is subject to rapid exchange, it seems that mild acidification should preferentially remove this material. All treatments, excluding NaOCl have at least one acidic phase and apparently reduce the CO_3 present in samples (Table 2.1, Fig. 2.2). Much of this carbonate loss is probably attributable to removal of the highly exchangeable fraction, but some structural CO_3 may be lost in the process as well.

Removal of organics is common practice in analyses of bone and tooth mineral despite a lack of studies on the specific interference caused by the presence of organic matter. Here we have shown that the presence of organic matter in samples leads to changes in measured $\delta^{18}O$ that are dependent on time spent in the Kiel before

analysis. This is clearly a phenomenon that should be avoided. Thus, some pretreatment to remove organic material is necessary if $\delta^{18}O$ values are of interest.

Treatment with NaOCl causes large shifts in $\delta^{18}O$ and $\delta^{13}C$. This may be due to precipitation of a carbonate mineral or adsorption of bicarbonate. The isotope shifts appear to be reversed to some degree by subsequent treatment with AACA, suggesting that NaOCl-AACA is an acceptable treatment process. However, it is desirable to avoid conditions under which carbonate or bicarbonate might contaminate samples. H_2O_2 treatment is sufficient to remove organic material and avoid the time-dependent $\delta^{18}O$ effects observed in untreated and AACA-only-treated samples. Furthermore, the acidic conditions under which the removal of organics occurs should prevent precipitation of carbonate minerals. In addition, H_2O_2 removes some of the high-solubility fraction of carbonate in the sample as evidenced by reduced weight percent CO_3. This is also suggested by the minor effect on δ values of subsequent AACA treatment on H_2O_2-treated samples.

Oxidation of organics with tube caps closed leads to δ values that differ from those measured on samples for which oxidation was conducted with caps open. This effect is ameliorated by subsequent AACA treatment. Leaving caps closed also results in increased pressure within the tubes, particularly in the case of H_2O_2 treatment, and this may lead to spontaneous opening of caps and loss of sample. It is recommended that this treatment be conducted with caps open. The effect of AACA treatment on δ values does not appear to be affected by the status of the cap, although sample loss is greater when the cap is closed.

Given the observations made in this study, and those of Zazzo et al. (2006), treatment of modern dentin with NaOCl should be avoided. Treatment with H_2O_2 followed by AACA is preferable. In the case of small sample sizes for which sample loss must be minimized, H_2O_2 treatment alone may remove organics and high-solubility carbonate to a sufficient degree. The difference in δ values between H_2O_2-only- and H_2O_2-AACA-treated samples is small and not significant.

It should be stated that these recommendations apply only to modern dentin, and, given the similarity of the materials, perhaps also to bone. They may be inapplicable to modern enamel or fossil materials.

Table 2.1. Results from isotope analyses. Data for treatments conducted with caps on are italicized and not included in the calculated means and standard deviations (s.d.) of the relevant treatment group. $\delta^{13}C$ and $\delta^{18}O$ are reported relative to VPDB. Mass of untreated sample represented in treated samples was used in calculation of the adjusted weight percent CO_3. This was calculated by multiplying the actual sample mass by 1/(proportion of sample remaining after treatment). Two samples with anomalous values were exlcuded from these data (an H_2O_2 with $\delta^{13}C$= -13.35‰, $\delta^{18}O$=2.17‰, and an NaOCl with $\delta^{13}C$=-12.33‰, $\delta^{18}O$=0.46‰). Means and values for capped samples are plotted in Figure 2.1. Mean weight percent carbonate is shown in Figure 2.2.

Treatment	Run	Time (minutes into run)	$\delta^{18}O$	$\delta^{13}C$	µmol CO_3	Adjusted wt % CO_3
Untreated	1	212	2.64	-13.05	0.469	2.75
Untreated	1	377	2.59	-13.08	0.474	2.79
Untreated	1	613	2.45	-13.09	0.466	2.84
Untreated	1	848	2.39	-13.09	0.474	2.88
Untreated	1	1173	2.25	-13.06	0.474	2.88
Untreated	1	1348	2.20	-13.04	0.501	2.88
Untreated	1	1603	2.08	-13.04	0.474	2.78
mean			**2.37**	**-13.06**	**0.48**	**2.83**
s.d.			**0.21**	**0.02**	**0.01**	**0.05**
NaOCl (cap on)	*1*	*650*	*1.11*	*-13.26*	*0.824*	*2.77*
NaOCl	1	81	1.05	-12.34	0.844	3.06
NaOCl	1	244	1.27	-12.39	0.819	3.12
NaOCl	1	413	1.37	-12.32	0.819	3.11
NaOCl	1	883	0.99	-12.40	0.892	3.18
NaOCl	1	1206	0.93	-12.35	0.852	3.15
mean			**1.12**	**-12.36**	**0.85**	**3.13**
s.d.			**0.19**	**0.03**	**0.03**	**0.05**
H_2O_2 (cap on)	*2*	*777*	*3.30*	*-13.34*	*0.623*	*2.55*
H_2O_2	2	388	3.03	-13.40	0.583	2.24
H_2O_2	2	469	2.99	-13.38	0.573	2.21
H_2O_2	2	1180	3.04	-13.35	0.627	2.54
H_2O_2	2	1502	2.98	-13.30	0.607	2.45
mean			**3.01**	**-13.36**	**0.60**	**2.36**
s.d.			**0.03**	**0.05**	**0.02**	**0.17**
AACA (cap on)	*1*	*698*	*2.39*	*-13.55*	*0.488*	*1.84*
AACA	1	126	2.88	-13.47	0.440	1.92
AACA	1	294	2.53	-13.44	0.454	1.89
AACA	1	461	2.83	-13.55	0.496	1.92
AACA	1	936	2.19	-13.51	0.501	1.99
AACA	1	1258	1.78	-13.49	0.480	1.90
AACA	1	1521	1.86	-13.41	0.451	1.92
mean			**2.34**	**-13.48**	**0.47**	**1.92**
s.d.			**0.47**	**0.05**	**0.03**	**0.04**
NaOCl-AACA (cap on)	*1*	*800*	*1.97*	*-13.34*	*0.690*	*1.78*
NaOCl-AACA	1	161	2.14	-13.26	0.720	1.73
NaOCl-AACA	1	327	2.05	-13.26	0.670	1.67
NaOCl-AACA	1	566	2.05	-13.36	0.697	1.74
NaOCl-AACA	1	1126	2.00	-13.34	0.690	1.75
NaOCl-AACA	1	1291	2.10	-13.38	0.701	1.78
NaOCl-AACA	1	1555	1.92	-13.31	0.631	1.76
mean			**2.04**	**-13.32**	**0.68**	**1.74**
s.d.			**0.08**	**0.05**	**0.03**	**0.04**
H_2O_2-AACA (cap on)	*2*	*822*	*3.28*	*-13.37*	*0.560*	*1.74*
H_2O_2-AACA	2	276	3.04	-13.49	0.551	1.62
H_2O_2-AACA	2	429	3.24	-13.49	0.560	1.66
H_2O_2-AACA	2	429	3.11	-13.54	0.533	1.59
H_2O_2-AACA	2	1222	3.17	-13.45	0.564	1.71
H_2O_2-AACA	2	1544	3.08	-13.40	0.570	1.70
mean			**3.13**	**-13.47**	**0.56**	**1.66**
s.d.			**0.08**	**0.05**	**0.01**	**0.05**

Table 2.1. continued.

Treatment	Run	Time (minutes into run)	$\delta^{18}O$	$\delta^{13}C$	µmol CO_3	Adjusted wt % CO_3
NBS 19	1	0	-2.29	1.92	-	-
NBS 19	1	38	-2.22	1.94	-	-
NBS 19	1	497	-2.15	1.97	-	-
NBS 19	1	727	-2.16	1.90	-	-
NBS 19	1	756	-2.07	1.94	-	-
NBS 19	1	969	-2.18	1.95	-	-
NBS 19	1	1006	-2.28	1.94	-	-
NBS 19	1	1046	-2.23	1.98	-	-
NBS 19	1	1084	-2.21	1.96	-	-
NBS 19	1	1393	-2.32	1.93	-	-
NBS 19	1	1431	-2.25	1.93	-	-
NBS 19	1	1642	-2.16	1.97	-	-
NBS 19	1	1683	-2.12	1.95	-	-
mean			**-2.20**	**1.94**		
s.d.			**0.07**	**0.02**		
					-	-
NBS 19	2	0	-2.18	1.95	-	-
NBS 19	2	34	-2.17	1.93	-	-
NBS 19	2	309	-2.24	1.95	-	-
NBS 19	2	540	-2.14	1.95	-	-
NBS 19	2	855	-2.35	1.95	-	-
NBS 19	2	938	-2.22	1.92	-	-
NBS 19	2	1291	-2.23	1.91	-	-
mean			-2.22	1.94		
s.d.			0.07	0.02		

Table 2.2. Significance of regressions of δ values on time in run. Those regressions with p-values greater than 0.05 are considered not significant (n.s.). Capped samples were not included in the data. Note the highly significant trend in $\delta^{18}O$ for untreated samples.

Treatment	Significance of regression on time (p-value) $\delta^{18}O$	$\delta^{13}C$
Untreated	< 0.001	n.s.
NaOCl	n.s.	n.s.
H_2O_2	n.s.	0.040
AACA	0.006	n.s.
NaOCl-AACA	n.s.	n.s.
H_2O_2-AACA	n.s.	0.050
NBS 19 (run 1)	n.s.	n.s.
NBS 19 (run 2)	n.s.	n.s.

Table 2.3. Bonferroni-corrected p-values from pairwise Cramér tests. Significant differences ($p < 0.05$) between groups are indicated by the bold figures. Cramér tests were carried out with 10000 bootstrap replicates. AACA has little effect on H_2O_2-treated samples as is shown by the lack of significant difference between the H_2O_2 and H_2O_2-AACA groups.

	Untreated	NaOCl	H_2O_2	AACA	NaOCl-AACA	H_2O_2-AACA
Untreated	-					
NaOCl	**0.003**	-				
H_2O_2	**0.015**	**0.028**	-			
AACA	0.151	**0.007**	0.304	-		
NaOCl-AACA	**0.013**	**0.012**	**0.016**	0.624	-	
H_2O_2-AACA	**0.009**	**0.012**	0.172	0.153	**0.007**	-

Table 2.4. Predicted offsets in $\delta^{18}O$ and $\delta^{13}C$ after 24 hours in Kiel based on regressions of treatment data on time. Predicted offsets are shown only for significant regressions. Untreated and AACA-treated samples exhibit substantial, time-dependent shifts in $\delta^{18}O$.

	Predicted offset (‰) at 24 hours	
Treatment	$\delta^{18}O$	$\delta^{13}C$
Untreated	-0.57	-
NaOCl	-	-
H_2O_2	-	0.11
AACA	-1.15	-
NaOCl-AACA	-	-
H_2O_2-AACA	-	0.12
NBS 19 (run 1)	-	-
NBS 19 (run 2)	-	-

Table 2.5. Percent sample loss during treatments (based on dry mass before and after). Bold figures in the column representing percent sample loss in capped treatments identify loss outside of the 3σ range for uncapped treatments. Sample loss is greater in capped NaOCl, AACA, and NaOCl-AACA than in uncapped equiivalent treatments. Sample loss is reduced in capped H_2O_2. * The AACA phase of this treatment was conducted on material remaining after removing 1-mg samples for analysis of the H_2O_2-only treatment. The proportion lost in the second phase of treatment was used to calculate the loss that would have occurred during the two-phase treatment had the 1-mg samples not been removed.

Treatment	% Sample loss	% Sample loss in capped
NaOCl	36.4	**42.3**
H_2O_2	33.9	**32.7**
AACA	31.7	**35.8**
NaOCl-AACA	56.9	**62.2**
H_2O_2-AACA*	50.9	49.7

Table 2.6. pH of treatment solutions at start and end of treatments. pH was not measured on AACA with the cap closed. Note that pH of NaOCl treatment remains basic over the 24-hour period, while the H_2O_2 treatment remains acidic.

Treatment	pH at start	pH after 24 hours	pH after 24 hours capped
NaOCl	10	8	6.5
H_2O_2	4.9	5.5	5.1
AACA	4.6	4.6	-

Figure 2.1. Mean $\delta^{13}C$ and $\delta^{18}O$ of treatment groups. Error bars are 1σ. Small symbols without error bars represent values for treatments conducted with the caps on the tubes closed. NaOCl has a pronounced effect on both $\delta^{13}C$ and $\delta^{18}O$ (as compared to untreated samples), which is somewhat counteracted by subsequent AACA treatment (NaOCl-AACA). The large $\delta^{18}O$ errors for AACA and untreated groups are due to the time-dependent effect discussed in the text. Leaving caps closed during treatment has only moderate effects on isotope values except in the case of NaOCl.

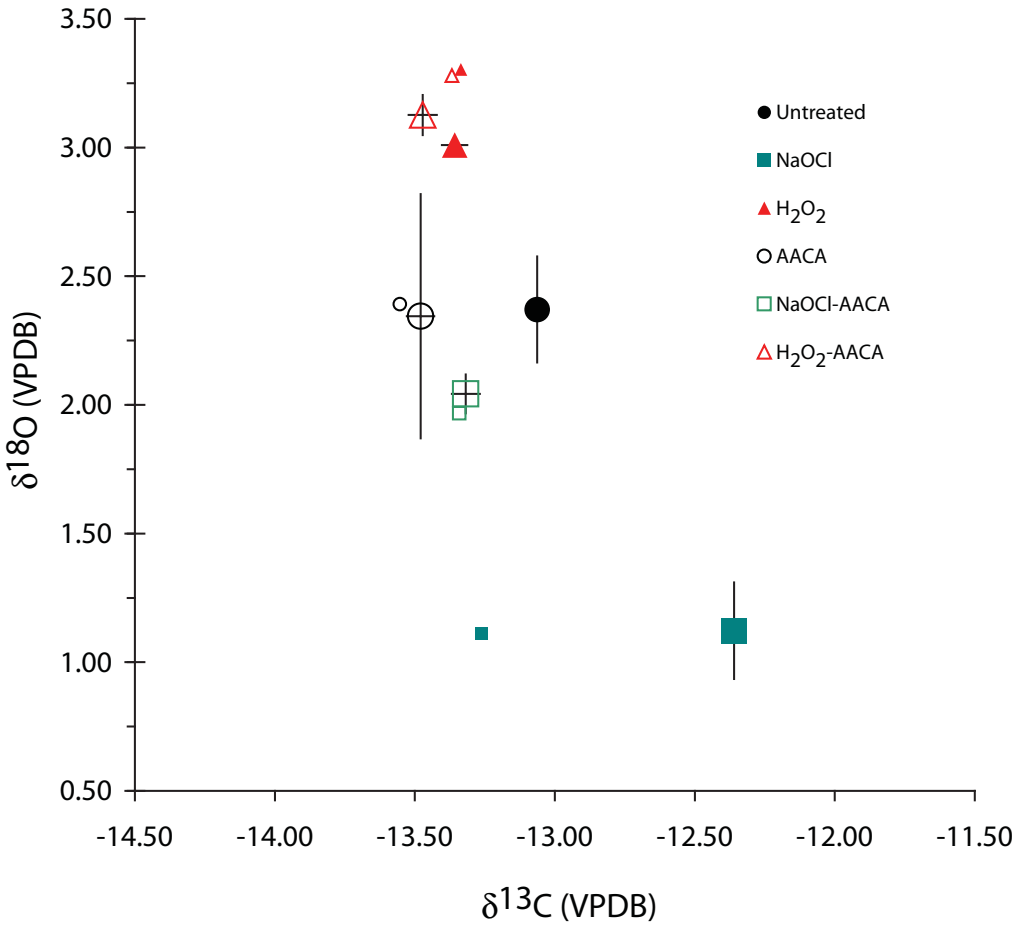

Figure 2.2. Adjusted weight percent CO_3. See Table 2.1 for description of adjustment. Error bars represent 1σ. Note that adjusted weight percent carbonate is higher in NaOCl-treated samples than in untreated samples.

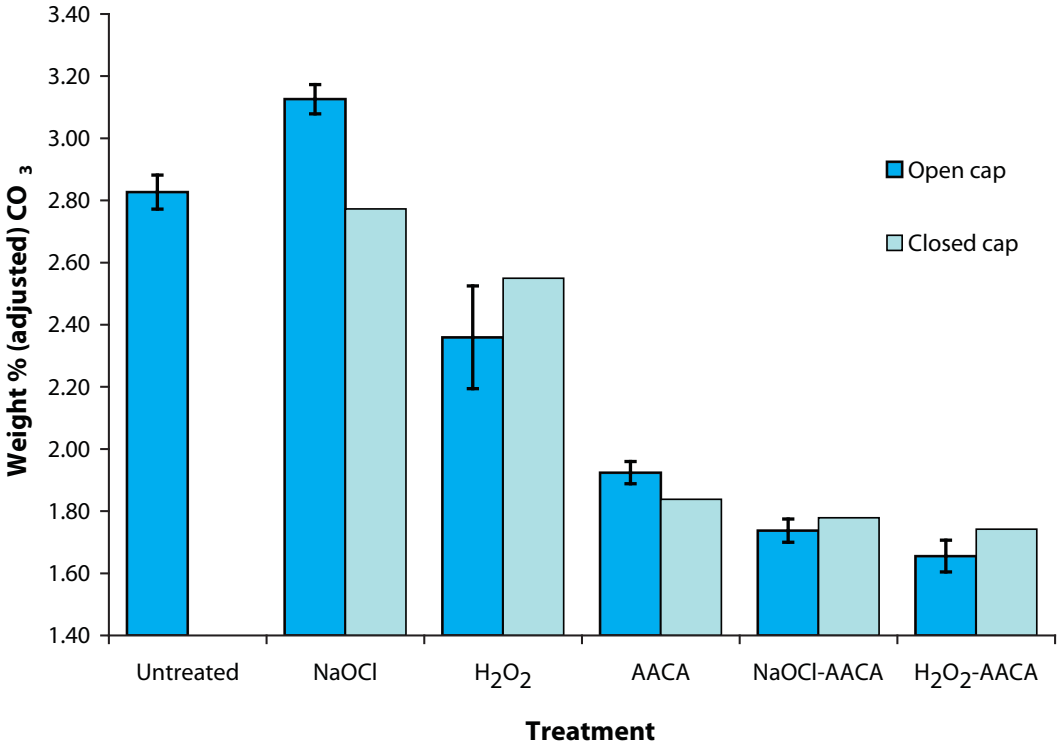

References

Baringhaus, L., Franz, C., 2004. On a new multivariate two-sample test. Journal of Multivariate Analysis 88, 190–206.

Beshah, K., Rey, C., Glimcher, M.J., Schimizu, M., Griffin, R.G., 1990. Solid state carbon-13 and proton NMR studies of carbonate-containing calcium phosphates and enamel. Journal of Solid State Chemistry 84, 71–81.

Cazalbou, S., Combes, C., Eichert, D., Rey, C., Glimcher, M.J., 2004. Poorly crystalline apatites: evolution and maturation in vitro and in vivo. Journal of Bone and Mineral Metabolism 22, 310–317.

Cerling, T.E, Harris, J.M., MacFadden, B.J., Leakey, M.G., Quade, J., Eisenmann, V., Ehleringer, J.R., 1997. Global vegetation change through the Miocene/Pliocene boundary. Nature 389, 153–158.

DeNiro, M.J., Epstein, S., 1978. Carbon isotopic evidence for different feeding patterns in two hyrax species occupying the same habitat. Science 201(4359), 906–908.

Franz, C., 2006. Cramer: Multivariate nonparametric Cramer-Test for the two-sample-problem. R package version 0.8-1.

Garvie-Lok, S.J., Varney, T.L., Katzenberg, M.A., 2004. Preparation of bone carbonate for stable isotope analysis: the effects of treatment time and acid concentration. Journal of Archaeological Science 31(6) 763–776.

Haynes, V., 1968. Radiocarbon: Analysis of inorganic carbon of fossil bone and enamel. Science 161(3842) 687–688.

Jiang, T., Ma, X., Wang, Y., Zhu, Z., Tong, H., Hu, J., 2007. Effects of hydrogen peroxide on human dentin structure. Journal of Dental Research 86, 1040–1045.

Kawamoto, K., Tsujimoto Y., 2004. Effects of the hydroxyl radical and hydrogen peroxide on tooth bleaching. Journal of Endodontics 30(1), 46–50.

Koch, P.L., 1989. Paleobiology of late Pleistocene mastodonts and mammoths from southern Michigan and western New York. Unpublished doctoral dissertation, University of Michigan.

Koch, P.L., Fisher, D.C., Dettman, D., 1989. Oxygen isotope variation in the tusks of extinct proboscideans: A measure of season of death and seasonality. Geology 17, 515–519.

Koch, P.L., Tuross, N., Fogel, M.L., 1997. The effects of sample treatment and diagenesis on the isotopic integrity of carbonate in biogenic hydroxylapatite. Journal of Archaeological Science 24, 417–429.

Krueger, H.W., 1991. Exchange of carbon with biological apatite. Journal of Archaeological Science 18, 355–361.

Lee-Thorp, J.A., Sealy, J.C., van der Merwe, N.J., 1989. Stable carbon isotope ratio differences between bone collagen and bone apatite, and their relationship to diet. Journal of Archaeological Science 16, 585–599.

Lee-Thorpe, J.A., van der Merwe, N.J., 1991. Aspects of the chemistry of modern and fossil biological apatites. Journal of Archaeological Science 18, 343–354.

LeGeros, R., 1991. Calcium phosphates in oral biology and medicine. Monographs in Oral Science 15. Karger, Basel.

Lowenstam, H.A., Epstein, S., 1957. On the origin of sedimentary aragonite needles of the Great Bahama Bank. Geology 65(4), 364–375.

Munro, L.E., Longstaffe, F.J., White, C.D., 2008. Effects of heating on the carbon and oxygen-isotope compositions of structural carbonate in bioapatite from modern deer bone. Palaeogeography, Palaeoclimatology, Palaeoecology 266, 142–150.

Neuman, W.F., Mulryan, B.J., 1967. Synthetic hydroxyapatite crystals: III. The carbonate system. Calcified Tissue Research 1, 94–104.

Posner, A.S., Tannenbaum, P.J., 1984. The mineral phase of dentin. In: Linde, A., (Ed.), Dentin and Dentinogenesis Vol. 2. CRC Press, Boca Raton.

Poyart, C.F., Busaux, E., Fréminet, A., 1975. The bone CO_2 compartment: Evidence for a bicarbonate pool. Respiration Physiology 25, 89–99.

Poyart, C.F., Fréminet, A., Bursaux, E., 1975b. The exchange of bone CO_2 *in vivo*. Respiration Physiology 25, 101–107.

R Development Core Team, 2008. R: A language and environment for statistical computing. R Foundation for Statistical Computing, Vienna, Austria.

Rey, C., Combes, C., Drouet, C., Sfihi, H., Barroug, A., 2007. Physico-chemical properties of nanocrystalline apatites: Implications for biominerals and biomaterials. Materials Science and Engineering C 27, 198–205.

Sullivan, C.H., Krueger, H.W., 1983. Carbon isotope ratios of bone apatite and animal diet reconstruction. Nature 301, 177.

Urey, H.C., Lowenstam, H.A., Epstein, S., McKinney, C.R., 1951. Measurement of paleotemperatures and temperatures of the upper Cretaceous of England, Denmark, and the southeastern United States. Bulletin of the Geological Society of America 62, 399–416.

Wright, L.E., Schwarcz, H.P., 1998. Stable carbon and oxygen isotopes in human tooth enamel: Identifying breastfeeding and weaning in prehistory. American Journal of Physical Anthropology 106, 1–18.

Zazzo, A., Balasse, M., Patterson, W.P., 2006. The reconstruction of mammal individual history: refining high-resolution isotope record in bovine tooth dentine. Journal of Archaeological Science 33, 1177–1187.

Zazzo, A., Lécuyer, C., Mariotti, A., 2004. Experimentally-controlled carbon and oxygen isotope exchange between bioapatites and water under inorganic and microbially-mediated conditions. Geochimica et Cosmochimica Acta 68(1), 1–12.

Zioupos, P., Rogers, K.D., 2006. Complementary physical and mechanical techniques to characterize tooth: A bone-like tissue. Journal of Bionic Engineering 3, 19–31.

Chapter 3

Temporal variation in stable isotope and elemental ratios in the tusk of a juvenile African elephant

Introduction

Animal recording structures are those structures that accumulate in layers and change in response to changing physiological condition (Klevezal, 1996). These structures include teeth, otoliths, mollusc shells, and other animal parts that are formed by accretion and persist for a relatively long period of time. Recording structures offer a data source for age determinations as well as life history reconstructions. In addition to changes in structure, such as the increased thickness of dentin growth increments in teeth associated with favorable nutritional status (Fisher, 1996), the composition of recording structures also changes in response to physiological and environmental factors (e.g., Koch, 1989; Fisher and Fox, 2003; Cerling et al., 2004). Methods combining analyses of structural and compositional features allow for detailed reconstruction of individual life histories, and these methods are a powerful means of collecting data on organisms that are difficult or impossible to study by direct observation.

Dentin in the tusks of proboscideans is a nearly ideal recording structure because it is laid down throughout life, it contains temporally periodic incremental growth features (Fisher, 2001), and it is not (usually) subject to resorption. The incremental features in dentin occur at three scales. First-order increments are annual, third-order increments are daily, and second-order increments (in elephants and mammoths) represent sets of around seven days (Fisher, 2001; Fisher pers. comm.). Thus, tusks contain relatively permanent, long-term records of the physiological and environmental changes experienced by an animal. Furthermore, the temporally periodic nature of incremental growth features permits assignment of events to intervals of time on the order of one to two weeks (e.g., Fisher, 1996; Fisher, 2008). All of these attributes allow the use of tusk data to test hypotheses that otherwise would be testable only by field observations.

Fisher (1996) has proposed that documenting changes in the life history parameters of late Pleistocene proboscideans , as determined through tusk analyses, can offer new insights into the causes of their extinction. The tusks of juveniles are of particular importance in understanding the paleobiology of mammoths or mastodons because they offer an opportunity to investigate the early years of life. The dentin formed during these early years is often worn away in the tusks of adults. In order to develop a reference for work on juvenile mammoths, we have conducted an analysis of the tusk of a juvenile African elephant.

While there has been some work on patterns of structural and compositional variation in modern elephant tusks (e.g., Koch, 1989 dissertation, Koch et al., 1995), to

our knowledge, no high-resolution, serial compositional analyses have been performed on an elephant tusk that retains the earliest formed dentin. Information on the variation in composition that occurs seasonally as well as over longer periods in this early phase of life is needed to serve as a reference for interpretations of data from mammoth tusks. Additionally, elemental concentrations in a presumably unaltered tusk provide a general baseline against which potentially diagenetically altered samples can be compared. Thus, we undertook an extensive structural and compositional analysis of the tusk of a juvenile African elephant.

Elephants in Hwange National Park

The tusk analyzed in this study was collected at the Shabi Shabi seep (-19.323389, 26.174525) in Hwange National Park (HNP), Zimbabwe by G. Haynes in mid-1984 as part of a study of elephant mass death assemblages. The seep is located in the southwestern Kalahari Sands portion of the park (Fig. 3.1), which is characterized by the presence of parallel, east-west oriented, Pleistocene dunes. The areas between the dunes consist of finer grained sands, and the lowest points in the troughs often contain seeps or pans (Flint and Bond, 1968). The sediment in these pans has a much higher proportion of clay, which inhibits flow and creates small perched aquifers (Flint and Bond, 1968). Due to the highly seasonal patterns of precipitation in the park, these perched aquifers are an important water resource during certain periods of the year when surface water is scarce or unavailable (Haynes, 1991). Most precipitation in the park occurs during the warm wet season, which falls between November and

March. Mean annual precipitation at HNP Main Camp in the northeast part of the park is approximately 600 mm (Dudley et al. 2001), but the Shakwanki region in which the Shabi Shabi seep is located probably receives less precipitation (Haynes, 1991; Swap et al. 2004).

The distribution of elephants within the park is, in large part, controlled by water availability (Williamson, 1975). Elephants occur at lower densities in the rainy season, and herds enter areas of the park that are not frequented in the dry season (Williamson, 1975). The diet shifts from browse to grass in the rainy season, with maximum grass/browse ratios occurring from January to March (Williamson, 1975b). Similar patterns have been observed in other areas with comparable climate regimes (Barnes, 1982). During the dry season, elephants concentrate in areas of water availability, and their diets consist of mostly browse (Williamson, 1975b). In the northern part of the park, dry-season water may be obtained from either perennial rivers or borehole-fed pans. However, in the southwest region of the park, the majority of dry-season water sources is at seeps such as Shabi Shabi (Chamaille-Jammes et al., 2007) . Accessing this water requires digging (Williamson, 1975).

Elephants obtain water at the seeps by digging wells and using their trunks to extract water from them (Haynes 1991). During drought years, the depth of the water table may be such that young elephants are unable to reach it with their trunks (Williamson, 1975). Dudley et al. (2001) suggest that this may account for the high mortality of juvenile elephants at the seeps in drought years such as 1994. Juvenile mortality was also high at the seeps in the dry years of 1982 and 1983 (Haynes, 1991).

As the dry season progresses, the concentrated elephant population depletes forage near the seeps, and individuals must travel progressively greater distances from the water source to obtain food (Haynes, 1991). Juveniles might be under greater stress during these times as they probably have more difficulty making these treks. The individual from which this tusk was collected most likely died as a result of starvation and/or water stress between July and October of 1983 after having survived the more severe die-off of 1982. There is some evidence that during drought years at HNP, juvenile elephants are more likely to become separated from their herds and fall victim to lion predation (Loveridge et al., 2006), but the carcass of this individual showed no signs of utilization by predators.

Stable Isotopes

$\delta^{13}C$

The $\delta^{13}C$ values of proteins and structural carbonate in mineralized tissues have been used in many studies as indicators of diet. The primary interpretive basis for much of this work has been the existence of a difference in the $\delta^{13}C$ of plants using the C_3 photosynthetic pathway versus plants using the C_4 photosynthetic pathway (Smith and Epstein, 1971). The $\delta^{13}C$ of animal tissues reflects the proportions of C_3 and C_4 plants in the diet (DeNiro and Epstein, 1978); thus, isotopic analyses of animal tissues can be used to determine aspects of dietary history.

Ambrose and Norr (1993) showed that the $\delta^{13}C$ of collagen depends primarily on the $\delta^{13}C$ of the protein portion of the diet, but that it is also influenced by the

isotopic composition of carbohydrates and lipids. The $\delta^{13}C$ of carbonate in hydroxyapatite more closely represents the isotopic composition of bulk diet (Ambrose and Norr 1993). For large ungulates, the diet to enamel (carbonate in hydroxyapatite) enrichment of ^{13}C is about +14.1 ‰ (Cerling and Harris, 1999), while that for diet to collagen is about +5 ‰ (Sullivan and Krueger, 1981). Thus, the carbon isotopic composition of collagen and carbonate in hydroxyapatite can be used to determine the isotopic composition of both the bulk diet and the (predominately) protein portion of the diet. By serially sampling a structure that grows by accretion, such as a tusk, shifts in the isotopic composition of diet can be tracked.

The dominant factor influencing the C isotopic composition of elephants in HNP should be the relative proportions of C_3 browse and C_4 grass in the diet. Based on examinations of stomach contents, grass makes up the between 10 and 98 % of the diet during the rainy season, while browse makes up the majority of the diet of during the dry season (Williamson, 1975b).

No data on the isotopic composition of plants in HNP was available, but Swap et al. (2004) provide compiled data for localities in southern Africa with similar mean annual precipitation (MAP) levels to HNP. For C_3 plants at Maun (MAP = 460 mm), in north-central Botswana, they report a mean $\delta^{13}C$ of -26.8 ‰ (n = 14, s.d. = 1.9). For C_4 plants at Kruger National Park, South Africa (MAP = 650 mm) they report a mean of -13.7 ‰ (n = 8, s.d. = 0.8). Using these values, one would expect an elephant eating only C_4 plants to have a $\delta^{13}C_{col}$ of around -8.7 ‰ and a $\delta^{13}C_{carb}$ of around 0.4 ‰, while an elephant eating only C_3 would have a $\delta^{13}C_{col}$ of around -21.8 ‰ and a $\delta^{13}C_{carb}$ of

around -12.7 ‰. Thus, in an elephant with a seasonally shifting diet, we expect to see seasonal variation in $\delta^{13}C$ between these endpoints.

This case is complicated somewhat by the fact that the individual analyzed in the current study was a nursing juvenile. An isotope study of diet and milk in cattle showed that shifts from C_3 to C_4 diets lead to shifts in the isotopic composition of milk (Wilson et al., 1988) suggesting that the $\delta^{13}C$ pattern observed in the tusk of a nursing juvenile elephant might vary with season even if the calf is primarily feeding on milk. However, a portion of the C in milk is also derived from maternal tissues, and the magnitude of this contribution may depend on the amount of milk being produced (Wilson et al., 1988). One can imagine complicating scenarios such as one in which maternal fat and protein stores are built up in the rainy season when C_4 plants are important in the diet, and these stores are then utilized for milk production during the dry season. The $\delta^{13}C$ data obtained in this study, in conjunction with weather data, will help to clarify whether or not such a scenario actually occurs.

$\delta^{15}N$

Because of tissue enrichment that occurs at each trophic level (Schoeninger and DeNiro, 1984), $\delta^{15}N$ of collagen (and other tissues such as hair) has been used to determine trophic level. In addition, enrichment in ^{15}N has been associated with nutritional stress (Hobson et al., 1993; Mekota et al., 2006;), water stress (in drought-tolerant herbivores, Ambrose and DeNiro, 1986), or differences in N isotopic composition of diet. In particular, young individuals feeding on their mothers' milk

often have higher collagen $\delta^{15}N$ than they do after weaning because they effectively feed one trophic level higher than a mature individual of their species (e.g., Hobson and Sease, 1998; Newsome and Koch, 2006).

In general, there is a +3 ‰ enrichment in collagen $\delta^{15}N$ per trophic level (Shoeninger and DeNiro, 1984), and as a nursing calf is one trophic level above its mother, the $\delta^{15}N$ of the calf's collagen might be 6 ‰ more positive than vegetation, and 3 ‰ more positive than its mother. Although, this enrichment has been observed in some studies (e.g., Hobson and Sease, 1998; Newsome et al. 2006), other studies have found less enrichment than expected (e.g., Dalerum et al., 2007; Polischuk, 2001). This may be attributable to complexities in diet-to-consumer enrichment. Sponheimer et al. (2003) observed a dependence of diet-to-consumer enrichment on the protein content of the diet. Greater enrichment occurred on high protein diets. Robbins et al. (2005) found that diets with high biological value (a measure of dietary protein quality), such as milk and fish lead to lower levels of diet-to-consumer enrichment than those of low biological value, such as ruminant plant diets. Based on the relationships presented in the Robbins et al. (2005) study, the expected enrichment on a milk diet would be about 2 ‰. Although Jenkins et al. (2001) reported that milk was depleted in ^{15}N (~1 ‰) relative to maternal plasma (possibly reducing any expected differences between mother and calf), Polischuk et al. (2001) reported that milk was enriched in ^{15}N relative to maternal (and cub) plasma. Based on the available data and assuming that the diet composition and diet-to-consumer enrichment for plant foods are similar in the calf and mother, the expected offset

between collagen formed during milk dependence and that formed during plant dependence should be between +1 and +3 ‰.

$\delta^{15}N$ of collagen also depends on the $\delta^{15}N$ of vegetation ingested. In hairs from adult elephants, Cerling et al. (2009) observed higher $\delta^{15}N$ (and $\delta^{13}C$) values in samples representing rainy season growth than in samples representing dry season growth. They also found that C_4 plants, which make up a larger portion of the diet during the rainy seasons, had higher $\delta^{15}N$ values than C_3 plants. In contrast, Codron (2008, unpublished dissertation) found that the mean $\delta^{15}N$ of C_3 plants in Kruger National Park, South Africa was significantly higher than that of C_4 plants. However, Codron (2008, unpublished dissertation) also found marked variation in $\delta^{15}N$ of plants in different regions of the park. She also observed no relationship between elephant fecal $\delta^{15}N$ and the $\delta^{15}N$ of available plants, which, in part, led to the conclusion that animal physiology rather than diet might be the primary controller of tissue $\delta^{15}N$. Based on this variability in patterns of $\delta^{15}N$ in elephants, it is not clear what seasonal-scale patterns might be expected in this individual. However, high $\delta^{15}N$ would still be expected early in life when dependence on milk is high.

$\delta^{18}O$

The $\delta^{18}O$ of structural carbonate in the hydroxyapatite of large herbivores is largely dependent on the $\delta^{18}O$ of drinking water (Koch et al., 1989). Meteoric water is often seasonally variable in its isotopic composition (Gat, 1996), and drinking water is generally derived from local meteoric water. Thus, the $\delta^{18}O$ of serial samples of

mineralized structures that grow by accretion can exhibit seasonal-scale variation (Koch et al., 1989).

As precipitation occurs in HNP only on a seasonal basis, full-scale seasonal variation in $\delta^{18}O$ cannot occur. However, as there is no surface water available during the dry season (Haynes, 1991), during that time elephants must be drinking from water sources that have been enriched in ^{18}O by evaporation (Gat, 1996). Thus, it is hypothesized that $\delta^{18}O_{carb}$ in this tusk should show a seasonal pattern in which higher values occur during the dry season.

There may also be some unique factors affecting $\delta^{18}O$ that apply to this juvenile. Wright and Schwarcz (1998) suggested that, because milk is derived from body water, and body water is enriched in ^{18}O relative to drinking water, nursing infants might show higher $\delta^{18}O$ than weaned individuals. In their study, they found $\delta^{18}O_{carb}$ in enamel was higher in younger individuals assumed to be nursing.

Elemental Ratios

Mg/Ca

Mg concentration or Mg/Ca ratios have been used as paleodietary indicators of vegetation in diet because the Mg concentration in plant foods is higher than in animal foods (Klepinger, 1984). Mg levels in bone (and presumably dentin) are correlated with dietary levels (Miller et al. 1965), but Klepinger (1990) suggests this may only be true in cases of extreme dietary deficiency or excess. The Mg/Ca of elephant milk is about 150 (mmol/mol) (based on data from McCullagh and

Widowson, 1970), while the mean Mg/Ca of leaves from 30 species of trees in western Zimbabwe (near HNP) is about 799 (mmol/mol) (based on data from Holdo, 2003). Thus, increasing intake of vegetation and decreased dependence on milk may be recorded in the dentin as increasing Mg/Ca.

Mn/Ca and Fe/Ca

Mn/Ca and Fe/Ca are included in this analysis to determine expected levels in unaltered juvenile dentin for comparison with fossil juvenile mammoth dentin. Mn and Fe are found in low concentrations in modern enamel and at concentrations ~2 to 3 orders of magnitude greater in fossil enamel and dentine (Kohn et al., 1999).

Zn/Ca

Zn has been used in paleodietary studies as a means of determining carnivory vs. herbivory (reviewed by Ezzo, 1994). Ezzo (1994) points out that there are problems with the use of bone Zn as a paleodietary indicator because there are a variety of factors that can influence Zn concentrations. In this study, we are primarily concerned with the elevated levels of Zn that may occur around the time of birth.

Jeswani and Vani (1982) observed that serum Zn concentrations of human fetuses increased through gestation, and Dauncey et al. (1977) note accelerated accumulation of Zn occurring in the third trimester. Furthermore, Zn concentrations in human milk are highest in the early stages of lactation and decrease thereafter (Vuori and Kuitunen, 1979). Based on these studies, one could hypothesize that Zn/Ca

would show a marked high around the time of birth. Indeed, Drzaga et al. (2007) observed significant decreases in bone Zn/Ca in 7 to 28 day old rats, suggesting that levels were high around the time of birth. Ando-Mizobata et al. (2006) noted that Zn/Ca in the dentin of Steller sea lions was high in the first year of life and then decreased and showed little variability after this, and Evans et al. (1995) found the highest concentrations of Zn in the earliest-formed cementum of walrus teeth. Based on these studies, we hypothesize that if the tusk of this elephant began forming before the time of birth, Zn/Ca will show a peak early in the record that represents the late gestation/neonatal period.

Zn/Ca could also vary seasonally. Dufty et al. (1977) observed seasonal variation in plasma Zn in cattle, in which high levels were associated with the season of rapid pasture growth. Thus, if Zn/Ca varies seasonally, highs might occur during the rainy season, a time of much new plant growth.

Sr/Ca

Sr is discriminated against relative to Ca in the guts of terrestrial vertebrates, and has been used to determine trophic level (Sr/Ca decreases with increasing trophic level) (reviewed by Sillen and Kavanagh, 1982). For example, Toots and Voorhies (1965) found that Sr concentrations in bones of Pliocene carnivores were lower than the concentrations in herbivores.

Sr/Ca has also been used to identify nursing and weaning as Sr is discriminated against during absorption by the mother, then again in milk production (reviewed in

Sillen and Kavanagh, 1982). One would expect low Sr/Ca in the tissues of nursing infants. However, use of this system is complicated by the fact that discrimination against Sr in the digestive system of infants and children increases with age (reviewed in Sillen and Kavanagh, 1982). While knowledge of the changes in discrimination with age allows Sr/Ca to be used to identify nursing/weaning in humans, the pattern of changing discrimination in elephants is unknown. Thus, we measure Sr/Ca in an exploratory manner with no hypotheses regarding expected patterns.

Sr/Ca is also dependent on soil Sr and Ca concentrations (reviewed by Sillen and Kavanagh, 1982). Feeding in areas with different soil Sr/Ca could affect Sr/Ca observed in the tusk.

Ba/Ca

Ba behaves similarly to Sr, with increasing discrimination with age (Taylor et al. 1962), and decreasing Ba/Ca with trophic level (Pate, 1994). Trends in Ba/Ca in the tusk are expected to be similar to those in Sr/Ca. However, if soil Sr/Ba is variable, Sr and Ba may exhibit different patterns.

P/Ca and Pb/Ca

P/Ca and Pb/Ca were included for exploratory purposes.

Materials and Methods

The tusk under study (Figs. 3.2A, B) is the left tusk of a pair collected from one individual. The tusk is 40.0 cm in length along the outside curve, and it has a maximum circumference of 12.2 cm. Additional measurements are listed in Table 3.1. Several details of the tusk's morphology are notable. The distal (abapical) end of the tusk has a segment extending 6.2 cm proximally (apically) from the tip which lacks cementum (Figs. 3.2A, B). Patches of enamel, which is present only at the tips of elephant tusks, cover parts of the dentin surface in this segment, indicating that some of the underlying, first-formed dentin is still present. The thickness of the enamel is variable, but it is generally thinner near the tip (~0.18 mm) and thicker proximally (0.38 mm). Cementum overlays the enamel in some areas, with the proximalmost observed enamel being 7.8 cm from the tip on the medial surface of the tusk.

The distalmost cementum shows staining and etching (Figs. 3.2A, B), marking the portion of the tusk that had erupted and was exposed to saliva prior to death (Elder, 1970). The boundary between stained and unstained cementum shows the position of the gingival margin. As noted by Elder (1970) this boundary does not follow a simple circle of locally minimal diameter, but rather it undulates as it encircles the tusk. The distalmost position of the boundary is located 10.8 cm from the tip, while the proximalmost position of the boundary is located 13.8 cm from the tip. Taking the midpoint (12.3 cm from the tip), this implies that the proximal 27.7 cm of the tusk was contained within the alveolus and gingiva at the time of death.

Elder (1970) showed that the tusks of male and female elephants differ in the ratio of pulp cavity depth to length of unexposed ivory. Generally the depth of the

pulp cavity in a male's tusk is greater than the length of unexposed tusk, while in females, the depth of the pulp cavity is less than the length of unexposed tusk (Elder, 1970). There are few tusks in Elder's data set that are similar in size to the tusk used in this study. However, these few tusks follow the generally observed pattern. The depth of the pulp cavity, as determined by insertion of a 2 mm-wide steel ribbon was 23.2 cm. This is less than the length of unexposed tusk suggesting that the individual from which this tusk was collected was female. It is also notable that Elder (1970) used a 0.5 inch-wide steel tape to measure pulp cavity depth, leading to artificially shortened pulp cavity depths, particularly in individuals with very acute pulp cavities. Following this procedure, the pulp cavity of the tusk of interest was measured at 18.3 cm.

There is a prominent, rapid increase in circumference that occurs between 29.0 and 30.5 cm from the tip (Figs. 3.2A, B). This "bulge" has also been observed in the tusks of juvenile mammoths (Rountrey et al., 2007; Rountrey pers. obs.). The cause of the rapid increase in circumference is unknown, but as it is present only in the tusks of juveniles, it may represent a shift in condition associated with changes in the shape and or size of the skull and alveolus, or it may result from the change in stresses exerted on the tusk as it erupts and begins to be used for manipulation of objects.

In order to obtain thin-sections for the measurement of growth increment thicknesses through life, and to allow serial compositional sampling of the interior dentin, it was necessary to cut the tusk. In order to document the original morphology of the tusk, prior to any cutting, the tusk was molded using silicone molding materials.

In addition, a three-dimensional computer model was produced using a Microscribe-3DLX (Immersion Corporation, San Jose) point digitizer and the software package Geomagic Studio 2.0 (Raindrop Geomagic, Inc., Research Triangle Park, NC). Alignment points were placed on the tusk such that additional features, such as the interior surface of the pulp cavity, could be digitized after cuts were made and incorporated into the three-dimensional model (Fig. 3.2C).

The tusk was first cut longitudinally (Fig. 3.3). Following this cut, each half of the tusk was again molded with silicone molding materials, and the pulp cavity surface was digitized. The result of digitization is a three-dimensional model that shows the relationship of the pulp cavity to the external surface of the tusk (Fig. 3.2C). On the longitudinal cut surface (Fig. 3.3), dark-light couplets, which appear as a series of nested "V"s with their apices directed toward the tip, show how the cut plane intersects the conical layers that represent previous positions of the pulp cavity. These dark-light couplets are the first-order incremental features, which have been observed in the tusks of proboscideans (e.g., Fisher, 1984; Koch, 1989; Fisher, 2001) as well as in the teeth of other mammals (Klevezal 1996). As each couplet, or first-order increment, represents a year of dentin apposition, the increments can be used as an aid in the planning of transverse cuts, to make sure that all years are well represented in the thin-sections and compositional sampling blocks. Careful planning of transverse cuts is necessary because growth increments thin near the cementum-dentin junction. In order for measurements of second-order increment thicknesses to be comparable, the measurements need to be made in areas of the dentin away from the cementum

dentin junction. Furthermore, the temporal resolution provided by serial compositional sampling is increased when samples are taken in areas where the growth increments are thicker.

One half of the tusk was left intact, while nine transverse cuts were made in its counterpart. An initial proximalmost cut was made using a coping saw. Subsequent cuts were made using an Isomet low speed saw with a diamond wafering blade. Segments were numbered 1 to 10 with numbers increasing from the tip of the tusk proximally. Each segment was sanded and polished on three sides. Each polished face was imaged on an Epson Perfection 4490 Photo flatbed scanner (Epson America, Inc., Long Beach, CA) at 9600 dpi. With contrast enhancement, the first-order features are easily identified on longitudinal and transverse surfaces (Fig. 3.4A, B). A thin-section was cut from the proximal surface of each segment for the measurement of second- and third-order increment thicknesses.

Following thin-section production, segments 1, 2, 4, and 8 were chosen for use in compositional sampling. These segments allow a series of compositional samples to be taken that cover the complete period of tusk formation. Each segment was again cut in half using the Isomet saw. The cut plane was oriented so that it passed through the tusk axis and followed a radius that bisected the sector in which the radii of curvature of second-order increments visible on the transverse surfaces were at their maxima (Fig. 3.5). The placement of this mediolateral cut allows compositional samples to be milled from the resultant cut face of either part. The fact that the cut bisected the sector in which the radii of curvature of second-order increments visible

on the transverse surfaces were at their maxima means that possible time averaging caused by milling across second order increments with increasing milling depth is minimized.

The surfaces exposed by the mediolateral cut were sanded and polished, then scanned on the flatbed scanner (e.g., Fig. 3.6A). These images were used to produce a plan for the compositional sampling. Ideally, samples are milled by following the path of second-order increments visible on the cut surface. In this specimen, and in well-preserved mammoth dentin, second-order increments are difficult or impossible to see under the stereomicroscope used for milling, so a technique for visualizing and marking the paths of these features was developed. First, the scan images were processed using the FFT Bandpass Filter plugin (J. Walter) for ImageJ (Rasband, 1997-2008) using filtering parameters to filter out large scale features down to 40 pixels and small scale features up to 3 pixels. This helps to diminish differences in luminance due to first-order increments, Schreger pattern, and random ccd noise. Additionally, vertical stripes were suppressed with a tolerance of direction of 5%. This suppression reduces artifacts that result from variation in the response of individual sensors in the CCD strip of the scanner as it is translated across the surface of the specimen. The autoscale and saturate features were enabled to increase the contrast of the image. Individual second-order increments are visible in the resulting image (Fig. 3.6C).

The enhanced images were aligned and specific second-order increments that were correlated among multiple images were used to define the boundaries within which samples would be collected in each segment. This ensured sampling of all

second-order increments present in the tusk. Sampling lines were marked on the images in Adobe Photoshop CS3 (Adobe Systems Inc., San Jose, CA) by tracing along second-order increments and spacing lines by 0.5 mm (the diameter of the bit to be used for sampling) (Fig. 3.6D). The sampling-line overlays were then printed on transparency film at actual size. The transparency was aligned on the polished cut surfaces using the corners of the surface as alignment points and adhered using two-sided tape. A pin was used to penetrate the transparency and produce dimples in the dentin surface along the lines to be sampled. While this was a time-consuming procedure, it was necessary to obtain high-resolution serial samples in this well-preserved dentin.

After marking, segments to be sampled were adhered to aluminum plates such that the cut surface to be sampled was parallel with the bottom of the plate. Samples were milled using a milling station consisting of a fixed dental drill and stereomicroscope. A carbide burr of 0.5 mm diameter was used to mill out powdered samples along the dimpled lines. Where possible, approximately half the length of each sampling line was milled. By alternating the direction in which the lines were milled, this allowed for extraction of both a powder and a solid block sample for each line position (Fig. 3.6E). Block samples were undercut for removal with a custom carbide bit. Because the sampling lines in the distalmost segments were short, this alternating method would produce individual powder or block samples too small for analysis. For samples in this area, every other sample line on both segment parts

resulting from the mediolateral cut was sampled, and the unsampled lines were removed as blocks.

Powder samples were retained for analysis of $\delta^{13}C$ and $\delta^{18}O$ in hydroxy-carbonate apatite. Due to constraints on the number of samples that could be analyzed, a subset of 13 samples was selected. Powder aliquots of 6 mg were weighed into 1.5mL microcentrifuge tubes. In order to oxidize organics in the dentin, 0.08 mL of 30% H_2O_2 was added for each milligram of dentin in the samples. Tubes were agitated and then left for 24 hours with the caps open to allow the escape of gasses produced in the reaction. Samples were then centrifuged for six minutes at 9000 rpm in an Eppendorf 5414 microcentrifuge. The supernatant was pipetted off, and samples were rinsed with 1 mL of ultrapure water five times. To remove adsorbed bicarbonate ions and any diagenetic carbonate that might be present, 0.08 mL of 1M buffered acetic acid was added for each milligram of dentin in the samples. Following agitation, samples were left for 24 hours with the caps open. The tubes were centrifuged and rinsed as before, then freeze-dried overnight. Subsamples of 1 mg were roasted under vacuum at 200° C to remove volatiles, then analyzed using a Finnegan Kiel-IV coupled to a Thermo MAT 253 isotope ratio mass spectrometer.

Approximately 10 mg (in some cases, less than 10 mg was available) of each block sample was weighed and placed in a baked (550° C overnight), acid-leached (1 M HCl Fisher TraceMetal grade) glass scintillation vial. To each sample, 3 mL of 0.5 M Fisher TraceMetal grade HCl was added and vials were placed in a refrigerator at 4° C for 36 hours. At the end of this period, 1 mL of each solution was pipetted off into a

1.5 mL metal-free microcentrifuge tube, then centrifuged for six minutes at 14,000 rpm. The solutions for elemental analysis were diluted with 1% HNO_3 (1 ppb In as an internal standard) to target between 6 and 13 ppm Ca. The diluted solutions were analyzed for concentrations of Mg, P, Ca, Mn, Fe, Zn, Sr, Ba, and Pb using a Finnigan MAT Element ICP-MS.

The collagenous blocks remaining after demineralization were rinsed five times with 10 mL of ultrapure water. In order to remove lipids from the blocks, 10 mL of 2:1 chloroform-methanol was added to each vial, and the vials were placed in an ultrasonicator for 30 minutes. The chloroform-methanol was discarded and samples were rinsed five times with 10 mL of ultrapure water. Samples were then freeze-dried and weighed. Sub-samples of 1.5 ± 0.1 mg were loaded into pressed silver capsules and analyzed for $\delta^{13}C$ and $\delta^{15}N$ at the Isotope Ratio Mass Spectrometry Laboratory, University of California, Santa Cruz.

Thin-sections were analyzed by first making scaled digital photomicrograph mosaics of transects corresponding to the mediolateral cut plane used to produce the sampling segments. Individual second-order increments were correlated among mosaics such that measurements made on multiple thin-sections could be assembled into a single series representing all increments present in the tusk. A plugin for ImageJ (Rasband, 1997-2008) was written which allowed boundaries between second order increments to be marked along a transect perpendicular to the lamination. The plugin outputs the thicknesses of second-order increments based on the locations of boundary points placed along the transect. Only those second-order increment

thicknesses that were measured in dentin centrally located between the cementum-dentin junction and the tusk axis were included in the final, complete series (with the exception of increments measured in the tip segment, some of which are only represented near the enamel-dentin junction).

In order to tie compositional samples to specific times in the elephant's life, the second-order increments present in each sample must be known. This was accomplished by digitally overlaying the thin section mosaics with marked and numbered second-order increments on the scanned images of the sampled segments (scanned prior to block sample removal) and identifying which increments were contained in the material removed for each sample.

Because an approximate date of death is known for this individual, and historical weather data are available for this area, this specimen allows for the examination of relationships among weather and tusk compositional data. If the second-order increments are formed with a seven day periodicity in African elephants (Codron, 2008 unpublished dissertation), determining the calendar days represented by each compositional sample should be relatively straightforward. However, as noted by Codron (2008, unpublished dissertation), there is some variation in the number of second-order increments counted per year. Rather than assume a seven day periodicity, we calculated the average second-order increment periodicity based on counts of third-order, daily increments. Measurements of third-order increments were taken at multiple locations in the dentin to determine the average daily growth.

This value was used to calculate the average number of days contained in second-order increments, which for this individual is close to nine (9.075).

Weather data for Hwange National Park Main Camp were obtained from the National Climatic Data Center (NOAA). The record is incomplete (~84% of days have entries), and the weather station is located 100km from the location at which the carcass was found, but rainfall and temperature patterns are likely similar enough to what the animal would have experienced to allow for comparison with tusk compositional data. From these data, mean daily precipitation and temperature values for the intervals of time represented in each compositional sample were calculated.

The data produced by these analyses include of measurements of $\delta^{13}C_{col}$,$\delta^{15}N_{col}$, and the ratios of Mg, P, Mn, Fe, Zn, Sr, Ba, and Pb to Ca for 33 serial dentin samples. Measurements of $\delta^{18}O$ and $\delta^{13}C$ are available for a subset of 13 samples spaced throughout the sample series. Furthermore, mean temperature and precipitation values were calculated for each sample. This is a relatively large data set, and potential relationships among variables might be difficult to discern simply by examining the series. Because the time of formation for each serial sample can be determined using growth increments, the data take the form of 13 time series with uneven sampling (i.e. the time between consecutive samples is variable), and methods used for analysis of time series can be employed to quantify relationships among variables.

One goal in analyzing these data is to identify correlations in the patterns among compositional measurements, and between compositional measurements and weather data. In order to assess these relationships, we chose to use sample cross-correlations. The sample cross-correlation is a normalized form of the sample cross-covariance. Sample cross-covariance is defined as

$$\hat{\gamma}_{xy}(h) = n^{-1} \sum_{t=1}^{n-h} (x_{t+h} - \bar{x})(y_t - \bar{y}),$$

where *x* and *y* are the two time series, and *h* is the lag. The cross-correlation is defined as

$$\hat{\rho}_{xy}(h) = \frac{\hat{\gamma}_{xy}(h)}{\sqrt{\hat{\gamma}_x(0)\hat{\gamma}_y(0)}},$$

where $\hat{\gamma}_x(0)$ and $\hat{\gamma}_y(0)$ are the sample autocovariances of series *x* and *y* at lag = 0 respectively (Shumway and Stoffer, 2006). Cross-correlation varies between -1 and 1 and provides a measure of similarity or dissimilarity between two time series at a series of lags or time offsets. The inclusion of lag is important for the analyses of these series, because there is no expectation that a variable such as $\delta^{13}C_{col}$ will respond instantaneously to a presumed causative factor such as precipitation, and the response times of different variables may differ due to, for example, body reservoir effects.

In order to deal with the problem of uneven sampling (time between consecutive samples is not equal for all consecutive pairs), the series were spline interpolated (R Development Core Team, 2008) to weekly sample resolution.

Cross-correlation requires two stationary series (Shumway and Stoffer, 2006), and some of the spline-interpolated tusk data series do not fulfill this requirement. Stationarity was determined using the Kwiatkowski-Phillips-Schmidt-Shin (KPSS) test (Trapletti and Hornik, 2009). Non-stationary series were detrended by taking the residuals from a cubic spline (4 d.f.) fit to the series (R Development Core Team, 2008).

To simplify the representation of cross-correlation results, only the maximum and minimum significant correlations (searching lags -70 to +70 weeks) are reported for each time series pair. Furthermore, values are reported only if this maximum or minimum significant correlation occurred with a lag between -6 and +6. This restriction means that, in almost all cases, only a single positive or negative correlation is reported. As an example, if two sinusoidal series (period = 52 weeks) sampled at weekly intervals with no phase offset were processed, maximum correlations would occur at lag = 0 and lag = +/- 52. Minimum (the most negative) correlations would occur at lags +/- 26. Using the system described above, only the maximum correlation at lag = 0 would be reported. If these two series were a weather measure and a compositional measure that might be affected by weather, one could argue that this correlation at lag = 0 is the appropriate value to report.

The significance of correlations was determined using a bootstrapping method in which a distribution of correlations for each pair of compositional series was

produced by cross-correlation of one sample series with 1000 series created by random sampling (with replacement) of the other series. Resampled series were equal in length to the original (i.e., not spline interpolated) series. The resampled series were then spline interpolated to weekly resolution and detrended (if non-stationary) prior to cross-correlation with the spline-interpolated, detrended (if non-stationary) sample series. Because there are slight differences in the bootstrap-derived p-values (but not the magnitudes of the correlations themselves) depending on which of the two series was resampled, results from both possibilities are reported. Correlations with p-values less than 0.025 are considered significant. In addition, correlations that are significant with Bonferroni correction (p-values less than 0.025 divided by the number of pairwise comparisons) are underlined.

Second-order increment thicknesses were also included in the cross-correlation analysis. In order to produce a series of the same temporal resolution and number of data points as the compositional series, a series of means of the second-order increment thicknesses of increments contained within each compositional sample was used.

Results

Compositional Data

The results of stable isotope analysis of collagen and carbonate hydroxyapatite are shown in Table 3.2, while elemental ratios are shown in Table 3.3. In Figure 3.7, isotope values are plotted as series along with precipitation and temperature data.

$\delta^{13}C_{col}$ values range from -21.7 to -16.3 ‰ with a mean of -19.45 ‰, while $\delta^{13}C_{carb}$ values range from -15.5 to -7.3 ‰ with a mean of -12.28 ‰. The mean offset between $\delta^{13}C_{col}$ and $\delta^{13}C_{carb}$ is 7.0 ‰, and the offset increases through time (positive slope in least squares regression, $p = 0.03$). $\delta^{15}N_{col}$ ranges from 10.5 to 14.1 ‰ with a mean of 12.1 ‰, while $\delta^{18}O_{carb}$ ranges from -2.0 to 4.5 ‰ with a mean of 1.4 ‰.

The most obvious seasonal-scale variation appears in $\delta^{13}C_{col}$ (Fig. 3.7B) which shows a pattern in which high $\delta^{13}C_{col}$ is associated with high precipitation and temperature in the warm wet season. To evaluate the associations statistically, the cross-correlation between the $\delta^{13}C_{col}$ series and the precipitation series was calculated. Figure 3.8A shows the sample cross-correlation. A positive lag *h* implies that series 1 ($\delta^{13}C_{col}$) has been shifted such that the sample at *t*+*h* is compared with the sample at *t* in series 2 (precipitation). The maximum positive cross-correlation between $\delta^{13}C_{col}$ and precipitation is 0.38 ($p < 0.025$), and it occurs at a lag of 0 (Fig. 3.8A, Table 3.4) implying that there is no delay between the series. However, the peak in correlation values near lag = 0 is broad; thus, support is roughly equivalent for hypotheses of an offset in the response of $\delta^{13}C_{col}$ to precipitation of between 0 and +/- 3 weeks. The large negative peak in the cross-correlation that occurs centered on a lag of +24 results from the alignment of more positive $\delta^{13}C_{col}$ values in the series with dry season low precipitation values (Fig. 3.8A). This result is expected given that the time series are shifted to an offset of almost six months. Following the same procedure, but comparing $\delta^{13}C_{col}$ to temperature, reveals a stronger correlation (0.60, $p < 0.025$) at a lag of +3 (Fig. 3.8B, Table 3.4) showing that high $\delta^{13}C_{col}$ values occur just after high temperature values.

The pattern observed in $\delta^{15}N_{col}$ is more complicated, including an early phase of high, non-seasonally variable values followed by lower, seasonally variable values, and finally a short excursion to higher values prior to death (Fig. 3.7A). When detrended (spline, d.f. = 4) (Fig. 3.9A), $\delta^{15}N_{col}$ values are negatively correlated with precipitation; a maximum negative correlation of -0.50 ($p < 0.025$) occurs at a lag of 0 (Fig. 3.9B, Table 3.4). $\delta^{15}N_{col}$ is also positively correlated with second order increment thickness (lag = -1) (Table 3.4).

The cross-correlation of $\delta^{15}N_{col}$ and temperature (Fig. 3.9C) shows a pattern in which three similar peaks in negative correlation occur at spacings of 50 and 52 weeks. This result highlights the regular periodicity of both series. The absolute values of peak correlations increase at higher lags because the aseasonal early portion of the $\delta^{15}N_{col}$ series is increasingly excluded from the calculation as lag values increase.

Due to the relatively sparse sampling of $\delta^{13}C_{carb}$ and $\delta^{18}O_{carb}$, analyses of these series may lead to spurious results. Ideally, additional samples should be analyzed. However, for completeness, we report the significant correlations here. The spline interpolated, detrended $\delta^{13}C_{carb}$ series shows significant positive correlations with $\delta^{13}C_{col}$ (0.69, lag = 0), precipitation (0.53, lag = +5), and temperature (0.65, lag = +5). The spline interpolated, detrended $\delta^{18}O$ series shows significant negative correlations with $\delta^{13}C_{col}$ (-0.50, lag = +1), $\delta^{15}N_{col}$ (-0.47, lag = -1), and $\delta^{13}C_{carb}$ (-0.42, lag = +2).

Mg, Sr, Ba, P, and Zn concentrations were above detection limits for all samples, while Mn was above detection limits for most samples (Table 3.3). Pb and Fe were below detection limits for most samples. Although low concentrations of these

elements were present, dilution of the samples was required to get the Ca concentration into an acceptable range, and this reduced the concentration of some elements below detection limits. Samples 1 and 2 have unusually low Mg/Ca and P/Ca as well as high Mn/Ca, Ba/Ca, and Fe/Ca. Sample 33 also has low Mg/Ca and lower than expected (based on the previous 10 samples) P/Ca. The pattern of increased Mn, Ba, and Fe exhibited by samples 1 and 2 is consistent with the diagenetic alteration of this more exposed dentin near the exterior surface of the tip of the tusk (Kohn et al., 1999). The low Mg in samples 1, 2, and 33 is also consistent with diagenetic alteration (Hola et al., 2008). Thus, these samples have been excluded from the plotted data (Fig. 3.10).

As a simple test for the presence of trends over the life of the animal (ontogenetic trends), least squares regressions of elemental ratios (and δ values) on time were conducted (excluding samples 1, 2 and 33 for elemental ratios). Significant slopes are present in $\delta^{15}N$ ($R^2 = 0.13$, $p = 0.021$), Mg/Ca ($R^2 = 0.83$, $p < 0.001$), P/Ca ($R^2 = 0.46$, $p < 0.001$) , and Fe/Ca ($R^2 = 0.80$, $p = 0.003$) with that of $\delta^{15}N$ being negative, while those of Mg/Ca, P/Ca, and Fe/Ca are positive. No other variables had significant slopes.

The relationships among elemental ratios, stable isotope ratios and weather data, excluding those samples apparently affected by diagenesis, are summarized in Table 3.5. Only the significant ($p < 0.025$) maximum/minimum correlations with lags between -6 and +6 are shown. Non-stationary series were detrended as described in the Materials and Methods section and are marked with asterisks. Correlations

between δ values and weather variables are described above for the full series (Table 3.4), and results for the restricted series are generally similar (Table 3.5).

Several elemental ratios are significantly correlated with the precipitation series. Mg/Ca, P/Ca, and Ba/Ca are positively correlated with precipitation (0.42, 0.48, and 0.47 respectively). There are also correlations of interest among other variables. Mg/Ca shows positive correlations with Sr/Ca (0.70, lag = +3) and P/Ca (0.81, lag = -1), and a negative correlation with $\delta^{15}N$ (-0.51, lag = -2). This suggests that in addition to their response to ontogeny, which has been removed by detrending, Mg/Ca, P/Ca, and $\delta^{15}N$ might be covarying on shorter time scales due to a common causative factor. Ba/Ca is positively correlated with $\delta^{13}C_{col}$ (0.44, lag = +1) and negatively correlated with $\delta^{18}O_{carb}$ (-0.57, lag = -2).

Growth Increments

A total of 142 second-order increments were identified in the dentin of this tusk. The periodicity of these features appears to be close to nine days as discussed above. The mean second-order increment thickness is 0.118 mm with a standard deviation of 0.040 indicating annual dentin accretion on the order of 5 mm. There is a significant ($p < 0.001$), but weak ($r^2 = 0.08$) trend toward greater thicknesses later in life (positive slope in least squares regression on time). Seasonal-scale variation in growth increment thicknesses occurs, but this pattern is apparent only in the latter half of the time represented in the tusk (Fig. 3.11). Cross-correlations (Tables 3.4, 3.5) reveal no significant association with precipitation or temperature. However, there is a positive

correlation with $\delta^{15}N_{col}$ with a lag of -1 weeks (Table 3.4) implying, for example, that peaks in tusk growth occur one week before the peaks in $\delta^{15}N_{col}$. In addition there is a negative correlation with Mn/Ca (lag = -1) (Table 3.5).

The darker (in reflected light) bands of dentin that are parts of the dark-light couplets of first-order, annual increments are formed during the mid to late dry season (and just into the rainy season; e.g., samples 22–25 representing ~408 to 299 days before death). Correspondingly, the lighter bands are formed in the rainy season and early dry season. Second-order increments in the darker band described above decrease in thickness through the band and continue this decline in the first sample of the light band (Fig. 3.11). Following this, they begin to increase.

Discussion

Diagenesis

Samples 1, 2, and 33 representing 1275, 1234, and 14 days before death are suspected as diagentically altered samples. Mg/Ca and P/Ca are low in these samples, and samples 1 and 2 also have high Mn/Ca, Ba/Ca, and Fe/Ca (Table 3.3). The low Mg/Ca and P/Ca probably result from the same process, namely preferential loss of Mg substituted hydroxyapatite. Hola et al. (2008) observed rapid Mg loss in a series of 2- to 25-year-old of fish scale samples recovered from lake sediments in the Czech Republic, and they warned that paleodietary interpretations based on Mg may be problematic with bones only one or two years old. The dentin samples that show Mg loss are those located on or near exposed surfaces of dentin (the tusk tip and pulp

cavity), which apparently allowed for their rapid diagenesis, as the carcass of this elephant was exposed for less than one year. However, the time during which tusk diagenesis can take place may not be restricted to the post-mortem. The tip of the tusk may begin to undergo alteration even during the life of an elephant, which perhaps explains why the tip samples show other signs (high Mn/Ca, Ba/Ca, and Fe/Ca) of diagenesis that are absent in the pulp cavity sample (Table 3.3).

The elevated Mn/Ca, Ba/Ca and Fe/Ca observed in samples 1 and 2 follows a pattern of diagenesis noted by Kohn et al. (1999). They measured the concentrations of a large set of elements in modern enamel and fossil dentin and enamel and found Mn and Fe concentrations several orders of magnitude greater in fossil dentin than in modern enamel. Ba concentrations were also higher in fossil dentin than in modern or fossil enamel. Furthermore, Kohn et al. (1999) noted staining of fossil teeth presumably caused by Fe- and Mn-oxides or oxyhydroxides. The outer portion of dentin at the tip of the tusk is the only area of dentin staining in the tusk.

Depletion in Mg/Ca and P/Ca suggests diagenetic alteration of the pulp cavity sample. Although this probably represents diagenetic Mg loss, it is possible that this is a primary signal. The most likely cause of death for this elephant was nutritional/water stress. If body Mg levels were low due to starvation, this might explain the low Mg/Ca (and P/Ca) observed in this sample. Hypomagnesemia is a condition that has a relatively high incidence in humans with eating disorders (Hall et al. 1988), but in this case, it is difficult to determine whether the low values represent the effects of diagenesis, hypomagnesemia, or some other factor.

Stable Isotopes

$\delta^{13}C$

The positive correlations between $\delta^{13}C_{col}$ and precipitation (0.39, lag = 0) and temperature (0.58, lag = +2) (Table 3.4) support the hypothesis of seasonal shifts to higher proportions of C_4 plants in the diet during the rainy season(Figs. 3.7B, D). This corroborates Williamson's (1975) observations that grass intake was higher during the rainy season. As death is known to have occurred in the late dry season and relatively low $\delta^{13}C_{col}$ values occur before death, one can also infer that the relatively more negative $\delta^{13}C_{col}$ values in each cycle represent the early to mid dry season.

Despite the possible complications anticipated for assessing the $\delta^{13}C$ patterns in a nursing juvenile, both $\delta^{13}C_{col}$ and $\delta^{13}C_{carb}$ show fairly regular seasonal variation consistent with known seasonal dietary shifts in adults.

In the last sample, representing the few weeks prior to death, $\delta^{13}C$ in carbonate and collagen is higher than previous values. It seems unlikely that this increase is attributable to increased C_4 plant intake as this dentin formed in the dry season. Some studies (e.g., Rau et al., 1983) have reported trophic-level effects in $\delta^{13}C$ in which animals feeding at higher trophic levels showed some enrichment in ^{13}C. It is possible that, in a manner similar to $\delta^{15}N$ (Hobson et al. 1993), $\delta^{13}C$ of collagen could show enrichment in an animal that was under severe nutritional stress (catabolizing proteins). Under moderate nutritional stress, one might expect $\delta^{13}C$ to decrease due to the use of stored lipids, which are depleted in ^{13}C, to meet needs for energy and

protein synthesis (Williams et al., 2007). However, under conditions of prolonged starvation, a threshold is reached after which so called "phase III" starvation begins (Goodman et al. 1980). In this phase of starvation, the importance of lipids is diminished, and protein catabolism increases (Goodman et al. 1980). Given that this elephant had lived through two drought years, it might be expected that its lipid stores were already in a poor state. In the few weeks prior to its death, this elephant may have been in phase III starvation.

The long term trend in the offset between $\delta^{13}C_{carb}$ and $\delta^{13}C_{col}$ might also record changes in the importance of milk in the diet. The expected offset between $\delta^{13}C_{carb}$ and $\delta^{13}C_{col}$ for an herbivore has been stated as about 9 ‰ (Fisher and Fox, 2003; based on data from Cerling and Harris, 1999, and Sullivan and Krueger, 1981) and about 6.8 (Lee-Thorp et al. 1989), some of the difference observed may be attributable to different apatite pretreatment methods (this dissertation Chapter 2). The pretreatment used in this study is most similar to that used by Cerling and Harris (1999), thus, the value of 9 ‰ will be used in this discussion. Based on this reference value, the observed offset for this individual (mean = 6.97 ‰, Table 3.2) is lower than expected in all samples with the exception of the last sample in the series (11.8 ‰ difference) (Table 3.2). As the two $\delta^{13}C$ measurements provide information about different parts of the diet ($\delta^{13}C_{col}$ mostly dependant on protein composition and $\delta^{13}C_{carb}$ reflecting bulk diet composition (Ambrose and Norr, 1993)), this below-average offset suggests several possibilities: (1) The protein source is enriched in ^{13}C leading to higher $\delta^{13}C_{col}$; (2) the energy source is depleted in ^{13}C leading to lower $\delta^{13}C_{carb}$; (3) both

1 and 2. Data on cattle from Wilson et al. (1988) show that casein is enriched in ^{13}C relative to diet, and that milk fat and lactose are depleted in ^{13}C relative to diet. If these patterns hold for elephants, this fits well with scenario 3 above, given that this individual is presumed to be feeding on milk and vegetation. Furthermore, the increasing offset through time may be related to decreasing milk intake. York et al. (2008), working with the teeth of Stellar sea lions, found that the $\delta^{13}C_{carb}$ of dentin formed in the first year of life when pups were nursing was depleted in ^{13}C (0.9 ‰) relative to dentin formed after weaning. Presumably, the more negative values they observed in the first year are associated with intake of ^{13}C-depleted milk fat (Hobson and Sease, 1998). This supports the hypothesis that at least $\delta^{13}C_{carb}$ is affected by changes in milk intake.

The offset between $\delta^{13}C_{col}$ and $\delta^{13}C_{carb}$ is 11.8 ‰ in the sample representing the last-formed dentin. As the $\delta^{13}C_{col}$ value is not unusually low, this large offset can be attributed to the unusually high $\delta^{13}C_{carb}$ value. This high value may represent diagenetic alteration near the pulp cavity surface, and the low Mg/Ca and P/Ca for this sample lend support to that hypothesis. Interestingly, the $\delta^{18}O_{carb}$ of this sample does not appear unusual. This apparent diagenesis affecting only $\delta^{13}C_{carb}$ has been previously noted (e.g., Koch, 1989 dissertation), but the phenomenon remains unexplained.

$\delta^{15}N$

It was hypothesized that $\delta^{15}N$ would be high in the earlier-formed dentin, as the individual would be more dependent on milk during this time. Indeed, dentin $\delta^{15}N$ values are highest in the first year recorded in the tusk, but are only about 1 ‰ more positive than later annual peak values (Fig. 3.7A) No long-term decline in $\delta^{15}N$ is apparent after the about 1.5 years.

It seems likely that these early, elevated values and the lack of seasonality in early $\delta^{15}N_{col}$ represent a time of higher relative intake of milk than occurs later in life. The lack of any decline after the first 1.5 years recorded in the tusk suggests either that further long-term (i.e. not seasonal) changes in the contribution of milk protein to total dietary protein intake were minimal, or that, after reaching about 1.5 years of age, the milk/vegetation protein ratio was sufficiently low that further long-term decreases in the proportion of milk protein had little effect on collagen $\delta^{15}N$. Although the relative contributions of milk versus plant protein to juvenile elephant diet are unknown, data on time spent feeding on vegetation provide some information. By the age of 10 to 12 months, elephant calves spend about 40 % of daily time feeding on vegetation (Lee and Moss, 1986). This increases further to about 55 % at ~ 24 months at which time calves are considered nutritionally self-sufficient (though nursing typically continues for at least another 1.5 years)(Lee and Moss, 1986). Thus, it seems possible that the relative intake of milk protein in this individual was sufficiently low after 1.5 years that its effect on collagen $\delta^{15}N$ was minimal. However, it is also possible that, following the first year, the relative importance of milk in the diet fluctuated seasonally with no apparent, underlying, long-term trends.

The detrended $\delta^{15}N$ series also shows seasonal variation (Fig. 3.9), in which high values are generally associated with the dry season, and lows with the rainy season. The pattern of $\delta^{15}N$ values exhibited in the tusk of this juvenile differs from the data presented by Cerling et al. (2009) in that $\delta^{15}N_{col}$ peaks generally occur offset from $\delta^{13}C_{col}$ peaks rather than in-phase with them, and low $\delta^{15}N_{col}$ occurs during the rainy season rather than high $\delta^{15}N_{col}$ in the rainy season. It is possible that the elephants in the Shabi Shabi area of HNP that congregate at overgrazed seeps during dry seasons experience greater nutritional stress than those in northern Kenya or Kruger National Park leading to high values during the dry season.

Alternatively, the lack of an in-phase relationship between $\delta^{15}N_{col}$ and $\delta^{13}C_{col}$ might be a phenomenon specific to juveniles. If the relative intake of milk were seasonally variable, such that relative intake was higher in the dry season, this might explain the occurrence of higher $\delta^{15}N_{col}$ during this time. The negative correlation between detrended Mg/Ca (which might be lower when feeding on milk) and detrended $\delta^{15}N_{col}$ (which might be higher when feeding on milk) lends some support to this hypothesis (Table 3.5), although other factors could also produce seasonal Mg/Ca fluctuations.

As occurs in $\delta^{13}C$, $\delta^{15}N_{col}$ shows increases in the weeks prior to the death of this elephant (Fig. 3.7A). $\delta^{15}N_{col}$ of the last dentin sample is higher than any values in the previous ~2.5 years. This elevated value probably reflects enrichment in ^{15}N caused by severe nutritional stress and the catabolization of body proteins (Hobson et al. 1993).

$\delta^{18}O$

It was hypothesized that $\delta^{18}O_{carb}$ would be higher in the dry season due to ingestion of evaporatively ^{18}O-enriched waters during this time. While $\delta^{18}O_{carb}$ is negatively correlated with $\delta^{13}C_{col}$ (Table 3.4), suggesting that $\delta^{18}O_{carb}$ might be higher during the dry season, there is no significant correlation with precipitation or temperature. Analyzing additional samples might help with interpretation, but there does not seem to be a seasonal pattern in $\delta^{18}O_{carb}$.

Elemental Ratios

Mg/Ca, P/Ca, and Sr/Ca

Mg/Ca and P/Ca show increasing, long-term trends in the tusk of this individual (Fig. 3.10). The high correlation between Mg/Ca and P/Ca (Table 3.5) is expected because increased substitutions of Mg for Ca in the hydroxyapatite lattice will cause increases in both Mg/Ca and P/Ca. The majority of variation in P/Ca is attributable to variation in Mg/Ca (least squares regression on all data: $r^2 = 0.85$, $p < 0.001$); thus, interpretation is focused on the Mg/Ca series.

It was hypothesized that Mg/Ca might be lower when dependence on milk was high, due to the low Mg/Ca of milk compared with vegetation. It seems plausible that the increasing Mg/Ca in the tusk data series might represent the increasing contribution of plant Mg to the diet of this juvenile. Furthermore, Mg/Ca indicates that there may be seasonal variation in the importance of milk in the diet as detrended Mg/Ca is negatively correlated with detrended $\delta^{15}N$ (Table 3.5).

While detrended Mg/Ca is negatively correlated with detrended $\delta^{15}N_{col}$, detrended Mg/Ca is positively correlated with detrended Sr/Ca. This further supports the hypothesis that Mg/Ca fluctuations might be related to fluctuating milk intake. As with Mg/Ca, the Sr/Ca of milk is generally low, while the Sr/Ca of plant foods is high (reviewed by Sillen and Kavanagh, 1982). Thus, a high milk intake could lead to high $\delta^{15}N_{col}$, and low Mg/Ca and Sr/Ca. Complications associated with the use of Sr/Ca to identify milk intake derive from the fact that in human infants, gastro-intestinal discrimination against Sr is lower than that which occurs in adults (Sillen and Kavanagh, 1982). Increasing Sr discrimination occurring with increasing Sr intake from plant foods might result in a damped or even reversed long-term trend (perhaps this accounts for the lack of a long-term trend in Sr/Ca). However, variation on the shorter, seasonal time scales being discussed might still be evident.

The variation in Sr/Ca and Mg/Ca could also be due to variation in non-milk dietary sources or other factors. For example, if rainy season (when $\delta^{15}N_{col}$ is low) forage has higher Mg/Ca and Sr/Ca than dry season forage, or if soils in the areas in which elephants feed during the rainy season have higher Mg/Ca and Sr/Ca than areas frequented in the dry season, the seasonal-scale shifts in dentin might be associated with these differences.

There is also some evidence that calcium deficiency (reviewed in Sillen and Kavanagh, 1982) and starvation (Taylor et al., 1962) can cause increased relative absorption of Sr. As the Ca content of browse exceeds that of grass (Sillen, 1988), one might expect any calcium deficiency, and associated higher relative Sr absorption, if it

were to occur, would occur in the rainy season. Nutritional stress, on the other hand, is more likely to occur in the dry season. Thus, based on the positive correlation between detrended Mg/Ca and detrended Sr/Ca, and the negative correlation between detrended Mg/Ca and detrended $\delta^{15}N_{col}$, the data could support a hypothesis of calcium deficiency during the rainy season. However, Sr/Ca itself is not significantly correlated with precipitation or temperature (Table 3.5).

Zn/Ca

It was hypothesized that if the tusk began to develop before (or very near) the time of birth, a period of high Zn/Ca might mark the late gestation/neonatal period. There is no neonatal line evident in the dentin, and no period of unusually high Zn/Ca in the tusk record, both suggesting that tusk formation began after birth.

No regular patterns appear in the Zn/Ca series (Fig. 3.10D), but there is a positive correlation with Mg/Ca (lag = -1) (Table 3.5). This correlation is difficult to interpret.

Fe/Ca

After removal of apparently diagenetically altered samples, Fe/Ca appears to increase through the life of this individual; however, as Fe was below detection for many samples, this apparent increase is based on only seven values. Furthermore, only one value represents dentin accreted in the last ~2 years of life. However, it is worth mentioning possible causative factors for trends in Fe/Ca.

If the increasing trend reflects a pattern in the calf's Fe status, it may be related to milk intake. In humans, the concentration of Fe in milk is low (though bioavailability is high), and infants use Fe reserves accumulated during gestation for most red blood cell synthesis (Dewey et al., 1998). As the relative importance of milk in the diet of elephants decreases with age, increasing Fe levels may be associated with this pattern. Although there has been little work on temporal trends in the Fe content of mineralized tissues, in a study of elemental concentrations in the tusk dentin of a dugong, Edmonds et al. (1997) observed a marked increase in the Fe (and Mg) concentration in the first few years of life that may be due to the factors described above.

Ba/Ca

Ba/Ca exhibits a positive correlation with $\delta^{13}C_{col}$ and a negative correlation with $\delta^{18}O_{carb}$, indicating higher intake or absorption when C_4 plants are being consumed. Ba generally behaves in a similar manner to Sr, with discrimination against Ba occurring during absorption, increased relative absorption occurring associated with starvation, and less discrimination occurring in young individuals (Taylor et al., 1962). Given this similar behavior, it is of interest that Ba/Ca is positively correlated with $\delta^{13}C_{col}$ while Sr/Ca is negatively correlated with $\delta^{13}C_{col}$. This may reflect different soil Ba/Sr in rainy season feeding areas as compared to dry season feeding areas, but no further data is available to evaluate this hypothesis.

Growth Increments

Growth increment thicknesses in tusks are expected to be dependent on nutritional status (Fisher, 1996). McCullagh (1969) found that the ratio of hydroxyproline to creatinine in the urine of elephants in Uganda was lower during the dry season than during the rainy season, indicating a period of slower growth in the dry season. Thus, one would expect the thickness of dentin growth increments to be less during the dry season. There is no significant correlation between detrended increment thickness and precipitation (Table 3.4). However, the positive correlation with detrended $\delta^{15}N_{col}$ (Table 3.4) suggests that the thickness of increments does vary in connection with changes in diet or physiology. Unexpectedly, thicker increments occur in the dry season when elevated $\delta^{15}N_{col}$ seemed to suggest either increased nutritional stress or increased milk intake (associated with low plant food availability) (Figs. 3.7A and E, 3.11). It is not clear what might lead to higher tusk growth rates in the dry season. Further studies on the tusks of adults from this area might help to clarify the issue.

Consistent with the patterns noted by Koch et al. (1989), darker bands of dentin that form parts of first-order increments are associated with decreasing tusk growth rate (in the last two years of life) in seasons associated with nutritional stress (i.e. winter or dry season) (Figs. 3.7E, 3.11) . However, in this case, some dark, slow-growth dentin also forms in the early rainy season (Fig. 3.7E). Presumably, this represents some delay in the recovery from nutritional stress encountered during the dry season.

Conclusions

Tusks can provide an excellent record of life history through serial compositional analyses, though the dependence of compositional variables on multiple factors complicates interpretation. In an effort to maximize interpretability and asses the cumulative support for various hypotheses, we have analyzed a set of compositional measures including $\delta^{13}C_{col}$, $\delta^{15}N_{col}$, $\delta^{18}O_{carb}$, $\delta^{13}C_{carb}$, Mg/Ca, Mn/Ca, Fe/Ca, Zn/Ca, Sr/Ca, Ba/Ca, and Pb/Ca for each sample. Results show that diagenesis, ontogentic trends, seasonal patterns, and signs of starvation are detectable.

Seasonal patterns with correlations to weather data are apparent in $\delta^{13}C_{col}$, $\delta^{13}C_{carb}$, and $\delta^{15}N_{col}$, $\delta^{18}O_{carb}$, Mg/Ca, P/Ca, and Ba/Ca. $\delta^{13}C$ values are highest in the warm rainy season during which C_4 grasses are known to make up a larger proportion of elephant diet in HNP. $\delta^{15}N_{col}$ is negatively correlated with precipitation indicating one or more of the following: 1) nutritional stress during the dry season, 2) differences in the $\delta^{15}N$ of rainy season versus dry season plant diet, 3) differences in the protein biological value of rainy season versus dry season plant diet, or 4) seasonal patterns in the relative importance of milk in the diet.

Long-term trends are present in $\delta^{15}N_{col}$, Mg/Ca, and P/Ca. It is hypothesized that these trends result from decreasing importance of milk in the diet as the animal is gradually weaned. Elevated $\delta^{15}N_{col}$ has been observed in juvenile mammoths thought to be feeding on milk (Rountrey et al., 2007), and this study further corroborates the hypothesis that $\delta^{15}N_{col}$ is elevated when dependence on milk is high. To our knowledge, Mg/Ca has not been used previously to identify nursing/weaning.

Controlled experiments are necessary to determine if Mg/Ca in dentin is, in fact, related to milk intake. However, even if controlled experiments reveal that Mg/Ca can be used as a proxy for milk intake, the rapid loss of Mg during diagenesis might limit its applicability.

In addition to the long-term increase in Mg/Ca, detrended Mg/Ca is also negatively correlated with detrended $\delta^{15}N$ and positively correlated with detrended Sr/Ca. Because Mg/Ca and Sr/Ca are lower in milk than in plants, and because elevated $\delta^{15}N_{col}$ is expected in a nursing juvenile, this pattern may indicate seasonal scale fluctuations in the relative importance of milk in the diet.

Ba/Ca is positively correlated with $\delta^{13}C_{col}$ while Sr/Ca is negatively correlated with $\delta^{13}C_{col.}$ Given that Ba and Sr are expected to behave similarly with respect to their absorption, it is hypothesized that soil, and therefore plant, Ba/Sr differs in rainy season versus dry season foraging areas.

Diagenesis of samples on exposed surfaces is indicated by low Mg/Ca and P/Ca, high Mn/Ca, Fe/Ca, and Ba/Ca, and possibly by high $\delta^{13}C_{carb}$. The fact that Mg/Ca and Ba/Ca, two values of interest for paleodietary analyses, appear altered by exposure of less than one year suggests that care should be taken when making interpretations based on these measures. Analysis of a series of samples from locations with high to low probability of diagenesis (e.g., outer surface to interior) may provide some means of assessing the degree to which mineralized tissue has been altered in cases where homogenization has not occurred.

Second-order growth increments show apparent seasonal patterns in the second half of life, with growth rate being unexpectedly lower in the rainy season. Furthermore, growth increment thickness is positively correlated with $\delta^{15}N_{col}$. This pattern is difficult to explain, and further work on the tusks of adult elephants is needed.

While this study provides much needed reference information on the composition and patterns of change in composition in the tusk of a juvenile elephant, it also highlights the difficulties associated with interpreting stable isotope and elemental concentration data in nursing juveniles. The complexities that result from the animals having two nutrient sources (milk and vegetation) and the possibility of variable relative importance in diet allow for many possible interpretations of the same patterns. The inclusion of multiple proxies can aid in the accuracy of life history interpretations by allowing cumulative support for competing hypotheses to be evaluated. In the case of this elephant, multiple factors ($\delta^{15}N_{col}$, Mg/Ca, and Sr/Ca) all support a hypothesis of seasonally fluctuating relative importance of milk in the diet.

Because of differences in climate and vegetation structure (such as the very low abundance of C_4 vegetation in the arctic) some of these results cannot serve as direct references for data from juvenile, arctic mammoths. However, patterns apparently resulting from declines in milk intake are likely to be similar in mammoths. In addition, the elemental ratios observed in this tusk can also serve as baselines for detecting diagenetic alteration in mammoth tusks. Data from additional juvenile elephants, particularly from those that have been under observation, as well as data from adults,

will likely lead to the establishment of a more robust characterization of the factors leading to compositional variation in tusks.

Table 3.1. Circumference of tusk taken at measured distances from the tusk tip.

Distance from tip (cm)	Circumference (cm)
1	4.1
5	7.4
10	9.2
15	10.5
20	10.5
25	11.1
28	11.1
30	11.5
32	12.5
35	12.2
40	11.6

Table 3.2. Results from stable isotope analyses. All $\delta^{13}C$ and $\delta^{18}O$ values are relative to VPDB. $\delta^{15}N$ values are relative to AIR. C/N is the molar ratio of carbon to nitrogen in the collagen samples. Errors on measurement are 1σ based on standards that ran with the samples. Isotope data are plotted in Figures 3.7A, B, C, and D.

Sample	Days before death	$\delta^{13}C_{col}$	$\delta^{15}N_{col}$	$\delta^{18}O_{carb}$	$\delta^{13}C_{carb}$	C/N_{col}	$\delta^{13}C_{carb}$ - $\delta^{13}C_{col}$
1	-1275	-20.11 ± 0.09	13.00 ± 0.06			3.21 ± 0.02	
2	-1234	-20.46 ± 0.09	13.07 ± 0.06	1.39 ± 0.05	-12.85 ± 0.02	3.20 ± 0.02	7.61 ± 0.09
3	-1189	-19.91 ± 0.09	13.31 ± 0.06			3.20 ± 0.02	
4	-1134	-19.30 ± 0.09	13.35 ± 0.06			3.18 ± 0.02	
5	-1075	-18.68 ± 0.09	14.14 ± 0.06	-0.85 ± 0.05	-14.33 ± 0.02	3.18 ± 0.02	4.35 ± 0.09
6	-1035	-18.58 ± 0.09	13.22 ± 0.06			3.18 ± 0.02	
7	-1003	-18.40 ± 0.09	11.65 ± 0.06	1.62 ± 0.05	-12.20 ± 0.02	3.17 ± 0.02	6.19 ± 0.09
8	-962	-17.37 ± 0.09	12.04 ± 0.06			3.17 ± 0.02	
9	-926	-16.34 ± 0.09	12.57 ± 0.06	-1.98 ± 0.05	-10.66 ± 0.02	3.18 ± 0.02	5.67 ± 0.09
10	-903	-18.95 ± 0.09	12.40 ± 0.06			3.17 ± 0.02	
11	-867	-21.31 ± 0.09	11.72 ± 0.06			3.18 ± 0.02	
12	-808	-21.72 ± 0.09	11.90 ± 0.06	4.14 ± 0.05	-15.47 ± 0.02	3.18 ± 0.02	6.25 ± 0.09
13	-767	-21.65 ± 0.09	11.61 ± 0.06			3.19 ± 0.02	
14	-731	-21.24 ± 0.09	11.76 ± 0.06			3.17 ± 0.02	
15	-699	-19.96 ± 0.09	11.99 ± 0.06	0.81 ± 0.05	-13.97 ± 0.02	3.16 ± 0.02	5.99 ± 0.09
16	-658	-20.27 ± 0.09	10.84 ± 0.06			3.18 ± 0.02	
17	-603	-19.08 ± 0.09	10.53 ± 0.06			3.18 ± 0.02	
18	-535	-18.56 ± 0.09	11.02 ± 0.06	2.67 ± 0.05	-11.98 ± 0.02	3.17 ± 0.02	6.58 ± 0.09
19	-499	-18.68 ± 0.09	11.65 ± 0.06			3.18 ± 0.02	
20	-467	-19.76 ± 0.09	12.03 ± 0.06			3.18 ± 0.02	
21	-436	-20.34 ± 0.09	12.14 ± 0.06			3.19 ± 0.02	
22	-408	-20.23 ± 0.09	12.52 ± 0.06	0.10 ± 0.05	-13.86 ± 0.02	3.17 ± 0.02	6.37 ± 0.09
23	-381	-20.10 0.09	12.13 0.06			3.18 0.02	
24	-345	-19.68 ± 0.09	12.00 ± 0.06			3.17 ± 0.02	
25	-299	-19.37 ± 0.09	10.79 ± 0.06			3.16 ± 0.02	
26	-245	-19.10 ± 0.09	10.60 ± 0.06	3.61 ± 0.05	-11.22 ± 0.02	3.20 ± 0.02	7.88 ± 0.09
27	-191	-17.53 ± 0.09	11.66 ± 0.06			3.17 ± 0.02	
28	-150	-17.04 ± 0.09	12.01 ± 0.06	-0.47 ± 0.05	-9.52 ± 0.02	3.19 ± 0.02	7.51 ± 0.09
29	-113	-18.21 ± 0.09	12.39 ± 0.06			3.16 ± 0.02	
30	-86	-20.07 ± 0.09	11.91 ± 0.06	3.66 ± 0.05	-13.11 ± 0.02	3.17 ± 0.02	6.96 ± 0.09
31	-64	-20.53 ± 0.09	12.21 ± 0.06	4.46 ± 0.05	-13.10 ± 0.02	3.15 ± 0.02	7.43 ± 0.09
32	-41	-20.25 ± 0.09	12.37 ± 0.06			3.16 ± 0.02	
33	-14	-19.09 ± 0.09	13.07 ± 0.06	-0.55 ± 0.05	-7.33 ± 0.02	3.18 ± 0.02	11.77 ± 0.09
mean		-19.45	12.11	1.43	-12.28	3.18	6.97
s.d.		1.29	0.83	2.13	2.19	0.01	1.73

Table 3.3. Results of elemental analysis. Sample 23 was lost in processing, thus no measurements are reported. Other missing data represent analyses in which the concentration of the element was not above the lower limit of detection for the run. Errors are 1σ and are based on the relative standard deviation (RSD) of standards that were run with the samples. These data (excluding Pb/Ca and Fe/Ca) are plotted in Figure 3.10. Note the high Mn/Ca and Fe/Ca, and low Mg/Ca in samples 1 and 2 indicating alteration near the exposed exterior surface of the tusk tip.

Sample	Days before death	Mg/Ca	Sr/Ca	Ba/Ca	Pb/Ca	P/Ca	Mn/Ca	Fe/Ca	Zn/Ca
1	-1275	49.87 ± 0.33	1.80 ± 0.01	0.839 ± 0.007	0.0010 ± 0.0003	644.62 ± 10.65	1.0259 ± 0.0141	1.57 ± 0.20	0.198 ± 0.004
2	-1234	59.24 ± 0.39	1.56 ± 0.01	0.461 ± 0.004		639.52 ± 10.56	0.2396 ± 0.0033	0.80 ± 0.20	0.143 ± 0.003
3	-1189	164.95 ± 1.08	1.20 ± 0.01	0.180 ± 0.002		760.64 ± 12.57	0.0034 ± 0.0007	0.42 ± 0.20	0.138 ± 0.003
4	-1134	170.71 ± 1.12	1.40 ± 0.01	0.166 ± 0.001	0.0013 ± 0.0003	786.60 ± 12.99	0.0037 ± 0.0007		0.223 ± 0.005
5	-1075	158.14 ± 1.04	1.12 ± 0.01	0.109 ± 0.001		694.48 ± 11.47	0.0022 ± 0.0007	0.34 ± 0.20	0.112 ± 0.003
6	-1035	170.07 ± 1.12	1.83 ± 0.01	0.133 ± 0.001		690.47 ± 11.41	0.0032 ± 0.0007		0.143 ± 0.003
7	-1003	195.76 ± 1.29	2.13 ± 0.01	0.183 ± 0.002	0.0010 ± 0.0003	800.42 ± 13.22	0.0034 ± 0.0007	0.47 ± 0.20	0.190 ± 0.004
8	-962	190.82 ± 1.25	1.42 ± 0.01	0.173 ± 0.001		823.35 ± 13.60	0.0031 ± 0.0007		0.139 ± 0.003
9	-926	191.97 ± 1.26	1.36 ± 0.01	0.163 ± 0.001		761.41 ± 12.58	0.0032 ± 0.0007	0.49 ± 0.20	0.180 ± 0.004
10	-903	199.69 ± 1.31	1.49 ± 0.01	0.156 ± 0.001		812.47 ± 13.42	0.0032 ± 0.0007		0.131 ± 0.003
11	-867	188.78 ± 1.24	1.66 ± 0.01	0.103 ± 0.001		773.76 ± 12.78	0.0032 ± 0.0007		0.119 ± 0.003
12	-808	197.38 ± 1.30	1.54 ± 0.01	0.090 ± 0.001		787.82 ± 13.01	0.0027 ± 0.0007		0.120 ± 0.003
13	-767	201.83 ± 1.33	1.94 ± 0.01	0.075 ± 0.001		818.51 ± 13.52	0.0039 ± 0.0007	0.51 ± 0.20	0.202 ± 0.005
14	-731	208.96 ± 1.37	2.28 ± 0.02	0.082 ± 0.001		821.66 ± 13.57	0.0030 ± 0.0007	0.47 ± 0.20	0.119 ± 0.003
15	-699	211.86 ± 1.39	2.36 ± 0.02	0.110 ± 0.001		820.76 ± 13.56			0.149 ± 0.003
16	-658	224.62 ± 1.48	2.56 ± 0.02	0.101 ± 0.001		852.84 ± 14.09	0.0024 ± 0.0007		0.122 ± 0.003
17	-603	211.70 ± 1.39	1.47 ± 0.01	0.136 ± 0.001		808.83 ± 13.36	0.0028 ± 0.0007		0.124 ± 0.003
18	-535	202.46 ± 1.33	1.45 ± 0.01	0.098 ± 0.001		816.83 ± 13.49			0.104 ± 0.002
19	-499	206.02 ± 1.35	1.28 ± 0.01	0.099 ± 0.001		826.22 ± 13.65	0.0029 ± 0.0007		0.126 ± 0.003
20	-467	215.25 ± 1.41	1.47 ± 0.01	0.116 ± 0.001		822.25 ± 13.58	0.0028 ± 0.0007		0.239 ± 0.005
21	-436	216.34 ± 1.42	1.73 ± 0.01	0.126 ± 0.001		815.86 ± 13.48	0.0028 ± 0.0007		0.100 ± 0.002
22	-408	214.63 ± 1.41	1.93 ± 0.01	0.181 ± 0.002		825.95 ± 13.64	0.0030 ± 0.0007		0.087 ± 0.002
23	-381								
24	-345	224.25 ± 1.47	1.99 ± 0.01	0.085 ± 0.001		822.75 ± 13.59	0.0029 ± 0.0007		0.101 ± 0.002
25	-299	226.48 ± 1.49	1.85 ± 0.01	0.086 ± 0.001		847.84 ± 14.01	0.0032 ± 0.0007		0.217 ± 0.005
26	-245	228.41 ± 1.50	1.48 ± 0.01	0.114 ± 0.001		835.45 ± 13.80	0.0058 ± 0.0007	0.69 ± 0.20	0.124 ± 0.003
27	-191	224.14 ± 1.47	1.31 ± 0.01	0.138 ± 0.001		840.79 ± 13.89			0.102 ± 0.002
28	-150	229.13 ± 1.51	1.33 ± 0.01	0.139 ± 0.001		818.07 ± 13.51			0.129 ± 0.003
29	-113	229.27 ± 1.51	1.73 ± 0.01	0.155 ± 0.001		838.71 ± 13.86			0.123 ± 0.003
30	-86	231.57 ± 1.52	1.63 ± 0.01	0.119 ± 0.001		835.14 ± 13.80	0.0029 ± 0.0007		0.213 ± 0.005
31	-64	231.38 ± 1.52	2.18 ± 0.01	0.121 ± 0.001		838.02 ± 13.84			0.112 ± 0.003
32	-41	230.41 ± 1.51	2.19 ± 0.02	0.129 ± 0.001	0.0011 ± 0.0003	869.30 ± 14.36	0.0034 ± 0.0007		0.147 ± 0.003
33	-14	126.82 ± 0.83	2.05 ± 0.01	0.094 ± 0.001		712.89 ± 11.78	0.0093 ± 0.0007		0.119 ± 0.003
mean		194.78	1.71	0.158	0.001	795.76	0.0518	0.64	0.144
s.d.		44.32	0.37	0.141	0.000	58.57	0.2040	0.38	0.041

Table 3.4. Correlations between pairs of detrended (if non-stationary), spline-interpolated isotope, weather, and increment thickness series. See Materials and Methods for description of statistical methods. Only significant ($p < 0.025$) correlations are shown. Underlined values are significant with Bonferroni correction. Asterisks mark series that were detrended. Color scale indicates the lag associated with each correlation. Positive lag means that the column series is shifted such that y_{t+lag} in the column series is aligned with y_t in the row series. Precip. = precipitation, Temp. = temperature, Avg. Inc. Thick. = average thickness of second-order increments contained within each compositional sample. As an example of the kind of information portrayed here, note the positive correlations between $\delta^{13}C_{col}$ and the weather data series (precipitation and temperature). Elevated $\delta^{13}C_{col}$ during the warm wet season is due to an increased proportion of C_4 plants in the diet.

	$\delta^{13}C_{col}$	$\delta^{15}N_{col}$*	$\delta^{18}O_{carb}$*	$\delta^{13}C_{carb}$*	Precip.	Temp.	Avg. Inc. Thick. *
$\delta^{13}C_{col}$			<u>-0.50</u>	<u>0.69</u>	0.38	<u>0.60</u>	
$\delta^{15}N_{col}$*			-0.47		<u>-0.50</u>		0.42
$\delta^{18}O_{carb}$*		-0.47					
$\delta^{13}C_{carb}$*	<u>0.69</u>		-0.42		0.53	0.65	
Precip.	0.38	-0.50		<u>0.53</u>			
Temp.	<u>0.60</u>			<u>0.65</u>			
Avg. Inc. Thick. *		0.42					

Lag (weeks)

-6 -5 -4 -3 -2 -1 0 1 2 3 4 5 6

Table 3.5. Correlations between pairs of detrended (if non-stationary), spline-interpolated series excluding altered samples. Samples that appeared to have been diagenetically altered (samples 1, 2, and 33- see text and Table 3.3) were excluded from the series. See Materials and Methods for description of statistical methods. Only significant ($p < 0.025$) correlations are shown. Underlined values are significant with Bonferroni correction. Asterisks mark series that were detrended. Color scale indicates the lag associated with each correlation. Positive lag means that the column series is shifted such that y_{t+lag} in the column series is aligned with y_t in the row series. Precip. = precipitation, Temp. = temperature, Avg. Inc. Thick. = average thickness of second-order increments contained within each compositional sample. Of particular interest are the negative correlation between $\delta^{15}N_{col}$ and Mg/Ca, and the positive correlation between Mg/Ca and Sr/Ca. This pattern may indicate seasonal differences in the importance of milk in the diet.

	$\delta^{13}C_{col}$*	$\delta^{15}N_{col}$*	$\delta^{18}O_{carb}$*	$\delta^{13}C_{carb}$*	Mg/Ca*	P/Ca*	Mn/Ca*	Zn/Ca*	Sr/Ca*	Ba/Ca*	Precip.*	Temp.	Avg. Inc. Thick.*
$\delta^{13}C_{col}$*			-0.39	**0.86**					-0.42	0.44		**0.70**	
$\delta^{15}N_{col}$*					-0.51	-0.48	-0.57				**-0.58**	-0.51	
$\delta^{18}O_{carb}$*						-0.47				-0.57			
$\delta^{13}C_{carb}$*	**0.86**								-0.53	0.47	0.53	**0.77**	
Mg/Ca*		-0.51				**0.81**		0.36	**0.70**		0.42		
P/Ca*		-0.48	-0.47		**0.81**				0.49		0.48		
Mn/Ca*		-0.57		0.44									-0.44
Zn/Ca*													
Sr/Ca*	-0.42			-0.53	**0.70**	0.49							
Ba/Ca*	0.44		-0.57	0.47		0.35					0.47		
Precip.*		-0.58	0.38	0.53	0.42	0.48				0.47			
Temp.	**0.70**	-0.51		**0.77**									
Avg. Inc. Thick.*							-0.44						

Lag (weeks)

-6 -5 -4 -3 -2 -1 0 1 2 3 4 5 6

Figure 3.1. Location at which tusk was collected. The Shabi Shabi seep is located in the central, western part of Hwange National Park (HNP) in Zimbabwe. Coordinates of the seep are -19.323389 °lat., 26.174525 °lon. (Modified from Haynes, 1991).

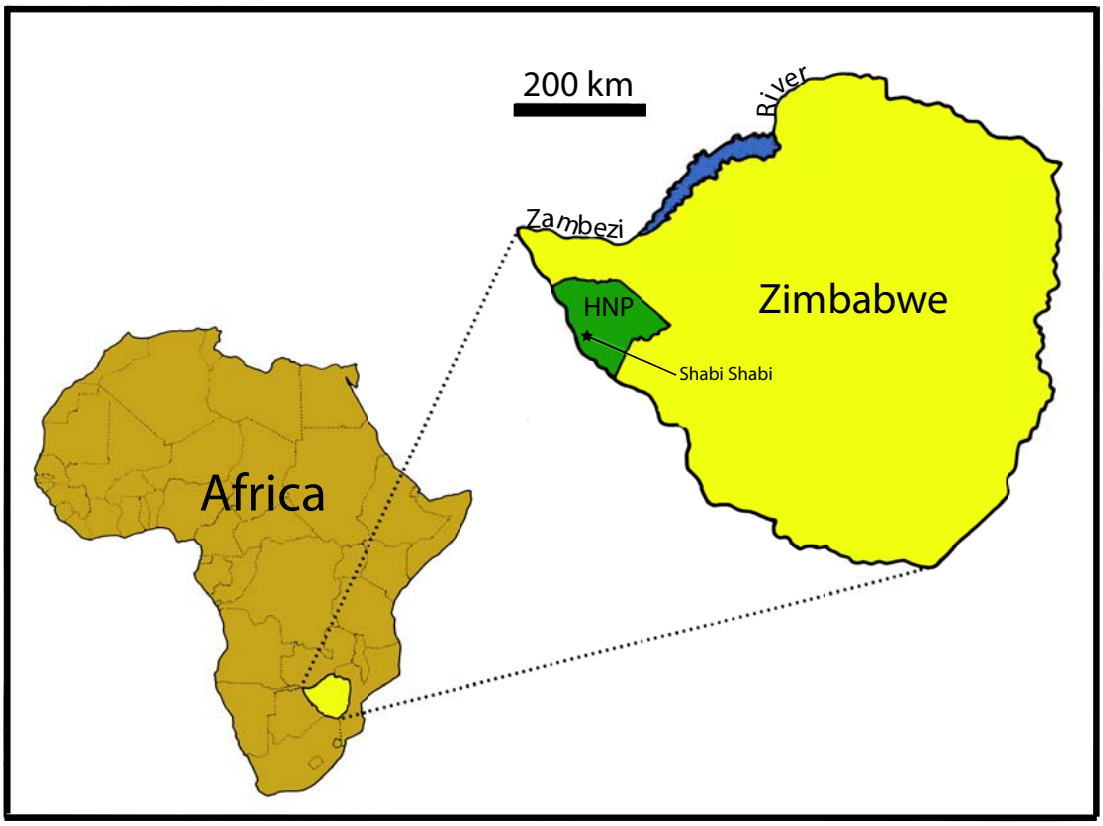

Figure 3.2, A-C. Images of tusk and three-dimensional model. A) Medial aspect of tusk. B) Lateral aspect of tusk. C) Translucent rendering of three-dimensional, digitized model of tusk showing extent of pulp cavity (medial aspect). Patches of enamel are present near the tip of the tusk (more easily seen in B). Staining and etching near the tip of the tusk mark the portion of the tusk exposed during life. The depth of the pulp cavity is less than the length of unexposed tusk indicating that this tusk probably came from a female calf.

Figure 3.3. Unpolished surfaces resulting from the initial longitudinal cut. Contrast has been increased so that first-order, annual growth increments are visible as dark-light couplets in the dentin.

Figure 3.4, A-B. Contrast-enhanced longitudinal and transverse cut surfaces.
A) Polished and contrast enhanced longitudinal cut surfaces of segments. First-order, annual growth increments are clearly visible as nested "V"s. Just over three years of growth are represented. B) As in A, but with the proximal surfaces of each segment included in the image. Thin sections were made from the transverse surfaces to allow measurements of second-order increment thicknesses.

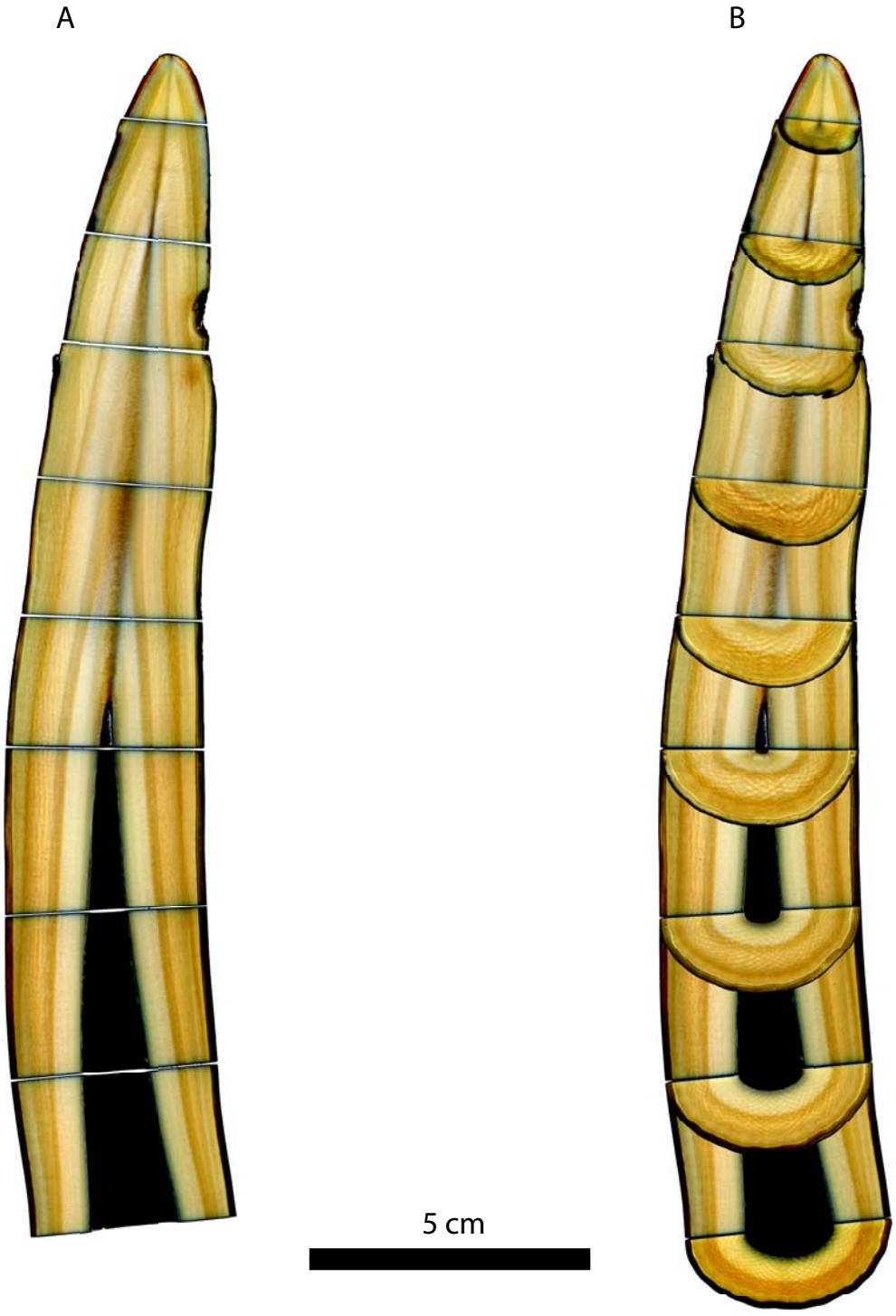

Figure 3.5. Cutting strategy for segments in which sampling was performed. The cut plane is oriented so that it passes through the tusk axis and follows a radius that bisects the sector in which the radii of curvature of second-order (and first-order) increments on the transverse surfaces are at their maxima.

Figure 3.6, A-E. Tusk segment 8 sampling. A) Unaltered scan of sampling surface. The small white circles on the corners serve as alignment landmarks. B) as in A, but contrast enhanced. C) as in B, but with FFT filtering to enhance visibility of second-order increments. D) Sampling plan. E) Segment after powdered samples have been removed. Block samples remain in place.

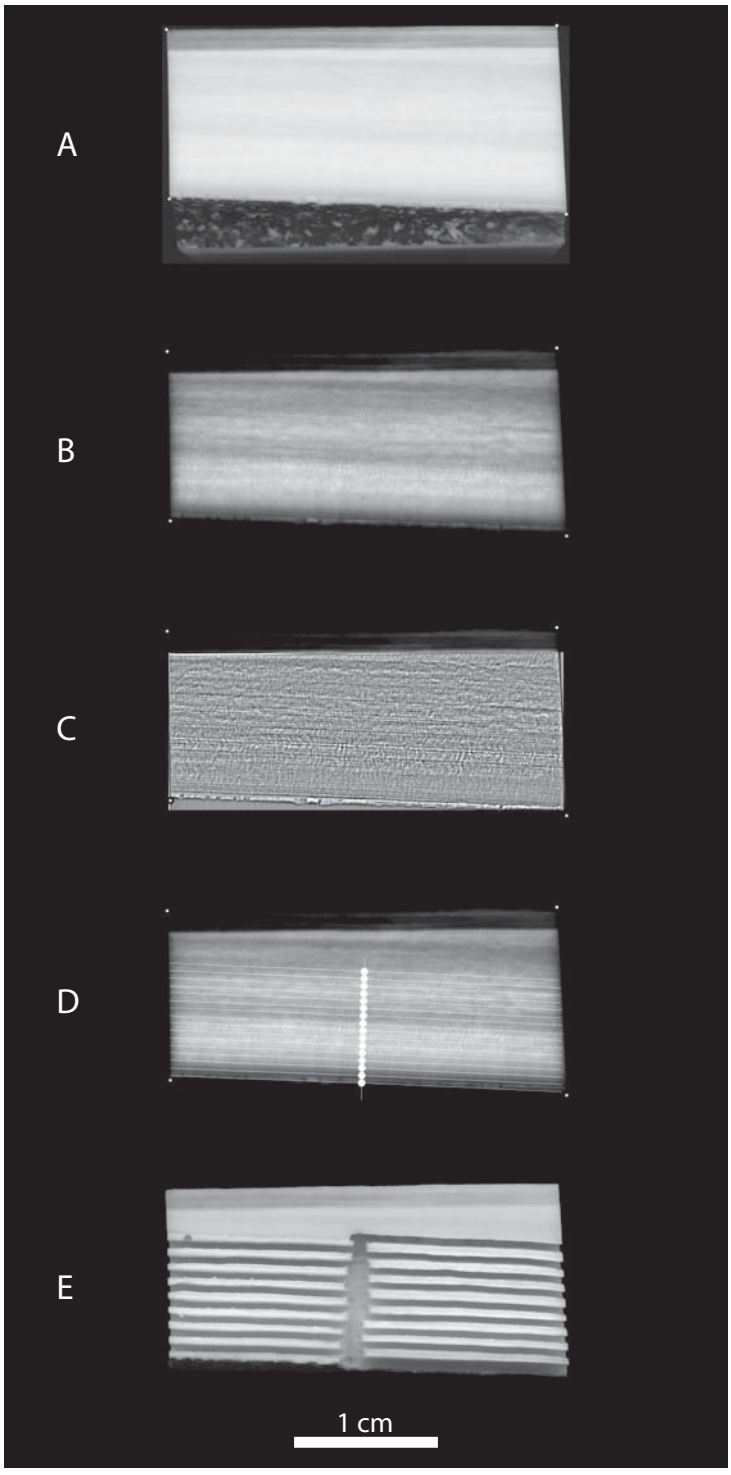

Figure 3.7, A-F. Stable isotope data and weather data (sampled to equivalent temporal resolution as compositional samples). Dotted lines mark years before death. Bars above abscissae indicate dark bands in dentin. A) $\delta^{15}N$ of collagen samples (relative to AIR). B) $\delta^{13}C$ of collagen samples (relative to VPDB). C) $\delta^{18}O$ of structural carbonate (relative to VPDB). D) $\delta^{13}C$ of structural carbonate (relative to VPDB). E) Mean daily precipitation (mm) during the interval in which a corresponding compositional sample formed. F) Mean daily temperature (°C) during the interval in which a corresponding compositional sample formed. Seasonal variation in composition is evident in A, B, and D. For example, low $\delta^{13}C_{col}$ values (B) occur when temperature (F) is low (when diet includes more C_3 plants). The sample cross-correlation of these two series is shown in Figure 3.8B, and it indicates that these series are significantly positively correlated with a lag of +3 weeks. See Tables 3.4 and 3.5 for other correlations.

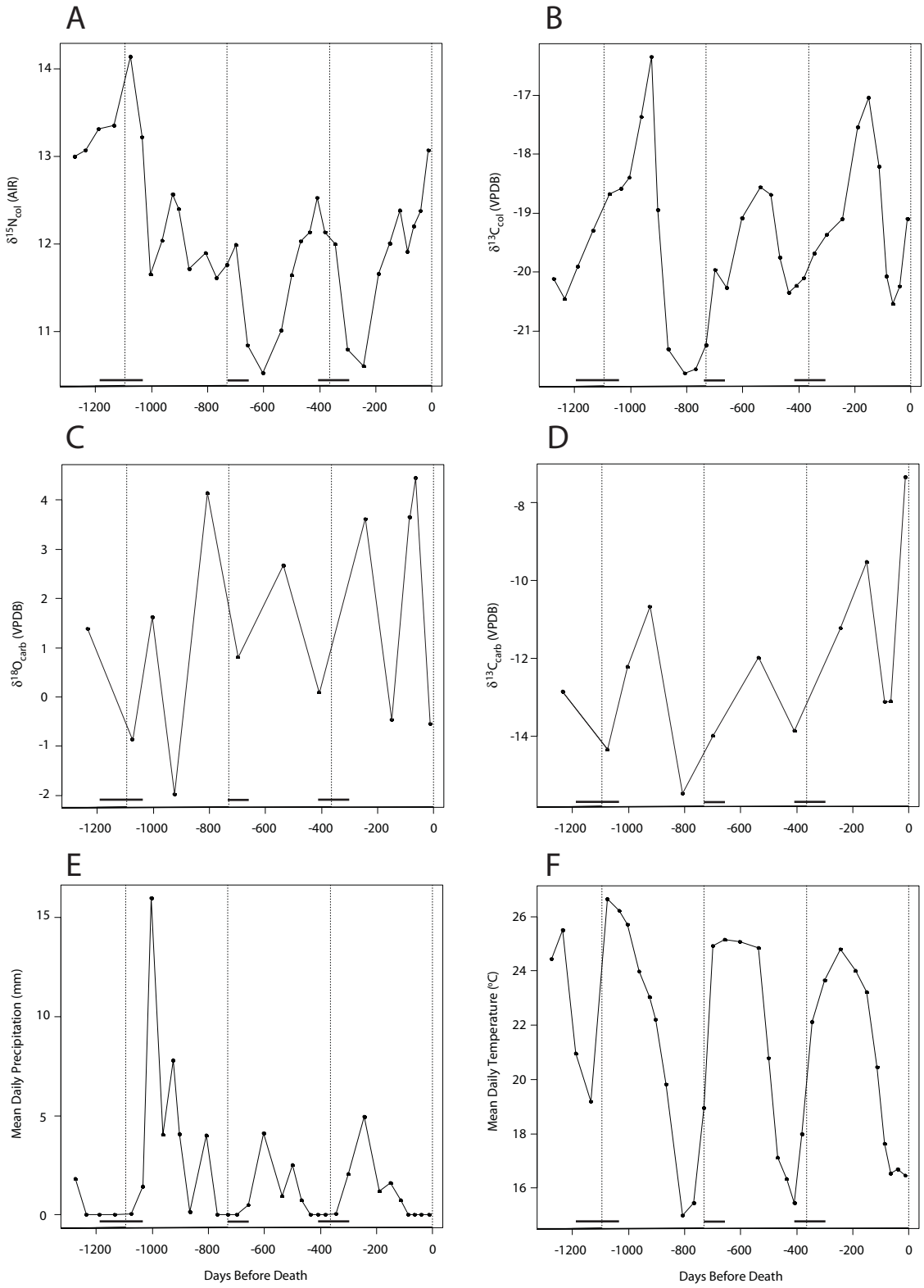
A
B
C
D
E
F
$\delta^{15}N_{col}$ (AIR)
$\delta^{13}C_{col}$ (VPDB)
$\delta^{18}O_{carb}$ (VPDB)
$\delta^{13}C_{carb}$ (VPDB)
Mean Daily Precipitation (mm)
Mean Daily Temperature (°C)
Days Before Death
Days Before Death

Figure 3.8, A-B. Sample cross-correlations for $\delta^{13}C_{col}$ against precipitation and temperature. Series were interpolated to weekly resolution. Dashed lines mark bootstrap-derived 95% confidence intervals for correlations between the compositional series and randomly resampled weather series. A) $\delta^{13}C_{col}$ against precipitation. There is a significant positive correlation of 0.38 at lag = 0, which is of greater magnitude than at any other lag from -70 to +70 (also shown in Table 3.4). B) $\delta^{13}C_{col}$ against temperature. There is a significant positive correlation of 0.60 at lag = +3, which is of greater magnitude than at any other lag from -70 to +70 (also shown in Table 3.4).

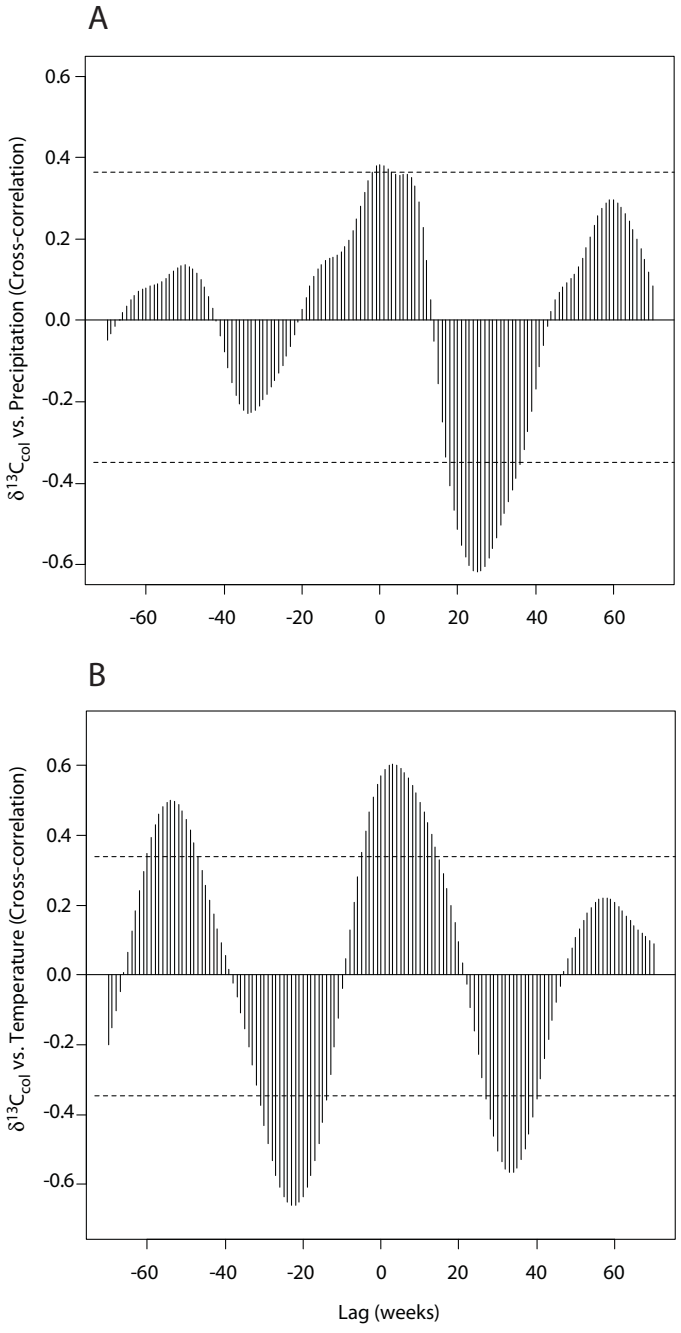

Figure 3.9, A-C. Spline-interpolated, detrended collagen $\delta^{15}N$ series and sample cross-correlations with precipitation and temperature. A) Spline-interpolated, detrended collagen $\delta^{15}N$ (residuals from cubic spline fit d.f. = 4). Dashed lines mark years before death. B) Sample cross-correlation for detrended $\delta^{15}N$ versus precipitation. Dashed lines mark bootstrap-derived 95% confidence intervals for correlations between the compositional series and randomized samples of the weather series. There is a significant positive correlation of 0.50 at lag = 0, which is of greater magnitude than at any other lag from -70 to +70 (also shown in Table 3.4) C) Sample cross-correlation for detrended $\delta^{15}N$ versus temperature. Dashed lines as in B. There is a significant negative correlation of -0.49 at lag = +6, but this is not of greater magnitude than at any other lag from -70 to +70. Thus, it is not shown in Table 3.4 (see Methods and Materials for description of statistical method).

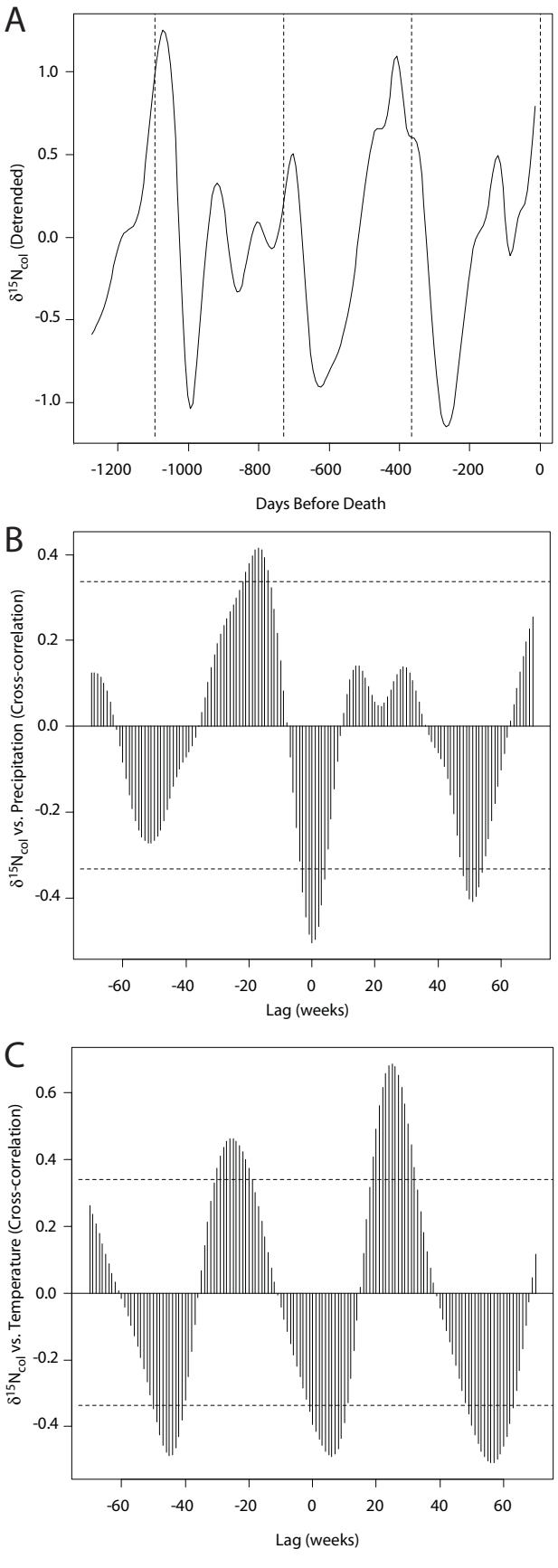
A
1.0
0.5
0.0
-0.5
-1.0
δ15Ncol (Detrended)
-1200
-1000
-800
-600
-400
-200
0
Days Before Death
B
0.4
0.2
0.0
-0.2
-0.4
δ15Ncol vs. Precipitation (Cross-correlation)
-60
-40
-20
0
20
40
60
Lag (weeks)
C
0.6
0.4
0.2
0.0
-0.2
-0.4
δ15Ncol vs. Temperature (Cross-correlation)
-60
-40
-20
0
20
40
60
Lag (weeks)

Figure 3.10, A-D. Elemental concentrations relative to calcium. Dotted lines mark years before death. Bars above abscissae indicate dark bands in the dentin. Sample 23 (381 days before death) was lost for all elements and has been estimated by spline interpolation. Samples 1 (earliest),2, and 33 (latest)) are diagentically altered and are not shown here, their values are listed in Table 3.3. A) Magnesium:Calcium. B) Phosphorus:Calcium. C) Manganese:Calcium. Missing values had Mn below limit of detection. D) Zinc:Calcium. Of particular interest in these plots is the increase in Mg/Ca with time. This may be due to decreasing importance of milk in the diet.

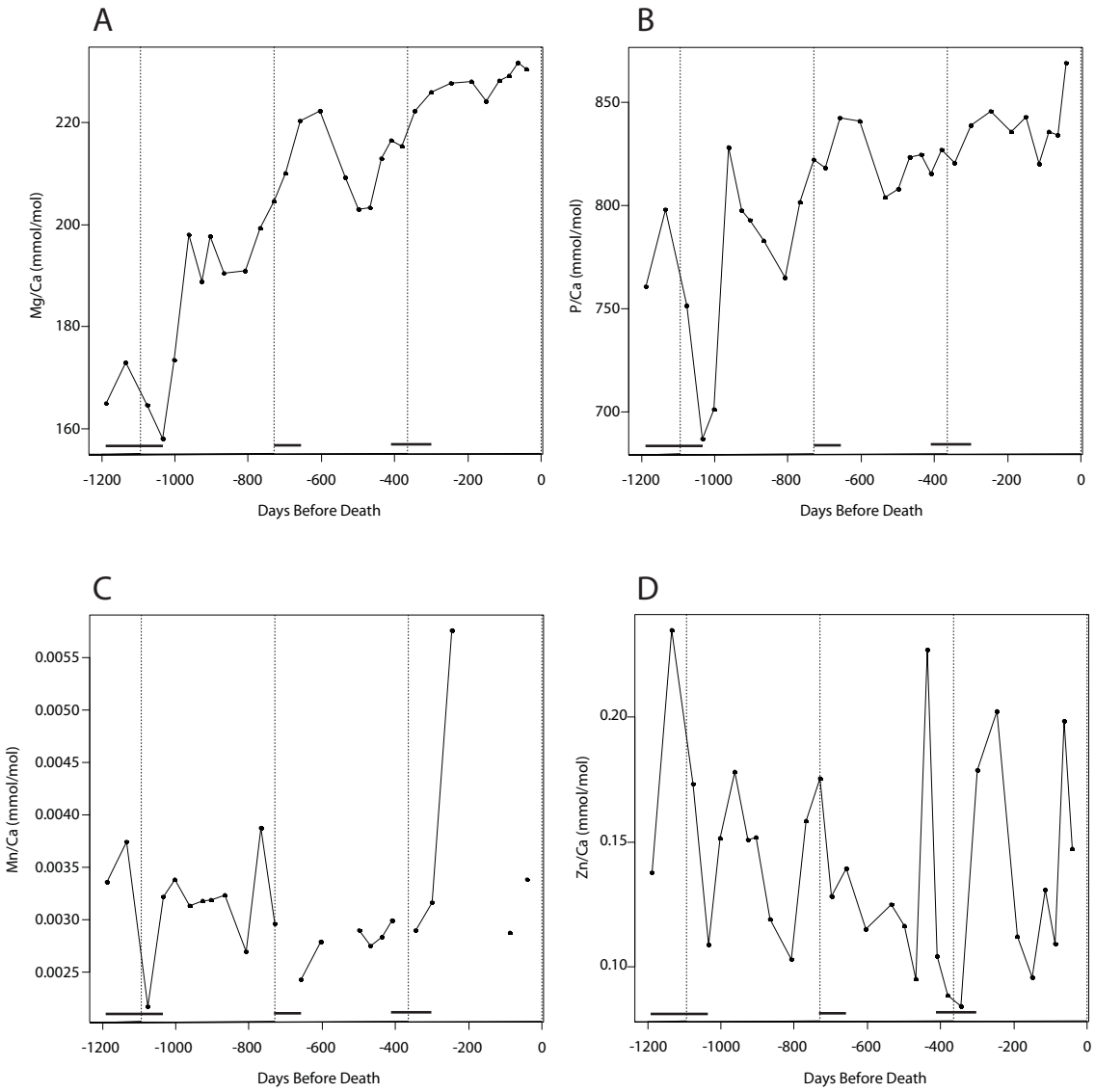

Figure 3.10, E-F. Elemental concentrations relative to calcium. Dotted lines mark years before death. Bars above abscissae indicate dark bands in the dentin. Sample 23 (381 days before death) was lost for all elements and has been estimated by spline interpolation. Samples 1 (earliest),2, and 33 (latest)) are diagentically altered and are not shown here, their values are listed in Table 3.3. E) Strontium:Calcium. Note the seasonal-scale variation in Sr/Ca in the last two years of life. F) Barium:Calcium. Ba/Ca may vary seasonally (it is significantly correlated with precipitation (see Table 3.5), but the pattern is not as consistent as that seen in the last two years of life for Sr/Ca.

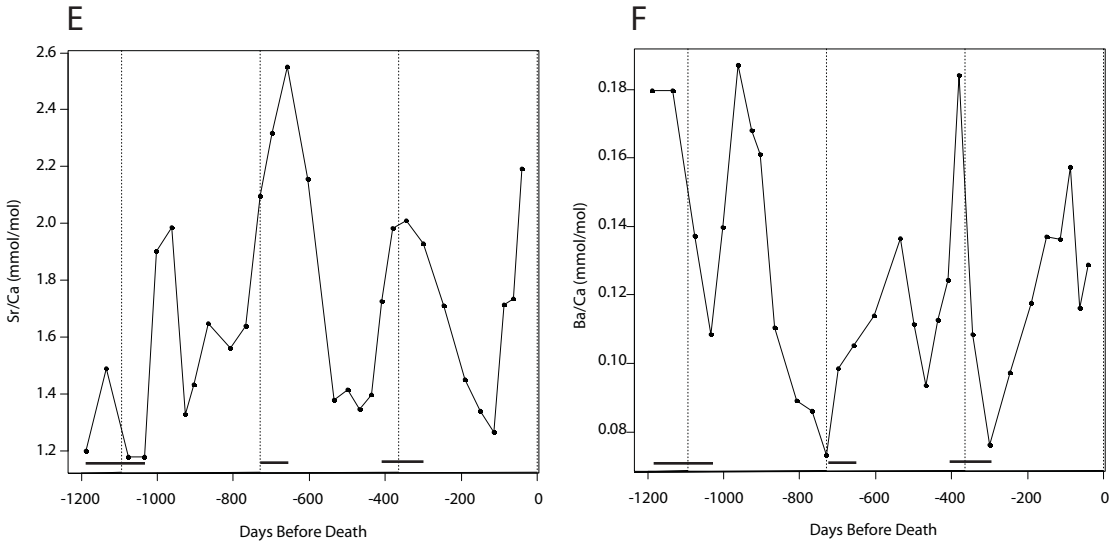

Figure 3.11. Second-order growth increment thicknesses through time. Dotted lines mark years before death. Bars above abscissa indicate dark bands in the dentin. In the last two years of life, increments are thicker in the late rainy season and early dry season (see Fig. 3.7E for precipitation data).

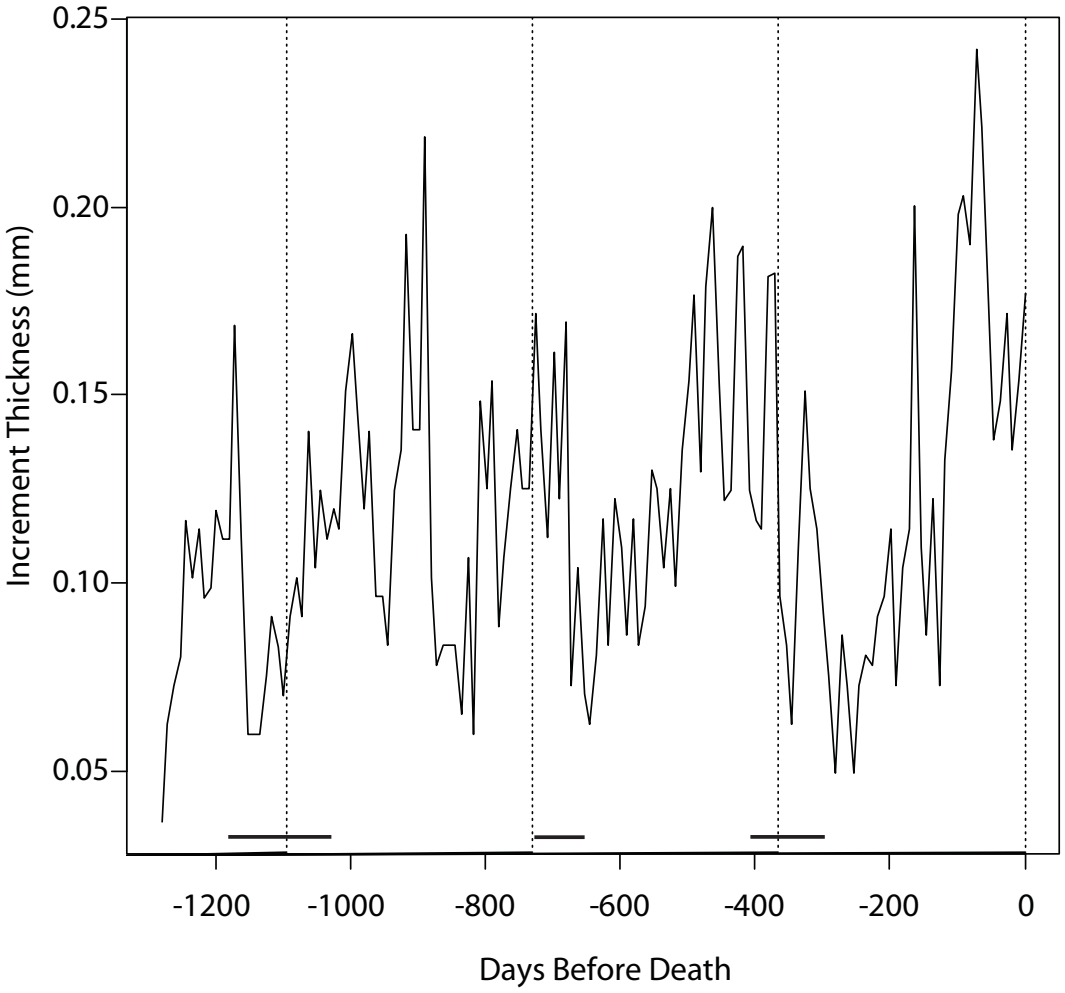

References

Ambrose, S.H., DeNiro, M.J., 1986. The isotopic ecology of East African mammals. Oecologia 69, 395–406.

Ambrose, S.H., Norr, L., 1993. Experimental evidence for the relationship of the carbon isotope ratios of whole diet and dietary protein to those of bone collagen and carbonate. In: Lambert, J.B., Groupe, G. (Eds.), Prehistoric Human Bone: Archaeology at the Molecular Level. Springer, Berlin, pp. 1–37.

Ando-Mizobata, N., Sakai, M., Sakurai, Y., 2006. Trace-element analysis of Steller sea lion (*Eumetopias jubatus*) teeth using scanning X-ray analytical microscope. Mammal Study 31, 65–68.

Cerling, T.E., Harris, J.M., 1999. Carbon isotope fractionation between diet and bioapatite in ungulate mammals and implications for ecological and paleoecological studies. Oecologia 120, 347–363.

Cerling, T.E., Passey, B.H., Ayliffe, L.K., Cook, C.S., Ehleringer, J.R., Harris, J.M., Dhidha, M.B., Kasiki, S.M., 2004. Orphans' tales: seasonal dietary changes in elephants from Tsavo National Park, Kenya. Palaeogeography, Palaeoclimatology, Palaeoecology 206, 367–376.

Cerling, T.E., Wittemyer, G., Ehleringer, J.R., Remien, C.H., Douglas-Hamilton, I., 2009. History of Animals using Isotope Records (HAIR): A 6-year dietary history of one family of African elephants. Proceedings of the National Academy of Sciences of the United States of America DOI: 10.1073/pnas.0902192106.

Chamaillé-Jammes, S., Fritz, H., Murindagomo, F., 2007. Climate-driven fluctuations in surface-water availability and the buffering role of artificial pumping in an African savanna: Potential implication for herbivore dynamics. Austral Ecology 32, 740–748.

Codron, J. 2008. Annals of Ivory: Perspectives on African Elephant *Loxodonta africana* (Blumenberg 1797) feeding ecology from a multi-decadal record. Unpublished dissertation, University of Cape Town.

Dalerum, F., Bennett, N.C., Clutton-Brock, T.H., 2007. Longitudinal differences in ^{15}N between mothers and offspring during and after weaning in a small cooperative mammal, the meerkat (*Suricata suricatta*). Rapid Communications in Mass Spectrometry 21, 1889–1892.

Dauncey, M.J., Shaw, J.C.L., Urman, J., 1977. The absorption and retention of magnesium, zinc, and copper by low birth weight infants fed pasteurized human breast milk. Pediatric Research 11, 991–997.

DeNiro, M.J., Epstein, S., 1978. Carbon isotopic evidence for different feeding patterns in two hyrax species occupying the same habitat. Science 201(4359), 906–908.

Dewey, K.G., Cohen, R.J., Rivera, L.L., Brown, K.H., 1998. American Journal of Clinical Nutrition 67, 878–884.

Drzazga, Z., Michalik, K., Maciejewska, K., Trzeciak, H., Kaszuba, M., 2007. Role of endogenous zinc in bones of newborn rats. Biofactors 30, 243–248.

Dudley, J.P., Criag, G.C., Gibson, D.St.C., Haynes, G., Klimowicz, J., 2001. Drought mortality of bush elephants in Hwange National Park, Zimbabwe. African Journal of Ecology 39, 187–194.

Dufty, J.H., Bingley, J.B., Cove, L.Y., 1977. The plasma zinc concentration of nonpregnant, pregnant, and parturient Hereford cattle. Australian Veterinary Journal 53, 519–522.

Edmonds, J.S., Shibata, Y., Prince, R.I.T., Preen, A.R., Morita, M., 1997. Elemental composition of a tusk of a dugong, *Dugong dugon*, from Exmouth, Western Australia. Marine Biology 129, 203–214.

Evans, R.D., Richner, P., Outridge, P.M., 1995. Micro-spatial variations of heavy metals in the teeth of walrus as determined by laser ablation ICP-MS: The potential for reconstructing a history of metal exposure. Archives of Environmental Contamination and Toxicology 28, 55–60.

Ezzo, J. A., 1994. Zinc as a paleodietary indicator: An issue of theoretical validity in bone-chemistry analysis. American Antiquity 59(4), 606–621.

Fisher, D.C., 2008. Taphonomy and paleobiology of the Hyde Park mastodon. In: Allmon, W.D., Nester, P.L. (Eds.), Mastodon Paleobiology, Taphonomy, and Paleoenvironment in the Late Pleistocene of New York State: Studies on the Hyde Park, Chemung, and North Java Sites, Palaeontogrphica Americana 61, pp. 197–289.

Fisher, D.C., 2008b. Paleobiology and extinction of proboscideans in the Great Lakes region of North America. In: Haynes, G. (Ed.), American Megafaunal Extinctions at the End of the Pleistocene. Springer, pp. 55–75.

Fisher, D.C., 2001. Season of Death, Growth Rates, and Life History of North American

Mammoths. In: West, D. (Ed.), Proceedings of the International Conference on Mammoth Site Studies, Publications in Anthropology 22. University of Kansas, Lawrence, pp. 121–135.

Fisher, D.C., 1996. Extinction of proboscideans in North America. In: Shoshani, J., Tassy, P. (Eds.), The Proboscidea: Evolution and Paleoecology of Elephants and Their Relatives. Oxford University Press, Oxford, pp. 296–315.

Fisher, D.C., 1984. Taphonomic analysis of late Pleistocene mastodon occurrences: Evidence of butchery by North American Paleo-Indians. Paleobiology 10(3), 338–357.

Fisher, D.C., Beld, S.G., Rountrey, A.N., 2008. Tusk record of the North Java mastodon. In: Allmon, W.D., Nester, P.L. (Eds), Mastodon Paleobiology, Taphonomy, and Paleoenvironment in the Latre Pleistocene of New York State: Studies on the Hyde Park, Chemung, and North Java Sites, Palaeontographica Americana 61, pp. 399–445.

Fisher, D.C., Fox, D.L., 2003. Season of death and terminal growth histories of Hiscock mastodons. In: Laub, R.S. (Ed.), The Hiscock Site: Late Pleistocene and Holocene Paleoecology and Archaeology of Western New York State, Bulletin of the Buffalo Society of Natural Sciences, 37, pp. 83–101.

Flint, R.F., Bond, G., 1968. Pleistocene sand ridges and pans in western Rhodesia. Geological Society of America Bulletin 79, 299–314.

Gat, J.R., 1996. Oxygen and hydrogen isotopes in the hydrologic cycle. Annual Review of Earth and Planetary Sciences 24, 225–262.

Goodman, M.N., Larsen, P.R., Kaplan, M.M., Aoki, T.T., Young, V.R., Ruderman, N.B., 1980. Starvation in the rat. II. Effect of age and obesity on protein sparing and fuel metabolism. American Journal of Physiology- Endocrinology and Metabolism 239(4), E277–E286.

Hall, R.C.W., Hoffman, R.S., Beresford, T.P., Wooley, B., Tice, L., Hall, A.K., 1988. Hypomagnesemia in patients with eating disorders. Psychosomatics 29(3) 264–272.

Haynes, G., 1991. Mammoths, mastodonts, and elephants: Biology, behavior, and the fossil record. Cambridge University Press, Cambridge, UK.

Hobson, K.A., Alisauskas, R.T., Clark, R.G., 1993. Stable-Nitrogen isotope enrichment in avian tissues due to fasting and nutritional stress: Implications for isotopic analyses of diet. The Condor 95 (2), 388–394.

Hobson, K.A., Sease, J.L., 1998. Stable isotope analyses of tooth annuli reveal temporal dietary records: an example using Stellar sea lions. Marine Mammal Science 14, 116–129.

Holá, M., Kalvoda, J., Bábek, O., Brzobohatý, R., Holoubek, I., Kanický, V., Skoda, R., 2008. LA-ICP-MS heavy metal analyses of fish scales from sediments of the Oxbow Lake Certak of the Morava River (Czech Republic). Environmental Geology DOI: 10.1007/s00254-008-1501-z.

Holdo, R.M., 2003. Woody plant damage by African elephants in relation to leaf nutrients in western Zimbabwe. Journal of Tropical Ecology 19, 189–196.

Jenkins, S.G., Partridge, S.T., Stephenson, T.R., Farley, S.D., Robbins, C.T., 2001. Nitrogen and carbon isotope fractionation between mothers, neonates, and nursing offspring. Oecologia 129, 336–341.

Jeswani, R.M., Vani, S.N., 1991. A study of serum zinc levels in cord blood of neonates and their mothers. Indian Journal of pediatrics 58(5), 683–686.

Klepinger, L.L, 1990. Magnesium ingestion and bone magnesium concentration in paleodietary reconstruction: Cautionary evidence from an animal model. Journal of Archaeological Science 17, 513–517.

Klepinger, L.L., 1984. Nutritional assessment from bone. Annual Review of Anthropology 13, 75–96.

Klevezal, G.A., 1996. Recording Structures of Mammals: Determination of Age and Reconstruction of Life History. A. A. Balkema, Rotterdam.

Koch, P.L., Fisher, D.C., Dettman, D., 1989. Oxygen isotope variation in the tusks of extinct proboscideans: A measure of season of death and seasonality. Geology 17, 515–519.

Kohn, M.J., Schoeninger, M.J., Barker, W.W., 1999. Altered states: Effects of diagenesis on fossil tooth chemistry. Geochimica et Cosmochimica Acta 63(18), 2737–2747.

Lee, P.C., Moss, C.J., 1986. Early maternal investment in male and female African elephant calves. Behavioral Ecology and Sociobiology 18, 353–361.

Lee-Thorp, J.A., Sealy, J.C., van der Merwe, N.J., 1989. Stable carbon isotope ratio differences between bone collagen and bone apatite, and their relationship to diet. Journal of Archaeological Science 16, 585–599.

Loveridge, A.J., Hunt, J.E., Murindagomo, F., Macdonald, D.W., 2006. Influence of drought on predation of elephant (*Loxodonta africana*) calves by lions (*Panthera leo*) in an African wooded savannah. Journal of Zoology 270, 523–530. Elder, W.H, 1970. Morphometry of elephant tusks. Zoologica Africana 5(1), 143–159.

McCullagh, K., 1969. The growth and nutrition of the African elephant. East African Wildlife Journal 7, 85–90.

McCullagh, K.G., Widdowson, E.M., 1970. The milk of the African elephant. British Journal of Nutrition 24, 109–117.

Mekota, A., Grupe, G., Ufer, S., Cuntz, U., 2006. Serial analysis of stable nitrogen and carbon isotopes in hair: monitoring starvation and recovery phases of patients suffering from anorexia nervosa. Rapid Communications in Mass Spectrometry 20, 1604–1610.

Miller, E.R., Ullrey, D.E., Zutaut, C.L., Baltzer, B.V., Schmidt, D.A., Hoefer, J.A., Luecke, R.W., 1965. Magnesium requirement of the baby pig. The Journal of Nutrition 85, 13–20.

Newsome, S.D., Koch, P.L., Etnier, M.A., Aurioles-Gamboa, D., 2006. Using carbon and nitrogen isotope values to investigate maternal strategies in northeast Pacific otariids. Marine Mammal Science 22(3), 556–572.

Pate, F.D., 1994. Bone chemistry and paleodiet. Journal of Archaeological Method and Theory 1(2), 161–209.

Polischuk, S.C., Hobson, K.A., Ramsay, M.A., 2001. Use of stable-carbon and –nitrogen isotopes to assess weaning and fasting in female polar bears and their cubs. Canadian Journal of Zoology 79, 499–511.

R Development Core Team, 2008. R: A language and environment for statistical computing. R Foundation for Statistical Computing, Vienna, Austria.

Rasband, W.S., 1997-2008. ImageJ, U.S. National Institutes of Health, Bethesda, Maryland, USA, http://rsb.info.nih.gov/ij.

Rau, G.H., Mearns, A.J., Young, D.R., Olson, R.J., Schafer, H.A., Kaplan, I.R., 1983. Animal $^{13}C/^{12}C$ correlates with trophic level in pelagic food webs. Ecology 64(5), 1314–1318.

Raubenheimer, E.J., van Heerden, W.F.P, van Niekerk, P.J, de Vos, V., Turner, M.J., 1995. Morphology of the deciduous tusk (tush) of the African elephant (*Loxodonta africana*). Archives of Oral Biology 40(6), 571–576.

Robbins, C.T., Felicetti, L.A., Sponheimer, M., 2005. The effect of dietary protein quality on nitrogen isotope discrimination in mammals and birds. Oecologia 144, 534–540.

Rountrey, A.N, Fisher, D.C., Vartanyan, S., Fox, D.L., 2007. Carbon and nitrogen isotope analyses of a juvenile woolly mammoth tusk: Evidence of weaning. Quaternary International 169–170, 166–173.

Schoeninger M.J., DeNiro, M.J., 1984. Nitrogen and carbon isotopic composition of bone collagen from marine and terrestrial animals. Geochimica et Cosmochimica Acta 48, 625–639.

Shumway, R.H., Stoffer, D.S., 2006. Time Series Analysis and Its Applications With R Examples (2nd ed.). Springer, New York.

Sillen, A., 1988. Elemental and isotopic analyses of mammalian fauna from southern Africa and their implications for paleodietary research. American Journal of Physical Antropology 76, 49–60.

Sillen, A., Kavanagh, M., 1982. Strontium and paleodietary research: A review. Yearbook of Physical Anthropology 25, 67–90.

Smith, B.N., Epstein, S., 1971. Two categories of $^{13}C/^{12}C$ ratios for higher plants. Plant Physiology 47, 380–384.

Sponheimer, M., Robinson, T., Ayliffe, L., Roeder, B., Hammer, J., Passey, B., West, A., Cerling, T., Dearing, D., Ehleringer, J., 2003. International Journal of Osteoarchaeology 13, 80–87.

Sullivan, C.H., Krueger, H.W., 1981. Carbon isotope analysis of separate chemical phases in modern and fossil bone. Nature 292, 333–335.

Swap, R.J., Aranibar, J.N., Dowty, P.R., Gilhooly, W.P., Macko, S.A., 2004. Natural abundance of ^{13}C and ^{15}N in C_3 and C_4 vegetation of southern Africa: patterns and implications. Global Change Biology 10, 350–358.

Taylor, D.M., Bligh, P.H., Duggan, M.H., 1962. The absorption of calcium, strontium, barium, and radium from the gastrointestinal tract of the rat. Biochemical Journal 83, 25–29.

Toots, H., Voorhies, M.R., 1965. Strontium in fossil bones and the reconstruction of food chains. Science 149(3686), 854–855.

Trappletti, A., Hornik, K., 2009. tseries: Time Series Analysis and Computational Finance. R package version 0.10-18.

Vuori, E., Kuitunen, P., 1979. The concentrations of copper and zinc in human milk. Acta Paediatrica Scandinavica 68, 33–37.

Williams, C.T., Buck, C.L., Sears, J., Kitaysky, A.S., 2007. Effects of nutritional restriction on nitrogen and carbon stable isotopes of growing seabirds. Oecologia 153, 11–18.

Williamson, B.R., 1975. Seasonal distribution of elephant in Wankie National Park. Arnoldia (Rhodesia) 7(11) 1–16.

Williamson, B.R., 1975b. The condition and nutrition of African elephant in Wankie National Park. Arnoldia (Rhodesia) 7(12) 1–20.

Wilson, G.F., Mackenzie, D.D.S., Brooks, I.M., Lyon, G.L., 1988. Importance of body tissues as sources of nutrients for milk synthesis in the cow, using ^{13}C as a marker. British Journal of Nutrition 60, 605–617.

Wright, L.E., Schwarcz, H.P., 1998. Stable carbon and oxygen isotopes in human tooth enamel: Identifying breastfeeding and weaning in prehistory. American Journal of Physical Anthropology 106, 1–18.

York, A.E., Thomason, J.R., Sinclair, E.H., Hobson, K.A., 2008. Stable carbon and nitrogen isotope values in teeth of Stellar sea lions: age of weaning and the impact of the 1975–1976 regime shift in the North Pacific Ocean. Canadian Journal of Zoology 86, 33–44.

Chapter 4

Life histories of juvenile woolly mammoths: Stable isotope and elemental analyses of tusk dentin

Introduction

The similarity in anatomy, behavior, and habitat preference between the extant species of elephants (*Loxodonta africana* and *Elephas maximus*) (Haynes, 1991), which phylogenetically bracket the genus *Mammuthus* (Rohland et al., 2007), suggests that these species are reasonable references for hypotheses related to the life history characteristics of mammoths. However, particularly in the case of woolly mammoths (*Mammuthus primigenius*), habitat dissimilarity is such that one might expect differences in life history and behavior relative to these modern species. Behavior and life history are typically difficult to study in fossil organisms, though functional morphology and ichnofossils can serve this goal to some extent. In the case of mammoths, additional information related to life history is contained in the tusks.

The tusks of mammoths are continuously growing recording structures. Animal recording structures are those structures that accumulate in layers and change aspects of their structure and/or composition in response to changing physiological condition (Klevezal, 1996). Data on age, nutritional status (Fisher, 1996), diet (Fisher

and Fox, 2003), climate (Fox et al., 2007), and life history events (e.g., weaning and maturation) (Fisher, 2008) can be extracted through the study of growth increments and the isotopic composition of tusks. These types of data enable the evaluation of hypotheses that typically can only be evaluated in extant species on which field observations can be made. For example, using growth increment data, Fisher (2008) has investigated the possible causes of the late Pleistocene extinction of mastodons. He has shown that the age of sexual maturation for Great Lakes-region mastodons did not increase near the time of their extinction, a pattern more consistent with human hunting than climate-driven nutritional stress as a primary cause for extinction.

Tusks are nearly ideal recording structures due to their evergrowing nature, the presence of temporally periodic growth increments (Fisher, 1987; Koch et al., 1989), and a composite collagen/mineral structure allowing analyses of the composition of both proteins and hydroxyapatite (e.g., Fisher and Fox, 2003). However, they are subject to abrasion and breakage that leads to loss of information. The tips of adult tusks are typically worn and/or broken such that the record of life is incomplete. The material lost from the tusks is that which formed early in life. As most analyses that have been conducted have used adult tusks, very little is known about early mammoth (or mastodon) life history. In addition, the loss of early dentin means that the ages of individuals determined by growth increment counts are minimum estimates. An approximation of the number of years missing can be produced by comparison of the minimum circumference at an unworn position along the tusk to circumferences of other tusks that retain earlier dentin (Fisher et al., 2008). However,

in order to make accurate estimates, the relationship between circumference and age must be determined, and this requires that tusks retaining the very earliest formed dentin be analyzed.

Furthermore, as tusk dentin formation in elephants appears to begin around the time of birth (Raubenheimer, 2000;), tusks of juvenile elephants and mammoths record information about early life history events such as weaning (Rountrey et al., 2007) and possibly birth, but few life history studies have been conducted on juvenile tusks. Analyses of juvenile tusks could provide data on season of birth, nursing patterns, and nutritional stress, in addition to weaning age. Weaning age is a life history parameter of particular interest because it is sensitive to environmental conditions. In a study of African elephants, Lee and Moss (1986) found that weaning was completed at around 5.6 years of age during times of drought, and at around 3.5 years of age under favorable conditions. In a study using recording structures (teeth) to track life history changes, York et al. (2008), identified a trend of increasing weaning ages in Steller sea lions from the early 1960s to the mid 1980s that they associated with declines in resource availability. If weaning ages for a large set of juvenile mammoths from times leading up to their eventual extinction can be determined, it may be possible to determine whether changing resource availability played a role in the extinction. In this study, we begin this work by analyzing growth increments and isotopic/elemental composition in the tusks of five juvenile woolly mammoths.

Tusk growth

The tusks of mammoths are modified upper incisors (I^2) (Luckett, 1996), and their early development follows the typical sequence for mammalian teeth. Enamel is present only on the tips of mammoth and elephant tusks. The outer surface of adult tusks is composed of cementum (or exposed dentin when cementum has been abraded away). The enamel does not seem to have a function in juveniles, and its occurrence is probably related to the interactions between epithelial and mesenchymal tissues required for tooth development. In order for a tooth to develop, both epithelium, which gives rise to ameloblasts (enamel-secreting cells), and mesenchyme, which gives rise to odontoblasts (dentin-secreting cells) must be present (Piesco and Avery, 2002). Early in development, oral epithelium induces the mesenchyme to form the tooth bud, and later in development, the mesenchyme induces epithelial cells to form the enamel organ (Piesco and Avery, 2002).

Odontoblasts, which line the pulp cavity, produce dentin by secreting a collagenous matrix of predentin that later mineralizes and becomes dentin. As dentin is laid down, odontoblasts migrate inward, away from the dentin-enamel junction. The rate of matrix secretion varies with 24-hour periodicity, the greater secretion occurring during light hours versus dark hours (Ohtsuka et al. 1998). This leads to the development of daily growth lines or incremental lines in the dentin. In addition to these daily lines, which will be referred to as third-order, incremental features are present at two other scales in mammoth dentin. First-order increments are annual in periodicity, and second-order increments have a period of around seven days (Fisher, 2001). The thickness of a growth increment is associated with the nutritional status of

the animal during the period of formation (Fisher, 1996). Thus, a record of the changes in the nutritional status of an animal through time can be produced by measuring the thicknesses of all growth increments in a tusk. The presence of these incremental features also allows for the determination of the temporal position of compositional samples taken from tusks.

In evergrowing tusks, as the volume of the pulp cavity is decreased with dentin apposition, the volume is increased by extension of the apical margin. This is accomplished through the differentiation of new odontoblasts. The pulp cavity of a tusk is conical in shape. As a result, the process of incrementally marked apposition and extension leads to dentin that appears to contain a series of stacked cones (Fig. 4.1), with the earliest cone at the tip of the tusk, and subsequent cones stacked inside progressively through the length of the tusk. The dentin at the pulp cavity surface represents material formed just before death.

Dentin Composition

Dentin consists of a collagenous matrix and a mineral fraction. In this study compositional analysis of the collagenous matrix is restricted to measurement of $\delta^{15}N$ and $\delta^{13}C$. The mineral fraction is nominally hyroxyapatite ($Ca_{10}[PO_4]_6[OH]_2$), with substitutions occurring at the Ca, PO_4, and OH sites. In this study, analysis of the mineral fraction includes measurement of $\delta^{13}C$ and $\delta^{18}O$ in substituted CO_3 as well as the ratios of Mg, P, Mn, Fe, Cu, Zn, Sr, Ba, and Pb to Ca. Serial samples from each tusk

are analyzed to allow observation of both long-term (multi-year) and seasonal-scale patterns of compositional change.

$\delta^{13}C$

The $\delta^{13}C$ of proteins and structural carbonate in mineralized tissues have been used in many studies as indicators of diet. The primary interpretive basis for much of this work has been the existence of a difference in the $\delta^{13}C$ of plants using the C_3 photosynthetic pathway versus plants using the C_4 photosynthetic pathway (Smith and Epstein, 1971). The $\delta^{13}C$ of animal tissues reflects the proportions of C_3 and C_4 in the diet (DeNiro and Epstein, 1978); thus, isotopic analyses of animal tissues can be used to determine aspects of dietary history.

Ambrose and Norr (1993) showed that the $\delta^{13}C$ of collagen depends primarily on the $\delta^{13}C$ of the protein portion of the diet, but that it is also influenced by the isotopic composition of carbohydrates and lipids. The $\delta^{13}C$ of carbonate in hydroxyapatite more closely represents the isotopic composition of bulk diet (Ambrose and Norr 1993). For large ungulates, the diet to enamel (carbonate in hydroxyapatite) enrichment of ^{13}C is about +14.1 ‰ (Cerling and Harris, 1999), while that for diet to collagen is about +5 ‰ (Sullivan and Krueger, 1981). Using these offsets, the carbon isotopic composition of collagen and carbonate in hydroxyapatite can be used to determine the isotopic composition of both the bulk diet and the (predominately) protein portion of the diet. Shifts in the isotopic composition of diet can be tracked by serially sampling a structure that grows by accretion, such as a tusk.

The conditions of the arctic limit the possible causes of variation in $\delta^{13}C$. C_4 plants are generally absent where the mean minimum temperature in the growing season is less than 8 – 10°C (Long, 1983). Furthermore, in an isotope study, Bocherens (2003) found no evidence for the inclusion of C_4 plants in the diets of herbivores of the mammoth steppe fauna of northern Europe, Siberia, and Alaska. Any variation in $\delta^{13}C$ of arctic mammoth dentin is likely to result from either environmentally mediated differences in isotopic composition of C_3 plants, or physiological changes occurring in mammoths. Bocherens (2003) reviewed those factors (excluding photosynthetic pathway) affecting the isotopic composition of plants. More negative plant $\delta^{13}C$ is associated with low light, lower temperature, and low nutrient availability, while more positive (less negative) values are associated with water stress and saline stress. Physiological factors include utilization of isotopically light (DeNiro and Epstein, 1977) fat reserves. Use of these fat reserves might lead to depleted $\delta^{13}C$.

Interpretation of variation is complicated in the case of analyses performed on dentin from juveniles as their diets consist of a vegetation component and a milk component. Furthermore, the isotopic composition of milk could vary due to dietary and physiological factors in the mother. Although weaning age may have varied, mammoths probably nursed for three to six years based on data from African elephants (Lee and Moss, 1986) and previous isotope studies (Rountrey et al. 2007). Juvenile elephants are completely dependent on milk in the first three months of life (Lee and Moss, 1986). The relative importance of milk in the diet of juvenile elephants

decreases thereafter, with nutritional independence being reached at about 24 months (Lee and Moss, 1986).

There may also be seasonal variation in the contribution of milk to total diet (this dissertation, Chapter 3). African elephant milk is composed of (by weight) approximately 79.7 % water, 9.4% fat, 5.1 % protein, 3.7 % lactose, and 0.74% ash (McCullagh and Widdowson, 1970). Milk fat is depleted in ^{13}C relative to other components of the organism (Polischuk et al. 2001). Ingestion of significant amounts of milk fat, and its utilization as an energy source, could lead to more negative values in $\delta^{13}C_{carb}$ in the calf (e.g., Hobson and Sease, 1998). $\delta^{13}C_{col}$ might also be depleted if carbon from milk lipids is incorporated into proteins (Newsome et al. 2006). In cattle, milk fat is depleted in ^{13}C versus diet (~ -1.9 ‰), but the protein casein is enriched (~ +1.8 ‰) (Wilson et al. 1988). If little carbon from fat is incorporated into collagen, $\delta^{13}C_{col}$ might be enriched when milk is a primary protein source versus when vegetation is the primary food source.

$\delta^{15}N$

Because of tissue enrichment that occurs at each trophic level (Schoeninger and DeNiro, 1984), $\delta^{15}N$ of collagen (and other tissues such as hair) has often been used to determine the trophic level of organisms. In addition, enrichment in ^{15}N has been associated with nutritional stress (Hobson et al., 1993; Mekota et al., 2006;), water stress (in drought-tolerant herbivores) (Ambrose and DeNiro, 1986), and differences in N isotopic composition of diet. In particular, young individuals feeding on their

mothers' milk often have higher collagen $\delta^{15}N$ than they do after weaning because they effectively feed one trophic level higher than a mature individual of their species (e.g., Hobson and Sease, 1998; Newsome and Koch, 2006).

In addition to possible enrichment of $\delta^{15}N$ due to milk intake or nutritional stress, the types of plants eaten (by the calf or its lactating mother) may also lead to variation in collagen $\delta^{15}N$. Schulze et al. (1994) found that, in northern Alaska, $\delta^{15}N$ was different in different plant types. The values of $\delta^{15}N$ were ordered, tree<dwarf shrub<grass (Schulze et al., 1994). Similarly Michelsen et al. (1996) observed that non-mycorrhizal monocots (mostly grasses) had higher $\delta^{15}N$ than ericoid mycorrhizal dicots (dwarf shrubs) and ectomycorrhizal dicots (shrub, dwarf shrub, forb) in the subarctic of Sweden. They attribute the differences to utilization of different nitrogen sources (Michelsen et al., 1996). Thus, if mammoth plant preferences changed seasonally, one might expect to observe seasonal variation in $\delta^{15}N$.

Nutritional stress may also be an important factor affecting $\delta^{15}N$ in mammoths. The enrichment in $\delta^{15}N$ that occurs during nutritional stress is a result of the increased relative contribution of nitrogen from catabolized body proteins to the nitrogen pool available for protein synthesis during starvation (Hobson et al., 1993). Recovery from nutritional stress results in decreasing $\delta^{15}N$ (Mekota et al., 2006). In the case of nursing juveniles, nutritional stress in either the mother or the calf (or both) might lead to elevated $\delta^{15}N_{col}$.

$^{\delta 18}O$

The $\delta^{18}O$ of body water in herbivorous mammals is mostly dependent on the $\delta^{18}O$ of surface water (Kohn, 1996). Carbonate in the hydroxyapatite of mineralized tissue forms in isotopic equilibrium with body water (Iacumin et al., 1996). The majority of oxygen taken in by an herbivore is in the form of free water in food and drinking water, the compositions of which are related to the composition of surface water (Kohn, 1996). As meteoric water is often seasonally variable in its isotopic composition (Gat, 1996), and drinking water (and plant water) is generally derived from local meteoric water, the $\delta^{18}O$ of serial samples of mineralized structures that grow by accretion can exhibit seasonal-scale variation (Koch et al., 1989).

The general movement of moisture over Siberia in the present is from west to east with progressive rainout leading to progressively depleted $\delta^{18}O$ of meteoric water from west to east during the winter. Subarctic, eastern, coastal sites are less depleted than one would expect given this pattern due to the influence of other vapor sources (Kurita et al., 2004). In summer, moisture from terrestrial sources exerts a strong influence on the isotopic composition of precipitation (Kurita et al. 2004). Nevertheless, seasonal patterns in $\delta^{18}O$ of meteoric water at a single location vary in a similar manner to that noted by Koch et al. (1989), with more depleted values occurring in the winter, and more enriched values in the summer (Fig. 4.2). In this study, we are primarily interested in the seasonal variation in $\delta^{18}O$ and its use in determining the season in which variations in other compositional variables occur.

Despite the consistent seasonal pattern in meteoric water, there are complications associated with permafrost and snow melt. In a study of plant water

sources conducted near Yakutsk, Yakutia, Russian Federation, the presence of permafrost and snow melt were shown to be factors affecting plant water source (Sugimoto et al., 2002). Early in the growing season (late May – early June), much of the water taken up by plants is derived from snow melt, which has a depleted oxygen isotope composition (~ -32.0 ‰) relative to spring/summer rain (~ -15 ‰) (Sugimoto et al., 2002). As a result, plant (stem) water composition is lowest in early June, and then gradually becomes more enriched through August (Sugimoto et al., 2002). In years with little rainfall, soil water ($\delta^{18}O$ ~ -24 ‰) appears to make a larger contribution to plant water, resulting in a damped seasonal pattern and more depleted summer plant $\delta^{18}O$ (Sugimoto et al., 2002). Presumably, at the end of the growing season, as temperatures begin to drop and soil begins to freeze, plant water with late summer/autumn enriched values becomes locked into plants, where it remains until the following growing season. This is evidenced by similarity in plant water $\delta^{18}O$ in mid-May and August (Sugimoto et al., 2002). For an herbivore, free water in food makes up a larger proportion of the oxygen intake than drinking water (Kohn, 1996); thus, one might expect seasonal $\delta^{18}O$ patterns to follow those observed in plants.

During the summer, drinking water for Siberian mammoths could include water from large or small lakes as well as rivers and streams. In general, the pattern in $\delta^{18}O$ of water available for drinking is similar to that observed in plant water (Ichiyanagi et al., 2003; Sugimoto et al., 2002). However, possibly due to evaporative enrichment, some lakes show considerable enrichment through the summer (e.g.,

from -22.47 ‰ in May to -9.63 ‰ in August), while others show very little change (e.g., from -11.42 ‰ in May to -9.22 ‰ in August) (Ichiyanagi et al., 2003). River water $\delta^{18}O$ also increases through the summer, with values for the Lena River near Yakutsk rising from -21.32 ‰ in May to -17.62 ‰ in August.

Water could be obtained during the winter from plant water, snow, or ice. Plant water $\delta^{18}O$ during the winter might be similar to that which occurs in late summer/autumn, with perhaps some additional enrichment due to desiccation. The $\delta^{18}O$ of snow is much more depleted than summer precipitation and late summer plant water (Sugimoto et al., 2002), while the $\delta^{18}O$ of ice (i.e. frozen lake or river water) should be similar to late summer/ early autumn values. What the winter source of water for Siberian mammoths might have been may have depended on the relative availability of water from each of these possible sources.

There may also be some unique factors affecting $\delta^{18}O$ that apply to juveniles. Wright and Schwarcz (1998) suggested that, because milk is derived from body water, and body water is enriched in ^{18}O relative to drinking water, nursing infants might show higher $\delta^{18}O$ than weaned individuals. In their study they found $\delta^{18}O_{carb}$ in enamel was higher in younger individuals assumed to be nursing.

Mg/Ca

Mg concentration or Mg/Ca ratios have been used as paleodietary indicators of vegetation in diet because the concentration in plant foods is higher than the

concentration in animal foods (Klepinger, 1984). Mg levels in bone (and presumably dentin) are correlated with dietary levels (Miller et al. 1965), but Klepinger (1990) suggests this may only be true in cases of extreme dietary deficiency or excess. Mg/Ca in African elephant milk is about 1/5 the ratios in plants (McCullagh and Widdowson, 1970; Holdo, 2003). In a study of a juvenile African elephant tusk, Mg/Ca was observed to increase with age and vary seasonally, possibly indicating the seasonal and long-term shifts in the relative importance of milk in the diet (this dissertation, Chapter 3). Though increasing Mg/Ca may be an indicator of weaning, the susceptibility of Mg in dentin to diagenetic loss makes its interpretation difficult in fossil materials (this dissertation, Chapter 3).

Mn/Ca

Mn occurs at low concentrations in modern enamel and at concentrations ~2 to 3 orders of magnitude greater in fossil enamel and dentine (Kohn et al. 1999). Furthermore, in apparently unaltered dentin from a modern African elephant, Mn/Ca was ~ 0.003 mmol/mol, while slightly altered dentin in the same tusk had a value of 1.026 mmol/mol (this dissertation, Chapter 3). In this study Mn/Ca is used as an indicator of diagenesis.

Fe/Ca

Similar to Mn, Fe occurs at low concentrations in modern enamel, but at concentrations several orders of magnitude higher in fossil enamel and dentin (Kohn

et al., 1999). Fe/Ca in unaltered modern African elephant dentin is about 0.5 mmol/mol and three times higher in apparently altered dentin in the same tusk (this dissertation, Chapter 3). Fe/Ca can be used as an indicator of diagenesis, but Fe/Ca in unaltered specimens may also have some sensitivity to changes in juvenile diet. The Fe concentration in milk is low, and infants use reserves accumulated during gestation for most early red blood cell synthesis (Dewey et al., 1998). With decreasing importance of milk in the diet, available Fe may increase and lead to higher Fe/Ca in the dentin, although there is little previous work on how Fe status affects dentin Fe/Ca.

Cu/Ca

A variety of factors can influence plasma or serum copper levels including food intake, age, pregnancy/hormonal changes, and locality (Sarkar, 1994). In humans, serum copper is low at birth, rises in the first month, decreases in the second month, then rises to steady values similar to adults by three to eight months (Sarkar, 1994). A similar pattern occurs in pigs in which serum Cu levels increase from birth to three weeks of age (Ullrey et al., 1967). Low serum Cu has also been associated with nutritional stress (Barboza and Reynolds, 2004). This suggests that identification of a pattern in dentin might allow identification of birth/infancy or nutritional stress. However, it is not known if the pattern that occurs in serum would also be seen in dentin.

Zn/Ca

Zn has been used in paleodietary studies as a means of determining carnivory versus herbivory (reviewed by Ezzo, 1994). In this study, we are primarily concerned with one pattern that has been observed in many studies. Serum Zn concentrations increase through gestation (Jeswani and Vani, 1982), with the rate of accumulation accelerating in late pregnancy (Dauncey et al., (1977). Furthermore, Zn concentrations in human milk are highest in the early stages of lactation and decrease thereafter (Vuori and Kuitunen, 1979). Based on these studies, it is hypothesized that Zn/Ca in dentin might show a marked high around the time of birth. Indeed, in a study of human enamel, Ca-normalized Zn concentration was elevated around the neonatal line (a prominent incremental feature marking the time of birth in enamel) (Kang et al., 2004). Drzaga et al. (2007) observed significant decreases in bone Zn/Ca in 7 to 28 day old rats, and Ando-Mizobata et al. (2006) showed that Zn/Ca in the dentin of Steller sea lions was high in the first year of life and then decreased and showed little variability after. Evans et al. (1995) also found the highest concentrations of Zn in the earliest-formed cementum of walrus teeth. Based on these studies, it is hypothesized that if this early period in development is recorded in the tusks of juvenile mammoths, Zn/Ca will show a peak early in the record that represents the late gestation/neonatal period. In a study of a juvenile African elephant tusk, there was no pattern in Zn/Ca that would corroborate this hypothesis (this dissertation, Chapter 3), but it is not known if the pattern was absent due to formation of the tusk after birth (suggested by the absence

of a neonatal line), or failure of the dentin to record the changes in systemic Zn concentration.

There is also a possibility that Zn/Ca will show seasonal patterns. Dufty et al. (1977) observed seasonal variation in plasma Zn in cattle, in which high levels were associated with the season of rapid pasture growth.

Sr/Ca

Because Sr is discriminated against in the guts of terrestrial vertebrates, Sr/Ca has been used to determine trophic level (Sr/Ca decreases with increasing trophic level) (reviewed by Sillen and Kavanagh, 1982). Sr/Ca has also been used to identify nursing and weaning as Sr is discriminated against relative to calcium during absorption by the mother, and then again in milk production (reviewed in Sillen and Kavanagh, 1982). Thus, one would expect low Sr/Ca in the tissues of nursing infants.

However, use of this system is complicated by the fact that discrimination against Sr in the digestive system of infants and children increases with age (reviewed in Sillen and Kavanagh, 1982). In a study of a juvenile African elephant, no long-term trend in Sr/Ca was observed. However there was some seasonal variation with higher dentin Sr/Ca occurring in the dry seasons (this dissertation, Chapter 3). Sr/Ca is also dependent on soil Sr and Ca concentrations (reviewed by Sillen and Kavanagh, 1982). So, feeding in areas with different Sr/Ca during different seasons could account for the apparent seasonal variation observed in the elephant.

Ba/Ca

Ba behaves similarly to Sr, with increasing discrimination with age (Taylor et al. 1962) and decreasing Ba/Ca with trophic level (Pate, 1994). Trends in Ba/Ca in tusks are expected to be similar to Sr/Ca, although this pattern was not observed in the juvenile African elephant studied in this dissertation (Chapter 3). In this animal, Ba/Ca was positively correlated with $\delta^{13}C_{col}$, which varied seasonally (higher in the rainy season) (this dissertation, Chapter 3). This may indicate that Ba/Ca of soils and plants in the seasonal feeding areas differed.

P/Ca

P/Ca is included as an indicator of diagenetic alteration. In unaltered dentin from a juvenile African elephant tusk, the P/Ca averaged 795.76 ± 58.57 mmol/mol and increased with age (this dissertation, Chapter 3). P/Ca was positively correlated with Mg, which, compared to other analyzed elements, occurred in high concentrations in the dentin (this dissertation, Chapter 3). As Mg substitutes for Ca in the hydroxyapatite lattice, the changes in P/Ca were attributed to changes in Mg/Ca.

Pb/Ca

Pb/Ca shows increases from prenatal to postnatal enamel in humans (Dolphin et al., 2005). If this change is due to differential transfer of Pb across the placenta versus through milk, this change in concentration may also occur in mammoths. The increase might mark the time of birth. Pb was generally below detection in the

analysis of a juvenile elephant, and no trends in Pb/Ca were observed (this dissertation, Chapter 3).

Materials and Methods

The tusks of five juvenile woolly mammoths from Siberia are included in this analysis. The sample set includes one tusk recovered from Wrangel Island, two tusks from Bolshoi Lyakhovskii Island, one from Oimyakon, and one of unknown geographic origin (Fig 4.3).

Oimyakon

In 2004, a partial carcass of a mummified mammoth calf was recovered from the Ol'chan Mine in the Oimyakonskii region, Yakutia, Russian Federation (Boeskorov et al., 2007) (Fig. 4.3). The carcass, which has been dated to 41300 ± 900 years before present (Boeskorov et al., 2007), consists of the head and the anterior portion of the thorax (Fig. 4.4). DNA analysis indicates the sex as male (H. Poinar, pers. comm.). At the time of discovery, the carcass was damaged by excavation equipment with one result being the separation of the premaxillae from the rest of the skull. Only the right premaxilla was recovered, and it was found to contain a small, unerupted permanent (I^2) tusk (Fig. 4.5). No deciduous tusk was present. The darkly-stained permanent tusk (Fig. 4.6) is 7.6 cm in length, with a maximum circumference of 5.9 cm at the apical margin (i.e., the proximal margin; there is some splaying of the tusk near this margin, and the maximum circumference may be closer to 5.5 cm). The circumference 1 cm

from the tip is 3.2 cm. The length of the pulp cavity is 5.5 cm measured along the tusk axis.

The enamel of the tusk is relatively intact just proximal to the tip, but it has spalled off of the dentin in many places (Fig 4.6). The margin of the original extent of enamel, which extends further ventrally than dorsally, is marked by a change in dentin surface texture. A thin layer of cementum is present only near the apical end of the tusk (Fig. 4.6) and is, in most areas, less than 0.25 mm thick. Of particular interest in this specimen is the presence of a prominent, annular ridge in the dentin surface and a change in the color of the dentin, which occur 4.2 cm from the tip (Figs. 4.6, 4.7). Upon first inspection it was hypothesized that this might be the surface expression of a neonatal line, a well-defined growth increment formed near the time of birth. Subsequent longitudinal sectioning revealed a well-defined growth line terminating at the ridge on the exterior surface (Fig. 4.8).

Boeskorov et al., (2007) estimate the age at death to be between 1 and 1.5 years based on body size, and tusk/tooth development. In the maxilla, dP^{3-4} are present, as are their counterparts in the mandible (Boeskorov et al., 2007). In addition, there is evidence of some development of M1. The dP3s show wear extending back to the penultimate plate (the dP_3s have eight or nine plates (Boeskorov et al., 2007)), and no wear is apparent on the developing dP4s (Boeskorov et al., 2007). Interplate cementum deposition in dP4 is complete only in anterior plates.

Bolshoi Lyakhovskii (MMY 7916)

The nearly complete skull and mandible of a mammoth calf were collected near the mouth of the Bolshoi Eterikan River on Bolshoi Lyakhovskii Island (New Siberian Islands, Yakutia, Russian Federation) (Fig. 4.3). The remains have been dated to 24700 ± 170 radiocarbon years before present (Mashchenko et al., 2005). Both permanent tusks are present. Only the left tusk (Fig. 4.9) is included in this study. The tusk measures 16.9 cm along the outside curve, although there is some breakage at the apical margin indicating that actual tusk length may have been closer to 17.2 cm. The circumference is about 7.2 cm at a position 15 cm from the tip. Cementum is present over the length of the tusk with the exception of the tip (Fig. 4.9).

Enamel is present on the unworn tip of the tusk, and this extends apically beneath the cementum. As in the Oimyakon tusk, the enamel extends further apically on the ventral surface of the tusk than the dorsal. In this tusk, the enamel extends back from the tip 4.1 cm dorsally, and 7.0 cm ventrally.

The occluding dentition includes dP3 and dP4, with both showing wear. Seven plates remain in the dP^3s, while six remain in the dP_3s. Six to seven anterior plates are in wear on the dP^4s, while six are in wear on the dP_4s. Based on tooth eruption and wear, and comparison to patterns in Asian elephants (Roth and Shoshani, 1988), the age at death for this individual would be between 2.5 and about 4.5 Asian-elephant-equivalent years.

Mol (UM 115960)

The specimen analyzed in this study (Fig. 4.10) is the right tusk of a pair recovered from Bolshoi Lyakhovskii Island. The tusk has not yet been dated. Along the outside curve, the length is 22.9 cm, with circumferences of 7.0, 7.4, 7.4, and 7.7 cm at positions 5, 10, 15, and 20 cm from the tip, respectively. The tusk retains enamel on the tip, although enamel at the tip and several millimeters apically shows some polish indicating that this portion of the tusk was probably erupted and exposed during life.

As on the other tusks described above, enamel is present beneath the cementum, and it extends further apically on the ventral surface than on dorsal surface. In this case, the dorsal enamel extends to 3.3 cm from the tip, while the ventral enamel extends to 6.9 cm from the tip.

44-M (UM 115961)

Specimen 44-M is the left tusk of a juvenile woolly mammoth that was collected near the Neizvestnaya River on Wrangel Island, Chukotka (Fig. 4.3). The isotopic compositions of collagen samples from this tusk were previously reported by Rountrey et al. (2007). This tusk has not yet been radiocarbon-dated.

The tusk measures 38.9 cm along the outside curve with an apical/proximal circumference of 11.7 cm and an abapical/distal circumference of approximately 7.3 cm. Cementum is present over the length of the tusk with the exception of the fractured/worn area near the tip (Fig. 4.11). Although enamel is present near the tip, much has been lost to spalling. The apicalmost enamel visible in this tusk is 2.9 cm from the (fractured/worn) tip and is located on the ventrolateral surface of the dentin.

Taking MMY 7916 and the Mol tusk as references, this indicates that approximately 4 cm of material may have been lost to breakage or abrasion.

In a study of a tusk from a juvenile African elephant, it was noted that an abrupt increase in the circumference of the tusk occurred at a distance from the apical margin that might suggest that the ramp indicated the position of the apical margin at the time of tusk eruption (this dissertation, Chapter 3). Tusk 44-M also shows an abrupt change in morphology 6.9 cm from the apical margin (Fig. 4.11), although in this case it appears as more of a lateral shift in the position of the previous apical margin. This may be due to stresses imposed on the tusk near the time of eruption. If this interpretation is correct, it implies that ~6.9 cm of the tusk was exposed during life, with ~32 cm contained within the alveolus.

Allen (UM 115959)

This specimen is a darkly-stained tusk fragment with breaks occurring both apically and abapically (Figs. 4.12A,B). No specific locality information is available for this tusk, although it is reported to have been collected in Russia. Due to fracture and loss, cementum covers less than half of the outer surface of the tusk (Figs. 4.12A,B). The fragment is 15.1 cm in length, and the circumference of the dentin core is 6.5 cm at 3 cm from the tip and 7.9 cm at 12.9 cm from the tip. No enamel is visible. The exposed dentin is marked by three dark bands that probably correspond to an annual occurrence such as the transition from winter to spring (Fig. 4.12A).

Cutting

A single procedure for cutting the tusks to gain access to interior dentin and for the production of thin sections was not possible due to differences in size, and also, for loaned specimens, permissions. Molds and casts of all tusks were produced to document original morphological features. In addition, three dimensional, digitized models were produced using either a Microscribe-3DLX (Immersion Corporation, San Jose) point digitizer and the software package Geomagic Studio 2.0 (Raindrop Geomagic, Inc., Research Triangle Park, NC) or a HandyScan 3D portable laser scanner (Creaform, Inc., Lévis, Québec, Canada).

The loan requirements for the Mol, Oimyakon, and Bolshoi Lyakhovskii tusks allowed removal of material from only one half of the tusk. These tusks were first cut longitudinally using a low speed band saw or, in the case of the Oimyakon tusk, an Isomet low speed diamond wafering saw (Buehler, Lake Bluff, Illinois). Subsequent transverse cuts were made with the Isomet. The Allen tusk was also first cut longitudinally, and transverse cuts were made on one half of the tusk. The cutting procedure for the 44-M tusk is described in Rountrey et al. (2007).

Thin Sections and Analysis of Increments

Thin sections of transverse or longitudinal surfaces were made from the transversely cut segments such that each growth increment present in a tusk, aside from those located in the tusk tip, was visible in at least two thin sections. This allowed correlation of growth increments among sections and the construction of a

complete series of growth increment thicknesses. Thin sections were cut using the Isomet, and the slides were subsequently ground and polished to ~50 μm in thickness.

Second-order increment thicknesses were measured using a petrographic microscope and either OPTIMAS image analysis software, or ImageJ (Rasband, 1997-2008) and a custom plugin (this dissertation, Chapter 3).

Compositional Sampling

Samples for analysis of isotopic and elemental composition were taken from the Mol and Bolshoi Lyakhovskii tusks as outlined in Chapter 3 (this dissertation). A 0.5-mm carbide burr was used. The procedures differed for extraction of the samples from 44-M, Oimyakon, and Allen.

In the 44-M and Allen tusks, transverse surfaces from which thin sections had been produced were milled using a milling station consisting of a fixed dental drill with a 1-mm-diameter diamond bit and adjustable stage. Milling followed the alternating pattern described in Chapter 3 (this dissertation) such that both block and powder samples were available from each sampled interval.

The small size of the Oimyakon tusk, and its condition required that different techniques be utilized. Particularly near the tip of the tusk, there is insufficient material to permit the alternating milling pattern described in Chapter 3 (this dissertation). However, the dentin of this tusk contains many concentric fractures that propagate along prominent second-order features, and these fractures often extend for some length along the tusk allowing correlation of fractures in different transverse

segments. These fractures isolate blocks of dentin representing fixed intervals of time. Near the tip, blocks of dentin bordered by fractures were extracted using a scalpel and forceps. The specific growth increments contained in these blocks could be determined by noting the bounding fractures and correlating them to fractures visible in the thin sections. Powder samples were obtained by milling with a fixed dental drill and 0.5-mm carbide burr. In addition, some alternating block/powder samples were taken further from the tip of the tusk.

In all tusks, the locations of samples were recorded by taking high resolution (1600 dpi) scans of the surfaces of segments before and after removal of each sample. Images obtained during analysis of thin sections, which contain marked and numbered second-order increments can be digitally overlaid on these scans to allow determination of which second order increments are included in each sample.

Isotope Analysis- $\delta^{13}C$ and $\delta^{18}O$ in CO_3

Pretreatment procedures are different for 44-M versus other tusks because this tusk was analyzed before results from a pretreatment effects study (this dissertation, Chapter 2) were available. For 44-M, powder samples of around 10 mg were weighed into 15-mL centrifuge tubes and 0.08 mL/mg of 3% NaOCl was added. After 24 hours, samples were centrifuged and the supernatant was removed. Samples were rinsed five times in ultrapure water and 0.08 mL/mg of 1.0 M acetic acid/1.0 M Ca-acetate (pH ~4.6) was added to each sample. After 24 hours, the supernatant was removed. Samples were rinsed five times in ultrapure water and then allowed to dry at room

temperature for several days. 1-mg subsamples were taken and loaded into small stainless steel cups and roasted at 200 °C for 1 hour before loading into glass vessels for the Kiel. Samples were analyzed on a Finnegan Kiel-IV coupled to a Thermo MAT 253 isotope ratio mass spectrometer in the Stable Isotope Lab, Department of Geological Sciences, University of Michigan.

A different procedure was used for the Oimyakon and Bolshoi Lyakhovskii [to be completed July 10] tusks. 6-mg or 4-mg powder samples were weighed into 1.5 mL microcentrifuge tubes, and 0.08 mL/mg of 30% H_2O_2 was added (caps were left open). After 24 hours, samples were centrifuged and the supernatant was removed. Samples were rinsed five times with ultrapure water, and then 0.08 mL/mg of 1.0 M acetic acid/1.0 M Ca-acetate was added. The samples were allowed to sit for 24 hours (caps open), after which they were centrifuged, rinsed five times, then freeze-dried. After this step, preparation and analysis were identical to the procedure described above for the 44-M tusk.

Isotope Analysis- $\delta^{13}C$ and $\delta^{15}N$ in Collagen

Approximately 10 mg (in some cases, less than 10 mg was available) of each block sample was weighed and placed in a baked (550° C overnight) glass scintillation vial. To each sample, 10 mL of 0.5 M HCl was added, and vials were placed in a refrigerator at 4° C for about 36 hours (until the collagen block was translucent and flexible). The collagenous blocks remaining after demineralization were rinsed five times with 10 mL of ultrapure water. In order to remove lipids from the blocks, 10 mL

of 2:1 chloroform-methanol was added to each vial, and the vials were placed in an ultrasonicator for 30 minutes. The chloroform-methanol was discarded and samples were rinsed five times with 10 mL of ultrapure water. Samples were then freeze-dried and weighed. Sub-samples of 1.5 ± 0.1 mg were loaded into pressed silver capsules and analyzed for $\delta^{13}C$ and $\delta^{15}N$ at the Isotope Ratio Mass Spectrometry Laboratory, University of California, Santa Cruz.

Elemental Concentrations

1.0-mg powder samples were weighed into metal-free 1.5 mL microcentrifuge tubes (pre-weighed). 0.5 mL of ultrapure water was added to each tube. Tubes were agitated, and left to sit for < 30 minutes. Following centrifugation and removal of the supernatant, samples were freeze-dried overnight and re-weighed. 1.0 mL of 0.5 M TraceMetal grade HCl was added to each tube, and samples were refrigerated at 5 ^{o}C for 24 hours. Tubes were then centrifuged, and the supernatant was removed for analysis. The remaining collagen was rinsed, centrifuged, freeze-dried, and weighed.

The subsamples of solutions were diluted with 1% HNO_3 (1ppb In internal standard) to target Ca concentrations between 10 and 14 ppm, and analyzed using a Finnegan Element ICP-MS.

Statistical Analysis

In order to assess the relationships among compositional variables, we use sample cross-correlations. The technique is described in detail in Chapter 3 (this dissertation). Cross-correlation varies between -1 and 1 and provides a measure of

similarity or dissimilarity between two time series at a series of lags or time offsets. Significance was assessed using a bootstrapping technique, and non-stationary series were detrended by taking residuals from a cubic spline (d.f. = 4) fit to the series. The temporal position of each sample was defined by the mean increment number contained within the sample. All series (including resampled series for bootstrapping) were spline-interpolated (R Development Core Team, 2008) to second-order increment resolution.

In two cases, two compositional samples in tusks had overlap in the increments covered in the samples such that the average increment contained in the samples was identical. To avoid problems with spline-interpolation, sample 7 of the 44-M series, and sample 7 of the Mol series (see Appendices 4A, B) were removed and not included in the cross-correlation analyses (though they do appear in the plotted compositional data). Additionally some $\delta^{13}C_{col}$ and $\delta^{15}N_{col}$ data were interpolated (cubic spline) for samples lost during analysis. In some cases, data were interpolated so that the average increment contained in the collagen samples would match the average increment contained in samples used for determination of $\delta^{18}O_{carb}$, $\delta^{13}C_{carb}$, and elemental ratios (Appendix 4A).

Second-order increment thicknesses were also included in the cross-correlation analysis. In order to produce a series of the same temporal resolution and number of data points as the compositional series, a series of means of the second-order increment thicknesses of increments contained within each compositional sample was used.

Original data series were tested for the presence of long-term trends by assessing the significance of least squares regressions (R Development Core Team, 2008) of the variable of interest on increment number. Regressions with p-values less than 0.05 were considered significant.

Results

44-M

There are 246 second-order increments present in the tusk with a mean thickness of 0.13 mm (s.d. = 0.06). Assuming a second-order increment periodicity of 7 days, the dentin in the tusk represents 4.7 years of life. No neonatal line is visible in the dentin.

Isotope and elemental data are plotted in Figures 4.13A-N. The $\delta^{15}N_{col}$ and $\delta^{13}C_{col}$ data were previously reported in Rountrey et al. (2007). The $\delta^{15}N_{col}$ series (Fig. 4.13B) shows a significant negative slope ($p = 0.008$) with a superimposed seasonal-scale fluctuation in values. No other isotope series from this individual have significant regressions. The $\delta^{13}C_{col}$ series (Fig. 4.13A) also shows seasonal-scale fluctuations and is strongly positively correlated ($p < 0.001$) with detrended $\delta^{15}N_{col}$ with a lag of +2 second-order increments (e.g., peaks in $\delta^{15}N_{col}$ occur slightly after peaks in $\delta^{13}C_{col}$) (Table 4.1). $\delta^{18}O_{carb}$ also has apparent seasonal-scale cyclicity (Fig. 4.13C) and is positively correlated with $\delta^{13}C_{col}$ (lag = -5) and strongly negatively correlated with Sr/Ca (lag = +2) (Table 4.1).

The detrended $\delta^{13}C_{carb}$ series is correlated with $\delta^{13}C_{col}$ (lag = -2) (Table 4.1) as might be expected based on previous studies (this dissertation, Chapter 3), but the original series has an unusual pattern with higher values occurring early and late in life (Fig. 4.13D). The inverse of this pattern is observed in Mg/Ca (Fig. 4.13E), and the detrended series also have a highly significant negative correlation (lag = -1) (Table 4.1).

The Mg/Ca, Ba/Ca, and P/Ca series (Figs. 4.13E, L, F) exhibit patterns that may be linked in their origin. In the raw data, it is observed that Mg/Ca and P/Ca have low values in early samples and also in the samples taken near the pulp cavity (late in the series). Conversely Ba/Ca is high in early and late samples, and low between. The detrended Ba/Ca series is also negatively correlated with detrended Mg/Ca (lag = -2) (Table 4.1). Similarly, although many samples were below detection limits, Mn/Ca is higher in the earliest and latest samples (Fig. 4.13G), and Fe/Ca is high in the latest sample (Fig. 4.13H).

Detrended Cu/Ca is positively correlated with detrended $\delta^{13}C_{carb}$ (lag = +4) and negatively correlated with detrended Mg/Ca (lag = +2) (Table 4.1). The Zn/Ca series is not correlated with any other series (Table 4.1), but one sample has an unusually high value relative to others in the series (Fig. 4.13J).

The second-order growth increment profile for this individual does not show seasonal-scale patterns (Fig. 4.14), and the detrended series is not correlated with any other series (Table 4.1).

Mol

There are 164 increments present in the dentin of this tusk with a mean thickness of 0.13 mm (s.d. = 0.04). Assuming 7-day periodicity for second-order increments, the dentin of this tusk records 3.2 years of life. No neonatal line is present in the dentin.

Compositional data are shown in Figures 4.15A-L. The $\delta^{15}N_{col}$ series from this individual generally declines through life (negative regression slope, $p < 0.001$) (Fig. 4.15). Seasonal-scale fluctuations are not apparent in $\delta^{15}N_{col}$ (Fig. 4.15B) although they do appear in $\delta^{13}C_{col}$ (Fig. 4.15A). Both Sr/Ca and Ba/Ca also exhibit seasonal-scale variation (Figs. 4.15I, J). These series are strongly positively correlated with each other (Table 4.2), but of these, only Ba/Ca is correlated with $\delta^{13}C_{col}$ (as the sample set for elemental analysis included three early samples on which collagen isotopic analyses were not conducted, all cross correlation caluculations were conducted on only the overlapping time represented) (Table 4.2).

Both Mg/Ca and P/Ca have significant ($p < 0.001$) positive slopes, with values generally increasing through time (Figs. 4.15C, D). Detrended P/Ca is not correlated with any other series (Table 4.2), but detrended Mg/Ca is positively correlated with Zn/Ca (lag = +1) (Table 4.2).

The growth increment profile (Fig. 4.16) for this individual does not show obvious seasonal-scale patterns, though there are lows in the series that appear to occur with near annual periodicity. The series is positively correlated with Sr/Ca (lag = -6) (Table 4.2).

Bolshoi Lyakhovskii

There are 119 increments present in this tusk with a mean thickness of 0.10 mm (s.d. = 0.03). Assuming an increment periodicity of 7 days, the dentin in this tusk records 2.3 years of life. No neonatal line is present in the dentin.

Compositional data are plotted in Figures 4.17A-N. The $\delta^{15}N_{col}$ and $\delta^{13}C_{col}$ series (Figs. 4.17B, A) show significant declines over the time recorded in this tusk ($p < 0.001$). $\delta^{13}C_{carb}$ increases significantly with time ($p < 0.001$), while $\delta^{18}O_{carb}$ decreases significantly with time ($p = 0.003$). Seasonal-scale variation is apparent in $\delta^{13}C_{col}$ and $\delta^{18}O_{carb}$ (Figs. 4.17A, C) and may occur in $\delta^{15}N$ in the earliest ~80 second-order increments, although the pattern is damped by the declining trend (Fig. 4.17B). The detrended $\delta^{15}N_{col}$ and detrended $\delta^{13}C_{col}$ series are not correlated (Table 4.3), but the patterns appear similar until around increment 100, at which point the series diverge (Figs. 4.17A, B). Detrended $\delta^{13}C_{col}$ is positively correlated with detrended Mg/Ca. Detrended $\delta^{15}N_{col}$ is positively correlated with detrended $\delta^{18}O_{carb}$ and detrended $\delta^{13}C_{carb}$. There are also positive correlations with detrended P/Ca and Cu/Ca. Detrended $\delta^{15}N_{col}$, detrended $\delta^{13}C_{col}$, and detrended $\delta^{18}O_{carb}$ are negatively correlated with second-order increment thickness (Table 4.3). $\delta^{18}O_{carb}$ is also positively correlated with Ba/Ca (Table 4.3).

From second-order increment ~40 on, Ba/Ca appears to vary at a seasonal scale (Fig. 4.17L). In contrast, Sr/Ca steadily increases through time ($p < 0.001$) and plateaus around increment 60 with a slight decrease in values near the end of life (Fig. 4.17K).

Mn and Fe were below limits of detection for most samples, but in both Mn/Ca and Fe/Ca the final samples have much higher values than others in the respective series (Figs. 4.17G, H). Pb was detectable in many samples, and there is a tailed peak that occurs midway through the series (Fig. 4.17M). As observed in the 44-M data, the Zn/Ca series contains one sample for which the value is an order of magnitude higher than others, although in this case, the spike occurs quite early in the series (Fig. 4.17J).

The growth increment profile (Fig. 4.18) dips slightly from around increment 60 to increment 90, suggesting a reduced growth rate during this time.

Allen

There are 132 second-order growth increments present in this tusk with a mean thickness of 0.16 mm (s.d. = 0.04). Assuming a periodicity of seven days for second-order increments, this tusk records 2.5 years of life. No neonatal line is present in the dentin.

Compositional data are plotted in Figures 4.19A-L. Both $\delta^{13}C_{col}$ and $\delta^{15}N_{col}$ show seasonal-scale variations and no long-term trends (Figs. 4.19A, B). These series are negatively correlated with high significance (lag = -2 for detrended $\delta^{13}C_{col}$ vs $\delta^{15}N_{col}$, $p < 0.001$) (Table 4.4).

No seasonal patterns are apparent in elemental data (Figs. 4.19C-K), and only Mg/Ca (Fig. 4.19C) shows a marginally significant long-term trend (positive, $p = 0.04$). However, there are four highly significant ($p < 0.001$) correlations in element pairs. Sr/Ca is positively correlated with detrended Fe/Ca (lag = 0), Zn/Ca and Cu/Ca are

positively correlated (lag = 0), and detrended Mg/Ca is positively correlated with Zn/Ca and Cu/Ca (lags = 0) (Table 4.4). In the case of Mg/Ca, high significance of the correlations is achieved only when the Mg/Ca series is resampled in the bootstrap p-value calculation, and not when Zn/Ca or Cu/Ca are resampled (Table 4.4).

Second-order increment thickness (Figs. 4.19L, 4.20) is positively correlated with detrended $\delta^{13}C_{col}$ (lag = +5), Sr/Ca (lag = -5), and detrended Ba/Ca (lag = -4), and negatively correlated with detrended P/Ca (lag = +2) and detrended Mn/Ca (lag = +4) (Table 4.4).

Oimyakon

This tusk contains 75 second-order increments with a mean thickness of 0.08 mm (s.d. = 0.03), although second-order increments were difficult to identify near the tip. Assuming a periodicity of seven days, the dentin of this tusk records 1.4 years of life. A neonatal line is present in the dentin. There are 32 second-order increments from the neonatal line to the pulp cavity indicating an approximate age at death of 32 weeks (7.4 months).

Compositional data are plotted in Figures 4.21A-N. As the data series from this tusk were short (n = 8), no cross-correlations were calculated for this specimen. Furthermore, seasonal patterns are difficult to discern because little over 1 year of growth is represented in this tusk. The $\delta^{18}O_{carb}$ series may show a seasonal pattern with less than 2 cycles completed by the end of the series (Fig. 4.21C), but an alternative interpretation is introduced in the discussion. Although damped by a

significant increasing trend ($p = 0.003$), $\delta^{13}C_{carb}$ may also show just under 2 cycles of variation (Fig. 4.21D). $\delta^{13}C_{col}$ and $\delta^{15}N_{col}$ patterns appear similar to each other with high values early, then dropping to lower values later in life ($\delta^{13}C_{col}$ also returns to higher values in the last sample) (Figs. 4.21A, B). In these series, less than 1 cycle– if the pattern would be cyclic– of variation is present.

Mg/Ca decreases with time ($p = 0.046$) and is highest in the sample just preceding the inferred neonatal line (Fig. 4.21E). Sr/Ca varies in such a way that the pattern may represent seasonal variation over 1 cycle (Fig. 4.21K), while variation in Ba/Ca might represent less than 1 cycle (Fig. 4.21L). The Mn/Ca and Fe/Ca series are similar, with both having a pronounced low following the inferred neonatal line (Figs. 4.21G, H). Zn/Ca peaks in the sample just after the neonatal line (Fig. 4.21J), while the Cu/Ca series has one sample with a high value early in the series (Fig. 4.21I).

Second-order increment thickness (Fig. 4.22) increases significantly ($p < 0.001$) over time.

Mean Values

Table 4.5 shows the mean values for compositional measures from each individual in this study and also from an analysis of the tusk of a juvenile African elephant (this dissertation, Chapter 3). It should be noted that mammoth samples were rinsed prior to elemental analysis, while elephant samples were not. Rinsing leads to substantial decreases (e.g., from 198.5 mmol/mol to 143.2 mmol/mol in a sample from the Bolshoi Lyakhovskii tusk) in Mg/Ca (Rountrey, unpublished data)

making only broad comparisons between mammoth and elephant Mg/Ca appropriate. Mammoth $\delta^{13}C_{col}$ values are all similar to, but somewhat more depleted than modern elephant values. $\delta^{15}N_{col}$ is around 9.5 for mammoths with the exception of the two tusks from Bolshoi Lyakhovskii Island (Bolshoi Lyakhovskii and Mol), which have more enriched values similar to that of the modern elephant.

$\delta^{18}O_{carb}$ data are available from only three mammoths. The mean values are quite different, with more depleted values in the Oimyakon and Bolshoi Lyakhovskii tusks versus the 44-M tusk. $\delta^{13}C_{carb}$ also differs among these individuals, with 44-M enriched by more than 4 ‰ over Oimyakon and Bolshoi Lyakhovskii. Due to these differences, the $\delta^{13}C_{carb} - \delta^{13}C_{col}$ is much greater in 44-M than in Oimyakon, Bolshoi Lyakhovskii, or the modern elephant.

The C/N ratios, which are used as a rough measure of collagen integrity are all similar and suggest minimal alteration of the collagen (DeNiro, 1985).

Mean Mg/Ca values of mammoth samples are lower than modern elephant, with the most darkly stained tusks (Oimyakon and Allen) having the lowest values. As previously mentioned, the mammoth samples were rinsed prior to analysis, and the elephant samples were not. Rinsing leads to decreases in Mg/Ca (Rountrey unpublished data). Mg/Ca in the Bolshoi Lyakhovskii, Mol, and 44-M tusks are actually more similar to the values from the modern elephant (based on a few unrinsed samples), but samples from Oimyakon and Allen that were not rinsed prior to analysis are less than 10 and 20 mmol/mol respectively. This indicates that much of the magnesium in those tusks was lost prior to collection.

Similarly, P/Ca is slightly lower in all mammoth samples versus modern elephant, and the Allen tusk has the lowest value. Fe/Ca and Mn/Ca are higher in mammoths than in modern elephant, with darkly stained tusks having the highest values. Sr/Ca is variable, but values are similar in mammoths and modern elephant. The same is true for Ba/Ca. Zn/Ca is similar in the elephant and all mammoths except Oimyakon, which has a high value. Cu/Ca is roughly similar among mammoths.

Discussion

Age at death

Seasonal-scale oscillations in $\delta^{13}C_{col}$ occur in all tusks with the exception of Oimyakon. Assuming that these oscillations are indeed seasonal, they can be used to assess the approximate number of second-order increments per year in these tusks and refine estimates of the ages at death for these individuals. The number of second-order increments between seasonal lows in $\delta^{13}C_{col}$ is assumed to be the number of second-order increments per year. One exception is the Bolshoi Lyakhovskii tusk for which the spacing between lows in the $\delta^{18}O_{carb}$ series was used. This spacing yielded more consistent agreement between the inferred boundaries of years and seasonal scale variation in $\delta^{18}O_{carb}$, Mg/Ca, Ba/Ca, and increment thickness for this individual.

Using these techniques, and assuming the tusk began accreting dentin around the time of birth, the ages (in years) at death for these mammoths are: 44-M, 5.15 (4.15 in tusk, ~1 year missing from tip); Mol, 3.95 years; Bolshoi Lyakhovskii, 1.97 years. The Allen tusk fragment has a fractured tip and no pulp cavity, so the number of

increments present has no bearing on the actual age at death of the individual. In this tusk, 2.9 years of growth are recorded. Apparent second-order increment periodicities using this method are: 44-M, 6.2 days; Mol, 8.8 days; Bolshoi Lyakhovskii, 6.0 days; Allen, 8.0 days.

As there is an independent age estimate for the Bolshoi Lyakhovskii individual based on cheek tooth eruption and wear, a comparison of the two estimates is appropriate for discussion. Using data from Roth and Shoshani (1988) the Bolshoi Lyakhovskii calf was estimated to be between 2.5 and 4.5 years old at the time of its death. The estimate based on growth increments and isotope oscillation (1.97 years) is somewhat lower. There are several hypotheses regarding this offset. 1) High variation in eruption/wear rates of the modern elephant sample. Roth and Shoshani (1988) note such variation and also question the accuracy of some "known" ages. 2) A slower progression of eruption and wear in captive elephants. Many of the known-age elephants included in the Roth and Shoshani (1988) dataset were captive. The diets of these animals are likely less abrasive than the natural diets of elephants or mammoths, which might lead to lower rates of wear in captive individuals. 3) The $\delta^{18}O_{col}$ oscillations are not seasonal.

While assessment of hypotheses 1 and 2 is beyond the scope of this work, hypothesis 3 can be evaluated. The coincidence of oscillatory scale among $\delta^{18}C_{col}$, $\delta^{15}N_{col}$, and $\delta^{18}O_{carb}$ in 44-M (Figs. 4.13A, B, C), the individual for which the longest record is available, suggests that these are recurrent fluctuations that occur with approximately equivalent temporal spacing (based on number of second-order

increments and total thickness of accreted dentin). Seasonal changes are the most likely causes of these patterns.

A regression of age on $\log_{10}$ proximal (apical) tusk circumference for the four complete tusks in this study is significant only at the 0.10 level ($r^2 = 0.78$, $p = 0.077$). Additional data points are needed, but the preliminary equation, which could be used to approximate the ages of juveniles based on proximal tusk circumference is,

$$a = -10.424 + 14.9 \times log_{10}(c)$$

where *a* is the age in years, and *c* is the circumference of the permanent tusk at the apical margin in centimeters. Application of this relationship for determining ages in limited both by the low number of data points used to calculate the regression, and apparent differences in the onset of tusk formation. Of the three tusks in this study with intact, enamel-covered tips, only one contains a neonatal line. This suggests two non-exclusive possibilities: 1) there is individual variation in the timing of initial mineralization (possibly sex specific), or 2) that the expression of the neonatal line varies in such a way that, in some individuals, it cannot be detected.

Diagenesis

The tusks in this study are in variable states of preservation. While all retain collagen with C/N similar to modern materials (Table 4.5), they differ in degree of staining. The Mol, 44-M, and Bolshoi Lyakhovskii tusks exhibit little staining with the

exception of tips and pulp cavities. Thus, one might predict that these tusks are less likely to contain contaminating materials. Indeed, Fe/Ca and Mn/Ca are lower in these tusks than in the stained Oimyakon and Allen tusks, but the ratios are still greater than those observed in modern elephant (Table 4.5). Although mean Fe/Ca and Mn/Ca are higher in mammoth tusks than modern elephant, these values are largely influenced by the inclusion of a single high-value sample located either at the pulp cavity or the tip of the tusks. This implies that contamination with Fe- and Mn- oxides or hydroxides (Kohn et al., 1999) was largely limited to exposed dentin surfaces in these tusks.

The darkly stained tusks (Oimyakon and Allen) do not have high Fe/Ca and Mn/Ca only in exposed areas, but throughout the tusks (Figs. 4.19E,F, 4.21G, H). The one exception is Mn/Ca in the Allen tusk, which is higher near the (broken) tip (Fig. 4.19E). This suggests that the dentin of these tusks was, at some point in their diagenetic histories, completely saturated by diagenetic fluids facilitating the introduction of exogenous Fe and Mn (and possibly Ba (Kohn et al., 1999)) throughout the tusks. In addition, the Mg/Ca values of these specimens are quite low compared to other mammoth tusks and the modern elephant tusk (Table 4.5). Mg is quickly lost in diagenesis (Hola et al., 2008; this dissertation, Chapter 3).

To understand more fully the nature of diagenetic alteration of these tusks, one can examine the patterns in the 44-M tusk in more detail. High Mn/Ca and Fe/Ca are present only in samples taken near the pulp cavity (Mn/Ca is slightly elevated in the tip sample) (Figs. 4.13G, H), but other compositional profiles indicate partial alteration

concentrated near the tip and pulp cavity (i.e., the more exposed areas). In these areas, Mg/Ca and P/Ca are low (Figs. 4.13E, F), while Ba/Ca and $\delta^{13}C_{carb}$ are generally high (Figs. 4.13E, D). Although the detrended Mg/Ca and P/Ca series are not correlated (Table 4.1), the raw series show marked similarity. This suggests that loss of Mg and P are linked, which is reasonable considering the relatively high concentration of Mg in the dentin and its substitution for Ca in the apatite structure. Ba/Ca in the less altered middle portion of the tusk (Fig. 4.13L) is similar to Ba/Ca in the Mol (Fig. 4.15J) and Bolshoi Lyakhovskii (Fig. 4.17L) tusks. These two tusks show seasonal-scale variation in Ba/Ca; thus they are assumed to have been minimally altered. The higher Ba/Ca near the tip and pulp cavity of the 44-M tusk is assumed to result from diagenetic introduction of exogenous Ba.

The high $\delta^{13}C_{carb}$ of samples located in areas that appear to have been altered deserves consideration. High $\delta^{13}C_{carb}$ was also observed in the pulp cavity sample of modern elephant, which was assumed to have been altered (this dissertation, Chapter 3). Similar possible diagenetic enrichment of $\delta^{13}C_{carb}$ was observed by Koch (1989, unpublished dissertation). Interestingly, $\delta^{18}O_{carb}$ does not show evidence of spatially limited alteration other than a very slight increase in the amplitude of seasonal oscillation (Fig. 4.13C). A diagenetic mechanism that could alter $\delta^{13}C_{carb}$ without altering $\delta^{18}O_{carb}$ is unknown, but this pattern deserves further investigation.

Zn/Ca, Cu/Ca, and Sr/Ca in the 44-M tusk do not exhibit patterns of variation similar (or inverse) to the altered Mg/Ca, P/Ca, Ba/Ca, and $\delta^{13}C_{carb}$ series. This, and the similarity of mean values of these ratios in 44-M, apparently less altered tusks, and

modern elephant (Zn/Ca only) (Table 4.5) suggests that these ratios have not been greatly altered.

In the Allen tusk, the Sr/Ca and Fe/Ca series are similar, particularly in the first half of the series (Figs. 4.19I, F). As the pattern in Fe/Ca is likely the result of diagenetic alteration, this suggests that Sr/Ca values in this tusk have been altered. The Zn/Ca and Cu/Ca series are also very highly correlated (Table 4.4). This is not the case in any of the other tusks, and suggests that this pattern represents similar patterns of alteration of Zn and Cu concentrations.

Long-term Trends

As all of the tusks in this study, with the exception of the Allen tusk, are composed of dentin formed early in life, long-term, ontogenetic trends are expected. These are primarily associated with decreasing milk intake and increasing incorporation of vegetation in the diet. Expected trends associated with gradual weaning include decreasing $\delta^{15}N_{col}$, increasing Mg/Ca, Sr/Ca, and Ba/Ca. $\delta^{15}N$ is expected to be high early in life and later decline because the $\delta^{15}N$ of milk is enriched relative to vegetation (trophic level effect) (e.g., Hobson and Sease, 1998; Newsome and Koch, 2006). As vegetation progressively replaces milk in the diet, $\delta^{15}N_{col}$ should decrease. Sr/Ca and Ba/Ca are expected to be lower when a calf is feeding on milk because Sr and Ba are discriminated against relative to calcium by mammals (Sillen and Kavanagh, 1982; Pate, 1994). Thus, there is a trophic level effect similar to that which occurs in nitrogen. The Mg/Ca of milk is generally lower than the Mg/Ca of

plants (McCullagh and Widowson, 1970; Holdo, 2003), so there may also be an increase in Mg/Ca as more plant material is incorporated into the diet. This Mg/Ca pattern was observed in a juvenile African elephant in addition to a decreasing $\delta^{15}N_{col}$ in the first 1.5 years of life (this dissertation, Chapter 3). Sr/Ca and Ba/Ca do not increase with age in the juvenile elephant, but Sr/Ca in particular appears to vary in a seasonal manner over the last 2.5 years of life (this dissertation, Chapter 3).

All juvenile mammoths (Allen excluded) in this study show significantly decreasing $\delta^{15}N_{col}$ through life consistent with decreased inclusion of milk in the diet with age. However, it is not possible to determine accurate weaning ages from these data as there is too little time represented to identify post-weaning $\delta^{15}N_{col}$ patterns. Subjectively, the decreasing trend appears to continue through the life in 44-M (Fig. 4.13B), implying that this individual may not have been weaned at the time of its death (age ~5 years). On the other hand, the $\delta^{15}N_{col}$ series for Bolshoi Lyakhovskii (Fig. 4.17B) and Mol (Fig. 4.15B) show slight signs of leveling off late in life. Milk intake may have been minimal by around two years of age in Bolshoi Lyakhovskii and by just over two years of age in Mol, but the data from individuals that died at such young ages is difficult to interpret. The absence of a significant $\delta^{15}N_{col}$ trend in the Allen tusk suggests that the time represented in this tusk fragment represents post-weaning.

The rates of decrease in $\delta^{15}N_{col}$ vary among individuals. Based on regression of $\delta^{15}N_{col}$ on increment number, and assuming that cycles in $\delta^{13}C_{col}$ (or $\delta^{18}O_{carb}$ for Bolshoi Lyakhovskii) can be used to determine the number of increments in a year, the rates are: 44-M, -0.34 ‰/yr; Mol, -1.41‰/yr; Bolshoi Lyakhovskii, -1.74 ‰/yr; Oimyakon, -

2.54 ‰/yr. The 44-M tusk is missing material from the first year of life, and this may contribute to the exceptionally low rate observed in this individual. In addition, if the true decline follows a pattern of exponential decay, including more time in the linear regression would tend to decrease apparent rates. However, the differences in rate may suggest that rates of weaning differed among these individuals.

In the well-preserved Bolshoi Lyakhovskii and Mol tusks, trends in Mg/Ca, Sr/Ca, and Ba/Ca are not consistent. In the Mol tusk, Mg/Ca increases significantly over time, while Ba/Ca decreases. Sr/Ca shows no significant slope, but if the first three data points are excluded, values decrease significantly over time. Mg/Ca follows the pattern expected for decreasing relative importance of milk in the diet, but Ba/Ca and the abbreviated Sr/Ca series have trends that are opposite to expectations under a hypothesis that trophic level effects and decreasing relative milk intake are the primary drivers of trends in these variables. However, these trends are consistent with increasing discrimination against Sr and Ba relative to Ca in the digestive system. This discrimination is known to increase in humans during infancy and early childhood (Sillen and Smith, 1984). If this is the cause of the trend, it seems that the long-term effect of this changing discrimination dominates over the long-term effect of changing diet in juvenile mammoths. The fact that Sr/Ca is lowest in the samples representing the earliest material in the Mol tusk suggests that dietary change could be a primary driver of trends in Sr/Ca in the first year of life.

In the Bolshoi Lyakhovskii tusk, the increase in Mg/Ca is only marginally significant ($p = 0.0496$), Sr/Ca increases significantly through time, and Ba/Ca shows no

long-term trend. The increasing Sr/Ca may result from the short span of time covered in this tusk. Restricting the Mol Mg/Ca data to the first 97 increments (~2 years), the regression yields a significant positive slope. The increasing Sr/Ca in the Bolshoi Lyakhovskii tusk supports the hypothesis that, during the first year of life, Sr/Ca may be more affected by dietary change than changes in discrimination.

The lack of trends in the Mg/Ca and Ba/Ca of Bolshoi Lyakhovskii is difficult to explain. One hypothesis is that the trends observed in the Mol tusk actually represent diagenetic alteration near the tip of the tusk (early dentin). This might lead to elevated Ba/Ca and low Mg/Ca in early samples. Mean Mg/Ca is lower and mean Ba/Ca is higher in the Mol tusk (Table 4.5), supporting this hypothesis. However, the differences between the two tusks could also result from individual differences in feeding behavior, migratory patterns (source concentrations), or physiology. In the modern African elephant, Mg/Ca increases through time, but Ba/Ca and Sr/Ca do not show long-term trends (this dissertation, Chapter 3). Assessing the occurrence of long-term trends in these variables will likely require study of additional juvenile elephants.

There is also a long-term increase in $\delta^{13}C_{carb}$ in the Bolshoi Lyakhovskii tusk. Values in the early part of the record (Figure 4.17D) are more depleted than those measured on any other juvenile tusk, and are enriched by less than 5 ‰ over $\delta^{13}C_{col}$. This suggests that the energy source being utilized by this calf was depleted in ^{13}C. Milk fat is depleted in ^{13}C relative to other components of the organism (Polischuk et al. 2001). Ingestion of significant amounts of milk fat, and its utilization as an energy source is the likely cause of the depleted values early in life. The increasing trend

through time might result from decreasing importance of milk fat in the diet as the calf began to feed on more vegetation.

In the 44-M tusk, much of the variation in elemental ratios has been attributed to diagenesis. There is also a significant decrease in second-order increment thickness through time. In modern elephants, growth (shoulder height) rate increases and reaches a peak at about 1 year of age in females, and about 3 years of age in males (Lindeque and van Jaarsveld, 1993). Thus, the decreasing growth rates in this 4.7-year span of time may be reflecting this decrease in growth rate that occurs in young elephants.

There are no significant trends in growth-increment thicknesses for the Allen, Mol or Bolshoi Lyakhovskii tusks, but thicknesses increase significantly with time in the Oimyakon tusk. As this individual probably died before a peak growth rate would have been reached, this increase seems related to the normal, early, increasing growth rate observed in modern elephants.

The only other significant long-term trends observed in these specimens were a marginally significant ($p = 0.0464$) decrease in Mg/Ca and a marginally significant ($p = 0.04988$) increase in Sr/Ca in Oimyakon. There is also a significant increase in Mg/Ca through time in the Allen tusk, which is likely attributable to preferential loss of magnesium near the exterior surface of the fractured tip. Although the very low mean Mg/Ca for Oimyakon (Table 4.5) probably indicates diagenetic loss, a trend might still be evident if leaching were not spatially variable. As the Oimyakon tusk is thought to include a neonatal line (and thus, prenatal dentin), it is possible that the decreasing

trend is associated with changes in magnesium levels from prenatal to postnatal life. The increasing Sr/Ca in Oimyakon (Fig. 4.21K) might be explained by both changes in fetal uptake of Sr versus Ca and increasing intake of vegetation after birth. In rats, the fetal uptake of Sr vs. Ca increases from around day 17 of gestation to day 21 (i.e. late gestation) (Hartsook and Hershberger, 1973). A similar phenomenon may have occurred in mammoths, which would explain the initial increase in Sr/Ca. Sr/Ca in Oimyakon decreases after the neonatal line, then begins another increase (Fig. 4.21K). This second increase could be due to incorporation of plant foods in the diet.

Seasonal Patterns

There are few studies in which serial samples have been used to identify seasonal compositional patterns in Siberian mammoths. Fox et al. (2007) focused on $\delta^{18}O$ patterns in tusk dentin, while Iacumin et al. (2005) studied the variation in $\delta^{13}C$ and $\delta^{15}N$ in serial hair samples. Combining $\delta^{13}C$, $\delta^{15}N$, and $\delta^{18}O$ analyses allows a fuller characterization of the patterns of seasonal variability.

In temperate latitudes, $\delta^{18}O_{carb}$ of Pleistocene tusks and modern teeth varies following a pattern in which lighter $\delta^{18}O_{carb}$ values correspond to winter and heavier $\delta^{18}O_{carb}$ values correspond to summer (Koch et al., 1989). Thus, under these circumstances, one can assume $\delta^{18}O_{carb}$ can be used to identify season, and variation in other isotope ratios or elemental concentrations could be tied to dietary or physiological changes that occurred in specific seasons. However, seasonal $\delta^{18}O_{carb}$ patterns were not evident in tusks from the Taimir Peninsula in Siberia, and in

mammoth tusks from Chukotka and Wrangel Island, $\delta^{18}O_{carb}$ did not follow the expected depleted winter/enriched summer pattern noted by Koch et al. (1989) (as determined by comparison to growth increment thicknesses) (Fox et al., 2007).

As outlined in the introduction, plant water and drinking water isotope dynamics are complicated in permafrost regions. While the $\delta^{18}O$ of precipitation in northern Siberia roughly follows the pattern observed in temperate latitudes, the pattern in available surface water and plant water may be different. The $\delta^{18}O_{carb}$ record from the 44-M tusk, as it covers the longest period of time (i.e. the largest number of seasonal cycles) can serve as a reference in the current study. Most of the time covered in the series reflects a state in which $\delta^{18}O_{carb}$ remains at relatively enriched values, and this is punctuated by brief excursions to more depleted values (Fig. 4.13C). The pattern is similar in the data from the Bolshoi Lyakhovskii tusk (Fig. 4.17C). It is hypothesized that these excursions to low values represent the period during which snowmelt, which is depleted in ^{18}O, makes a large contribution to both surface water and plant water. In modern Yakutia, this occurs in May and June (Ichiyagagi et al., 2003; Sugimoto et al., 2002). Under this hypothesis, $\delta^{18}O_{carb}$ would be expected to remain relatively enriched throughout most of the year due to the preservation of late summer $\delta^{18}O$ in plants (and possibly ingested ice) through the late autumn, winter, and early spring. Decreases in $\delta^{18}O_{carb}$ might be relatively short in duration, occurring only in the late spring/early summer when snowmelt is a factor. Accepting this hypothesis for 44-M also implies that snow intake (which would lead to depleted values) in the winter was minimal relative to plant water (or ice) intake, and/or that this

individual was under water stress during winters leading to enrichment of body water $\delta^{18}O$ during those periods.

In the 44-M tusk, $\delta^{18}O_{carb}$ is positively correlated with $\delta^{13}C_{col}$ with high significance (lag = -5) (Table 4.1). The interpretation of Rountrey et al. (2007) regarding the $\delta^{13}C_{col}$ lows in this tusk was that they represented a relatively higher intake of plant proteins during the growing season. This interpretation seems valid, as the low $\delta^{13}C_{col}$ values occur about five weeks after low $\delta^{18}O_{carb}$, probably representing increased availability of early summer, high-protein vegetation at that time. The $\delta^{15}N_{col}$ series is not significantly correlated with $\delta^{18}O_{carb}$, although a positive correlation does exist for the Bolshoi Lyakovskii tusk (Table 4.3). In 44-M, $\delta^{15}N_{col}$ is correlated with $\delta^{13}C_{col}$ with high significance (lag = +2) (Table 4.1). The low $\delta^{15}N_{col}$ associated with low $\delta^{13}C$ may represent either decreased relative importance of isotopically enriched milk in the diet during this time of year, or a decrease in protein catabolism during this time of higher plant protein availability (Rountrey et al., 2007). An alternative hypothesis for the positive correlation between $\delta^{15}N_{col}$ and $\delta^{13}C_{col}$ is feeding on plants with different compositions in summer versus winter. Chapin (1996) observed that $\delta^{15}N$ of soils, moss, and arctic willow (*Salix arctica*) leaves in higher and drier areas was enriched relative to the same materials in a low wet area. Drier conditions might also lead to enriched $\delta^{13}C$ (Bocherens, 2003). If, due to less snow cover, mammoths fed on plants in high, dry windswept areas during the winter as modern reindeer do (Nellemann, 1996), and plants in wet low areas during the summer, this could result in an in-phase

pattern of variation in $\delta^{13}C_{col}$ and $\delta^{15}N_{col}$. Analyses on the tusks of adults, which would not have the complicating factor of milk intake, could be used to test this hypothesis.

The highly significant, negative correlation of Sr/Ca with $\delta^{18}O_{carb}$ (lag = -2) (Table 4.1) implies that Sr/Ca of diet was higher during the period in which snowmelt contributed to plant and surface water. As the Sr/Ca of plants is expected to be higher than that of milk, this is consistent with the hypothesis that ratio of plants to milk in the diet may have been lower during the early growing season. However, looking closely at the two series, one can see that the negative relationship is much more pronounced in the last 1.5 years of life (Figs. 4.13K, C). A correlation between these two variables is not present in any other tusk. The inverse relationship may be a phenomenon that occurs only in the late stages of a protracted weaning process, and, as such, it would be absent from the records of individuals that died younger. Alternatively, milk intake may not be a factor, and the pattern could result from feeding in different areas with different soil Sr/Ca in different seasons.

In the Mol tusk, seasonal patterns are apparent in $\delta^{13}C_{col}$, Sr/Ca, and Ba/Ca (Figs. 4.15A, I, J), and these all appear to vary in-phase, although the relationship is not significant for $\delta^{13}C_{col}$ and Sr/Ca (Sr/Ca and Ba/Ca, and $\delta^{13}C_{col}$ and Ba/Ca are positively correlated with high significance) (Table 4.2). As $\delta^{18}O_{carb}$ data are not available for this individual, it is assumed that the seasonal pattern in $\delta^{13}C_{col}$ is related to the same factors relevant to variation in the 44-M tusk, implying that the low $\delta^{13}C_{col}$ in each oscillation represents early summer. Low Sr/Ca and Ba/Ca in early summer is not consistent with the hypothesis that relative milk intake was low during this part of the

year. Furthermore, the lack of a seasonal pattern in $\delta^{15}N_{col}$ in the Mol tusk may indicate minimal seasonal variation in milk intake. Regarding the Sr/Ca and Ba/Ca patterns, it is also possible that higher plant productivity in the early summer leads to lower Ba and Sr concentrations in plants at this time (Markert and Weckert, 1989), and that this seasonal variation dominated any relative changes in milk intake. Feeding in areas with different soil Sr/Ca and Ba/Ca in different seasons could also account for these differences. Clearly, additional studies of seasonal variation in trace element concentration in mammalian tooth mineral are required for interpretation of these data.

In the Bolshoi Lyakhovskii tusk, $\delta^{13}C_{col,}$, $\delta^{18}O_{carb}$, and possibly $\delta^{15}N_{col}$ exhibit seasonal patterns. In the first 1.5 years of life $\delta^{15}N_{col}$ appears to vary roughly in-phase with $\delta^{13}C_{col}$ (Figs. 4.17B, A), although the two full series are not significantly correlated. The early pattern is similar to that observed in 44-M, and presumably, lows in $\delta^{13}C_{col}$ and $\delta^{15}N_{col}$ represent decreases in relative milk intake in early summer when $\delta^{18}O_{carb}$ is low. Ba/Ca appears to vary seasonally in the last ~1.5 years of life, with lows occurring when $\delta^{18}O_{carb}$ is low (the series are positively correlated (Table 4.3)). The higher values of Ba/Ca following these lows may indicate increased plant intake in the summer, but Sr/Ca shows no seasonal pattern, and Mg/Ca, which might be higher when relative milk intake is low, is lower during this time. Differences in the elemental composition of soils in winter versus summer feeding areas might account for these patterns. It is of interest that the relationships among $\delta^{13}C_{col}$, Sr,/Ca, and Ba/Ca differ between the Mol and Bolshoi Lyakhovskii tusks, as both of these were recovered from Bolshoi

Lyakhovskii Island. Although a radiocarbon date is not yet available for the Mol tusk, the differences suggest that juvenile life history in this region may have been different at different times.

The Allen tusk is the only specimen in this study for which $\delta^{13}C_{col}$ and $\delta^{15}N_{col}$ are negatively correlated (Table 4.4). This individual may have been fully weaned by the time this segment of tusk was produced as there is no long-term trend in $\delta^{15}N_{col}$. The anti-phase relationship offers no support to the winter/summer ridge/valley hypothesis mentioned above. In this case, the lows in $\delta^{13}C_{col}$ might represent times of increased fat utilization in late winter. The corresponding highs in $\delta^{15}N_{col}$ might be due to nutritional stress and increased recycling of body proteins in late winter. Increment thickness is positively correlated with $\delta^{13}C_{col}$ supporting the hypothesis that high $\delta^{13}C_{col}$ corresponds to summer in this individual.

It is difficult to assess seasonal variation in an individual such as Oimyakon, that lived for such a short period of time. In addition, approximately half of the time recorded in the tusk represents the prenatal period, which may introduce complexities into patterns of variation. The $\delta^{18}O_{carb}$ series does seem to exhibit a seasonal pattern, although $\delta^{13}C_{col}$ and $\delta^{15}N$ do not show a similar scale of pattern (Figs. 4.21C, A, B). There are complexities associated with possible seasonal-scale variation in juvenile $\delta^{18}O_{carb}$ including the influence of snowmelt, drinking from rivers versus ponds, winter water source, contributions from permafrost water, and possibly ^{18}O-enriched milk. In this case, as $\delta^{13}C_{col}$ and $\delta^{15}N_{col}$ show a similar scale of variation, and at least $\delta^{13}C_{col}$ shows seasonal-scale variation in all other individuals, it seems appropriate to accept

the patterns in these variables as marking the scale of seasonal variation in Oimyakon rather than $\delta^{18}O_{carb}$. If $\delta^{13}C_{col}$ and $\delta^{15}N_{col}$ define the scale of seasonal variation in this individual, with just under 1.0 year of growth represented, the second-order increment count for this individual may be erroneous. Indeed the mean increment thickness in the Oimyakon tusk (0.08 mm) is less than all others, suggesting the possibility that either the periodicity of the increments is less than seven days, or that some prominent third-order increments were included in the count/measurement. Increments were difficult to identify near the tip of the tusk, which may account for some error.

Using the 44-M tusk as a reference, lows in $\delta^{13}C_{col}$ and $\delta^{15}N_{col}$ indicate late spring/early summer. If this is correct, the location of the neonatal line indicates that this individual was born in early spring and survived only until autumn or early winter at an age of 7.4 months. The variation in $\delta^{18}O$ is difficult to interpret. It is possible that the brief increase in $\delta^{18}O_{carb}$ following birth represents the effect of intake of ^{18}O enriched milk (Wright and Schwarcz,1998) early in life followed by increasing intake of snowmelt-derived water leading to more depleted values. The increase in $\delta^{18}O_{carb}$ in the final sample might be due to increased intake of evaporatively enriched plant water in autumn. The Oimyakon data are discussed further below.

Oimyakon- Prenatal to Postnatal Patterns

Unlike other tusks in this study, the Oimyakon tusk appears to contain a neonatal line marking the time of birth. This provides an opportunity to study the

composition of prenatally deposited dentin, but also complicates interpretation. As mentioned above, intake of milk may cause enrichment in the $\delta^{18}O_{carb}$ of mineralized tissues because maternal body water (from which milk water is derived) could be enriched over dietary water values (Wright and Schwarcz, 1998). This may account for the brief excursion to higher values just after birth (Fig. 4.21C).

$\delta^{13}C_{col}$ is relatively high before birth, and declines thereafter until the final sample (Fig. 4.21A). The declining postnatal $\delta^{13}C_{col}$ values might be associated with either a high relative proportion of isotopically light lipids in the diet, a decreasing trophic level effect in C associated with increasing plant food intake, or a change in the feeding habits of the mother (a shift toward vegetation in lower, wetter areas). The higher $\delta^{13}C_{col}$ prior to birth could be due to high maternal $\delta^{13}C$ caused by eating plants in high dry areas in the winter, or due to preferential use of maternal protein stores for the production of fetal proteins (similar to ^{13}C- and ^{15}N-enriched fetal blood cells observed in caribou (Barboza and Parker, 2006)). In the same way, the higher $\delta^{15}N_{col}$ prior to birth could be due to either of these factors.

As evidenced by 44-M and the modern elephant (this dissertation, Chapter 3) $\delta^{13}C_{carb}$ appears to be susceptible to diagenesis. Given the high levels of Fe and low levels of Mg observed in the tusk, alteration seems likely. Thus, we do not offer any interpretation of the increasing trend.

Sr/Ca reaches a brief high before birth, then a decline in the two samples following birth, followed by another increase (Fig. 4.21K). In rats, Sr/Ca in the fetus increases in late gestation (Hartsook and Hershberger, 1973). This may account for the

increase observed in Oimyakon prior to birth. The decrease following birth might be due to low Sr/Ca in milk, which would be the only food source in very early life. A subsequent increase might suggest that some vegetation with a higher Sr/Ca than milk was being eaten by the calf after a few months.

If the interpretation of increased Sr/Ca just before birth is correct, one would expect a similar pattern to occur in Ba/Ca, but this is not the case. While increasing Ba/Ca occurs after birth, which could be attributed to increasing plant intake, the decline prior to birth is difficult to explain (Fig. 4.21L). The pattern exhibited in Ba/Ca may be predominately a maternal seasonal pattern associated with changes in substrate Ba/Ca that is transferred to the calf via the placenta and later through milk.

Zn/Ca shows a pronounced peak just after birth (Fig. 4.21J). In humans, fetal serum Zn concentrations increase through gestation (Jeswani and Vani, 1982). Furthermore, Zn concentrations in human milk are highest in the early stages of lactation and decrease thereafter (Vuori and Kuitunen, 1979). In a study of human enamel, Ca-normalized Zn concentration was elevated around the neonatal line (Kang et al., 2004). If dentin Zn concentration follows similar patterns to those in enamel, the peak in Zn/Ca may be an indicator of the neonatal period.

Cu/Ca spikes in the prenatal period of this individual, and no trends are apparent after this (Fig. 4.21I). In young pigs, serum copper levels are low around the time of birth and increase over the first two weeks of life (Ullrey et al., 1967), while in humans serum copper increases over the first five months of life (Shaw, 1980). No increasing trend is observed in the Oimyakon tusk. In muskoxen, protein-bound

hepatic Cu in fetuses increases tenfold in late gestation (Rombach et al., 2003). It is possible that the prenatal peak in Cu/Ca is associated with the accumulation of Cu in the liver, but studies of Cu concentrations in prenatal and postnatal dentin of extant mammals would be necessary to determine this.

Bolshoi Lyakhovskii- Possible Starvation Prior to Death

There are unusual patterns in $\delta^{13}C_{col}$ and $\delta^{15}N_{col}$ in the last six samples (Fig. 4.17B) from this individual. The relationship among the variables is different at the second low in $\delta^{18}O_{carb}$ that at the first low. $\delta^{15}N_{col}$ values decrease prior to the expected time assuming an in-phase relationship between $\delta^{18}O_{carb}$ and $\delta^{15}N_{col}$, then rise. This pattern could represent reduction or exclusion of milk from the diet (accounting for the decrease in $\delta^{15}N_{col}$) followed by nutritional stress in the months prior to death. However, contrary to expectations, growth increments do not decrease in thickness during this time indicating that some other dietary or physiological change may have led to this pattern. Furthermore, $\delta^{13}C_{carb}$ does not decrease during this increase in $\delta^{15}N_{col}$ (as might be expected if fat stores were being utilized during nutritional stress.

Conclusions

Serial compositional analyses of juvenile mammoth tusks can provide new information about early mammoth life history. While some patterns, such as decreasing $\delta^{15}N_{col}$ associated with weaning, and seasonal-scale oscillation in $\delta^{13}C_{col}$, are consistent among juveniles, others are not. The consistency of $\delta^{13}C_{col}$ and $\delta^{15}N_{col}$ patterns suggests that these measures can be profitably employed to determine scale

of seasonal patterns ($\delta^{13}C_{col}$) and age at weaning ($\delta^{15}N_{col}$) for juvenile mammoths. Furthermore, collagen preservation seems adequate in all tusks including those that are darkly stained and show evidence of diagenetic alteration of other compositional measures.

The factors leading to seasonal oscillation in $\delta^{13}C_{col}$ and $\delta^{15}N$ are not yet completely understood. The interpretation of Rountrey et al. (2007), that concomitant lows in $\delta^{13}C_{col}$ and $\delta^{15}N_{col}$ represent higher relative intake of plant proteins in spring or early summer and lower relative intake of milk at this time, seems reasonable. One presumably weaned individual in this set exhibited anti-phase patterns in these measures, and a similar anti-phase relationship was observed in the tusk of an adult mammoth from Chukotka (S. Gohman, D.L. Fox, and D.C. Fisher, in prep) and in hairs from another, presumably adult, mammoth from Bolshoi Lyakhovskii Island (Iacumin et al., 2005). Although additional analyses of adults and juveniles are necessary, this difference between young juveniles and older juveniles/adults may be a function of milk intake or a pattern of feeding in juveniles that differs from that exhibited by adults. In the case of dependence on milk intake, a transition from in-phase to anti-phase $\delta^{13}C_{col}$ and $\delta^{15}N_{col}$ might mark the time of weaning (in addition to the end of the declining trend in $\delta^{15}N_{col}$).

The $\delta^{18}O_{carb}$ patterns in the 44-M and Bolshoi Lyakhovskii tusks appear to confirm that the low $\delta^{13}C_{col}$ values occur in early summer when the influence of snowmelt leads to low $\delta^{18}O_{carb}$ values. Future work should include $\delta^{18}O_{carb}$, $\delta^{13}C_{col}$ and $\delta^{15}N_{col}$ analyses of adult tusks to determine if the apparent difference in $\delta^{13}C_{col}$ and

$\delta^{15}N_{col}$ phase relationship between adults and juveniles is caused by a shift in the $\delta^{13}C_{col}$ pattern or a shift in the $\delta^{15}N_{col}$ pattern as these would have different implications for understanding the dietary or physiological changes associated with the change.

The negative correlation of $\delta^{13}C_{carb}$ with Mg/Ca (which is easily lost during diagenesis) in a partially altered tusk, indicates that elevated $\delta^{13}C_{carb}$ may be due to diagentic alteration. This suggests that care should be taken when using dentin $\delta^{13}C_{carb}$ for dietary reconstruction. Furthermore, determination of Mg/Ca may be a simple test for detecting samples in which $\delta^{13}C_{carb}$ is likely to be altered.

In well-preserved tusks, Mg/Ca shows an increasing trend with age that may be due to decreasing milk intake, suggesting that it might be used as a weaning indicator. However, the susceptibility of Mg/Ca to diagenetic alteration probably precludes its use in paleodietary reconstruction for most specimens.

In some cases Ba/Ca and/or Sr/Ca show seasonal patterns, but at least in Ba/Ca, the phase relationship to $\delta^{13}C_{col}$ is not consistent among individuals. The patterns might be associated with seasonal variation in milk intake, plant trace element concentration, or feeding areas. Seasonal patterns in the elemental concentrations of mammalian herbivore dentin have not been well studied, but the occurrence of seasonal-scale patterns in tusks suggests that this may be a fruitful area for future research.

Elevated Fe/Ca and Mn/Ca often occur in tip and pulp cavity samples of well-preserved tusks, indicating diagenesis in these areas. In darkly stained tusks, values are elevated throughout (with the exception of Mn/Ca in one tusk).

Zn/Ca and Cu/Ca do not vary seasonally, and the series often contain spikes to high values. The spikes are troubling, and it is not known if this represents a primary signal or sample contamination. In the Oimyakon tusk, Zn/Ca is high in dentin deposited just after birth, which is consistent with patterns observed in other studies. If the factor causing spikes in Zn/Ca can be identified/eliminated, this suggests that Zn/Ca patterns in dentin might be used to identify the timing of birth. As the timing of initial tusk development and expression of the neonatal line in dentin appear to vary, having an independent means of determining the timing of birth would greatly improve our ability to study life history in tusks.

The results of this study indicate that combined isotope and elemental analyses have the potential to reveal new information about the paleobiology of mammoths. Similarities in patterns among individuals suggest that certain aspects of juvenile life history, such as weaning, can be relatively easily identified. However, individual variation in some seasonal patterns shows that feeding patterns or migrations may have varied regionally or through time. Expanding the number of both adult and juvenile tusks studied will aid in understanding the variation in life history both geographically and temporally.

Table 4.1. Cross-correlation results for the 44-M data. Correlations between pairs of detrended (if non-stationary), spline-interpolated series. See Materials and Methods for description of statistical methods. Only significant ($p < 0.025$) correlations are shown. Underlined values are significant with Bonferroni correction. Asterisks mark series that were detrended. Color scale indicates the lag associated with each correlation. Positive lag means that the column series is shifted such that y_{t+lag} in the column series is aligned with y_t in the row series. Avg. Inc. Thick. = average thickness of second-order increments contained within each compositional sample. As an example of the kind of information portrayed here, note the positive correlation between $\delta^{13}C_{col}$ and $\delta^{15}N_{col}$ (lag = -2 for $\delta^{13}C_{col}$ vs. $\delta^{15}N_{col}$). The similarity between the series can be observed in Figures 4.13A and B. In Figures 4.13A and B one can also see the temporal offset in the patterns that leads to the highest correlation at a lag of -2 (e.g., lows in $\delta^{15}N_{col}$ tend to occur just after lows in $\delta^{13}C_{col}$).

	$\delta^{13}C_{col}$	$\delta^{15}N_{col}$*	$\delta^{18}O_{carb}$	$\delta^{13}C_{carb}$*	Mg/Ca*	P/Ca*	Cu/Ca*	Zn/Ca	Sr/Ca	Ba/Ca*	Avg. Inc. Thick.*
$\delta^{13}C_{col}$		**0.70**	**0.54**	**0.40**		**-0.46**					
$\delta^{15}N_{col}$*	**0.70**					**-0.44**				**0.33**	
$\delta^{18}O_{carb}$	**0.54**								**-0.62**		
$\delta^{13}C_{carb}$*	**0.40**				**-0.62**	**-0.45**	**0.41**				
Mg/Ca*				**-0.62**			**-0.42**			**-0.33**	
P/Ca*	**-0.46**	**-0.44**		**-0.45**			**-0.30**				
Cu/Ca*				**0.41**	**-0.42**						
Zn/Ca											
Sr/Ca			**-0.62**								
Ba/Ca*		**0.33**			**-0.33**						
Avg. Inc. Thick.*											

Lag (second-order increments)

-6 -5 -4 -3 -2 -1 0 1 2 3 4 5 6

Table 4.2. Cross-correlation results for the Mol data. Correlations between pairs of detrended (if non-stationary), spline-interpolated series. See Materials and Methods for description of statistical methods. Only significant ($p < 0.025$) correlations are shown. Underlined values are significant with Bonferroni correction. Asterisks mark series that were detrended. Color scale indicates the lag associated with each correlation. Positive lag means that the column series is shifted such that y_{t+lag} in the column series is aligned with y_t in the row series. Avg. Inc. Thick. = average thickness of second-order increments contained within each compositional sample. As an example of the kind of information portrayed here, note the strong positive correlation between $\delta^{13}C_{col}$ and Ba/Ca (both detrended). Both vary seasonally. Similarities in the series can be observed in Figures 4.15A and J.

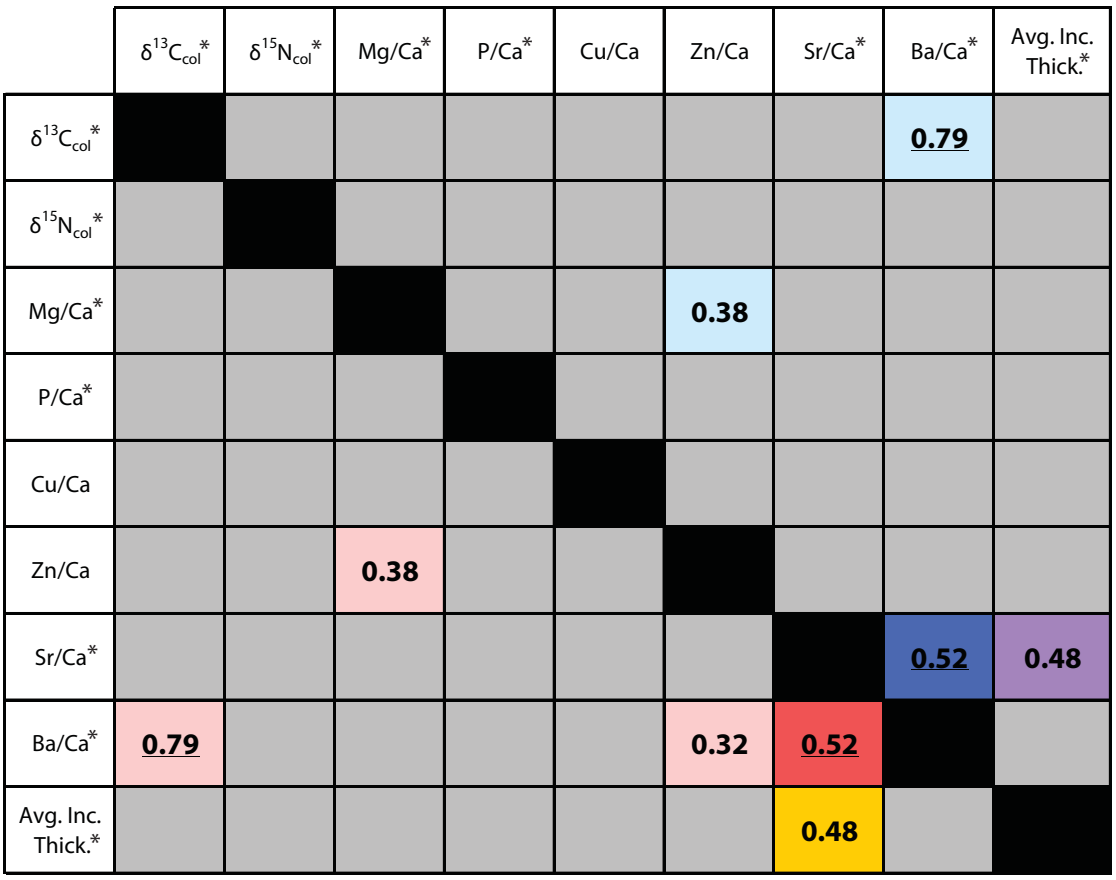

Lag (second-order increments)

-6 -5 -4 -3 -2 -1 0 1 2 3 4 5 6

Table 4.3. Cross-correlation results for the Bolshoi Lyakhovskii data. Correlations between pairs of detrended (if non-stationary), spline-interpolated series. See Materials and Methods for description of statistical methods. Only significant ($p < 0.025$) correlations are shown. Underlined values are significant with Bonferroni correction. Asterisks mark series that were detrended. Color scale indicates the lag associated with each correlation. Positive lag means that the column series is shifted such that y_{t+lag} in the column series is aligned with y_t in the row series. Avg. Inc. Thick. = average thickness of second-order increments contained within each compositional sample. As an example of the kind of information portrayed here, note the positive correlation between $\delta^{15}N_{col}$ and $\delta^{18}O_{carb}$ (both detrended). Similarities in the series can be observed in Figures 4.17B and C.

	$\delta^{13}C_{col}$*	$\delta^{15}N_{col}$*	$\delta^{18}O_{carb}$*	$\delta^{13}C_{carb}$*	Mg/Ca*	P/Ca*	Cu/Ca	Zn/Ca*	Sr/Ca*	Ba/Ca	Avg. Inc. Thick.
$\delta^{13}C_{col}$*					0.39						-0.55
$\delta^{15}N_{col}$*			0.57	0.51		0.50	0.39				-0.49
$\delta^{18}O_{carb}$*		0.57								0.46	-0.45
$\delta^{13}C_{carb}$*		0.51						0.40	0.56		
Mg/Ca*	0.39					0.59	-0.38			-0.45	-0.43
P/Ca*		0.50			0.59		-0.48				
Cu/Ca		0.39			-0.38	-0.48					
Zn/Ca*				0.40					0.42		
Sr/Ca*				0.56				0.42			
Ba/Ca			0.46		-0.45						
Avg. Inc. Thick.	-0.55	-0.49	-0.45		-0.43						

Lag (second-order increments)

-6 -5 -4 -3 -2 -1 0 1 2 3 4 5 6

Table 4.4. Cross-correlation results for the Allen data. Correlations between pairs of detrended (if non-stationary), spline-interpolated series. See Materials and Methods for description of statistical methods. Only significant ($p < 0.025$) correlations are shown. Underlined values are significant with Bonferroni correction. Asterisks mark series that were detrended. Color scale indicates the lag associated with each correlation. Positive lag means that the column series is shifted such that y_{t+lag} in the column series is aligned with y_t in the row series. Avg. Inc. Thick. = average thickness of second-order increments contained within each compositional sample. As an example of the kind of information portrayed here, note the strong negative correlation between $\delta^{15}N_{col}$ and $\delta^{13}C_{col}$. The inverse relationship can be observed in Figures 4.19A and B.

	$\delta^{13}C_{col}$*	$\delta^{15}N_{col}$	Mg/Ca*	P/Ca*	Mn/Ca*	Fe/Ca*	Cu/Ca	Zn/Ca	Sr/Ca	Ba/Ca*	Avg. Inc. Thick
$\delta^{13}C_{col}$*		**-0.79**	**0.40**	**-0.53**							**0.48**
$\delta^{15}N_{col}$	**-0.79**		**-0.36**	**0.38**							
Mg/Ca*	**0.40**						**0.47**	**0.47**		**-0.43**	
P/Ca*	**-0.53**						**-0.48**	**-0.46**			**-0.46**
Mn/Ca*							**-0.35**	**-0.35**			**-0.51**
Fe/Ca*									**0.78**		
Cu/Ca			**0.47**	**-0.48**	**-0.35**			**1.00**			
Zn/Ca			**0.47**	**-0.46**	**-0.35**		**1.00**				
Sr/Ca						**0.78**				**0.53**	**0.46**
Ba/Ca*			**-0.43**						**0.53**		**0.42**
Avg. Inc. Thick	**0.48**		**0.36**	**-0.46**	**-0.51**				**0.46**	**0.42**	

Lag (second-order increments)

-6 -5 -4 -3 -2 -1 0 1 2 3 4 5 6

Table 4.5. Mean values for compositional measures. Data for Shabi Shabi (*Loxodonta africana*) taken from Chapter 3 (this dissertation).

Specimen		$\delta^{13}C_{col}$	$\delta^{15}N_{col}$	$\delta^{18}O_{carb}$	$\delta^{13}C_{carb}$	C/N_{col}	$\delta^{13}C_{carb}$ - $\delta^{13}C_{col}$	Mg/Ca	P/Ca	Mn/Ca	Fe/Ca	Cu/Ca	Zn/Ca	Sr/Ca	Ba/Ca	Pb/Ca
44-M	**mean**	**-21.93**	**9.50**	**-8.05**	**-10.32**	**3.10**	**11.60**	**90.78**	**655.67**	**0.331**	**2.06**	**0.158**	**0.202**	**0.537**	**0.099**	**0.002**
	s.d.	0.47	0.83	0.56	0.98	0.03	1.02	63.12	59.59	0.918	3.82	0.131	0.293	0.029	0.056	0.002
Mol	**mean**	**-22.55**	**11.51**	**-**	**-**	**3.15**	**-**	**91.59**	**699.43**	**0.554**	**9.13**	**0.097**	**0.174**	**0.630**	**0.068**	**0.007**
	s.d.	0.49	1.61	-	-	0.02	-	19.18	39.93	1.530	18.23	0.076	0.096	0.088	0.023	0.009
Bolshoi Lyakhovskii	**mean**	**-22.10**	**11.16**	**-15.86**	**-15.40**	**3.14**	**6.51**	**125.51**	**721.17**	**0.262**	**3.38**	**0.084**	**0.215**	**0.748**	**0.046**	**0.002**
	s.d.	0.50	1.15	1.07	0.55	0.01	1.13	12.44	32.06	0.417	6.27	0.039	0.303	0.180	0.013	0.003
Allen	**mean**	**-22.13**	**9.28**	**-**	**-**	**3.25**	**-**	**18.39**	**636.63**	**0.937**	**85.27**	**0.390**	**0.285**	**1.680**	**0.564**	**0.002**
	s.d.	0.51	1.17	-	-	0.01	-	2.30	34.75	0.515	5.56	0.368	0.204	0.060	0.136	0.002
Oimyakon	**mean**	**-21.81**	**9.23**	**-14.22**	**-14.76**	**3.23**	**7.20**	**4.11**	**710.66**	**0.641**	**100.28**	**0.156**	**1.051**	**1.020**	**0.106**	**0.001**
	s.d.	0.22	0.74	0.94	0.24	0.01	0.51	0.91	27.54	0.034	4.59	0.240	0.435	0.080	0.013	0.001
ShabiShabi (Loxodonta africana)	**mean**	**-19.45**	**12.11**	**1.43**	**-12.28**	**3.18**	**6.97**	**194.78**	**795.76**	**0.052**	**0.64**	**-**	**0.144**	**1.710**	**0.158**	**0.001**
	s.d.	1.29	0.83	2.13	2.19	0.01	1.73	44.32	58.57	0.204	0.38	-	0.041	0.370	0.141	0.000

Figure 4.1. Computer-generated, three-dimensional model of a longitudinally sectioned tusk. Each color cycle represents one year of growth. The tusk appears as a series of stacked cones.

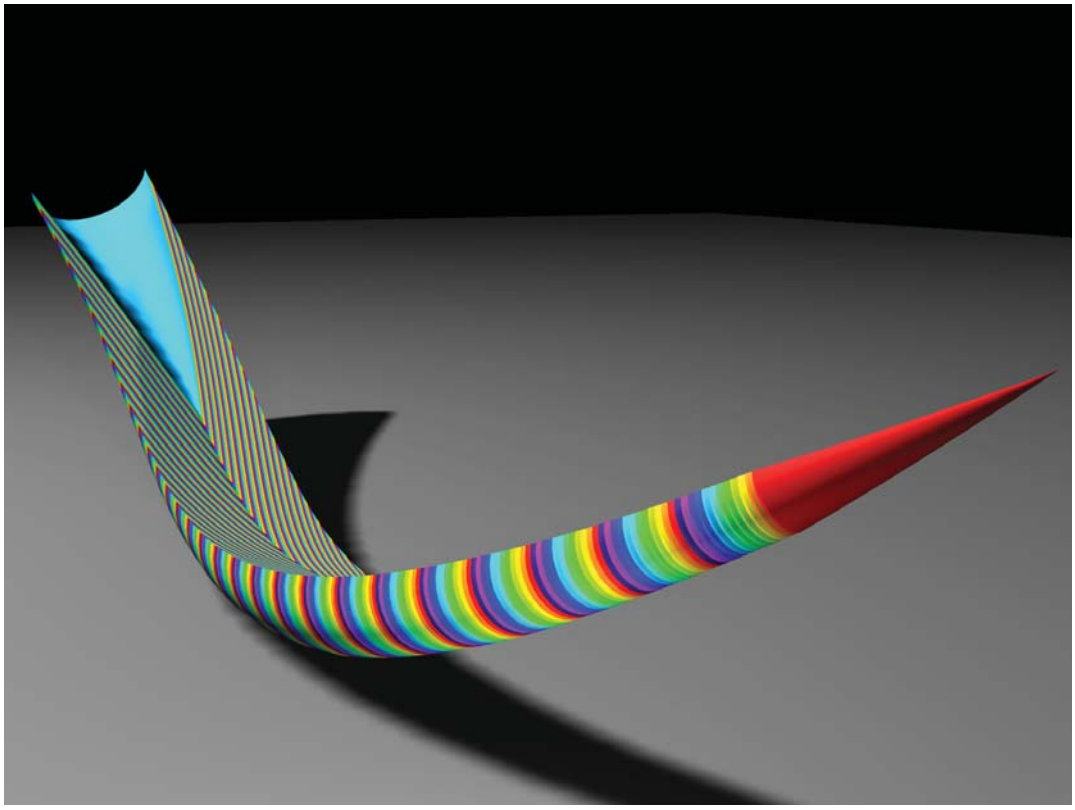

Figure 4.2. Winter (Dec.-Feb.)/Summer (Jun.-Aug.) $\delta^{18}O$ (VSMOW) of precipitation at weather stations in Russia (SNIP- Siberian Network of Isotopes in Precipitation). Data were collected from Jan. 1996 to Dec. 2000. The winter value at Ayon is based on a single month (Jan. 1998). Data from Kurita et al. (2004). Note winter values are more negative than summer values at all stations.

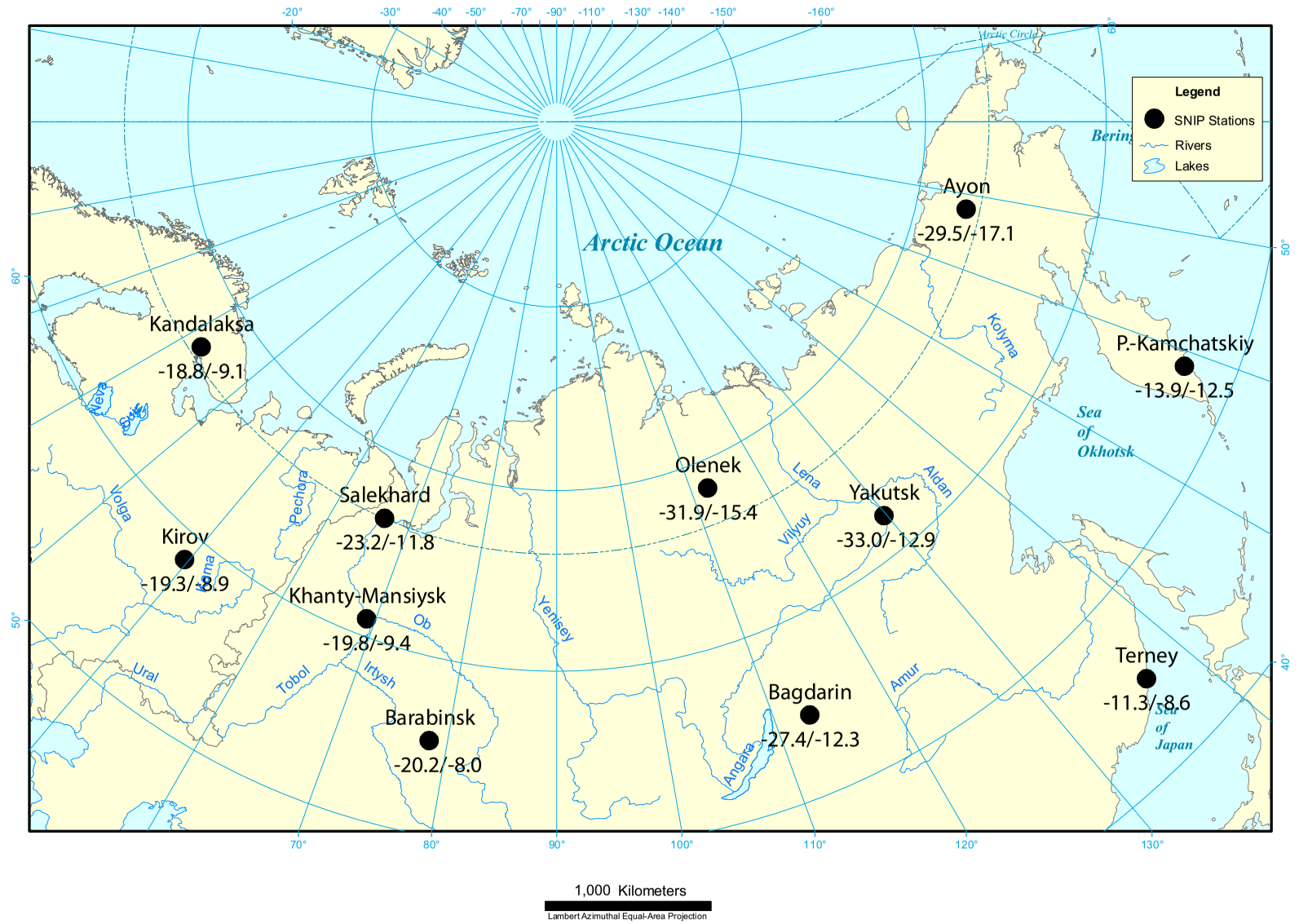
Legend
SNIP Stations
Rivers
Lakes
Arctic Ocean
Arctic Circle
Bering
Sea of Okhotsk
Sea of Japan
Ayon
-29.5/-17.1
Kandalaksa
-18.8/-9.1
P.-Kamchatskiy
-13.9/-12.5
Olenek
-31.9/-15.4
Salekhard
-23.2/-11.8
Yakutsk
-33.0/-12.9
Kirov
-19.3/-8.9
Khanty-Mansiysk
-19.8/-9.4
Terney
-11.3/-8.6
Bagdarin
-27.4/-12.3
Barabinsk
-20.2/-8.0
Neva
Svir
Volga
Kama
Pechora
Ural
Tobol
Irtysh
Ob
Yenisey
Angara
Lena
Vilyuy
Aldan
Kolyma
Amur
-20°
-30°
-40°
-50°
-70°
-90°
-110°
-130°
-140°
-150°
-160°
60°
50°
40°
70°
80°
90°
100°
110°
120°
130°
1,000 Kilometers
Lambert Azimuthal Equal-Area Projection

Figure 4.3. Map showing locations at which specimens were collected. There is no locality information available for the Allen tusk.

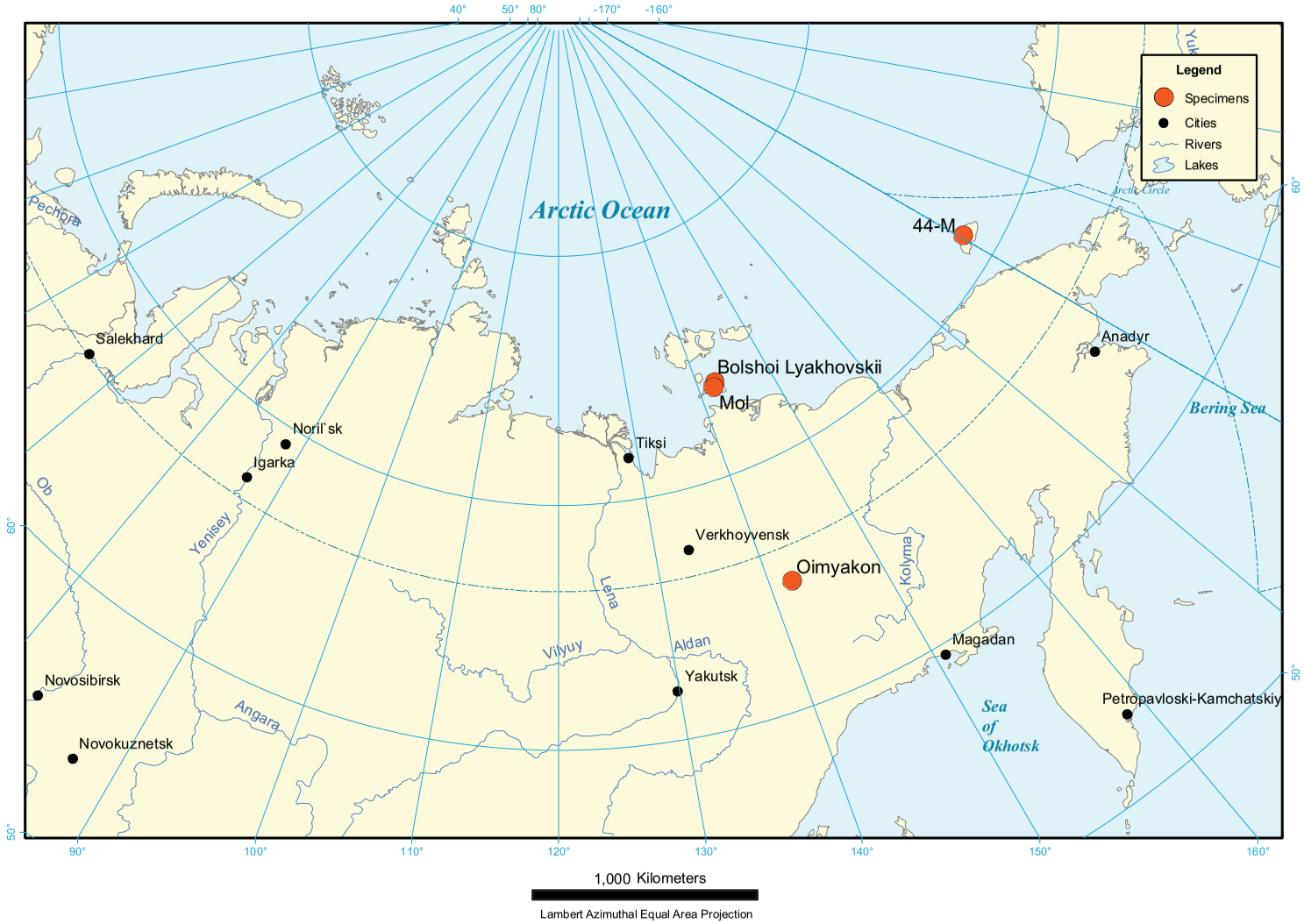
Legend
Specimens
Cities
Rivers
Lakes
Arctic Ocean
Bering Sea
Sea of Okhotsk
Arctic Circle
Pechora
Ob
Yenisey
Lena
Vilyuy
Aldan
Angara
Kolyma
44-M
Bolshoi Lyakhovskii
Mol
Salekhard
Noril`sk
Igarka
Tiksi
Verkhoyvensk
Oimyakon
Yakutsk
Anadyr
Magadan
Petropavloski-Kamchatskiy
Novosibirsk
Novokuznetsk
40°
50°
80°
-170°
-160°
60°
50°
90°
100°
110°
120°
130°
140°
150°
160°
1,000 Kilometers
Lambert Azimuthal Equal Area Projection

Figure 4.4. Anterior portion of the Oimyakon carcass. The trunk is severed from the face, but has been placed in approximately correct anatomical position.

Figure 4.5. Ventral aspect of the right premaxilla from the Oimyakon mammoth showing the permanent tusk within the alveolus. No deciduous tusk was present.

Figure 4.6. Medial aspect of the Oimyakon tusk. Patches of enamel (E) are visible on the distal third of the tusk, while cementum (C) is present on the dorsal surface proximally. The exterior expression of the neonatal line is visible (NnL).

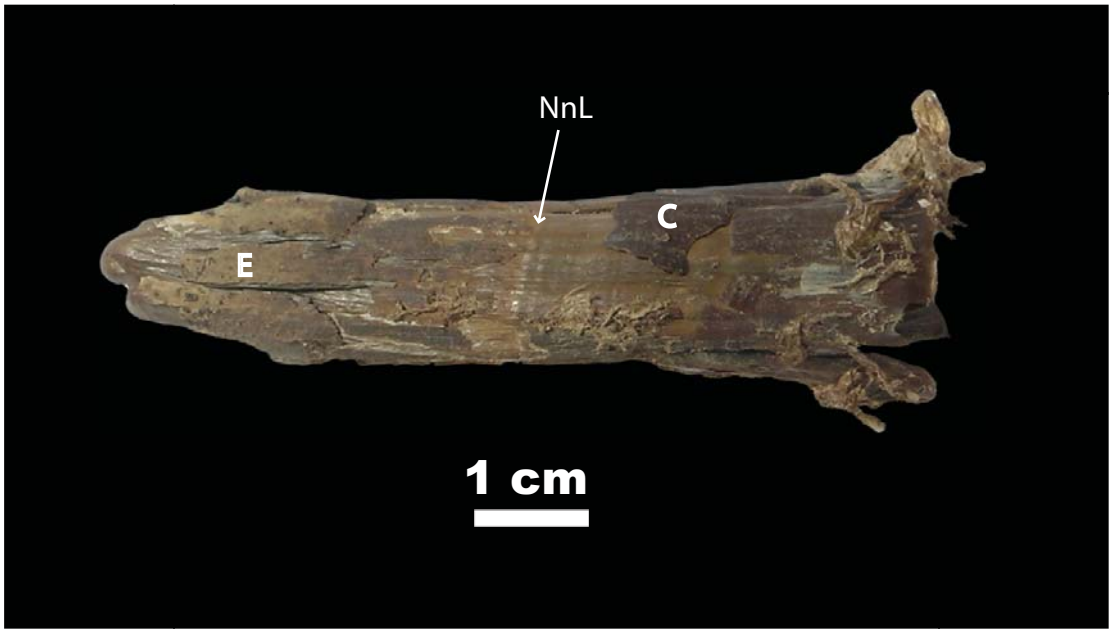

Figure 4.7. Under magnification, a prominent ridge marks the exterior expression of the neonatal line (NnL). The darker material near the bottom of the frame is immature enamel.

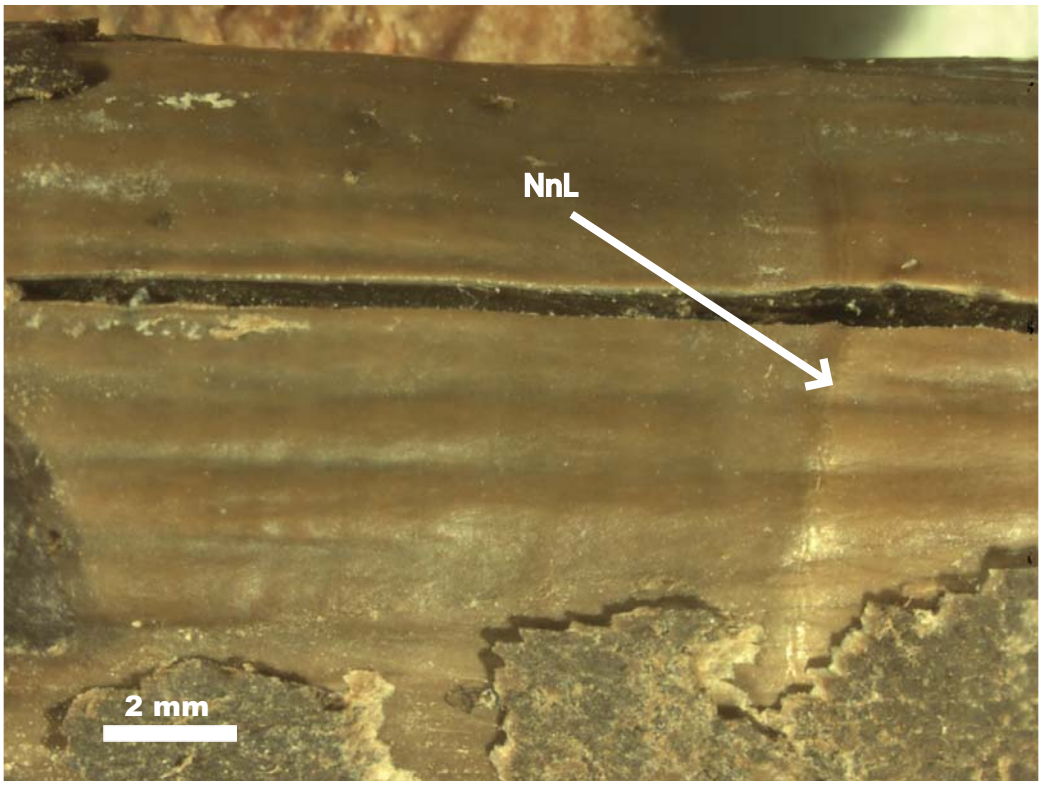

Figure 4.8. Cut surfaces following longitudinal sectioning. A prominent growth line (NnL) reaches the exterior of the tusk at the ridge shown in Figure 4.7.

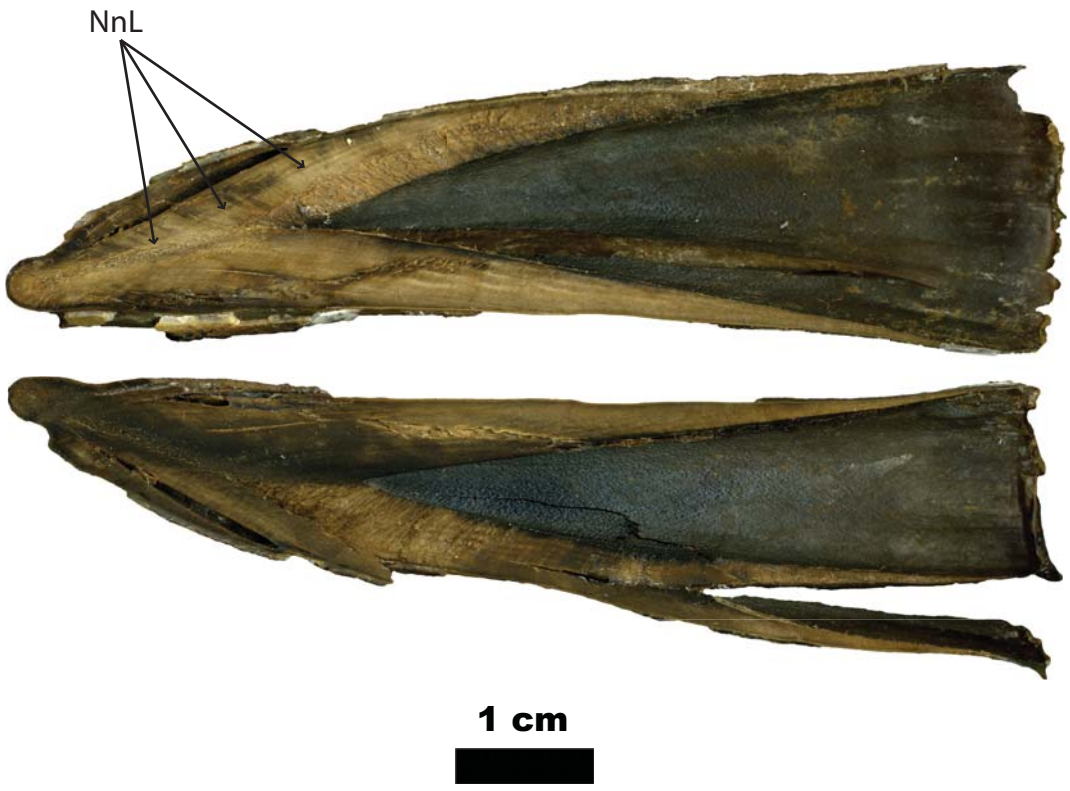

Figure 4.9. Lateral aspect of the Bolshoi Lyakhovskii tusk (MMY 7916).


1 cm

Figure 4.10. Medial aspect of the Mol tusk.


1 cm

Figure 4.11. Lateral aspect of the 44-M tusk.


5 cm

Figure 4.12. The Allen tusk fragment. A) Surface on outside curve. B) Surface on inside curve.


A
B
1 cm

Figure 4.13, A-F. Compositional series for the 44-M tusk. A) $\delta^{13}C_{col}$ relative to VPDB, B) $\delta^{15}N_{col}$ relative to AIR, C) $\delta^{18}O_{carb}$ relative to VPDB, D) $\delta^{13}C_{carb}$ relative to VPDB, E) Mg/Ca (mmol/mol), F) P/Ca (mmol/mol). Dashed lines represent approximate years and are separated by 59.25 increments. Missing points occur in the elemental ratio series when concentration was below detection. Note the seasonal patterns in A, B, and C, the inverse relationship between D and E, the similarity of E and F, and the long-term declinine in B.

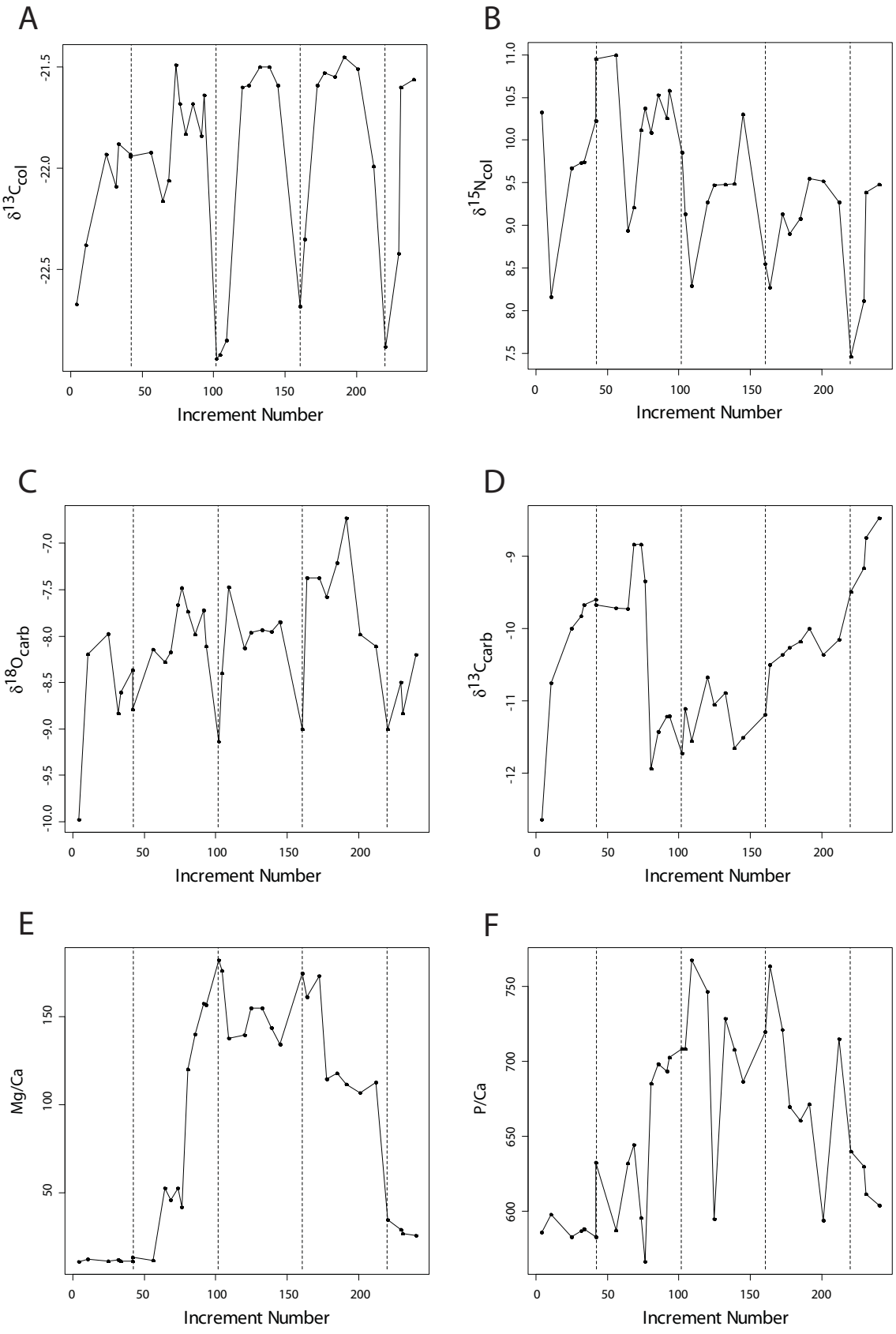
A
$\delta^{13}C_{col}$
-21.5
-22.0
-22.5
0
50
100
150
200
Increment Number
B
$\delta^{15}N_{col}$
11.0
10.5
10.0
9.5
9.0
8.5
8.0
7.5
0
50
100
150
200
Increment Number
C
$\delta^{18}O_{carb}$
-7.0
-7.5
-8.0
-8.5
-9.0
-9.5
-10.0
0
50
100
150
200
Increment Number
D
$\delta^{13}C_{carb}$
-9
-10
-11
-12
0
50
100
150
200
Increment Number
E
Mg/Ca
150
100
50
0
50
100
150
200
Increment Number
F
P/Ca
750
700
650
600
0
50
100
150
200
Increment Number

Figure 4.13, G-L. Compositional series for the 44-M tusk. G) Mn/Ca (mmol/mol) , H) Fe/Ca (mmol/mol), I) Cu/Ca (mmol/mol), J) Zn/Ca (mmol/mol), K) Sr/Ca (mmol/mol), L) Ba/Ca (mmol/mol). Dashed lines represent approximate years and are separated by 59.25 increments. Missing points occur in the elemental ratio series when concentration was below detection. Note the high Mn/Ca and Fe/Ca in the final sample, and the inverse relationship between L and E (see also Table 4.1).

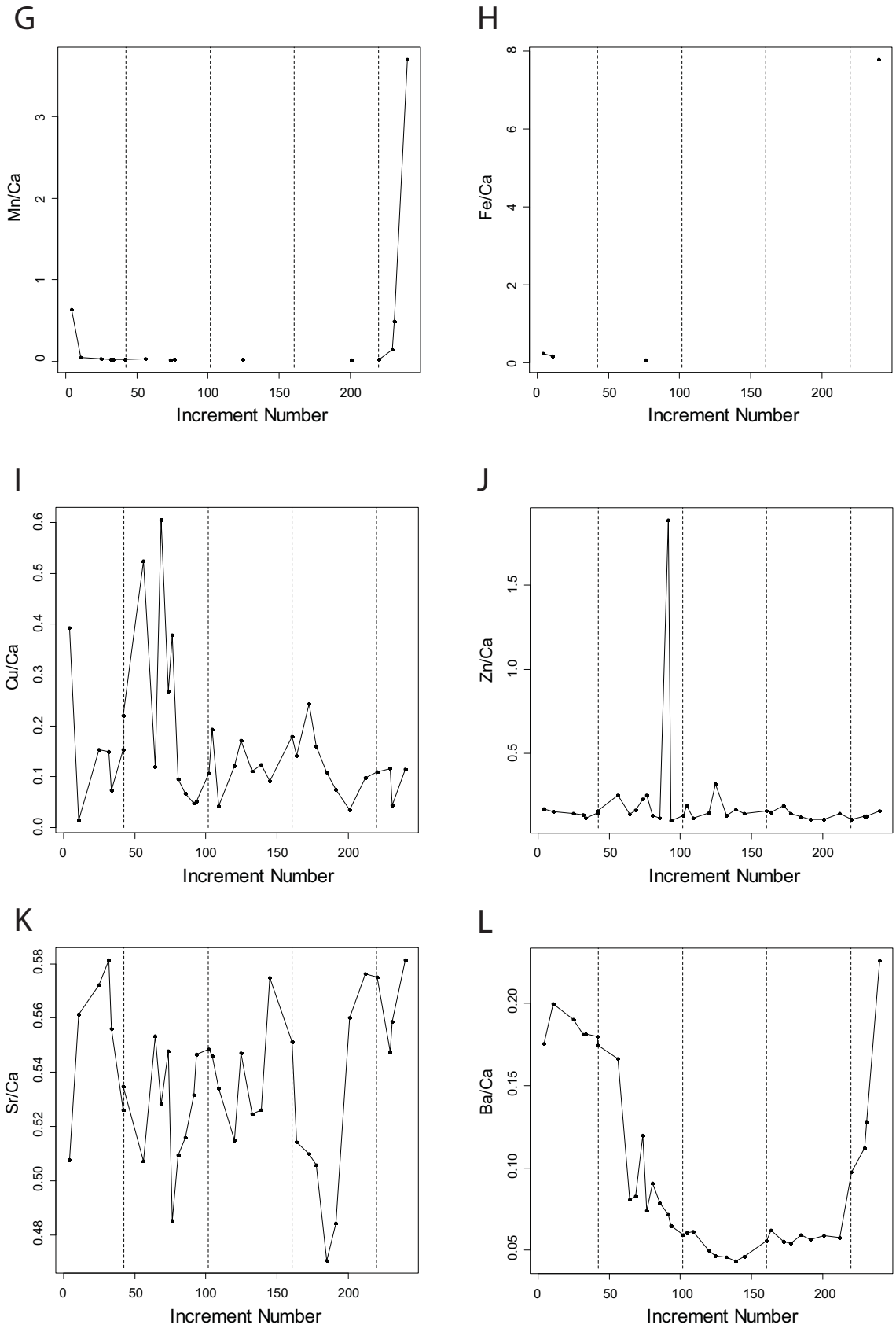
G
Mn/Ca
Increment Number
H
Fe/Ca
Increment Number
I
Cu/Ca
Increment Number
J
Zn/Ca
Increment Number
K
Sr/Ca
Increment Number
L
Ba/Ca
Increment Number

Figure 4.13, M-N. Compositional series for the 44-M tusk. M) Pb/Ca (mmol/mol), N) Average second-order increment thickness of increments contained within compositional samples (mm). Dashed lines represent approximate years and are separated by 59.25 increments. Missing points occur in the elemental ratio series when concentration was below detection. These series are difficult to interpret.

M

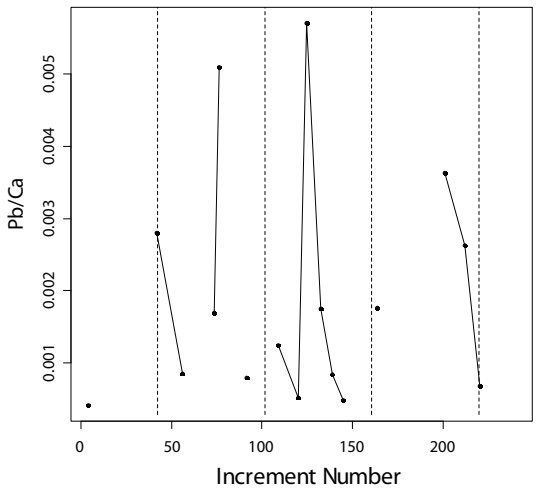
Pb/Ca
0.001
0.002
0.003
0.004
0.005
0
50
100
150
200
Increment Number

N

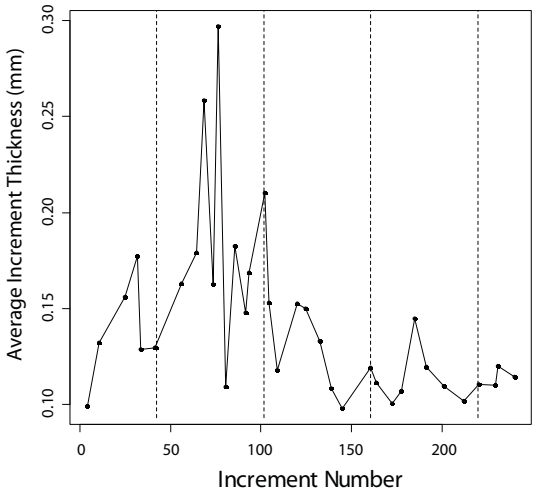
Average Increment Thickness (mm)
0.10
0.15
0.20
0.25
0.30
0
50
100
150
200
Increment Number

Figure 4.14. Second-order increment thicknesses for the 44-M tusk. Time proceeds from left to right. Dashed lines mark approximate years based on $\delta^{13}C_{col}$ and are evenly spaced at 59.25 increment intervals. No seasonal pattern is evident in the series.

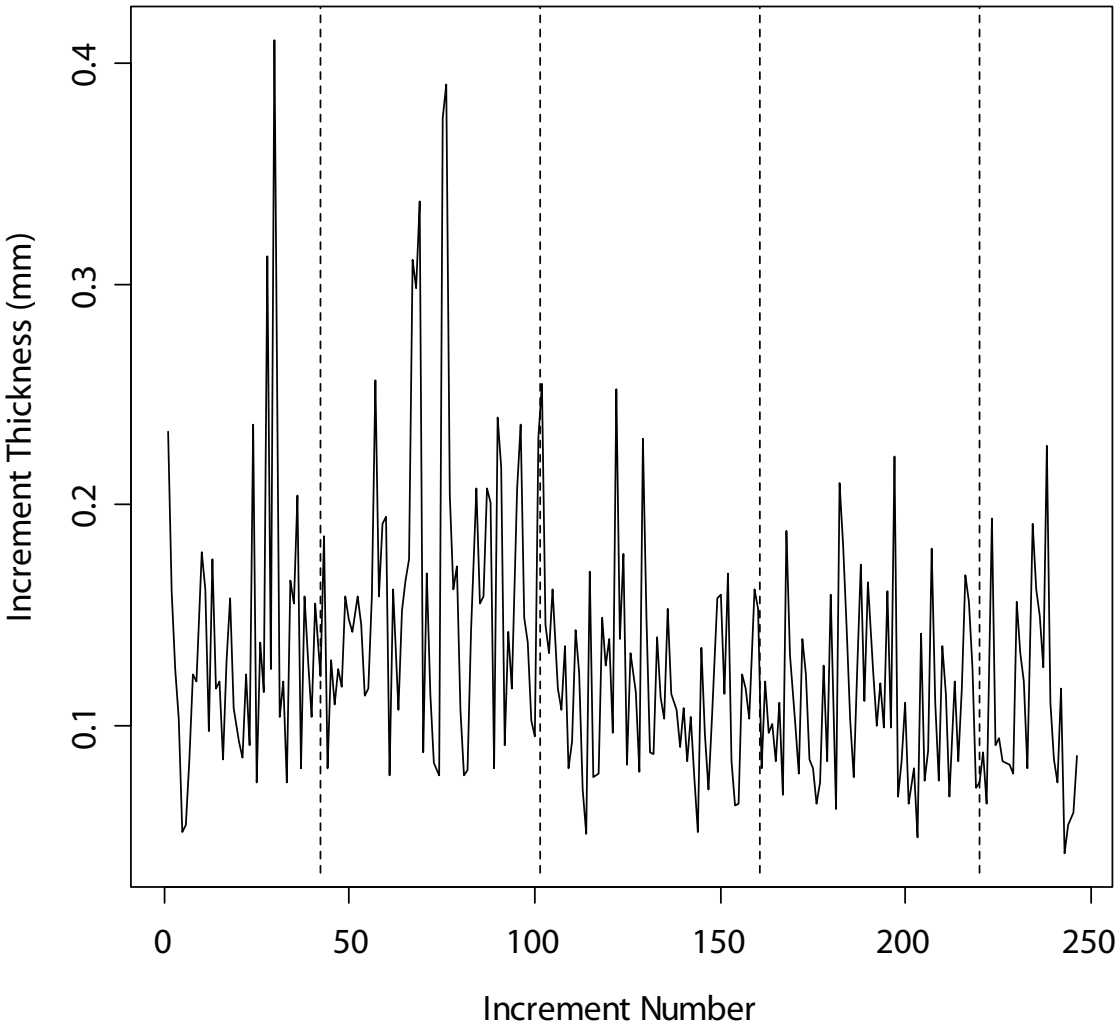

Figure 4.15, A-F. Compositional series for the Mol tusk. A) $\delta^{13}C_{col}$ relative to VPDB, B) $\delta^{15}N_{col}$ relative to AIR, C) Mg/Ca (mmol/mol), D) P/Ca (mmol/mol), E) Mn/Ca (mmol/mol), F) Fe/Ca (mmol/mol). Dashed lines represent approximate years and are separated by 41.5 increments. Collagen samples corresponding to the first three samples in the elemental series were not analyzed. Missing points occur in the elemental ratio series when concentration was below detection. Note the seasonal variation in A, the long-term decline in B, the long term increase in C and D, and the elevated values of the first samples (near the tip of the tusk) in E and F.

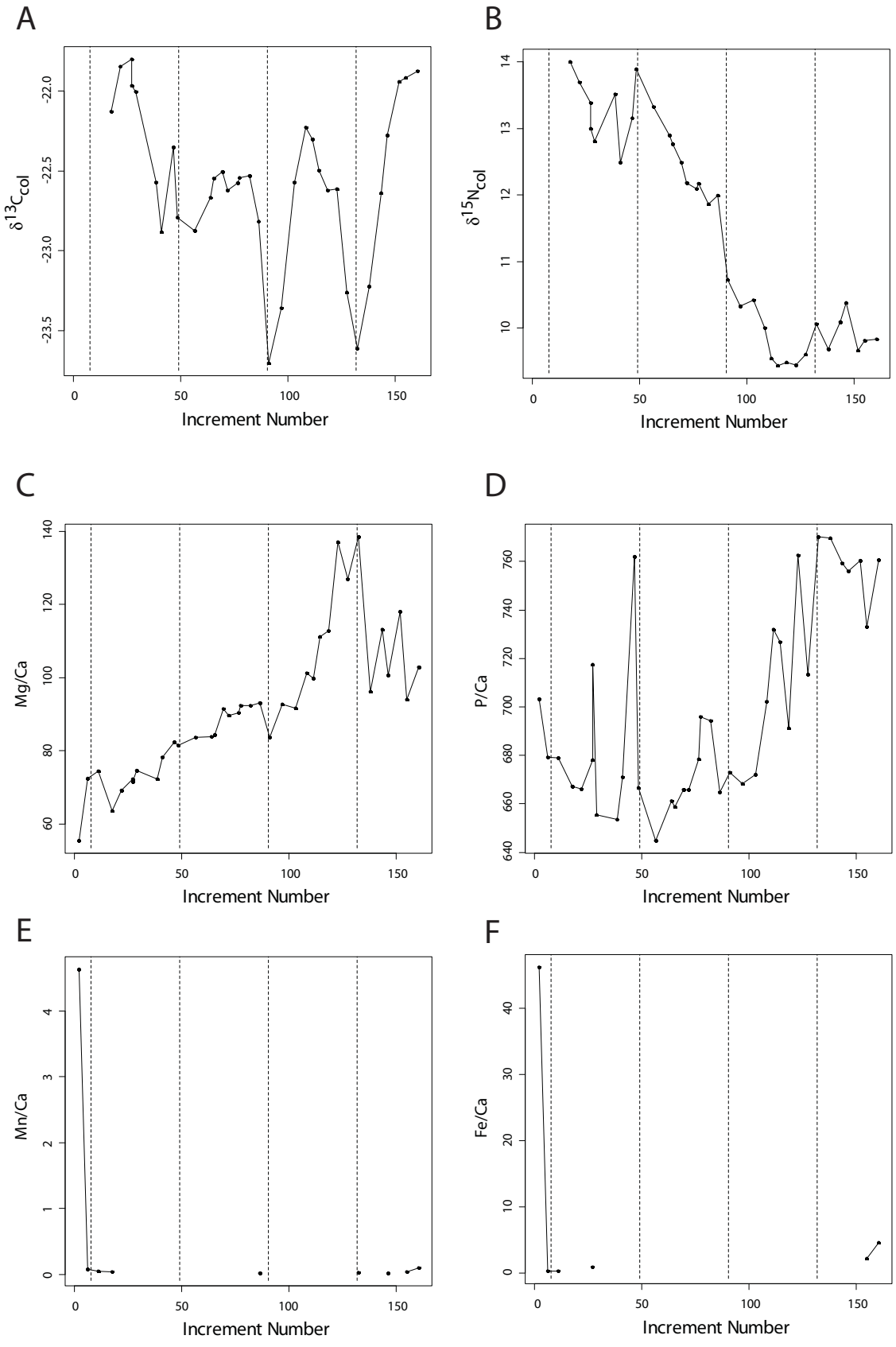
A
$\delta^{13}C_{col}$
-22.0
-22.5
-23.0
-23.5
0
50
100
150
Increment Number
B
$\delta^{15}N_{col}$
14
13
12
11
10
0
50
100
150
Increment Number
C
Mg/Ca
140
120
100
80
60
0
50
100
150
Increment Number
D
P/Ca
760
740
720
700
680
660
640
0
50
100
150
Increment Number
E
Mn/Ca
4
3
2
1
0
0
50
100
150
Increment Number
F
Fe/Ca
40
30
20
10
0
0
50
100
150
Increment Number

Figure 4.15, G-L. Compositional series for the Mol tusk. G) Cu/Ca (mmol/mol), H) Zn/Ca (mmol/mol), I) Sr/Ca (mmol/mol), J) Ba/Ca (mmol/mol), K) Pb/Ca (mmol/mol), F) Average second-order increment thickness of increments contained within compositional samples (mm). Dashed lines represent approximate years and are separated by 41.5 increments. Missing points occur in the elemental ratio series when concentration was below detection. Note the seasonal variation in I and J.

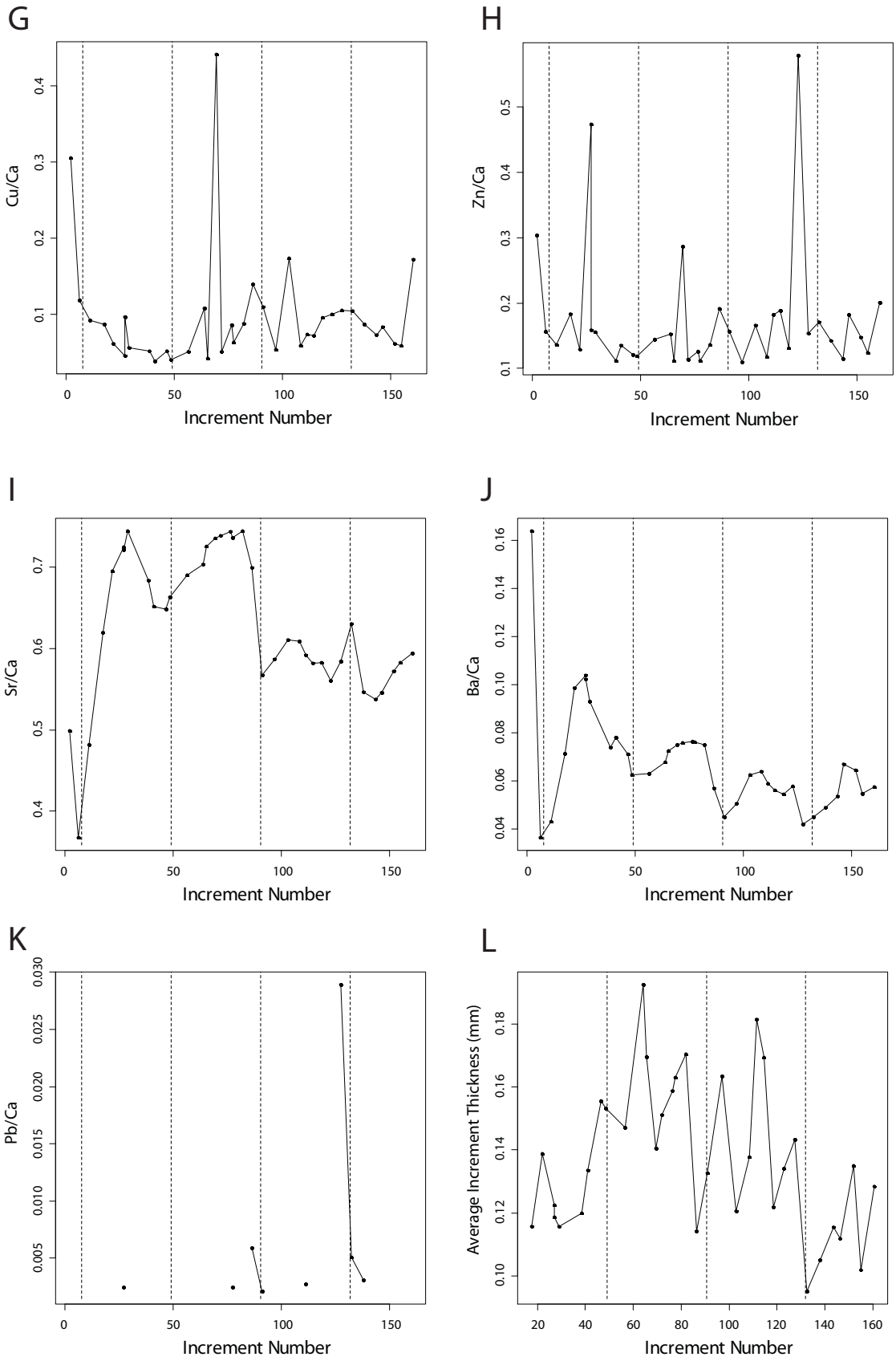
G
Cu/Ca
Increment Number
H
Zn/Ca
Increment Number
I
Sr/Ca
Increment Number
J
Ba/Ca
Increment Number
K
Pb/Ca
Increment Number
L
Average Increment Thickness (mm)
Increment Number

Figure 4.16. Second-order increment thicknesses for the Mol tusk. Time proceeds from left to right. Dashed lines mark approximate years based on $\delta^{13}C_{col}$ and are evenly spaced at 41.5 increment intervals. No seasonal pattern is evident in the series.

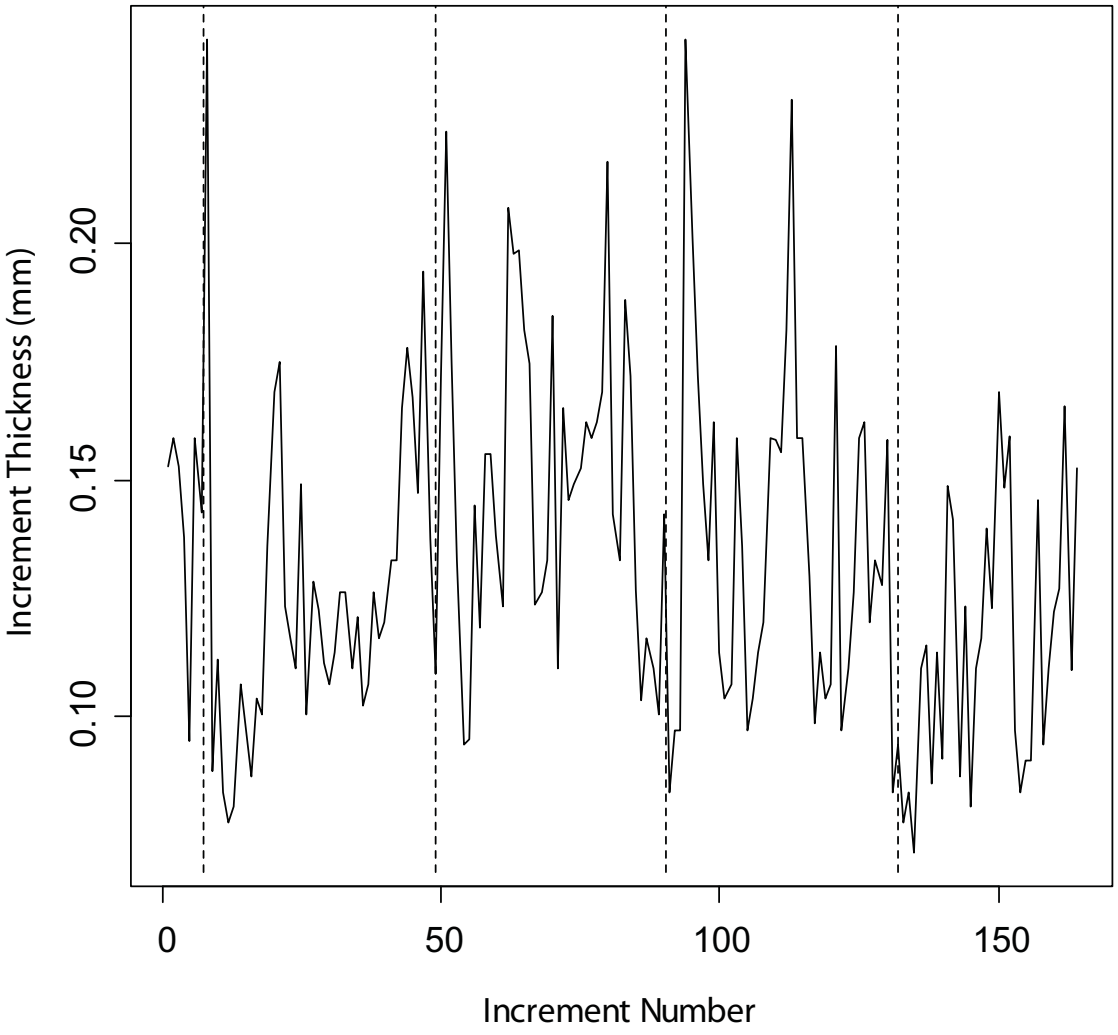

Figure 4.17, A-F. Compositional series for the Bolshoi Lyakhovskii tusk. A) $\delta^{13}C_{col}$ relative to VPDB, B) $\delta^{15}N_{col}$ relative to AIR, C) $\delta^{18}O_{carb}$ relative to VPDB, D) $\delta^{13}C_{carb}$ relative to VPDB, E) Mg/Ca (mmol/mol), F) P/Ca (mmol/mol). Dashed lines represent approximate years and are separated by 60.5 increments (based on number of increments between lows in the $\delta^{18}O_{carb}$ series). Missing points occur in the elemental ratio series when concentration was below detection. Note the seasonal-variation in A, B, and C, the long-term decline in B, the long-term increase in D, and possibly seasonal variation in E.

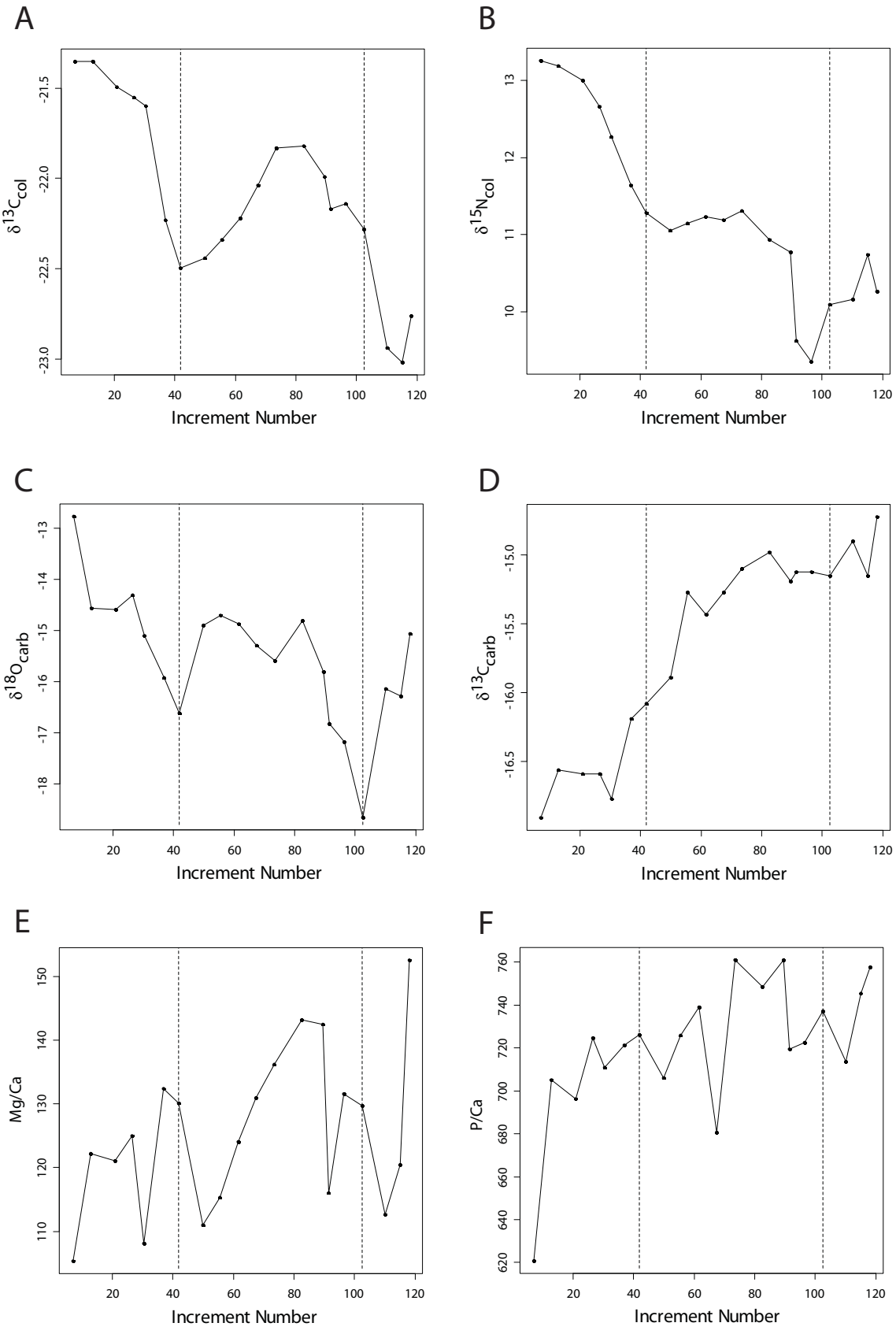
A
$\delta^{13}C_{col}$
-21.5
-22.0
-22.5
-23.0
20
40
60
80
100
120
Increment Number
B
$\delta^{15}N_{col}$
13
12
11
10
20
40
60
80
100
120
Increment Number
C
$\delta^{18}O_{carb}$
-13
-14
-15
-16
-17
-18
20
40
60
80
100
120
Increment Number
D
$\delta^{13}C_{carb}$
-15.0
-15.5
-16.0
-16.5
20
40
60
80
100
120
Increment Number
E
Mg/Ca
150
140
130
120
110
20
40
60
80
100
120
Increment Number
F
P/Ca
760
740
720
700
680
660
640
620
20
40
60
80
100
120
Increment Number

Figure 4.17, G-L. Compositional series for the Bolshoi Lyakhovskii tusk. G) Mn/Ca (mmol/mol) , H) Fe/Ca (mmol/mol), I) Cu/Ca (mmol/mol), J) Zn/Ca (mmol/mol), K) Sr/Ca (mmol/mol), L) Ba/Ca (mmol/mol). Dashed lines represent approximate years and are separated by 60.5 increments (based on number of increments between lows in the $\delta^{18}O_{carb}$ series). Missing points occur in the elemental ratio series when concentration was below detection. Note the elevated values of the last sample in G and H, the long-term increase in K, and the seasonal variation in L.

G

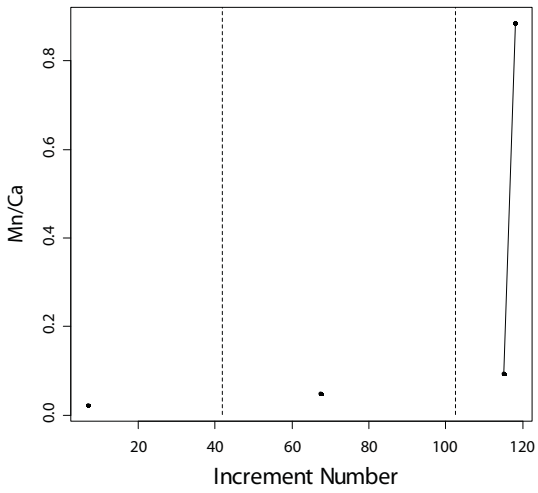
Mn/Ca
0.0
0.2
0.4
0.6
0.8
20
40
60
80
100
120
Increment Number

H

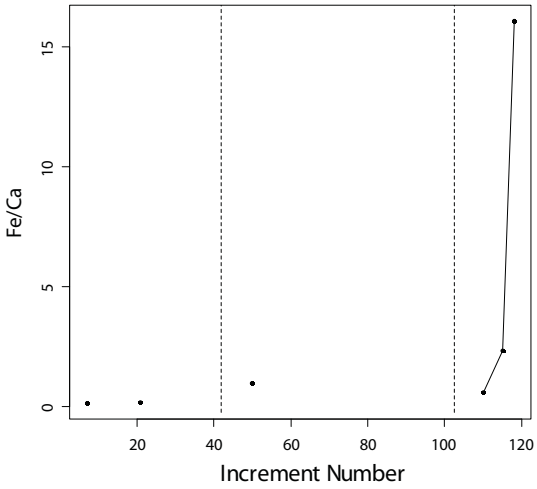
Fe/Ca
0
5
10
15
20
40
60
80
100
120
Increment Number

I

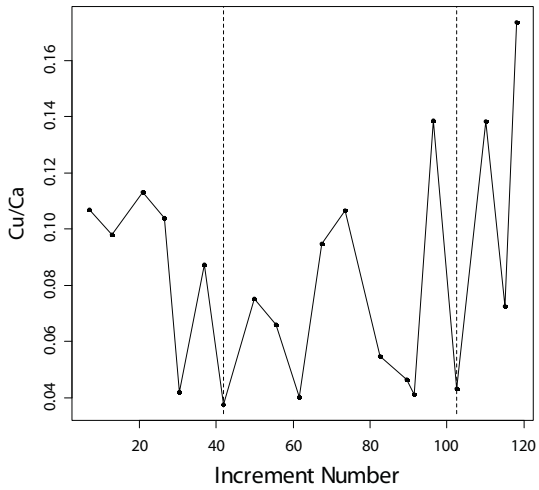
Cu/Ca
0.04
0.06
0.08
0.10
0.12
0.14
0.16
20
40
60
80
100
120
Increment Number

J

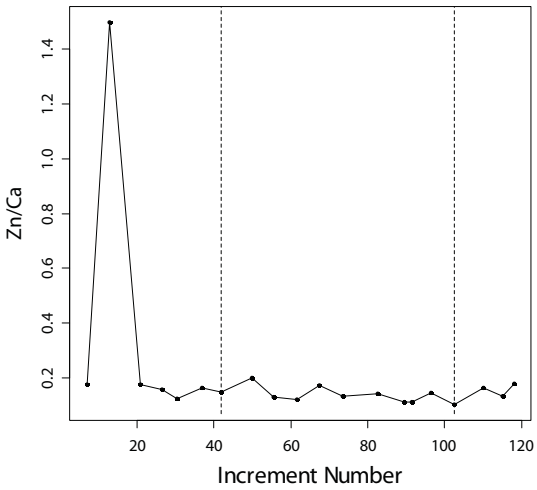
Zn/Ca
0.2
0.4
0.6
0.8
1.0
1.2
1.4
20
40
60
80
100
120
Increment Number

K

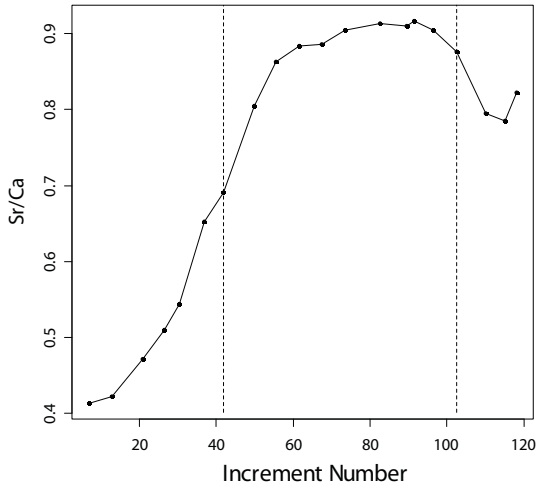
Sr/Ca
0.4
0.5
0.6
0.7
0.8
0.9
20
40
60
80
100
120
Increment Number

L

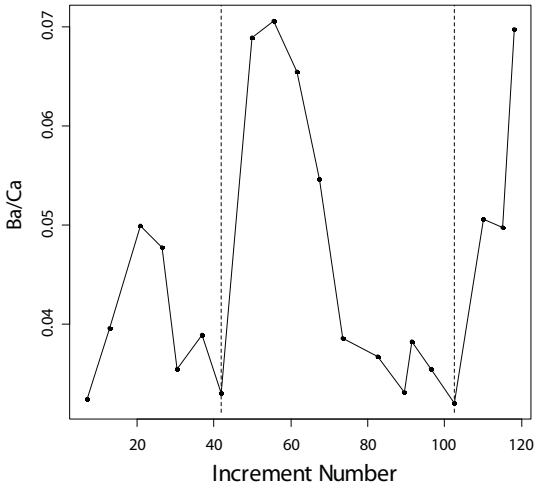
Ba/Ca
0.04
0.05
0.06
0.07
20
40
60
80
100
120
Increment Number

Figure 4.17, M-N. Compositional series for the Bolshoi Lyakhovskii tusk. M) Pb/Ca (mmol/mol), N) Average second-order increment thickness of increments contained within compositional samples (mm). Dashed lines represent approximate years and are separated by 60.5 increments (based on number of increments between lows in the $\delta^{18}O_{carb}$ series). Missing points occur in the elemental ratio series when concentration was below detection. The variation in N may be seasonal.

M

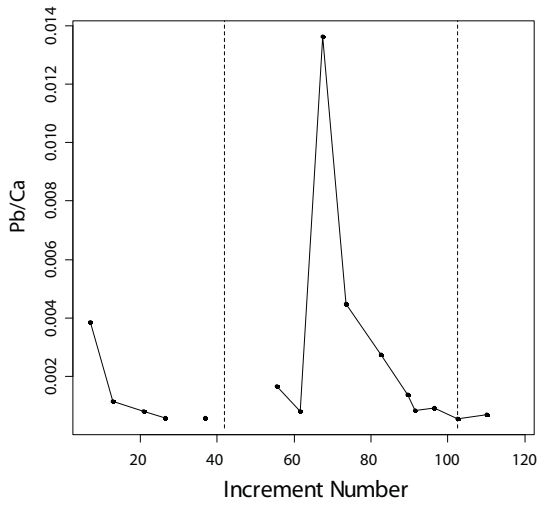
Pb/Ca
0.002
0.004
0.006
0.008
0.010
0.012
0.014
20
40
60
80
100
120
Increment Number

N

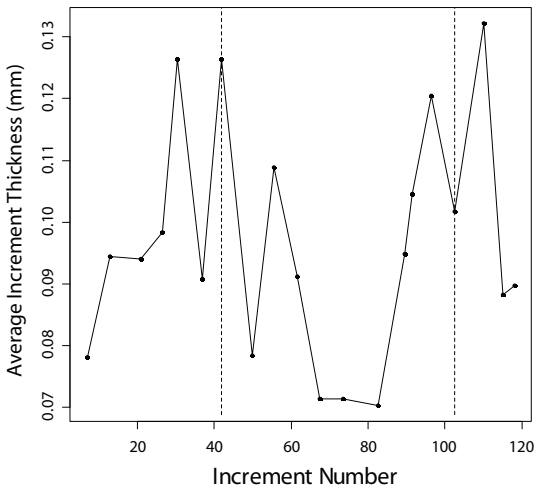
Average Increment Thickness (mm)
0.07
0.08
0.09
0.10
0.11
0.12
0.13
20
40
60
80
100
120
Increment Number

Figure 4.18. Second-order increment thicknesses for the Bolshoi Lyakhovskii tusk. Time proceeds from left to right. Dashed lines mark approximate years based on lows in $\delta^{18}O_{carb}$ (number of increments between dashed lines = 60.5). Accurate thicknesses for the first 8 increments could not be determined, and these increments are not shown. Increment thickness is negatively correlated with $\delta^{13}C_{col}$, $\delta^{15}N_{col}$, and $\delta^{18}O_{carb}$ (see Table 4.3). Note that thicknesses are reduced from around increment 65 to increment 85, a time when $\delta^{13}C_{col}$, $\delta^{15}N_{col}$, and $\delta^{18}O_{carb}$ are in the enriched phase of seasonal oscillation (Figs. 4.17A, B, C).

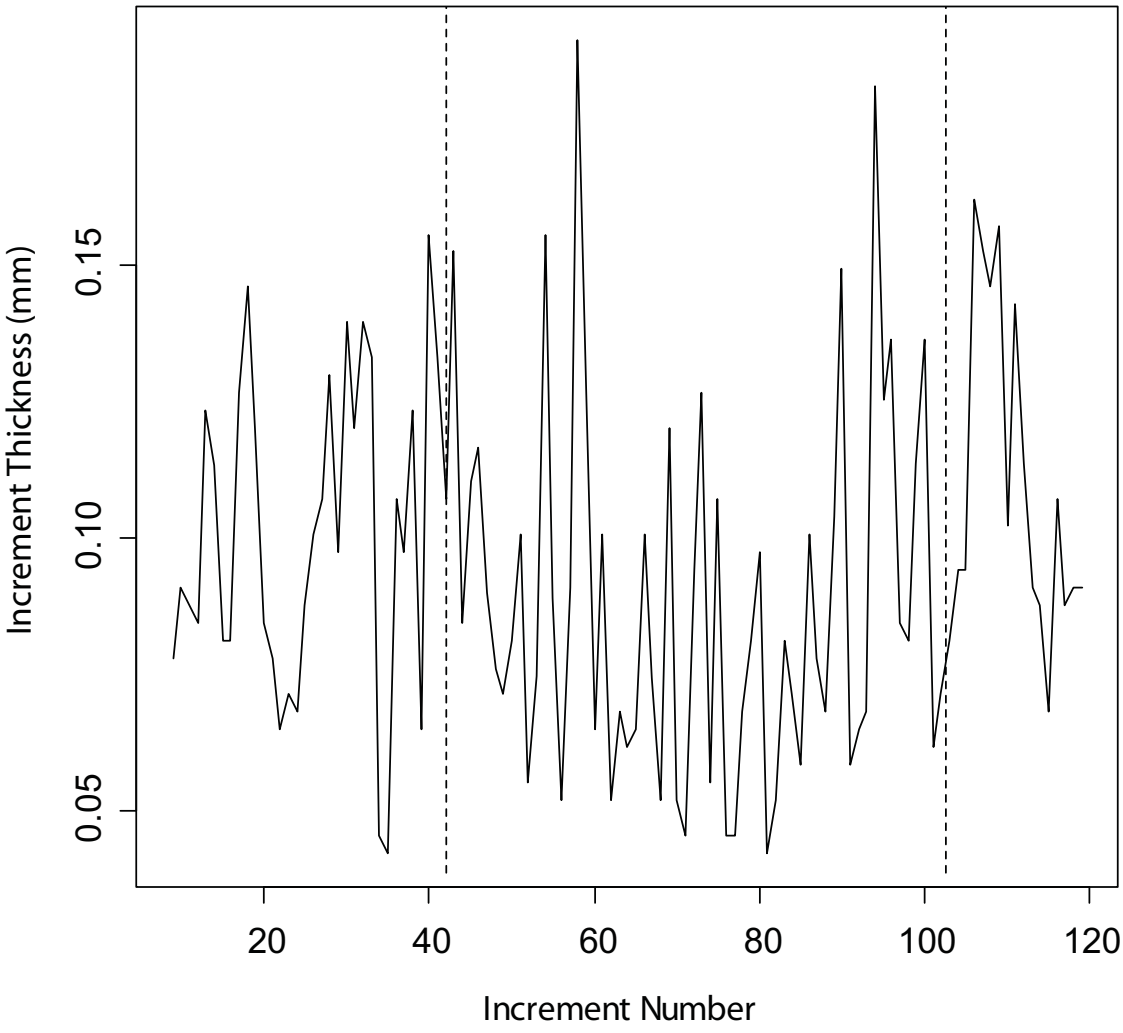

Figure 4.19, A-F. Compositional series for the Allen tusk. A) $\delta^{13}C_{col}$ relative to VPDB, B) $\delta^{15}N_{col}$ relative to AIR, C) Mg/Ca (mmol/mol), D) P/Ca (mmol/mol), E) Mn/Ca (mmol/mol), F) Fe/Ca (mmol/mol). Dashed lines represent approximate years and are separated by 45.5 increments. Note the anti-phase seasonal variation in A and B, the low values for all samples in C (see Table 4.5 for comparison), the elevated values of the first two samples in E, and the high values for all samples in F (see Table 4.5 for comparison).

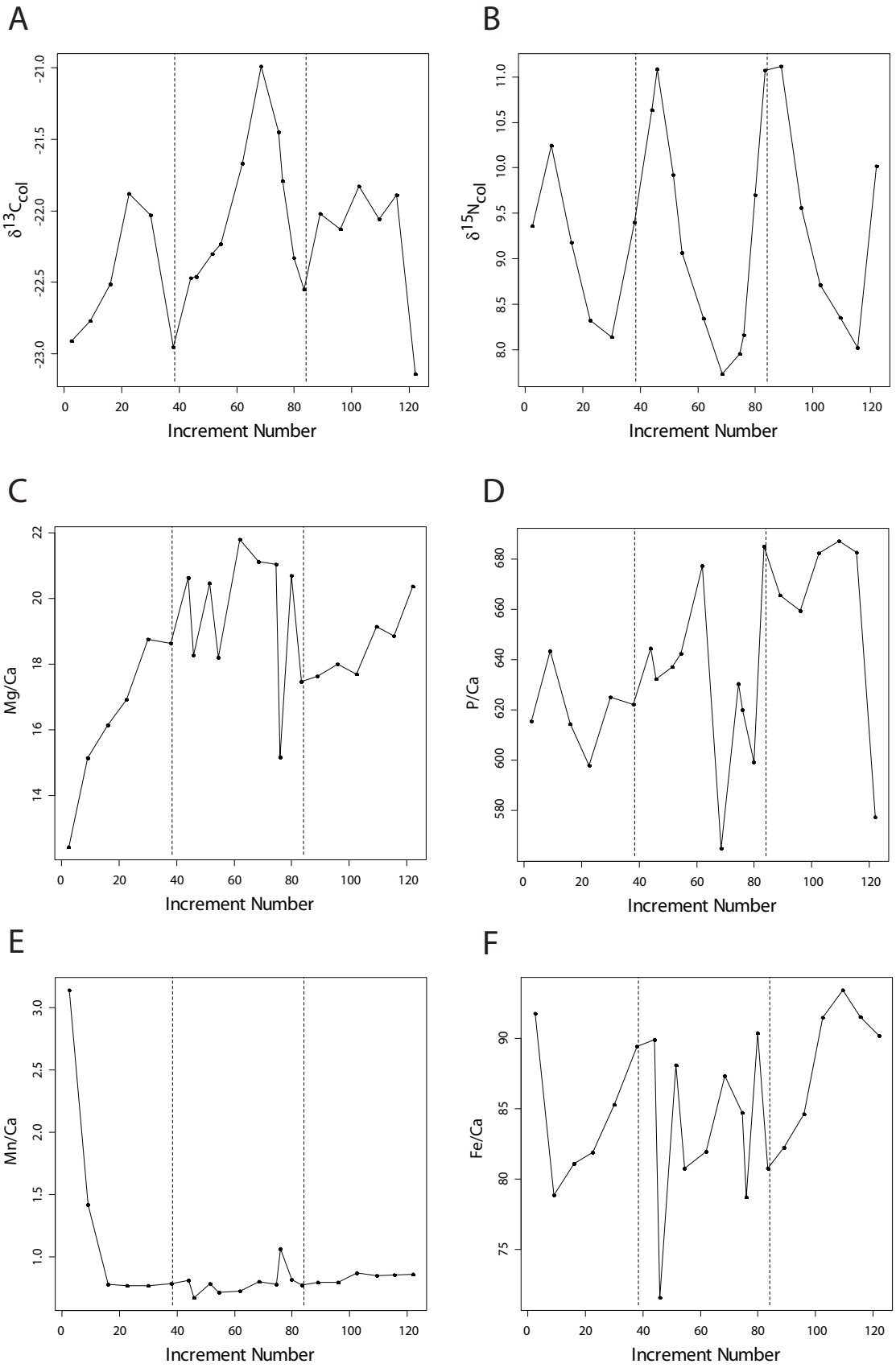
A
B
C
D
E
F
$\delta^{13}C_{col}$
$\delta^{15}N_{col}$
Mg/Ca
P/Ca
Mn/Ca
Fe/Ca
Increment Number

Figure 4.19, G-L. Compositional series for the Allen tusk. G) Cu/Ca (mmol/mol), H) Zn/Ca (mmol/mol), I) Sr/Ca (mmol/mol), J) Ba/Ca (mmol/mol), K) Pb/Ca (mmol/mol), F) Average second-order increment thickness of increments contained within compositional samples (mm). Missing points occur in the elemental ratio series when concentration was below detection. Dashed lines represent approximate years and are separated by 45.5 increments. These series are difficult to interpret. All values are relatively high in J (see Table 4.5 for comparison), and L is positively correlated with A (see Table 4.4).

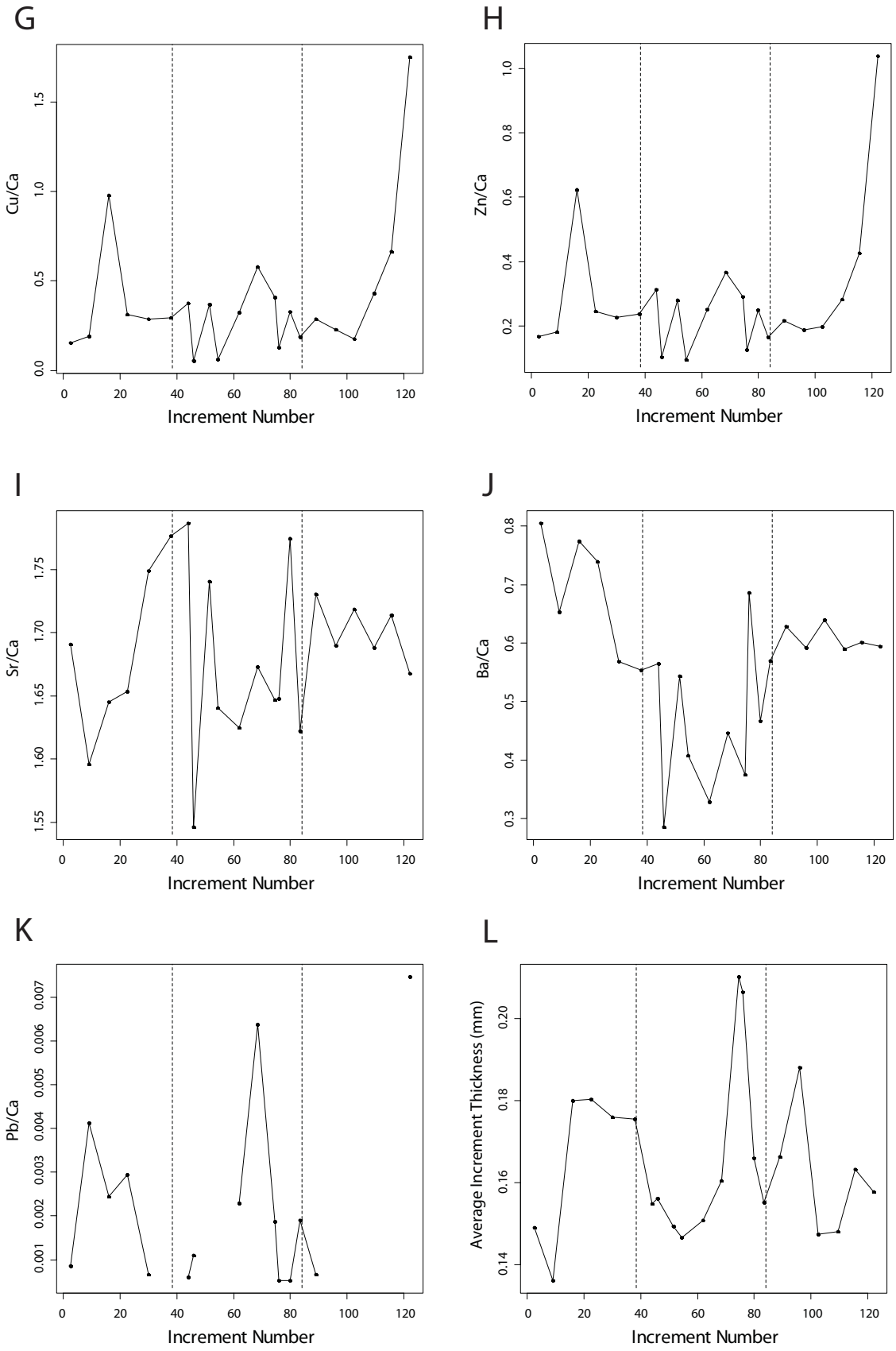
G
Cu/Ca
0.0
0.5
1.0
1.5
0
20
40
60
80
100
120
Increment Number
H
Zn/Ca
0.2
0.4
0.6
0.8
1.0
0
20
40
60
80
100
120
Increment Number
I
Sr/Ca
1.55
1.60
1.65
1.70
1.75
0
20
40
60
80
100
120
Increment Number
J
Ba/Ca
0.3
0.4
0.5
0.6
0.7
0.8
0
20
40
60
80
100
120
Increment Number
K
Pb/Ca
0.001
0.002
0.003
0.004
0.005
0.006
0.007
0
20
40
60
80
100
120
Increment Number
L
Average Increment Thickness (mm)
0.14
0.16
0.18
0.20
0
20
40
60
80
100
120
Increment Number

Figure 4.20. Second-order increment thicknesses for the Allen tusk. Time proceeds from left to right. Dashed lines mark approximate years based on $\delta^{13}C_{col}$ and are evenly spaced at 45.5 increment intervals. Increment thickness is positively correlated with $\delta^{13}C_{col}$ (and correlated with several other variables- see Table 4.4) suggesting that there is some association between diet/physiology and incremental growth rate in this individual.

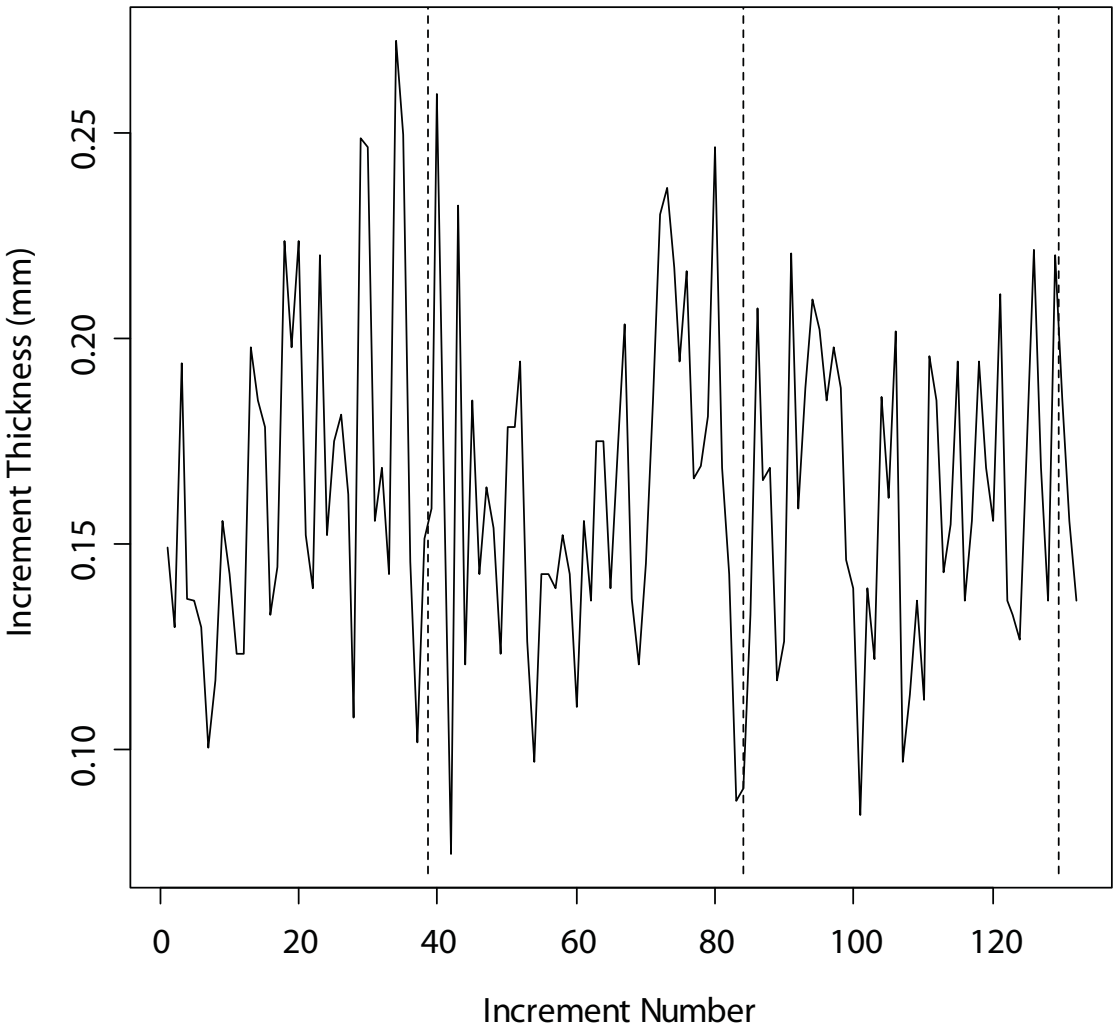

Figure 4.21, A-F. Compositional series for the Oimyakon tusk. A) $\delta^{13}C_{col}$ relative to VPDB, B) $\delta^{15}N_{col}$ relative to AIR, C) $\delta^{18}O_{carb}$ relative to VPDB, D) $\delta^{13}C_{carb}$ relative to VPDB, E) Mg/Ca (mmol/mol), F) P/Ca (mmol/mol). Dashed line indicates the position of the neonatal line. Note the declines in A and B following the neonatal line, and the low values for all samples in E (see Table 4.5 for comparison).

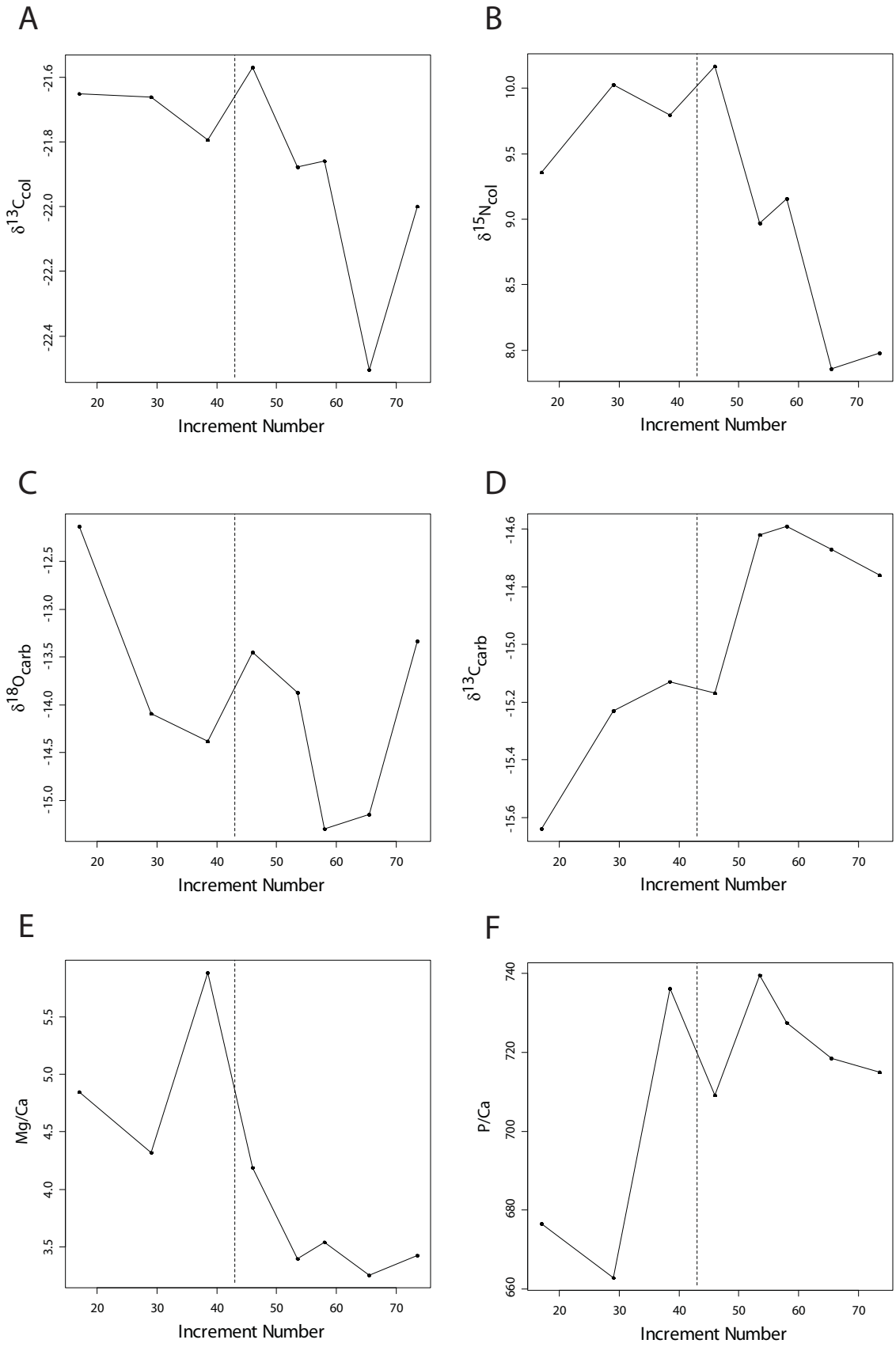
A
B
C
D
E
F
δ13Ccol
δ15Ncol
δ18Ocarb
δ13Ccarb
Mg/Ca
P/Ca
Increment Number

Figure 4.21, G-L. Compositional series for the Oimyakon tusk. G) Mn/Ca (mmol/mol) , H) Fe/Ca (mmol/mol), I) Cu/Ca (mmol/mol), J) Zn/Ca (mmol/mol), K) Sr/Ca (mmol/mol), L) Ba/Ca (mmol/mol). Dashed line indicates the position of the neonatal line. Note the elevated values for all samples in H (see Table 4.5 for comparison), the prenatal peak in I, the peak near the time of birth in J, a prenatal rise followed by a drop then another increase in K, and the possibly seasonal-scale variation in L.

G

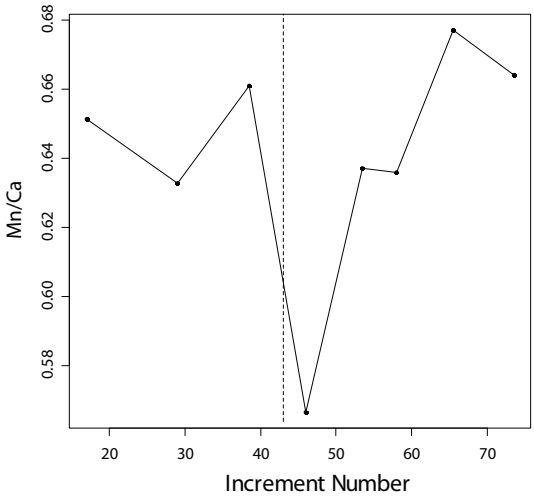
Mn/Ca
0.58
0.60
0.62
0.64
0.66
0.68
20
30
40
50
60
70
Increment Number

H

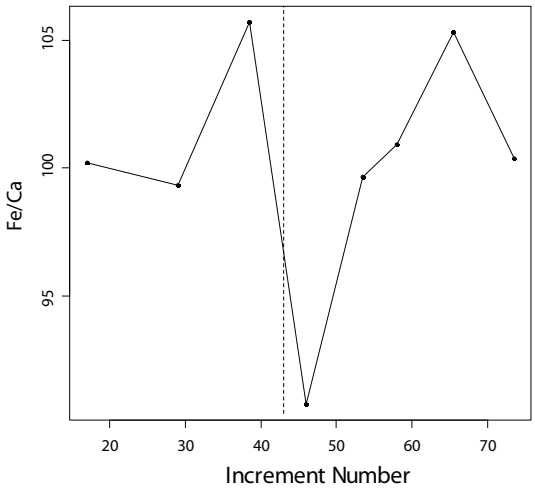
Fe/Ca
95
100
105
20
30
40
50
60
70
Increment Number

I

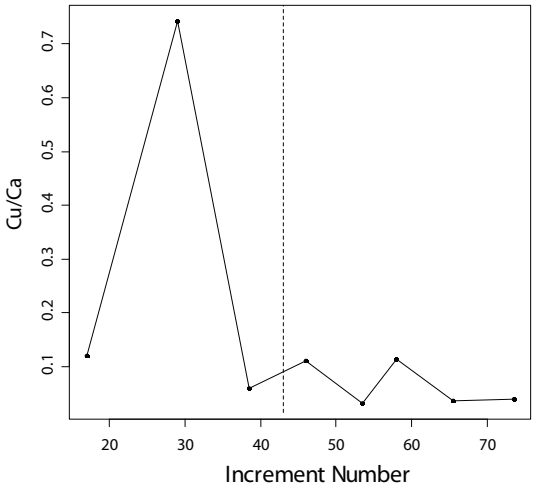
Cu/Ca
0.1
0.2
0.3
0.4
0.5
0.6
0.7
20
30
40
50
60
70
Increment Number

J

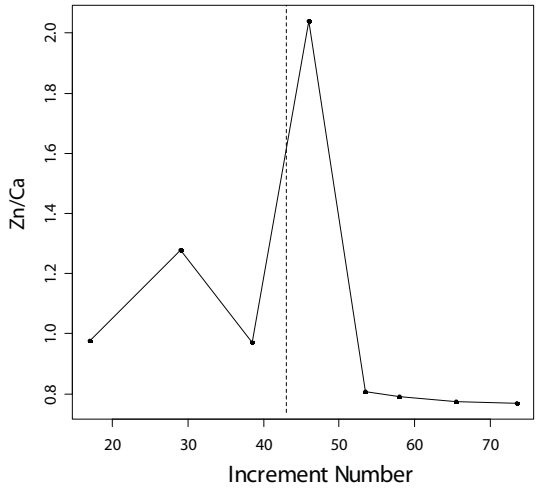
Zn/Ca
0.8
1.0
1.2
1.4
1.6
1.8
2.0
20
30
40
50
60
70
Increment Number

K

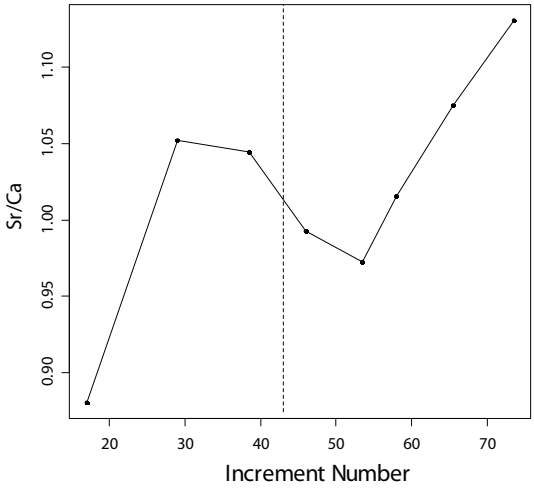
Sr/Ca
0.90
0.95
1.00
1.05
1.10
20
30
40
50
60
70
Increment Number

L

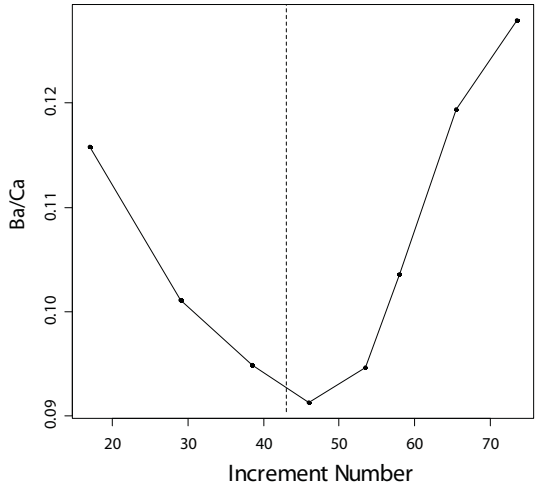
Ba/Ca
0.09
0.10
0.11
0.12
20
30
40
50
60
70
Increment Number

Figure 4.13, M-N. Compositional series for the Oimyakon tusk. M) Pb/Ca (mmol/mol), N) Average second-order increment thickness of increments contained within compositional samples (mm). Dashed line indicates the position of the neonatal line. Missing points occur in the elemental ratio series when concentration was below detection. M is difficult to interpret. See Figure 4.22 and text for discussion of patterns in increment thickness (N).

M

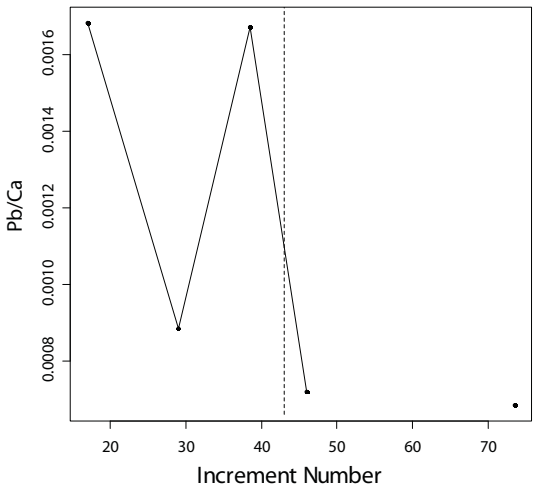
Pb/Ca
0.0008
0.0010
0.0012
0.0014
0.0016
20
30
40
50
60
70
Increment Number

N

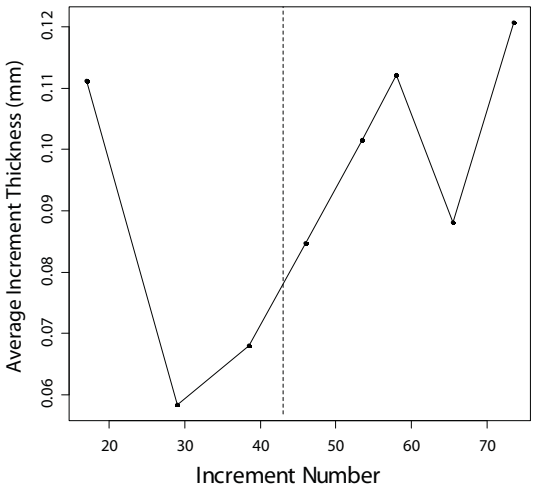
Average Increment Thickness (mm)
0.06
0.07
0.08
0.09
0.10
0.11
0.12
20
30
40
50
60
70
Increment Number

Figure 4.22. Second-order increment thicknesses for the Oimyakon tusk. Time proceeds from left to right. Dashed line marks the position of the neonatal line. Increment thickness increases significantly through time.

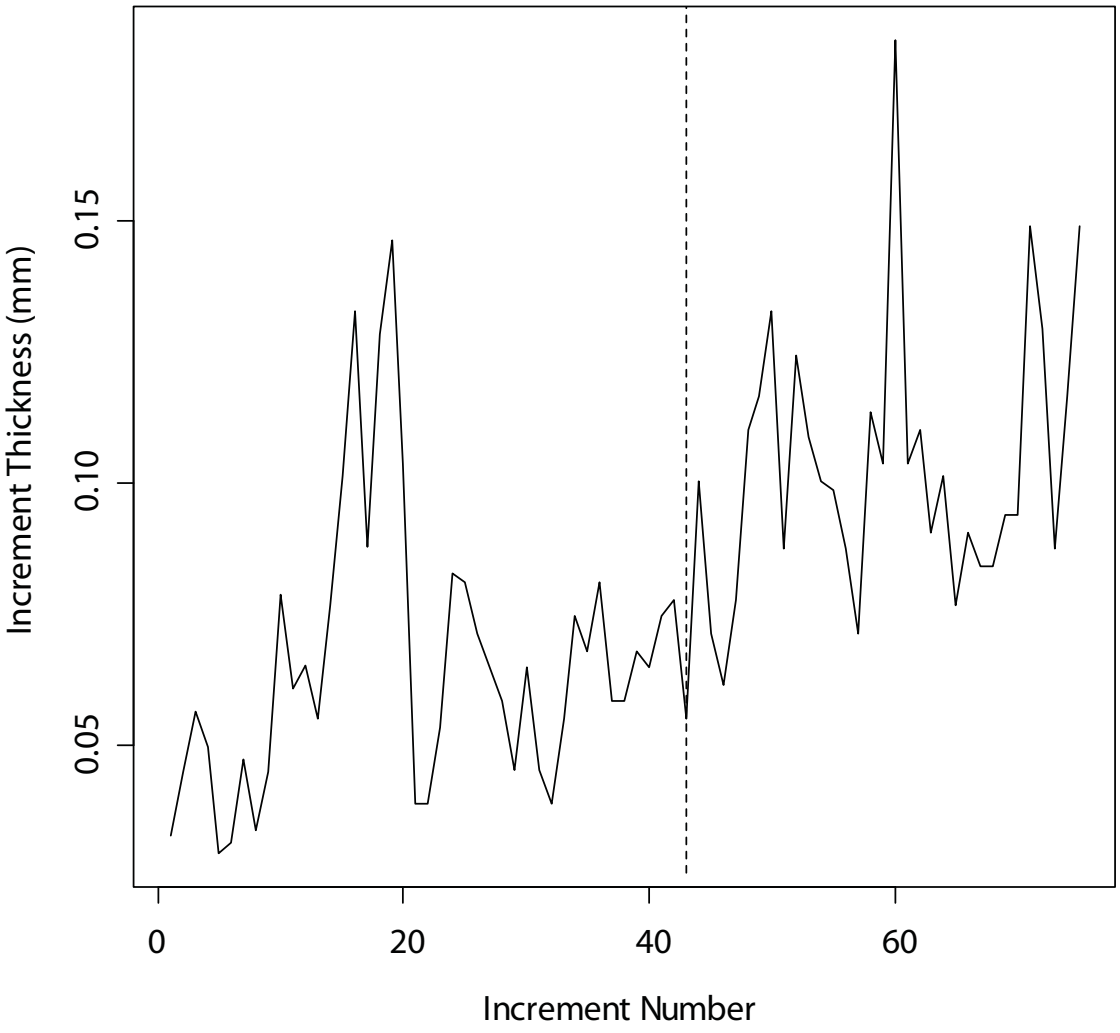

Appendix 4A

Isotope ratios and related data for the 44-M tusk. Sample 7 was excluded from calculation of cross-correlations.

Sample	Avg. Increment	$\delta^{13}C_{col}$	$\delta^{15}N_{col}$	$\delta^{18}O_{carb}$	$\delta^{13}C_{carb}$	C/N_{col}	$\delta^{13}C_{carb} - \delta^{13}C_{col}$
1	4.0	-22.67 ± 0.04	10.33 ± 0.10	-9.98 ± 0.05	-12.65 ± 0.03	3.08 ± 0.04	10.02 ± 0.05
2	10.5	-22.38 ± 0.04	8.16 ± 0.10	-8.19 ± 0.05	-10.76 ± 0.03	3.12 ± 0.04	11.63 ± 0.05
3	25.0	-21.93 ± 0.04	9.67 ± 0.10	-7.97 ± 0.05	-10.00 ± 0.03	3.11 ± 0.04	11.93 ± 0.05
4	31.5	-22.09 ± 0.04	9.73 ± 0.10	-8.83 ± 0.05	-9.83 ± 0.03	3.26 ± 0.04	12.26 ± 0.05
5	33.5	-21.88 ± 0.04	9.74 ± 0.10	-8.61 ± 0.05	-9.68 ± 0.03	3.12 ± 0.04	12.20 ± 0.05
6	42.0	-21.93 ± 0.04	10.23 ± 0.10	-8.36 ± 0.05	-9.60 ± 0.03	3.17 ± 0.04	12.33 ± 0.05
7*	42.0	-21.94 ± 0.04	10.95 ± 0.10	-8.79 ± 0.05	-9.68 ± 0.03	3.14 ± 0.04	12.26 ± 0.05
8	56.0	-21.92 ± 0.04	11.00 ± 0.10	-8.14 ± 0.05	-9.72 ± 0.03	3.13 ± 0.04	12.20 ± 0.05
9	64.5	-22.16 ± 0.04	8.94 ± 0.10	-8.28 ± 0.05	-9.73 ± 0.03	3.08 ± 0.04	12.43 ± 0.05
10	68.5	-22.06 ± 0.04	9.21 ± 0.10	-8.17 ± 0.05	-8.84 ± 0.03	3.04 ± 0.04	13.21 ± 0.05
11	73.5	-21.49 ± 0.04	10.12 ± 0.10	-7.66 ± 0.05	-8.84 ± 0.03	3.06 ± 0.04	12.66 ± 0.05
12	76.5	-21.68 ± 0.04	10.37 ± 0.10	-7.48 ± 0.05	-9.35 ± 0.03	3.10 ± 0.04	12.33 ± 0.05
13	80.5	-21.83 ± 0.04	10.09 ± 0.10	-7.74 ± 0.05	-11.94 ± 0.03	3.09 ± 0.04	9.89 ± 0.05
14	85.5	-21.68 ± 0.04	10.53 ± 0.10	-7.98 ± 0.05	-11.43 ± 0.03	3.07 ± 0.04	10.25 ± 0.05
15	91.5	-21.84 ± 0.04	10.26 ± 0.10	-7.72 ± 0.05	-11.22 ± 0.03	3.08 ± 0.04	10.63 ± 0.05
16	93.5	-21.64 ± 0.04	10.58 ± 0.10	-8.11 ± 0.05	-11.21 ± 0.03	3.16 ± 0.04	10.43 ± 0.05
17	102.0	-22.94 ± 0.04	9.86 ± 0.10	-9.13 ± 0.05	-11.73 ± 0.03	3.06 ± 0.04	11.21 ± 0.05
18	104.5	-22.92 ± 0.04	9.13 ± 0.10	-8.40 ± 0.05	-11.11 ± 0.03	3.08 ± 0.04	11.81 ± 0.05
19	109.0	-22.85 ± 0.04	8.29 ± 0.10	-7.47 ± 0.05	-11.56 ± 0.03	3.08 ± 0.04	11.29 ± 0.05
20	120.0	-21.60 ± 0.04	9.27 ± 0.10	-8.13 ± 0.05	-10.67 ± 0.03	3.09 ± 0.04	10.93 ± 0.05
21	124.5	-21.59 ± 0.04	9.47 ± 0.10	-7.96 ± 0.05	-11.05 ± 0.03	3.07 ± 0.04	10.53 ± 0.05
22	132.5	-21.50 ± 0.04	9.48 ± 0.10	-7.93 ± 0.05	-10.89 ± 0.03	3.08 ± 0.04	10.61 ± 0.05
23	139.0	-21.50 ± 0.04	9.49 ± 0.10	-7.95 ± 0.05	-11.65 ± 0.03	3.08 ± 0.04	9.85 ± 0.05
24	145.0	-21.59 ± 0.04	10.30 ± 0.10	-7.85 ± 0.05	-11.51 ± 0.03	3.09 ± 0.04	10.08 ± 0.05
25	160.5	-22.68 ± 0.04	8.55 ± 0.10	-9.00 ± 0.05	-11.19 ± 0.03	3.08 ± 0.04	11.48 ± 0.05
26	164.0	-22.35 ± 0.04	8.27 ± 0.10	-7.37 ± 0.05	-10.51 ± 0.03	3.15 ± 0.04	11.84 ± 0.05
27	172.5	-21.59 ± 0.04	9.13 ± 0.10	-7.37 ± 0.05	-10.37 ± 0.03	3.09 ± 0.04	11.22 ± 0.05
28	177.5	-21.53 ± 0.04	8.90 ± 0.10	-7.58 ± 0.05	-10.27 ± 0.03	3.11 ± 0.04	11.26 ± 0.05
29	185.0	-21.55 ± 0.04	9.08 ± 0.10	-7.21 ± 0.05	-10.19 ± 0.03	3.08 ± 0.04	11.37 ± 0.05
30	191.5	-21.45 ± 0.04	9.55 ± 0.10	-6.73 ± 0.05	-10.00 ± 0.03	3.11 ± 0.04	11.44 ± 0.05
31	201.0	-21.51 ± 0.04	9.52 ± 0.10	-7.98 ± 0.05	-10.36 ± 0.03	3.11 ± 0.04	11.15 ± 0.05
32	212.0	-21.99 ± 0.04	9.27 ± 0.10	-8.11 ± 0.05	-10.16 ± 0.03	3.08 ± 0.04	11.83 ± 0.05
33	220.5	-22.88 ± 0.04	7.46 ± 0.10	-9.00 ± 0.05	-9.49 ± 0.03	3.08 ± 0.04	13.38 ± 0.05
34	229.5	-22.42 ± 0.04	8.12 ± 0.10	-8.50 ± 0.05	-9.17 ± 0.03	3.12 ± 0.04	13.25 ± 0.05
35	231.0	-21.60 ± 0.04	9.39 ± 0.10	-8.83 ± 0.05	-8.75 ± 0.03	3.10 ± 0.04	12.86 ± 0.05
36	240.0	-21.56 ± 0.04	9.48 ± 0.10	-8.20 ± 0.05	-8.47 ± 0.03	3.10 ± 0.04	13.09 ± 0.05
mean		**-21.93**	**9.50**	**-8.05**	**-10.32**	**3.10**	**11.60**
s.d.		**0.47**	**0.83**	**0.56**	**0.98**	**0.03**	**1.02**

Appendix 4A

Isotope ratios and related data for the Mol tusk. Values in gray are spline interpolated and were not included in calculations of the means and standard deviations. No collagen samples were taken prior to increment 17.5. Sample 7 was excluded from calculation of cross-correlations.

Sample	Avg. Increment	$\delta^{13}C_{col}$	$\delta^{15}N_{col}$	C/N_{col}
1	2			
2	6			
3	11			
4	17.5	-22.13 ± 0.04	14.01 ± 0.02	3.16 ± 0.12
5	22	-21.84 ± 0.04	13.70 ± 0.02	3.18 ± 0.12
6	27	-21.80 ± 0.04	13.39 ± 0.02	3.15 ± 0.11
7	27	-21.97 ± 0.04	12.99 ± 0.02	3.14 ± 0.11
8	29	-22.00 ± 0.04	12.81 ± 0.02	3.14 ± 0.11
9	38.5	-22.57 ± 0.04	13.51 ± 0.02	3.16 ± 0.12
10	41	-22.88 ± 0.04	12.49 ± 0.02	3.15 ± 0.12
11	46.5	-22.35 ± 0.04	13.16 ± 0.02	3.17 ± 0.12
12	48.5	-22.79 ± 0.04	13.89 ± 0.02	3.15 ± 0.11
13	56.5	-22.87 ± 0.04	13.32 ± 0.02	3.11 ± 0.11
14	64	-22.67 ± 0.04	12.90 ± 0.02	3.17 ± 0.12
15	65.5	-22.55 ± 0.04	12.77 ± 0.02	3.13 ± 0.11
16	69.5	-22.51 ± 0.04	12.49 ± 0.02	3.13 ± 0.11
17	72	-22.62 ± 0.04	12.18 ± 0.02	3.14 ± 0.11
18	76.5	-22.58 ± 0.04	12.09 ± 0.02	3.14 ± 0.11
19	77.5	-22.54 ± 0.04	12.17 ± 0.02	3.11 ± 0.11
20	82	-22.53 ± 0.04	11.87 ± 0.02	3.13 ± 0.11
21	86.5	-22.82 ± 0.04	12.00 ± 0.02	3.12 ± 0.11
22	91	-23.70 ± 0.04	10.73 ± 0.02	3.19 ± 0.12
23	97	-23.36 ± 0.04	10.33 ± 0.02	3.18 ± 0.12
24	103	-22.57 ± 0.04	10.42 ± 0.02	
25	108.5	-22.23 ± 0.04	10.00 ± 0.02	3.17 ± 0.12
26	111.5	-22.30 ± 0.04	9.55 ± 0.02	3.16 ± 0.12
27	114.5	-22.50 ± 0.04	9.44 ± 0.02	3.21 ± 0.12
28	118.5	-22.62 ± 0.04	9.49 ± 0.02	3.19 ± 0.12
29	123	-22.61 ± 0.04	9.45 ± 0.02	3.16 ± 0.12
30	127.5	-23.26 ± 0.04	9.61 ± 0.02	3.17 ± 0.12
31	132.5	-23.61 ± 0.04	10.06 ± 0.02	3.15 ± 0.11
32	138	-23.22 ± 0.04	9.69 ± 0.02	3.12 ± 0.11
33	143.5	-22.64 ± 0.04	10.10 ± 0.02	3.15 ± 0.11
34	146.5	-22.28 ± 0.04	10.39 ± 0.02	3.14 ± 0.11
35	152	-21.94 ± 0.04	9.67 ± 0.02	3.16 ± 0.12
36	155	-21.92 ± 0.04	9.81 ± 0.02	3.13 ± 0.11
37	160.5	-21.88 ± 0.04	9.84 ± 0.02	3.18 ± 0.12
mean		**-22.55**	**11.51**	**3.15**
s.d.		**0.49**	**1.61**	**0.02**

Appendix 4A

Isotope ratios and related data for the Bolshoi Lyakhovskii tusk. Isotope values in gray are spline interpolated and were not included in calculations of means or standard deviations.

Sample	Avg. Increment	$\delta^{13}C_{col}$	$\delta^{15}N_{col}$	$\delta^{18}O_{carb}$	$\delta^{13}C_{carb}$	C/N_{col}	$\delta^{13}C_{carb} - \delta^{13}C_{col}$
1	7.0	-21.35 ± 0.04	13.26 ± 0.02	-12.77 ± 0.10	-16.91 ± 0.05	3.17 ± 0.12	4.44 ± 0.06
2	13.0	-21.35 ± 0.04	13.19 ± 0.02	-14.57 ± 0.10	-16.56 ± 0.05	3.18 ± 0.12	4.79 ± 0.06
3	21.0	-21.49 ± 0.04	13.00 ± 0.02	-14.59 ± 0.10	-16.59 ± 0.05		4.90 ± 0.06
4	26.5	-21.55 ± 0.04	12.66 ± 0.02	-14.31 ± 0.10	-16.59 ± 0.05	3.16 ± 0.12	4.96 ± 0.06
5	30.5	-21.60 ± 0.04	12.27 ± 0.02	-15.11 ± 0.10	-16.77 ± 0.05	3.15 ± 0.11	4.83 ± 0.06
6	37.0	-22.23 ± 0.04	11.64 ± 0.02	-15.93 ± 0.10	-16.19 ± 0.05	3.17 ± 0.12	6.04 ± 0.06
7	42.0	-22.50 ± 0.04	11.28 ± 0.02	-16.62 ± 0.10	-16.08 ± 0.05		6.41 ± 0.06
8	50.0	-22.44 ± 0.04	11.05 ± 0.02	-14.90 ± 0.10	-15.89 ± 0.05	3.15 ± 0.12	6.55 ± 0.06
9	55.5	-22.34 ± 0.04	11.14 ± 0.02	-14.71 ± 0.10	-15.27 ± 0.05		7.07 ± 0.06
10	61.5	-22.22 ± 0.04	11.23 ± 0.02	-14.88 ± 0.10	-15.43 ± 0.05	3.15 ± 0.11	6.79 ± 0.06
11	67.5	-22.04 ± 0.04	11.19 ± 0.02	-15.30 ± 0.10	-15.27 ± 0.05	3.14 ± 0.11	6.77 ± 0.06
12	73.5	-21.83 ± 0.04	11.31 ± 0.02	-15.60 ± 0.10	-15.10 ± 0.05	3.13 ± 0.11	6.73 ± 0.06
13	82.5	-21.82 ± 0.04	10.93 ± 0.02	-14.81 ± 0.10	-14.98 ± 0.05	3.15 ± 0.12	6.84 ± 0.06
14	89.5	-21.99 ± 0.04	10.77 ± 0.02	-15.81 ± 0.10	-15.19 ± 0.05	3.14 ± 0.11	6.80 ± 0.06
15	91.5	-22.17 ± 0.04	9.62 ± 0.02	-16.82 ± 0.10	-15.12 ± 0.05	3.14 ± 0.11	7.05 ± 0.06
16	96.5	-22.14 ± 0.04	9.35 ± 0.02	-17.18 ± 0.10	-15.12 ± 0.05	3.14 ± 0.11	7.02 ± 0.06
17	102.5	-22.28 ± 0.04	10.09 ± 0.02	-18.66 ± 0.10	-15.15 ± 0.05	3.13 ± 0.11	7.13 ± 0.06
18	110.0	-22.94 ± 0.04	10.16 ± 0.02	-16.14 ± 0.10	-14.90 ± 0.05	3.13 ± 0.11	8.04 ± 0.06
19	115.0	-23.02 ± 0.04	10.74 ± 0.02	-16.29 ± 0.10	-15.15 ± 0.05	3.16 ± 0.12	7.87 ± 0.06
20	118.0	-22.76 ± 0.04	10.26 ± 0.02	-15.07 ± 0.10	-14.72 ± 0.05	3.13 ± 0.11	8.04 ± 0.06
mean		**-22.10**	**11.16**	**-15.86**	**-15.40**	**3.14**	**6.51**
s.d.		**0.50**	**1.15**	**1.07**	**0.55**	**0.01**	**1.13**

Appendix 4A

Isotope ratios and related data for the Allen tusk.

Sample	Avg. Increment	$\delta^{13}C_{col}$	$\delta^{15}N_{col}$	C/N_{col}
1	2.5	-22.91 ± 0.01	9.36 ± 0.03	3.26 ± 0.03
2	9.0	-22.77 ± 0.01	10.25 ± 0.03	3.25 ± 0.03
3	16.0	-22.51 ± 0.01	9.18 ± 0.03	3.26 ± 0.03
4	22.5	-21.88 ± 0.01	8.32 ± 0.03	3.25 ± 0.03
5	30.0	-22.03 ± 0.01	8.14 ± 0.03	3.26 ± 0.03
6	38.0	-22.95 ± 0.01	9.40 ± 0.03	3.27 ± 0.03
7	44.0	-22.47 ± 0.01	10.64 ± 0.03	3.25 ± 0.03
8	46.0	-22.46 ± 0.01	11.09 ± 0.03	3.23 ± 0.03
9	51.5	-22.30 ± 0.01	9.92 ± 0.03	3.25 ± 0.03
10	54.5	-22.23 ± 0.01	9.07 ± 0.03	3.27 ± 0.03
11	62.0	-21.67 ± 0.01	8.34 ± 0.03	3.23 ± 0.03
12	68.5	-20.99 ± 0.01	7.73 ± 0.03	3.27 ± 0.03
13	74.5	-21.45 ± 0.01	7.95 ± 0.03	3.25 ± 0.03
14	76.0	-21.79 ± 0.01	8.16 ± 0.03	3.26 ± 0.03
15	80.0	-22.33 ± 0.01	9.70 ± 0.03	3.25 ± 0.03
16	83.5	-22.55 ± 0.01	11.07 ± 0.03	3.25 ± 0.03
17	89.0	-22.02 ± 0.01	11.12 ± 0.03	3.26 ± 0.03
18	96.0	-22.13 ± 0.01	9.56 ± 0.03	3.25 ± 0.03
19	102.5	-21.83 ± 0.01	8.71 ± 0.03	3.25 ± 0.03
20	109.5	-22.06 ± 0.01	8.35 ± 0.03	3.24 ± 0.03
21	115.5	-21.89 ± 0.01	8.02 ± 0.03	3.24 ± 0.03
22	122.0	-23.14 ± 0.01	10.02 ± 0.03	3.23 ± 0.03
mean		**-22.13**	**9.28**	**3.25**
s.d.		**0.51**	**1.17**	**0.01**

Appendix 4A

Isotope ratios and related data for the Oimyakon tusk. Isotope values in gray are spline interpolated and were not included in calculations of means and standard deviations for those variables. Samples marked with asterisks are those that appear in plots (Figures 4.21A-D).

Sample	Avg. Increment	$\delta^{13}C_{col}$	$\delta^{15}N_{col}$	$\delta^{18}O_{carb}$	$\delta^{13}C_{carb}$	C/N_{col}	$\delta^{13}C_{carb} - \delta^{13}C_{col}$
1	8.5	-21.65 ± <0.1	8.67 ± <0.1			3.20 ± 0.07	
2*	17.0	-21.65 ± <0.1	9.36 ± <0.1	-12.13 ± 0.05	-15.64 ± 0.02	3.23 ± 0.08	6.02 ± <0.1
3	24.5	-21.67 ± <0.1	10.00 ± <0.1			3.21 ± 0.07	
4*	29.0	-21.66 ± <0.1	10.03 ± <0.1	-14.09 ± 0.05	-15.23 ± 0.02		6.43 ± <0.1
5	32.5	-21.69 ± <0.1	9.91 ± <0.1			3.23 ± 0.08	
6*	38.5	-21.79 ± <0.1	9.80 ± <0.1	-14.38 ± 0.05	-15.13 ± 0.02		6.66 ± <0.1
7	39.5	-21.78 ± <0.1	9.84 ± <0.1			3.23 ± 0.08	
8*	46.0	-21.57 ± <0.1	10.17 ± <0.1	-13.45 ± 0.05	-15.17 ± 0.02		6.39 ± <0.1
9	47.0	-21.58 ± <0.1	10.07 ± <0.1			3.22 ± 0.08	
10	52.0	-21.85 ± <0.1	9.06 ± <0.1			3.23 ± 0.08	
11*	53.5	-21.88 ± <0.1	8.97 ± <0.1	-13.87 ± 0.05	-14.62 ± 0.02		7.25 ± <0.1
12*	58.0	-21.86 ± <0.1	9.16 ± <0.1	-15.30 ± 0.05	-14.59 ± 0.02		7.27 ± <0.1
13	60.0	-21.94 ± <0.1	9.07 ± <0.1			3.23 ± 0.08	
14	63.5	-22.31 ± <0.1	8.32 ± <0.1			3.23 ± 0.08	
15*	65.5	-22.51 ± <0.1	7.86 ± <0.1	-15.15 ± 0.05	-14.67 ± 0.02		7.83 ± <0.1
16*	73.5	-22.00 ± <0.1	7.98 ± <0.1	-13.33 ± 0.05	-14.76 ± 0.02	3.25 ± 0.08	7.24 ± <0.1
mean		**-21.81**	**9.23**	**-14.22**	**-14.76**	**3.23**	**7.20**
s.d.		**0.22**	**0.74**	**0.94**	**0.24**	**0.01**	**0.51**

Appendix 4B

Elemental ratios for the 44-M tusk.

Sample	Avg. Increment	Mg/Ca	P/Ca	Mn/Ca	Fe/Ca	Cu/Ca	Zn/Ca	Sr/Ca	Ba/Ca	Pb/Ca
1	4.0	10.51 ± 0.10	585.71 ± 41.90	0.6340 ± 0.0189	0.233 ± 0.048	0.393 ± 0.015	0.168 ± 0.005	0.508 ± 0.017	0.176 ± 0.003	0.0004 ± 0.0000
2	10.5	11.92 ± 0.11	597.65 ± 42.75	0.0510 ± 0.0015	0.157 ± 0.032	0.014 ± 0.001	0.153 ± 0.004	0.561 ± 0.019	0.200 ± 0.003	
3	25.0	10.98 ± 0.10	582.73 ± 41.68	0.0356 ± 0.0011		0.154 ± 0.006	0.145 ± 0.004	0.572 ± 0.019	0.190 ± 0.003	
4	31.5	11.56 ± 0.11	586.53 ± 41.95	0.0272 ± 0.0008		0.150 ± 0.006	0.136 ± 0.004	0.581 ± 0.020	0.181 ± 0.003	
5	33.5	11.03 ± 0.10	588.13 ± 42.07	0.0267 ± 0.0008		0.073 ± 0.003	0.115 ± 0.003	0.556 ± 0.019	0.181 ± 0.003	
6	42.0	11.09 ± 0.10	582.92 ± 41.70	0.0211 ± 0.0006		0.152 ± 0.006	0.149 ± 0.004	0.526 ± 0.018	0.180 ± 0.003	
7	42.0	13.22 ± 0.12	632.15 ± 45.22	0.0254 ± 0.0008		0.221 ± 0.008	0.159 ± 0.004	0.535 ± 0.018	0.175 ± 0.003	0.0028 ± 0.0001
8	56.0	11.27 ± 0.11	587.14 ± 42.00	0.0306 ± 0.0009		0.524 ± 0.020	0.250 ± 0.007	0.507 ± 0.017	0.166 ± 0.003	0.0009 ± 0.0000
9	64.5	52.37 ± 0.49	631.85 ± 45.19			0.120 ± 0.005	0.138 ± 0.004	0.553 ± 0.019	0.081 ± 0.001	
10	68.5	45.81 ± 0.43	644.29 ± 46.09			0.606 ± 0.023	0.164 ± 0.005	0.528 ± 0.018	0.083 ± 0.001	
11	73.5	52.49 ± 0.49	595.67 ± 42.61	0.0142 ± 0.0004		0.268 ± 0.010	0.227 ± 0.006	0.548 ± 0.019	0.120 ± 0.002	0.0017 ± 0.0001
12	76.5	41.68 ± 0.39	566.01 ± 40.49	0.0245 ± 0.0007	0.060 ± 0.012	0.379 ± 0.014	0.253 ± 0.007	0.485 ± 0.016	0.074 ± 0.001	0.0051 ± 0.0002
13	80.5	119.97 ± 1.13	685.12 ± 49.01			0.095 ± 0.004	0.132 ± 0.004	0.509 ± 0.017	0.091 ± 0.001	
14	85.5	139.76 ± 1.31	698.00 ± 49.93			0.067 ± 0.003	0.114 ± 0.003	0.516 ± 0.017	0.079 ± 0.001	
15	91.5	157.32 ± 1.48	693.36 ± 49.59			0.047 ± 0.002	1.888 ± 0.052	0.532 ± 0.018	0.071 ± 0.001	0.0008 ± 0.0000
16	93.5	156.85 ± 1.47	702.59 ± 50.26			0.051 ± 0.002	0.099 ± 0.003	0.547 ± 0.019	0.065 ± 0.001	
17	102.0	182.27 ± 1.71	708.20 ± 50.66			0.106 ± 0.004	0.132 ± 0.004	0.548 ± 0.019	0.059 ± 0.001	
18	104.5	176.04 ± 1.65	708.26 ± 50.66			0.193 ± 0.007	0.188 ± 0.005	0.546 ± 0.019	0.061 ± 0.001	
19	109.0	137.70 ± 1.29	767.52 ± 54.90			0.042 ± 0.002	0.116 ± 0.003	0.534 ± 0.018	0.061 ± 0.001	0.0012 ± 0.0000
20	120.0	139.52 ± 1.31	746.33 ± 53.38			0.121 ± 0.005	0.148 ± 0.004	0.515 ± 0.017	0.050 ± 0.001	0.0005 ± 0.0000
21	124.5	154.69 ± 1.45	594.54 ± 42.53	0.0250 ± 0.0007		0.172 ± 0.007	0.317 ± 0.009	0.547 ± 0.019	0.046 ± 0.001	0.0057 ± 0.0002
22	132.5	154.71 ± 1.45	728.31 ± 52.09			0.110 ± 0.004	0.130 ± 0.004	0.525 ± 0.018	0.046 ± 0.001	0.0017 ± 0.0001
23	139.0	143.45 ± 1.35	707.60 50.61			0.124 ± 0.005	0.167 0.005	0.526 0.018	0.043 0.001	0.0008 ± 0.0000
24	145.0	134.24 ± 1.26	686.24 ± 49.09			0.092 ± 0.003	0.141 ± 0.004	0.575 ± 0.019	0.046 ± 0.001	0.0005 ± 0.0000
25	160.5	174.52 ± 1.64	719.67 ± 51.48			0.179 ± 0.007	0.160 ± 0.004	0.551 ± 0.019	0.056 ± 0.001	
26	164.0	161.23 ± 1.51	763.19 ± 54.59			0.141 ± 0.005	0.152 ± 0.004	0.514 ± 0.017	0.062 ± 0.001	0.0018 ± 0.0001
27	172.5	173.20 ± 1.62	720.66 ± 51.55			0.244 ± 0.009	0.190 ± 0.005	0.510 ± 0.017	0.055 ± 0.001	
28	177.5	114.53 ± 1.07	669.59 47.89			0.159 ± 0.006	0.143 0.004	0.506 0.017	0.054 0.001	
29	185.0	118.01 ± 1.11	660.19 47.22			0.107 ± 0.004	0.123 0.003	0.471 0.016	0.059 0.001	
30	191.5	111.31 ± 1.04	671.38 48.02			0.075 ± 0.003	0.106 0.003	0.484 0.016	0.057 0.001	
31	201.0	106.72 ± 1.00	593.72 ± 42.47	0.0164 ± 0.0005		0.034 ± 0.001	0.108 ± 0.003	0.560 ± 0.019	0.059 ± 0.001	0.0036 ± 0.0001
32	212.0	112.67 ± 1.06	714.75 ± 51.13			0.097 ± 0.004	0.143 ± 0.004	0.576 ± 0.020	0.058 ± 0.001	0.0026 ± 0.0001
33	220.5	34.54 ± 0.32	639.56 ± 45.75	0.0249 ± 0.0007		0.109 ± 0.004	0.109 ± 0.003	0.575 ± 0.019	0.097 ± 0.001	0.0007 ± 0.0000
34	229.5	28.90 ± 0.27	629.53 ± 45.03	0.1421 ± 0.0042		0.115 ± 0.004	0.129 ± 0.004	0.548 ± 0.019	0.112 ± 0.002	
35	231.0	26.66 ± 0.25	611.25 ± 43.72	0.4919 ± 0.0147		0.044 ± 0.002	0.128 ± 0.004	0.559 ± 0.019	0.128 ± 0.002	
36	240.0	25.35 ± 0.24	603.64 ± 43.18	3.7042 ± 0.1105	7.785 ± 1.604	0.114 ± 0.004	0.159 ± 0.004	0.581 ± 0.020	0.226 ± 0.003	
mean		**90.78**	**655.67**	**0.3309**	**2.059**	**0.158**	**0.202**	**0.537**	**0.099**	**0.0019**
s.d.		**63.12**	**59.59**	**0.9181**	**3.818**	**0.131**	**0.293**	**0.029**	**0.056**	**0.0016**

Appendix 4B

Elemental ratios for the Mol tusk.

Sample	Avg. Increment	Mg/Ca	P/Ca	Mn/Ca	Fe/Ca	Cu/Ca	Zn/Ca	Sr/Ca	Ba/Ca	Pb/Ca
1	2	55.36 ± 0.94	703.26 ± 28.10	4.6334 ± 0.1519	46.183 ± 6.887	0.306 ± 0.012	0.303 ± 0.011	0.499 ± 0.026	0.164 ± 0.008	
2	6	72.44 ± 1.23	679.26 ± 27.14	0.0814 ± 0.0027	0.324 ± 0.048	0.118 ± 0.004	0.157 ± 0.006	0.367 ± 0.019	0.036 ± 0.002	
3	11	74.37 ± 1.27	678.92 ± 27.12	0.0438 ± 0.0014	0.371 ± 0.055	0.092 ± 0.003	0.137 ± 0.005	0.481 ± 0.025	0.043 ± 0.002	
4	17.5	63.60 ± 1.08	667.26 ± 26.66	0.0351 ± 0.0012		0.086 ± 0.003	0.183 ± 0.006	0.619 ± 0.032	0.071 ± 0.004	
5	22	69.16 ± 1.18	666.13 ± 26.61			0.061 ± 0.002	0.129 ± 0.005	0.695 ± 0.036	0.099 ± 0.005	
6	27	72.24 ± 1.23	678.20 ± 27.09		0.952 ± 0.142	0.045 ± 0.002	0.474 ± 0.017	0.725 ± 0.038	0.104 ± 0.005	
7	27	71.58 ± 1.22	717.36 ± 28.66			0.096 ± 0.004	0.159 ± 0.006	0.722 ± 0.038	0.102 ± 0.005	0.0025 ± 0.0001
8	29	74.64 ± 1.27	655.51 ± 26.19			0.056 ± 0.002	0.156 ± 0.006	0.745 ± 0.039	0.093 ± 0.005	
9	38.5	72.18 ± 1.23	653.56 ± 26.11			0.051 ± 0.002	0.112 ± 0.004	0.684 ± 0.036	0.074 ± 0.004	
10	41	78.23 ± 1.33	671.14 ± 26.81			0.038 ± 0.001	0.135 ± 0.005	0.652 ± 0.034	0.078 ± 0.004	
11	46.5	82.37 ± 1.40	761.90 ± 30.44			0.051 ± 0.002	0.121 ± 0.004	0.649 ± 0.034	0.071 ± 0.004	
12	48.5	81.43 ± 1.39	666.74 ± 26.64			0.040 ± 0.002	0.118 ± 0.004	0.664 ± 0.035	0.062 ± 0.003	
13	56.5	83.66 ± 1.42	644.73 ± 25.76			0.050 ± 0.002	0.144 ± 0.005	0.690 ± 0.036	0.063 ± 0.003	
14	64	83.82 ± 1.43	661.28 ± 26.42			0.108 ± 0.004	0.153 ± 0.005	0.704 ± 0.037	0.068 ± 0.004	
15	65.5	84.37 ± 1.44	658.71 ± 26.32			0.042 ± 0.002	0.111 ± 0.004	0.726 ± 0.038	0.072 ± 0.004	
16	69.5	91.38 ± 1.56	665.72 ± 26.60			0.442 ± 0.017	0.287 ± 0.010	0.735 ± 0.038	0.075 ± 0.004	
17	72	89.54 ± 1.53	665.94 ± 26.60			0.051 ± 0.002	0.114 ± 0.004	0.739 ± 0.038	0.076 ± 0.004	
18	76.5	90.40 ± 1.54	678.31 ± 27.10			0.086 ± 0.003	0.126 ± 0.004	0.744 ± 0.039	0.076 ± 0.004	
19	77.5	92.27 ± 1.57	695.95 ± 27.80			0.062 ± 0.002	0.112 ± 0.004	0.737 ± 0.038	0.076 ± 0.004	0.0025 ± 0.0001
20	82	92.42 ± 1.57	694.34 ± 27.74			0.087 ± 0.003	0.136 ± 0.005	0.744 ± 0.039	0.075 ± 0.004	
21	86.5	93.14 ± 1.59	664.69 ± 26.55	0.0177 ± 0.0006		0.139 ± 0.005	0.191 ± 0.007	0.699 ± 0.036	0.057 ± 0.003	0.0059 ± 0.0003
22	91	83.58 ± 1.42	672.80 ± 26.88			0.109 ± 0.004	0.157 ± 0.006	0.567 ± 0.030	0.045 ± 0.002	0.0021 ± 0.0001
23	97	92.74 ± 1.58	668.17 ± 26.69			0.053 ± 0.002	0.109 ± 0.004	0.587 ± 0.031	0.051 ± 0.003	
24	103	91.60 ± 1.56	672.15 ± 26.85			0.174 ± 0.007	0.166 ± 0.006	0.610 ± 0.032	0.062 ± 0.003	
25	108.5	101.26 ± 1.72	702.23 ± 28.05			0.059 ± 0.002	0.117 ± 0.004	0.609 ± 0.032	0.064 ± 0.003	
26	111.5	99.84 ± 1.70	732.07 ± 29.25			0.073 ± 0.003	0.182 ± 0.006	0.592 ± 0.031	0.059 ± 0.003	0.0027 ± 0.0001
27	114.5	111.24 ± 1.89	726.84 ± 29.04			0.071 ± 0.003	0.188 ± 0.007	0.582 ± 0.030	0.056 ± 0.003	
28	118.5	112.84 ± 1.92	691.12 ± 27.61			0.095 ± 0.004	0.131 ± 0.005	0.583 ± 0.030	0.054 ± 0.003	
29	123	137.13 ± 2.34	762.45 ± 30.46			0.100 ± 0.004	0.579 ± 0.021	0.561 ± 0.029	0.058 ± 0.003	
30	127.5	126.85 ± 2.16	713.32 ± 28.50			0.105 ± 0.004	0.153 ± 0.005	0.584 ± 0.030	0.042 ± 0.002	0.0289 ± 0.0015
31	132.5	138.59 ± 2.36	770.31 ± 30.77	0.0271 ± 0.0009		0.104 ± 0.004	0.170 ± 0.006	0.630 ± 0.033	0.045 ± 0.002	0.0051 ± 0.0003
32	138	96.09 ± 1.64	769.65 ± 30.75			0.086 ± 0.003	0.143 ± 0.005	0.547 ± 0.028	0.049 ± 0.003	0.0031 ± 0.0002
33	143.5	113.23 ± 1.93	759.28 ± 30.33			0.073 ± 0.003	0.115 ± 0.004	0.537 ± 0.028	0.053 ± 0.003	
34	146.5	100.60 ± 1.71	755.92 ± 30.20	0.0151 ± 0.0005		0.083 ± 0.003	0.182 ± 0.006	0.545 ± 0.028	0.067 ± 0.003	
35	152	118.00 ± 2.01	760.31 ± 30.37			0.061 ± 0.002	0.147 ± 0.005	0.572 ± 0.030	0.064 ± 0.003	
36	155	93.89 ± 1.60	732.98 ± 29.28	0.0420 ± 0.0014	2.258 ± 0.337	0.059 ± 0.002	0.124 ± 0.004	0.582 ± 0.030	0.055 ± 0.003	
37	160.5	102.91 ± 1.75	760.55 ± 30.38	0.0930 ± 0.0030	4.678 ± 0.698	0.172 ± 0.007	0.201 ± 0.007	0.594 ± 0.031	0.057 ± 0.003	
mean		**91.59**	**699.43**	**0.5543**	**9.128**	**0.097**	**0.174**	**0.630**	**0.068**	**0.0066**
s.d.		**19.18**	**39.93**	**1.5299**	**18.227**	**0.076**	**0.096**	**0.088**	**0.023**	**0.0091**

Appendix 4B

Elemental ratios for the Bolshoi Lyakhovskii tusk.

Sample	Avg. Increment	Mg/Ca	P/Ca	Mn/Ca	Fe/Ca	Cu/Ca	Zn/Ca	Sr/Ca	Ba/Ca	Pb/Ca
1	7.0	105.30 ± 0.99	620.69 ± 44.40	0.0214 ± 0.0006	0.132 ± 0.027	0.107 ± 0.004	0.175 ± 0.005	0.413 ± 0.014	0.0324 ± 0.0005	0.00386 ± 0.00013
2	13.0	122.22 ± 1.15	705.09 ± 50.43			0.098 ± 0.004	1.498 ± 0.042	0.422 ± 0.014	0.0396 ± 0.0006	0.00115 ± 0.00004
3	21.0	121.07 ± 1.14	696.24 ± 49.80		0.157 ± 0.032	0.113 ± 0.004	0.175 ± 0.005	0.471 ± 0.016	0.0499 ± 0.0008	0.00079 ± 0.00003
4	26.5	124.94 ± 1.17	724.68 ± 51.84			0.104 ± 0.004	0.157 ± 0.004	0.510 ± 0.017	0.0477 ± 0.0007	0.00058 ± 0.00002
5	30.5	108.15 ± 1.01	711.07 ± 50.86			0.042 ± 0.002	0.125 ± 0.003	0.544 ± 0.018	0.0354 ± 0.0005	
6	37.0	132.37 ± 1.24	721.24 ± 51.59			0.087 ± 0.003	0.163 ± 0.005	0.652 ± 0.022	0.0389 ± 0.0006	0.00059 0.00002
7	42.0	130.12 ± 1.22	726.11 ± 51.94			0.038 ± 0.001	0.150 ± 0.004	0.690 ± 0.023	0.0330 ± 0.0005	
8	50.0	110.95 ± 1.04	706.06 ± 50.50		0.974 ± 0.201	0.075 ± 0.003	0.201 ± 0.006	0.805 ± 0.027	0.0689 ± 0.0010	
9	55.5	115.29 ± 1.08	725.92 ± 51.92			0.066 ± 0.003	0.131 ± 0.004	0.863 ± 0.029	0.0706 ± 0.0011	0.00167 ± 0.00006
10	61.5	124.09 ± 1.16	739.03 ± 52.86			0.040 ± 0.002	0.123 ± 0.003	0.884 ± 0.030	0.0655 ± 0.0010	0.00080 ± 0.00003
11	67.5	130.90 ± 1.23	680.56 ± 48.68	0.0473 ± 0.0014		0.095 ± 0.004	0.173 ± 0.005	0.886 ± 0.030	0.0546 ± 0.0008	0.01364 ± 0.00048
12	73.5	136.15 ± 1.28	761.19 ± 54.45			0.107 ± 0.004	0.135 ± 0.004	0.905 ± 0.031	0.0386 ± 0.0006	0.00448 ± 0.00016
13	82.5	143.22 ± 1.34	748.56 ± 53.54			0.055 ± 0.002	0.144 ± 0.004	0.914 ± 0.031	0.0367 ± 0.0006	0.00273 ± 0.00010
14	89.5	142.48 ± 1.34	761.05 ± 54.44			0.047 ± 0.002	0.112 ± 0.003	0.910 ± 0.031	0.0331 ± 0.0005	0.00138 ± 0.00005
15	91.5	116.02 ± 1.09	719.36 ± 51.45			0.041 ± 0.002	0.113 ± 0.003	0.917 ± 0.031	0.0382 ± 0.0006	0.00083 ± 0.00003
16	96.5	131.51 ± 1.23	722.50 ± 51.68			0.139 ± 0.005	0.146 ± 0.004	0.904 ± 0.031	0.0355 ± 0.0005	0.00090 ± 0.00003
17	102.5	129.73 ± 1.22	737.20 ± 52.73			0.043 ± 0.002	0.103 ± 0.003	0.876 ± 0.030	0.0320 ± 0.0005	0.00054 ± 0.00002
18	110.0	112.64 ± 1.06	713.61 ± 51.04		0.590 ± 0.122	0.138 ± 0.005	0.165 ± 0.005	0.795 ± 0.027	0.0506 ± 0.0008	0.00069 ± 0.00002
19	115.0	120.48 ± 1.13	745.49 ± 53.32	0.0926 ± 0.0028	2.338 ± 0.482	0.073 ± 0.003	0.133 ± 0.004	0.785 ± 0.027	0.0497 ± 0.0007	
20	118.0	152.59 ± 1.43	757.82 ± 54.21	0.8858 ± 0.0264	16.076 ± 3.313	0.174 ± 0.007	0.180 ± 0.005	0.822 ± 0.028	0.0698 ± 0.0011	
mean		**125.51**	**721.17**	**0.2617**	**3.378**	**0.084**	**0.215**	**0.748**	**0.046**	**0.0023**
s.d.		**12.44**	**32.06**	**0.4171**	**6.274**	**0.039**	**0.303**	**0.180**	**0.013**	**0.0034**

Appendix 4B

Elemental ratios for the Allen tusk.

Sample	Avg. Increment	Mg/Ca	P/Ca	Mn/Ca	Fe/Ca	Cu/Ca	Zn/Ca	Sr/Ca	Ba/Ca	Pb/Ca
1	2.5	12.43 ± 0.12	615.48 ± 44.02	3.139 ± 0.094	91.76 ± 18.91	0.154 ± 0.006	0.167 ± 0.005	1.69 ± 0.06	0.805 ± 0.012	0.0009 ± 0.0000
2	9.0	15.15 ± 0.14	643.38 ± 46.02	1.419 ± 0.042	78.85 ± 16.25	0.192 ± 0.007	0.182 ± 0.005	1.60 ± 0.05	0.653 ± 0.010	0.0041 ± 0.0001
3	16.0	16.15 ± 0.15	614.38 ± 43.95	0.780 ± 0.023	81.09 ± 16.71	0.977 ± 0.037	0.624 ± 0.017	1.65 ± 0.06	0.774 ± 0.012	0.0024 ± 0.0001
4	22.5	16.93 ± 0.16	598.01 ± 42.77	0.768 ± 0.023	81.89 ± 16.88	0.315 ± 0.012	0.245 ± 0.007	1.65 ± 0.06	0.740 ± 0.011	0.0029 ± 0.0001
5	30.0	18.75 ± 0.18	625.16 ± 44.72	0.768 ± 0.023	85.30 ± 17.58	0.288 ± 0.011	0.228 ± 0.006	1.75 ± 0.06	0.568 ± 0.009	0.0007 ± 0.0000
6	38.0	18.63 ± 0.17	622.11 ± 44.50	0.782 ± 0.023	89.41 ± 18.43	0.296 ± 0.011	0.237 ± 0.007	1.78 ± 0.06	0.554 ± 0.008	
7	44.0	20.64 ± 0.19	644.52 ± 46.10	0.811 ± 0.024	89.89 ± 18.53	0.377 ± 0.014	0.314 ± 0.009	1.79 ± 0.06	0.565 ± 0.009	0.0006 ± 0.0000
8	46.0	20.47 ± 0.19	637.08 ± 45.57	0.786 ± 0.023	88.09 ± 18.15	0.368 ± 0.014	0.280 ± 0.008	1.74 ± 0.06	0.543 ± 0.008	0.0011 ± 0.0000
9	51.5	18.26 ± 0.17	632.33 ± 45.23	0.669 ± 0.020	71.56 ± 14.75	0.054 ± 0.002	0.105 ± 0.003	1.55 ± 0.05	0.285 ± 0.004	
10	54.5	18.20 ± 0.17	642.34 ± 45.95	0.713 ± 0.021	80.76 ± 16.64	0.061 ± 0.002	0.095 ± 0.003	1.64 ± 0.06	0.407 ± 0.006	
11	62.0	21.80 ± 0.20	677.13 ± 48.43	0.723 ± 0.022	81.96 ± 16.89	0.325 ± 0.012	0.251 ± 0.007	1.62 ± 0.06	0.328 ± 0.005	0.0023 ± 0.0001
12	68.5	21.13 ± 0.20	564.92 ± 40.41	0.801 ± 0.024	87.34 ± 18.00	0.579 ± 0.022	0.366 ± 0.010	1.67 ± 0.06	0.446 ± 0.007	0.0064 ± 0.0002
13	74.5	21.04 ± 0.20	630.44 ± 45.09	0.778 ± 0.023	84.71 ± 17.46	0.410 ± 0.016	0.292 ± 0.008	1.65 ± 0.06	0.375 ± 0.006	0.0019 ± 0.0001
14	76.0	15.16 ± 0.14	619.95 ± 44.34	1.061 ± 0.032	78.69 ± 16.22	0.129 ± 0.005	0.127 ± 0.004	1.65 ± 0.06	0.687 ± 0.010	0.0005 ± 0.0000
15	80.0	20.69 ± 0.19	599.30 ± 42.87	0.815 ± 0.024	90.38 ± 18.63	0.328 ± 0.012	0.249 ± 0.007	1.77 ± 0.06	0.467 ± 0.007	0.0005 ± 0.0000
16	83.5	17.46 ± 0.16	684.88 ± 48.99	0.773 ± 0.023	80.77 ± 16.65	0.188 ± 0.007	0.166 ± 0.005	1.62 ± 0.05	0.569 ± 0.009	0.0019 ± 0.0001
17	89.0	17.64 ± 0.17	665.57 ± 47.61	0.794 ± 0.024	82.23 ± 16.95	0.288 ± 0.011	0.217 ± 0.006	1.73 ± 0.06	0.628 ± 0.009	0.0007 ± 0.0000
18	96.0	18.00 ± 0.17	659.48 ± 47.17	0.792 ± 0.024	84.60 ± 17.44	0.230 ± 0.009	0.188 ± 0.005	1.69 ± 0.06	0.592 ± 0.009	
19	102.5	17.70 ± 0.17	682.24 ± 48.80	0.871 ± 0.026	91.45 ± 18.85	0.178 ± 0.007	0.198 ± 0.006	1.72 ± 0.06	0.640 ± 0.010	
20	109.5	19.14 ± 0.18	687.16 ± 49.15	0.847 ± 0.025	93.43 ± 19.25	0.430 ± 0.016	0.283 ± 0.008	1.69 ± 0.06	0.590 ± 0.009	
21	115.5	18.85 ± 0.18	682.56 ± 48.82	0.854 ± 0.025	91.52 ± 18.86	0.665 ± 0.025	0.426 ± 0.012	1.71 ± 0.06	0.602 ± 0.009	
22	122.0	20.37 ± 0.19	577.42 ± 41.30	0.858 ± 0.026	90.16 ± 18.58	1.751 ± 0.067	1.039 ± 0.029	1.67 ± 0.06	0.594 ± 0.009	0.0075 ± 0.0003
mean		**18.39**	**636.63**	**0.9365**	**85.27**	**0.390**	**0.285**	**1.68**	**0.564**	**0.0023**
s.d.		**2.30**	**34.75**	**0.5147**	**5.56**	**0.368**	**0.204**	**0.06**	**0.136**	**0.0022**

Appendix 4B

Elemental ratios for the Oimyakon tusk.

Sample	Avg. Increment	Mg/Ca	P/Ca	Mn/Ca	Fe/Ca	Cu/Ca	Zn/Ca	Sr/Ca	Ba/Ca	Pb/Ca
1	17.0	4.85 ± 0.05	676.56 ± 48.39	0.651 ± 0.019	100.20 ± 20.65	0.120 ± 0.005	0.976 ± 0.027	0.88 ± 0.03	0.116 ± 0.002	0.00168 ± 0.00006
2	29.0	4.32 ± 0.04	662.82 ± 47.41	0.633 ± 0.019	99.32 ± 20.47	0.743 ± 0.028	1.278 ± 0.036	1.05 ± 0.04	0.101 ± 0.002	0.00088 ± 0.00003
3	38.5	5.88 ± 0.06	736.20 ± 52.66	0.661 ± 0.020	105.72 ± 21.79	0.059 ± 0.002	0.971 ± 0.027	1.04 ± 0.04	0.095 ± 0.001	0.00167 ± 0.00006
4	46.0	4.19 ± 0.04	709.14 ± 50.72	0.567 ± 0.017	90.76 ± 18.70	0.110 ± 0.004	2.041 ± 0.057	0.99 ± 0.03	0.091 ± 0.001	0.00072 ± 0.00003
5	53.5	3.40 ± 0.03	739.59 ± 52.90	0.637 ± 0.019	99.64 ± 20.53	0.031 ± 0.001	0.808 ± 0.022	0.97 ± 0.03	0.095 ± 0.001	
6	58.0	3.54 ± 0.03	727.52 ± 52.04	0.636 ± 0.019	100.91 ± 20.80	0.114 ± 0.004	0.790 ± 0.022	1.02 ± 0.03	0.104 ± 0.002	
7	65.5	3.25 ± 0.03	718.54 ± 51.40	0.677 ± 0.020	105.31 ± 21.70	0.036 ± 0.001	0.775 ± 0.022	1.08 ± 0.04	0.119 ± 0.002	
8	73.5	3.43 ± 0.03	714.93 ± 51.14	0.664 ± 0.020	100.38 ± 20.69	0.038 ± 0.001	0.768 ± 0.021	1.13 ± 0.04	0.128 ± 0.002	0.00069 ± 0.00002
mean		**4.11**	**710.66**	**0.641**	**100.28**	**0.156**	**1.051**	**1.02**	**0.106**	**0.0011**
s.d.		**0.91**	**27.54**	**0.034**	**4.59**	**0.240**	**0.435**	**0.08**	**0.013**	**0.0005**

References

Ambrose, S.H., DeNiro, M.J., 1986. The isotopic ecology of East African mammals. Oecologia 69, 395–406.

Ambrose, S.H., Norr, L., 1993. Experimental evidence for the relationship of the carbon isotope ratios of whole diet and dietary protein to those of bone collagen and carbonate. In: Lambert, J.B., Groupe, G. (Eds.), Prehistoric Human Bone: Archaeology at the Molecular Level. Springer, Berlin, pp. 1–37.

Ando-Mizobata, N., Sakai, M., Sakurai, Y., 2006. Trace-element analysis of Steller sea lion (*Eumetopias jubatus*) teeth using scanning X-ray analytical microscope. Mammal Study 31, 65–68.

Barboza, P.S., Parker, K.L., 2006. Body protein stores and isotopic indicators of N balance in female reindeer (*Rangifer tarandus*) during winter. Physiological and Biochemical Zoology 79(3), 628–644.

Barboza, P.S., Reynolds, P.E., 2004. Monitoring nutrition of a large grazer: muskoxen on the Arctic Refuge. International Congress Series 1275, 327–333.

Bocherens, H., 2003. Isotopic biogeochemistry and the paleoecology of the mammoth steppe fauna. DEINSEA 9, 57–76.

Boeskorov, G.G., Tikhonov, A.N., Lazarev, P.A., 2007. A new find of a mammoth calf. Doklady Biological Sciences 417, 480–483.

Cerling, T.E., Harris, J.M., 1999. Carbon isotope fractionation between diet and bioapatite in ungulate mammals and implications for ecological and paleoecological studies. Oecologia 120, 347–363.

Chapin, D.M., 1996. Nitrogen mineralization, nitrification, and denitrfication in a high arctic lowland ecosystem, Devon Island, N.W.T., Canada. Arctic and Alpine Research 28(1), 85–92.

Dauncey, M.J., Shaw, J.C.L., Urman, J., 1977. The absorption and retention of magnesium, zinc, and copper by low birth weight infants fed pasteurized human breast milk. Pediatric Research 11, 991–997.

DeNiro, M.J., 1985. Postmortem preservation and alteration of *in vivo* bone collagen isotope ratios in relation to palaeodietary reconstruction. Nature 317, 806–809.

DeNiro, M.J., Epstein, S., 1978. Carbon isotopic evidence for different feeding patterns in two hyrax species occupying the same habitat. Science 201(4359), 906–908.

DeNiro, M.J., Epstein, S., 1977. Mechanism of carbon isotope fractionation associated with lipid synthesis. Science 197(4300), 261–263.

Dewey, K.G., Cohen, R.J., Rivera, L.L., Brown, K.H., 1998. American Journal of Clinical Nutrition 67, 878–884.

Dolphin, A.E., Goodman, A.H., Amarasiriwardena, D.D., 2005. Variation in elemental intensities among teeth and between pre- and postnatal regions of enamel. American Journal of Physical Anthropology 128, 878–888.

Drzazga, Z., Michalik, K., Maciejewska, K., Trzeciak, H., Kaszuba, M., 2007. Role of endogenous zinc in bones of newborn rats. Biofactors 30, 243–248.

Dufty, J.H., Bingley, J.B., Cove, L.Y., 1977. The plasma zinc concentration of nonpregnant, pregnant, and parturient Hereford cattle. Australian Veterinary Journal 53, 519–522.

Evans, R.D., Richner, P., Outridge, P.M., 1995. Micro-spatial variations of heavy metals in the teeth of walrus as determined by laser ablation ICP-MS: The potential for reconstructing a history of metal exposure. Archives of Environmental Contamination and Toxicology 28, 55–60.

Ezzo, J. A., 1994. Zinc as a paleodietary indicator: An issue of theoretical validity in bone-chemistry analysis. American Antiquity 59(4), 606–621.

Fisher, D.C., 2008. Paleobiology and extinction of proboscideans in the Great Lakes region of North America. In: Haynes, G. (Ed.), American Megafaunal Extinctions at the End of the Pleistocene. Springer, pp. 55–75.

Fisher, D.C., 2001. Season of Death, Growth Rates, and Life History of North American Mammoths. In: West, D. (Ed.), Proceedings of the International Conference on Mammoth Site Studies, Publications in Anthropology 22. University of Kansas, Lawrence, pp. 121–135.

Fisher, D.C., 1996. Extinction of proboscideans in North America. In: Shoshani, J., Tassy, P. (Eds.), The Proboscidea: Evolution and Paleoecology of Elephants and Their Relatives. Oxford University Press, Oxford, pp. 296–315.

Fisher, D.C., 1987. Mastodont procurement by paleoindians of the Great Lakes region: Hunting or scavenging? In: Nitecki, M.H., Nitecki, D.V. (Eds.), The Evolution of Human Hunting. Plenum Press, New York, pp.309–421.

Fisher, D.C., Beld, S.G., Rountrey, A.N., 2008. Tusk record of the North Java mastodon. In: Allmon, W.D., Nester, P.L. (Eds), Mastodon Paleobiology, Taphonomy, and Paleoenvironment in the Latre Pleistocene of New York State: Studies on the Hyde Park, Chemung, and North Java Sites, Palaeontographica Americana 61, pp. 399–445.

Fisher, D.C., Fox, D.L., 2003. Season of death and terminal growth histories of Hiscock mastodons. In: Laub, R.S. (Ed.), The Hiscock Site: Late Pleistocene and Holocene Paleoecology and Archaeology of Western New York State, Bulletin of the Buffalo Society of Natural Sciences, 37, pp. 83–101.

Fox, D.L., Fisher, D.C., Vartanyan, S., Tikhonov, A.N., Mol, D., Buigues, B. 2007. Paleoclimatic implications of oxygen isotopic variation in late Pleistocene and Holocene tusks of *Mammuthus primigenius* from northern Eurasia. Quaternary International 169–170, 154–165.

Gat, J.R., 1996. Oxygen and hydrogen isotopes in the hydrologic cycle. Annual Review of Earth and Planetary Sciences 24, 225–262.

Hartsook, E.W., Hershberger, T.V., 1973. Strontium-calcium discrimination during placental transfer and fetal uptake in rats: Effect of gestation duration. Proceedings of the Society for Experimental Biology and Medicine 143(2), 343–349.

Haynes, G., 1991. Mammoths, mastodonts, and elephants: Biology, behavior, and the fossil record. Cambridge University Press, Cambridge, UK.

Hobson, K.A., Alisauskas, R.T., Clark, R.G., 1993. Stable-Nitrogen isotope enrichment in avian tissues due to fasting and nutritional stress: Implications for isotopic analyses of diet. The Condor 95 (2), 388–394.

Hobson, K.A., Sease, J.L., 1998. Stable isotope analyses of tooth annuli reveal temporal dietary records: an example using Stellar sea lions. Marine Mammal Science 14, 116–129.

Holá, M., Kalvoda, J., Bábek, O., Brzobohatý, R., Holoubek, I., Kanický, V., Skoda, R., 2008. LA-ICP-MS heavy metal analyses of fish scales from sediments of the Oxbow Lake Certak of the Morava River (Czech Republic). Environmental Geology DOI: 10.1007/s00254-008-1501-z.

Holdo, R.M., 2003. Woody plant damage by African elephants in relation to leaf nutrients in western Zimbabwe. Journal of Tropical Ecology 19, 189–196.

Ichiyanagi, K., Sugimoto, A., Numaguti, A., Kurita, N., Ishii, Y., Ohata, T., 2003. Seasonal variation in stable isotopic composition of alas lake water near Yakutsk, Eastern Siberia.

Iacumin, P., Bocherens, H., Mariotti, A., Longinelli, A., 1996. Oxygen isotope analyses of co-existing carbonate and phosphate in biogenic apatite: a way to monitor diagenetic alteration of bone phosphate?. Earth and Planetary Science Letters 142, 1–6.

Iacumin, P., Davanzo, S., Nikolaev, V., 2005. Short-term climatic changes recorded by mammoth hair in the Arctic environment. Palaeogeography, Palaeoclimatology, Palaeoecology 218, 317–324.

Jeswani, R.M., Vani, S.N., 1991. A study of serum zinc levels in cord blood of neonates and their mothers. Indian Journal of pediatrics 58(5), 683–686.

Kang, D., Amarasiriwardena, D., Goodman, A.H., 2004. Application of laser ablation-inductively coupled plasma-mass spectrometry (LA-ICP-MS) to investigate trace metal spatial distributions in human tooth enamel and dentine growth layers and pulp. Analytical and Bioanalytical Chemistry 378, 1608–1615.

Klepinger, L.L, 1990. Magnesium ingestion and bone magnesium concentration in paleodietary reconstruction: Cautionary evidence from an animal model. Journal of Archaeological Science 17, 513–517.

Klepinger, L.L., 1984. Nutritional assessment from bone. Annual Review of Anthropology 13, 75–96.

Klevezal, G.A., 1996. Recording Structures of Mammals: Determination of Age and Reconstruction of Life History. A. A. Balkema, Rotterdam.

Koch, P.L., 1989. Paleobiology of late Pleistocene mastodonts and mammoths from southern Michigan and western New York. Unpublished doctoral dissertation, University of Michigan.

Koch, P.L., Fisher, D.C., Dettman, D., 1989. Oxygen isotope variation in the tusks of extinct proboscideans: A measure of season of death and seasonality. Geology 17, 515–519.

Kohn, M., 1996. Predicting animal $\delta^{18}O$: Accounting for diet and physiological adaptation. Geochimica et Cosmochimica Acta 60(23) 4811–4829.

Kohn, M.J., Schoeninger, M.J., Barker, W.W., 1999. Altered states: Effects of diagenesis on fossil tooth chemistry. Geochimica et Cosmochimica Acta 63(18), 2737–2747.

Kurita, N., Yoshida, N., Inoue, G., Chayanova, E.A., 2004. Modern isotope climatology of Russia: A first assessment. Journal of Geophysical Research 109(D03102), 1–15.

Lee, P.C., Moss, C.J., 1986. Early maternal investment in male and female African elephant calves. Behavioral Ecology and Sociobiology 18, 353–361.

Long, S.P., C_4 photosynthesis at low temperatures. 1983. Plant, Cell, and Environment 6, 345–363.

Luckett, W.P., 1996. Ontogenetic evidence for incisor homologies in proboscideans. In: Shoshani, J., Tassy, P. (Eds.), The Proboscidea: Evolution and Paleoecology of Elephants and Their Relatives. Oxford University Press, Oxford, pp. 26–31.

Mashchenko, E.N., Tikhonov, A.N., MacPhee, R.D.E., 2005. Mammoth calf from Bolshoi Lyakhovskii Island (New Siberian Islands, Arctic Siberia). Russian Journal of Theriology 4(1), 79–88.

McCullagh, K.G., Widdowson, E.M., 1970. The milk of the African elephant. British Journal of Nutrition 24, 109–117.

Mekota, A., Grupe, G., Ufer, S., Cuntz, U., 2006. Serial analysis of stable nitrogen and carbon isotopes in hair: monitoring starvation and recovery phases of patients suffering from anorexia nervosa. Rapid Communications in Mass Spectrometry 20, 1604–1610.

Michelsen, A., Schmidt, I.K., Jonasson, S., Quarmby, C., Sleep, D., 1996. Leaf ^{15}N abundance of subarctic plants provides field evidence that ericoid, ectomycorrhizal and non- and arbuscular mycorrhizal species access different sources of soil nitrogen. Oecologia 105, 53–63.

Miller, E.R., Ullrey, D.E., Zutaut, C.L., Baltzer, B.V., Schmidt, D.A., Hoefer, J.A., Luecke, R.W., 1965. Magnesium requirement of the baby pig. The Journal of Nutrition 85, 13–20.

Nellemann, C., 1996. Terrain selection by reindeer in late winter in central Norway. Arctic 49(4), 339–347.

Newsome, S.D., Koch, P.L., Etnier, M.A., Aurioles-Gamboa, D., 2006. Using carbon and nitrogen isotope values to investigate maternal strategies in northeast Pacific otariids. Marine Mammal Science 22(3), 556–572.

Ohtsuka, M., Saeki, S., Igarashi, K., Shinoda, H., 1998. Circadian rhythms in the incorporation and secretion of ^{3}H-proline by odontoblasts in relation to incremental lines in rat dentin. Journal of Dental Research 77(11), 1889–1895.

Pate, F.D., 1994. Bone chemistry and paleodiet. Journal of Archaeological Method and Theory 1(2), 161–209.

Piesco, N.P., Avery, J.K, 2002. Development of teeth:Crown formation. In: Avery, J.K., (Ed.), Oral Development and Histology (3rd ed.). Georg Thieme Verlag, Stuttgart, Germany.

Polischuk, S.C., Hobson, K.A., Ramsay, M.A., 2001. Use of stable-carbon and –nitrogen isotopes to assess weaning and fasting in female polar bears and their cubs. Canadian Journal of Zoology 79, 499–511.

R Development Core Team, 2008. R: A language and environment for statistical computing. R Foundation for Statistical Computing, Vienna, Austria.

Rasband, W.S., 1997-2008. ImageJ, U.S. National Institutes of Health, Bethesda, Maryland, USA, http://rsb.info.nih.gov/ij.

Raubenheimer, E.J., 2000. Development of the tush and tusk and tusklessness in the African elephant (*Loxodonta Africana*). Koedoe 43(2), 57–64.

Rohland, N., Malaspinas, A., Pollack, J.L., Slatkin, M., Matheus, P., Hofreiter, M., 2007. Proboscidean mitogenomics: Chronology and mode of elephant evolution using mastodon as outgroup. PLoS Biology 5(8), 1–9.

Rombach, E.P., Barboza, P.S., Blake, J.E., 2003. Costs of gestation in an Arctic ruminant: copper reserves in muskoxen. Comparative Biochemistry and Physiology Part C 134, 157–168.

Roth, V.L., Shoshani, J., 1988. Dental identification and age determination in *Elephas maximus*. Journal of Zoology 214(4), 567–588.

Rountrey, A.N, Fisher, D.C., Vartanyan, S., Fox, D.L., 2007. Carbon and nitrogen isotope analyses of a juvenile woolly mammoth tusk: Evidence of weaning. Quaternary International 169–170, 166–173.

Sarkar, B., 1994. Copper. In: Seiler, H.G., Sigel, A., Sigel, H., (Eds.), Handbook on Metals in Clinical and Analytical Chemistry. Marcel Dekker, New York, pp. 339–347.

Schulze, E.D., Chapin, F.S., III, Gebauer, G., 1994. Nitrogen nutrition and isotope differences among life forms at the northern treeline of Alaska. Oecologia 100, 406–412.

Schoeninger M.J., DeNiro, M.J., 1984. Nitrogen and carbon isotopic composition of bone collagen from marine and terrestrial animals. Geochimica et Cosmochimica Acta 48, 625–639.

Shaw, J.C.L., 1980. Trace elements in the fetus and young infant: II. Copper, Manganese, Selenium, and Chromium. American Journal of Diseases of Children 134, 74–81.

Sillen, A., Kavanagh, M., 1982. Strontium and paleodietary research: A review. Yearbook of Physical Anthropology 25, 67–90.

Sillen, A., Smith, P., 1984. Weaning patterns are reflected in strontium-calcium ratios of juvenile skeletons. Journal of Archaeological Science 11, 237–245.

Smith, B.N., Epstein, S., 1971. Two categories of $^{13}C/^{12}C$ ratios for higher plants. Plant Physiology 47, 380–384.

Sugimoto, A., Yanagisawa, N., Naito, D., Fujita, N., Maximov, T.C., 2002. Importance of permafrost as a source of water for plants in east Siberian taiga. Ecological Research 17, 493–503.

Sullivan, C.H., Krueger, H.W., 1981. Carbon isotope analysis of separate chemical phases in modern and fossil bone. Nature 292, 333–335.

Taylor, D.M., Bligh, P.H., Duggan, M.H., 1962. The absorption of calcium, strontium, barium, and radium from the gastrointestinal tract of the rat. Biochemical Journal 83, 25–29.

Ullrey, D.E., Miller, E.R., Brent, B.E., Bradley, B.L., Hoefer, J.A., 1967. Swine hematology from birth to maturity IV. Serum calcium, magnesium, sodium, potassium, copper, zinc, and inorganic phosphorus. Journal of Animal Science 26, 1024–1029.

Vuori, E., Kuitunen, P., 1979. The concentrations of copper and zinc in human milk. Acta Paediatrica Scandinavica 68, 33–37.

Wilson, G.F., Mackenzie, D.D.S., Brooks, I.M., Lyon, G.L., 1988. Importance of body tissues as sources of nutrients for milk synthesis in the cow, using ^{13}C as a marker. British Journal of Nutrition 60, 605–617.

Wright, L.E., Schwarcz, H.P., 1998. Stable carbon and oxygen isotopes in human tooth enamel: Identifying breastfeeding and weaning in prehistory. American Journal of Physical Anthropology 106, 1–18.

York, A.E., Thomason, J.R., Sinclair, E.H., Hobson, K.A., 2008. Stable carbon and nitrogen isotope values in teeth of Stellar sea lions: age of weaning and the impact of the 1975–1976 regime shift in the North Pacific Ocean. Canadian Journal of Zoology 86, 33–44.

Chapter 5

Stable isotope and elemental analyses of the dentin, bone and soft tissues of an exceptionally well-preserved woolly mammoth calf

Introduction

In May of 2007, the most complete mammoth carcass found to date was discovered on a bank of the Yuribei River, Yamal Peninsula, Yamal-Nenets Autonomous Okrug, Russian Federation (Fig. 5.1). The find is a nearly complete, mummified, female mammoth calf nicknamed "Lyuba", which has been dated (AMS-^{14}C on bone collagen) to 41910 + 550/-450 radiocarbon years before present (pers. comm. H. van der Plicht). Access to such a complete specimen allows study of aspects of mammoth paleobiology that have previously been difficult to evaluate. In this work we focus on the information that can be gained through analysis of carbon, nitrogen, and oxygen isotope ratios in the teeth and tissues, as well as elemental concentrations in the teeth.

The Carcass

The carcass (Fig. 5.2) is almost complete and is physically quite well preserved. Soft tissues are present, with the only apparently missing elements of the original anatomy being much of the hair, the nails, a portion of the tail, and a portion of the right pinna. Partial loss of the tail and pinna is attributed to recent scavenging activity around the time of discovery. The loss of hair and nails likely occurred around the time of death, as the release of hydrolytic enzymes at the boundary between the dermis and epidermis can lead to skin slippage (separation of the epidermis from the dermis) and loss of hair and nails (Clark et al., 1997).

The maximum height of the body is approximately 85 cm, with the shoulder height (R. manus to dorsal anterior thoracic region) is approximately 78 cm. The mass of the apparently desiccated carcass is approximately 50 kg. Additional measurements will be reported elsewhere.

Externally, the skin is intact, with few signs of decomposition, save some pitting that may be the result of superficial bacterial or fungal colonization. Some areas, particularly on the left side of the body, are also spotted with accumulations of vivianite. One of the more striking features of the carcass is the large hump located in the dorsal cervical region (Fig 5.2). A similar hump was present in this region of the Oimyakon mammoth calf (Boeskorov et al., 2007). In both calves, the hump was found to contain an accumulation of fatty tissue. Boeskorov et al. (2007) suggest that this fat reserve may have a function in aiding survival during severe winters. The presence of a significant fat reserve indicates that the calf probably did not experience nutritional stress prior to death.

In 2008, the carcass was partially thawed to allow collection of samples for histological, molecular, palynological, microbiological, and biogeochemical analysis. During this process, it was found that the internal organs were well preserved, and that the alimentary tract contained vegetation, sediment, and other materials. Samples for this work were collected at that time. Upper and lower left dP2s and dP3s, as well as several partially formed plates from the dP^4, were removed from the maxilla and mandible with little effort due to the apparent lack of periodontal ligament attachment. The left deciduous tusk (dI^2) was also extracted from the premaxilla. Samples of hump fat, orbital fat, subcutaneous abdominal fat, abdominal muscle, peritoneum, intestinal wall, caecal wall, and bone (rib) were collected in addition to intestinal and caecal contents. Teeth were stored in a sealed chamber above a small volume of ultrapure water and ethanol to prevent desiccation. All soft tissue samples were refrozen and stored at < -4 ^{o}C prior to analysis.

Teeth As Recording Structures

The tusks of mammoths, mastodons, and elephants are evergrowing, and changes in the structure and composition of tusk dentin can record information about an individual's age, as well as its nutritional status (Fisher, 1996), its diet (Fisher and Fox, 2003), and aspects of climate experienced during life (Fox et al., 2007). The dentin of tusks is marked by periodic growth lines that occur at different temporal scales. First-order growth increments are annual in periodicity, second-order increments have a period of around seven days, and third-order increments are daily (Fisher, 2001). The

thickness of a growth increment is associated with the nutritional status of the animal during the period of formation (Fisher, 1996). The presence of these incremental features also allows for the determination of the temporal position of compositional samples taken from tusks, which aids in understanding the temporal scale of the compositional oscillations that often occur in tusks (e.g. this dissertation, chapter 4).

Due to excellent soft-tissue preservation, Lyuba offers an opportunity to investigate not only the compositional and structural variation of recording structures, but also the composition of the tissues and intestinal contents from a young mammoth. For example, the isotopic composition of both dentin collagen and diet (based on intestinal contents) can be assessed. This allows determination of the diet-tissue fractionation for this individual. Other research goals, such as determination of the variation in stable isotope ratios of different tissues can also be addressed.

Lyuba has no permanent tusk, meaning that this preferred recording structure is unavailable for analysis. Its absence is also of note because there is some evidence, based on occurrence/absence of neonatal lines (a prominent growth line that occurs around the time of birth) in the dentin of permanent tusks from other juvenile mammoths, that the timing of initiation of permament tusk mineralization may have been variable in mammoths. Apparently, mineralization sometimes occurred prenatally, reflected by the presence of a neonatal line, but sometimes postnatally, indicated by the absence of a neonatal line. The deciduous tusk is present, but this is not an evergrowing tooth, and the apical margin is highly constricted, indicating formation of this tooth was completed before death (Fig. 5.3). Both the dP2s (Figs. 5.4,

5.5) and dP3s (Figs. 5.6, 5.7) have open roots, indicating formation was ongoing at the time of death. While the geometry of dentin accretion is more complex in deciduous premolars than in the permanent or deciduous tusk, these teeth offer the best source of material for analysis of a temporal interval that includes the time just before death.

Dentin Composition

Dentin consists of a collagenous matrix and a mineral fraction. In this study compositional analysis of the collagenous matrix is restricted to measurement of $\delta^{15}N$ and $\delta^{13}C$. The mineral fraction is nominally hydroxyapatite ($Ca_{10}[PO_4]_6[OH]_2$), with substitutions occurring at the Ca, PO_4, and OH sites. In this study, analysis of the mineral fraction includes measurement of $\delta^{13}C$ and $\delta^{18}O$ in substituted CO_3 as well as the ratios of Mg, P, Mn, Fe, Cu, Zn, Sr, Ba, and Pb to Ca. Serial samples are analyzed to allow observation of both long-term (multi-year) and seasonal-scale patterns of compositional change.

Variation in Compositional Measures

A description of factors likely to influence stable isotope and elemental ratios in juvenile mammoths is included in Chapter 4 (this dissertation). Here, this information is summarized.

$\delta^{13}C$

The $\delta^{13}C$ of collagen depends primarily on the $\delta^{13}C$ of the protein portion of the diet, but it is also influenced by the isotopic composition of carbohydrates and lipids (Ambrose and Norr, 1993). The $\delta^{13}C$ of carbonate in hydroxyapatite more closely represents the isotopic composition of bulk diet (Ambrose and Norr 1993). For large ungulates, the diet to enamel (carbonate in hydroxyapatite) enrichment of ^{13}C is about +14.1 ‰ (Cerling and Harris, 1999), while that for diet to collagen is about +5 ‰ (Sullivan and Krueger, 1981). By serially sampling accreted dentin, shifts in the isotopic composition of diet can be tracked.

The primary factors influencing $\delta^{13}C$ in the arctic are both dietary and physiological. More negative plant $\delta^{13}C$ is associated with low light, lower temperature, and low nutrient availability, while more positive values are associated with water and saline stress (Bocherens, 2003). Physiological factors include utilization of isotopically light (DeNiro and Epstein, 1977) fat reserves, which might lead to depleted $\delta^{13}C$. Intake of isotopically light milk lipids might also lead to more negative values (e.g. Newsome et al., 2006). Prenatally, $\delta^{13}C$ may be enriched due to preferential use of maternal protein stores in the production of fetal proteins (Barboza and Parker, 2006).

In all nursing juvenile mammoths previously studied, seasonal-scale oscillations in $\delta^{13}C_{col}$ occur, and these seem to be associated with decreased relative milk intake and increased relative plant protein intake in the early summer (this dissertation, chapter 4).

$\delta^{15}N$

$\delta^{15}N$ tends to increase with trophic level (Schoeninger and DeNiro, 1984) or nutritional stress. In young mammals, $\delta^{15}N$ of collagen formed during times of high milk dependency is often higher than that formed after weaning (Hobson and Sease, 1998; Newsome et al., 2006). In juvenile mammoths, $\delta^{15}N$ declines over the first few years of life in association with weaning (this dissertation, chapter 4). Prenatally, $\delta^{15}N$ may be enriched due to preferential use of maternal protein stores in the production of fetal proteins (Barboza and Parker, 2006).

$\delta^{18}O$

The $\delta^{18}O$ of body water in herbivorous mammals is mostly dependent on the $\delta^{18}O$ of surface water (Kohn, 1996). Meteoric water is often seasonally variable in isotopic composition (Gat, 1996), and this is true in modern Salekhard in the Yamal-Nenets Autonomous Okrug, where winter (Dec.-Feb.) precipitation has a $\delta^{18}O$ of -23.2 ‰, and summer (Jun.-Aug.) precipitation has a $\delta^{18}O$ of -11.8 ‰ (Kurita et al., 2004). However, the composition of food water and drinking water taken in by a mammoth is likely affected by the presence of permafrost and snow melt. In modern Yakutsk, Yakutia, Russian Federation, plant (stem) water is most depleted in ^{18}O in early June due to the contribution of snow melt (Sugimoto et al., 2002). $\delta^{18}O$ then increases through August, and presumably, late summer plant water $\delta^{18}O$ persists until the following May (this dissertation, Chapter 4; Sugimoto et al., 2002). Thus, lows in $\delta^{18}O$ oscillations may represent early summer.

Mg/Ca

While increasing Mg/Ca may be an indicator of decreased milk intake (this dissertation, chapter 3), the rapid diagenetic loss of Mg (Hola et al., 2008) makes this measure more useful as a determinant of diagenesis (this dissertation, Chapter 3). The mean value of samples from a modern juvenile African elephant with minimal alteration was 194.8 ± 44.3 mmol/mol, while the highest mean value of samples from a well-preserved juvenile mammoth tusk was 125.5 ± 12.4 mmol/mol (this dissertation, Chapter 4). However, the mammoth samples analyzed in Chapter 4 were rinsed prior to analysis while the elephant samples analyzed in Chapter 3 were not. An un-rinsed sub-sample from a well-preserved juvenile mammoth tusk had a value of 198.5 mmol/mol, while a rinsed sub-sample had a value of 143.2 mmol/mol (Rountrey, unpublished data). Values less than around 100 mmol/mol may indicate altered material.

Mn/Ca and Fe/Ca

Mn and Fe occur at low concentrations in modern enamel, but at concentrations several orders of magnitude higher in fossil enamel and dentine (Kohn et al., 1999). These measures are used as indicators of diagenesis in this study. In the tusk dentin of a modern juvenile African elephant mean Mn/Ca was 0.052 ± 0.204 mmol/mol, and mean Fe/Ca was 0.64 ± 0.38 mmol/mol (the high standard deviations are due to the inclusion of altered samples from the stained tip of the tusk), while in a

darkly stained juvenile mammoth tusk, the values were 0.641 ± 0.034 mmol/mol and 100.28 ± 4.59 mmol/mol respectively (this dissertation, Chapter 4).

Cu/Ca

In young pigs, serum copper levels are low around the time of birth and increase over the first two weeks of life (Ullrey et al., 1967), while in humans, serum copper increases over the first five months of life (Shaw, 1980). In muskoxen, protein-bound hepatic Cu in fetuses increases tenfold in late gestation (Rombach et al., 2003). Although it might be expected that dentin Cu/Ca would be low around the time of birth and increase over several months following the pattern in serum, no increasing trend was observed in a juvenile mammoth tusk in which a neonatal line marked the time of birth (this dissertation, Chapter 4). However, there was a late prenatal peak in Cu/Ca in that individual that could be related to the late prenatal accumulation of Cu in the liver (this dissertation, Chapter 4).

Zn/Ca

Serum Zn concentrations increase through gestation (Jeswani and Vani, 1982), and Zn concentrations in human milk are highest in the early stages of lactation (Vuori and Kuitunen, 1979). These factors might be expected to lead to elevated Zn/Ca around the time of birth. Indeed, in a study of human enamel, Ca-normalized Zn concentration was elevated in the vicinity of the neonatal line (Kang et al., 2004). Furthermore, in the tusk of a juvenile mammoth with a dentinal neonatal line, Zn/Ca

was elevated in dentin accreted just after birth (this dissertation, Chapter 4). These studies suggest that elevated Zn/Ca might mark the time of birth.

Sr/Ca

Sr/Ca of mineralized tissues is dependent upon the Sr/Ca of local soils (Sillen and Kavanagh, 1982). However, Sr is discriminated against relative to Ca in the guts of terrestrial vertebrates. Thus, decreasing Sr/Ca is associated with increasing trophic level (Sillen and Kavanagh, 1982). Sr/Ca has also been used to detect nursing and weaning as Sr is discriminated against during absorption by the mother, then again in milk production (Sillen and Kavanagh, 1982). This leads to low Sr/Ca in the tissues of nursing infants. Prenatally, the relative fetal uptake of Sr versus Ca in rats tends to increase in late gestation (Hartsook and Hershberger, 1973). Thus, it is hypothesized that dentin Sr/Ca should increase up to the time of birth. It is difficult to hypothesize about what pattern might be expected after birth because knowledge of differences in maternal-placental-fetal and maternal-milk-calf Sr discrimination is required. In a study of the composition of prenatal and postnatal human enamel, Dolphin et al. (2005) found no significant difference between prenatal and postnatal Sr/Ca in teeth from 36 individuals.

Ba/Ca

Ba generally behaves similarly to Sr, with decreasing values occurring with increasing trophic level (Pate, 1994). However, Dolphin et al. (2005) observed

significantly higher Ba/Ca in the postnatal enamel of humans versus the prenatal enamel, indicating a shift to lower total discrimination after birth. In the tusk of a juvenile mammoth with a dentinal neonatal line, Ba/Ca decreased until just after birth, then increased again (this dissertation, Chapter 4). Ba/Ca also varies seasonally in some juvenile mammoths (this dissertation, Chapter 4). Use of Ba/Ca as a paleodietary indicator is complicated by the association of high values with apparently diagenetically altered samples (this dissertation, Chapter 4).

P/Ca

P/Ca is included as an indicator of diagenetic alteration. In relatively unaltered dentin from a juvenile African elephant tusk, the P/Ca averaged 795.76 ± 58.57 mmol/mol, but increased with age (this dissertation, Chapter 3). This increase may be associated with increases in the Mg content of dentin with age (this dissertation, Chapter 3)

Pb/Ca

Pb/Ca increases from prenatal to postnatal enamel in humans (Dolphin et al. 2005). However, Pb levels are generally below detection using the methods of this study.

Materials and Methods

Cutting and Serial Sampling

Prior to any cutting or sampling, the dP2s and dI^2 were molded and cast using conventional methods. These teeth, as well as the dP3s were also μCT scanned to preserve a record of their original morphology.

Only the deciduous tusk and dP^2 were serially sampled. To gain access to the interior dentin of the deciduous tusk, it was longitudinally sectioned using an Isomet low-speed saw (Buehler, Lake Bluff, Illinois) and diamond wafering blade. To avoid contamination, ~70% ethanol in ultrapure water was used as the cutting lubricant. Powder samples were milled from a single cut surface following growth lines using the technique outlined in chapter 3 (this dissertation).

The dP^2 presented a challenge to conventional microsampling techniques. Due to the complex geometry of the dentin growth layers, and the small size of the tooth, milling would result in substantial time-averaging that would be difficult to characterize accurately. Following an observation from the μCT data, that many concentric fractures were present in the dentin, a plan was developed to use these fractures, which separate temporally discreet units of dentin (i.e. fractures propagate along incremental lines) to advantage. The fractures would be used as initiation points for a "peeling" method of collecting temporally discrete dentin layers.

The dP^2 was first cut along a mesial-distal plane using the Isomet saw. An additional cut was made along a roughly lingual-labial plane to isolate a lingual-distal fraction of the tooth (Fig. 5.8). An additional cut isolated a smaller portion of this fraction (Fig. 5.8). The purpose of isolating this part of the tooth was to obtain a portion of the tooth in which the growth laminae in dentin curved minimally, as it was

expected that attempting to separate curving layers of dentin might lead to additional fractures or tears. The natural fractures in the dentin were accentuated by repeatedly submerging the fragment in ~70% ethanol, then allowing much of the water and ethanol to evaporate prior to submerging again. This led to propagation of the existing fractures. Layers of dentin were then peeled away from the tooth using forceps. The fragment was scanned on a high-resolution flatbed scanner after removal of each sample, effectively recording the location of each sample. Use of this method produced relatively large (~7.5 mg) yet thin dentin sheets permitting analysis of this tooth at a higher temporal resolution than would have been possible using milling methods.

Thin Sections

Both ground and demineralized, paraffin-embedded (hematoxylin/eosin stained) thin sections of the cut teeth were produced to allow observation of incremental growth lines in the dentin.

$\delta^{13}C_{col}$ and $\delta^{15}N_{col}$

Subsamples of the powder or sheet samples were freeze-dried and weighed into 1.5 mL metal-free microcentrifuge tubes. 1.0 mL of 0.5 M TraceMetal Grade HCl was added to each sample. After 24 hours at 4° C, the samples were centrifuged (15 minutes at 14000 rpm) on an Eppendorf 5414 microcentrifuge, and the supernatant was pipetted off and retained for elemental analysis. Collagen samples were rinsed

five times in ultrapure water and then freeze-dried overnight. 0.5 mg of material from each sample was loaded into pressed tin capsules and analyzed for $\delta^{13}C$ and $\delta^{15}N$ at the Isotope Ratio Mass Spectrometry Laboratory at the University of California, Santa Cruz. A chloroform/methanol step, as is usually included in similar analyses to remove lipids, was not conducted on these samples. The use of powdered samples required that the samples remain in centrifuge tubes, and these tubes were not appropriate for containing chloroform. The lipid content of dentin is low (around 1.7 wt % of demineralized dentin (Wuthier, 1984), and no oils were used in the cutting process, so lipid contamination (and associated shifts toward light $\delta^{13}C$ values) should be minimal.

In addition to dentin samples, a bone (rib fragment) sample was also prepared for $\delta^{13}C$ and $\delta^{15}N$ analysis of collagen. The sample was placed in a roasted (550^{o}C overnight) glass scintillation vial, and 10 mL of 0.5 M TraceMetal Grade HCl was added. After 24 hours at 4^{o}C, 1 mL of the solution was pipetted off and reserved for elemental analysis. The sample was rinsed five times in ultrapure water; then 10 mL 2:1 chloroform/methanol was added to remove lipids. The vial was ultrasonicated for 30 minutes, after which the liquid was discarded, and the sample was rinsed five times in ultrapure water. The sample was then freeze-dried overnight, and a 1 mg subsample was loaded into a tin capsule for analysis on a Costech EA coupled to a Thermo DeltaV CF-IRMS at the Stable Isotope Laboratory, Department of Geological Sciences, University of Michigan, Ann Arbor, MI, USA.

Subsamples of tissue and gut contents were placed in 1.5 mL microcentrifuge tubes, rinsed with ultrapure water, and freeze dried. As the C/N of these materials was

expected to vary substantially, an initial subset of samples was loaded into pressed tin capsules and analyzed on a Costech (need info) EA coupled to a Thermo DeltaV CF-IRMS to determine C/N as well as $\delta^{13}C$ and $\delta^{15}N$ if C and/or N mass was appropriate. Following this initial reconnaissance run, appropriate masses of each sample were loaded into pressed tin capsules and analyzed for $\delta^{13}C$ and $\delta^{15}N$ at the Stable Isotope Laboratory, housed in the Department of Geological Sciences, University of Michigan, Ann Arbor, MI, USA. For some samples $\delta^{13}C$ and $\delta^{15}N$ were determined on separate subsamples due to very high C/N which precluded simultaneous determination. All $\delta^{15}N$ values are reported relative to air, while $\delta^{13}C$ is reported relative to VPDB.

$\delta^{13}C_{carb}$ and $\delta^{18}O_{carb}$

Powder samples from the deciduous tusk were analyzed for the $\delta^{13}C$ and $\delta^{18}O$ of structural carbonate in hydroxyapatite. As only small masses of sample were available, no chemical pretreatment was carried out. However, the samples were heated under vacuum at 200°C for 1 hour to remove volatiles. 1.0-mg samples were analyzed on a Thermo MAT 253 IRMS coupled to a Finnegan Kiel IV carbonate preparation device at the Stable Isotope Laboratory, Dept. Geological Sciences, University of Michigan, Ann Arbor. $\delta^{13}C$ and $\delta^{18}O$ are reported relative to VPDB.

Elemental Concentrations Relative to Calcium

Supernatant solutions resulting from the 0.5 M HCl demineralization of dentin samples (and one bone sample) to be used for collagen $\delta^{13}C$ and $\delta^{15}N$ analyses were

diluted with 1% HNO_3 (1 ppb In internal standard) to target ~10 ppm Ca. Solutions were analyzed using a Finnegan Element ICP-MS housed in the Keck Elemental Geochemistry Laboratory, Department of Geological Sciences, University of Michigan, Ann Arbor, MI, USA.

Results

Age at Death

Age Based on Tooth Eruption and Wear

The ages of mammoths are often determined by the state of eruption and wear of their premolars and molars and a comparison to the progression of eruption and wear in modern elephants. While ages determined by tooth growth increment counts are likely to be more accurate, particularly when a neonatal line is present, a description of the state of Lyuba's teeth, and her age in elephant-equivalent years is appropriate for discussion, as the information could be used to aid in calibrating this aging system for mammoths.

Lyuba's left maxilla contained a dP^2, dP^3, and partially formed plates from the dP^4. The crown of dP^2 consists of 5 fully formed lophs, yet cementum does not yet fill the space between these (Fig. 5.4). There is some polish and removal of enamel/dentin suggesting that the first three lophs were in wear at the time of death (Fig. 5.4). The crown of dP^3 consists of 9 fully formed lophs with no cementum filling the gaps between lophs (Fig. 5.6). Root formation is in an early stage. There are no signs of wear on the dP^3.

The left hemimandible contained a dP_2 and dP_3. The crown of dP_2 consists of 4 full lophs increasing in width distally and an additional distal loph that is of reduced width (Fig. 5.5). Cementum does not fill gaps between lophs. The mesial three lophs show some signs of wear, though this is difficult to assess because of some apparent spalling of enamel off of the crown (Fig. 5.5). Crown formation in dP_3 was incomplete. The crown consists of 10 lophs, but the distal three lophs are incompletely formed and are not joined to the rest of the tooth (Fig. 5.7). Cementum does not fill gaps between lophs, and there are no signs of wear on this tooth (Fig. 5.7).

Roth and Shoshani (1988) report that a three-day-old Asian elephant (*Elephas maximus*) showed wear in two dP_2 lophs, and that dP_3 was unerupted. In Asian elephants, dP_2 is lost at around 1.5-2.0 years (Roth and Shoshani, 1988). Based on these data Lyuba died at an age of between 3 days and 1.5 years (Asian elephant equivalent), though the age is likely closer to 3 days than 1.5 years.

Age Based on Dentin Growth Increments

A neonatal line was not apparent in the deciduous tusk. This, along with the narrow root canal (Fig. 5.3), suggests that its formation was completed before birth.

The roots of dP^2 and dP_2 show accentuated constrictions 1.5 and 3 mm from the apical margins respectively (Figs. 5.4, 5.5, 5.8). The original distance from the apical margin in dP^2 was probably greater, but some of the apical material appears to have been lost to decay. After the initial mesial-distal cut, it was discovered that this constriction corresponded to an accentuated growth line in dP^2 (Fig. 5.8). This line

appears to be a neonatal line marking the time of birth. Counts of third-order (daily) growth increments in the dentin from the neonatal line to the pulp cavity surface indicate an age at death of about 31 days.

Intestinal and Caecal Contents

The intestinal contents largely consist of four materials: 1) friable, white- to buff-colored granules up to ~2.5 mm in diameter (Fig 5.9A); 2) sheared and otherwise processed fragments of vegetation (Fig 5.9B); 3) sediment (medium to fine sand); 4) small (< 0.6 mm), translucent, amber-colored, botryoidal or spheroidal masses (Fig. 5.9C). Infrared spectroscopy shows that the friable granules are composed of calcium stearate or a similar calcium soap (possibly representing saponified milk fat), while the amber-colored masses contain calcium stearate, protein, and silicate or phosphate (M. McKelvy, pers. comm.). The contents of the caecum consist largely of processed vegetation and sediment.

Isotope and Elemental Composition

dP^2

Compositional data for the dP^2 samples are plotted in Figure 5.10A-K. Mean values are shown in Table 5.1. Sample 13 in this series represents dentin accreted after formation of the neonatal line (i.e. postnatal). $\delta^{13}C_{col}$ increases through time (Fig 5.10A), with significant ($p < 0.001$) positive slope (least squares regression). There may be a seasonal pattern present, though the increasing trend makes this difficult to

identify. The single postnatal sample is depleted relative to the previous three samples. No significant trend is present in $\delta^{15}N_{col}$, and an apparently seasonal pattern is observed (Fig. 5.10B). The postnatal sample is more enriched than all other samples.

Mg/Ca is low relative to values in a modern African elephant calf and well-preserved juvenile mammoth tusks (Table 5.1). Mn/Ca, Zn/Ca, Sr/Ca, and Ba/Ca are higher than observed in any of the juvenile mammoths previously studied (Table 5.1). Fe/Ca is also higher than in most other tusks (Table 5.1). Mg/Ca, Mn/Ca, Fe/Ca, Sr/Ca, and Ba/Ca all increase significantly ($p < 0.01$) with time, while Zn/Ca shows little variation prior to a pronounced increase in the last three samples (Fig. 5.10H). The Cu/Ca series peaks in sample 7, then generally declines until the postnatal sample, in which the measure rises again to a higher value (Fig. 5.10G). Pb was below detection limits in most samples (Fig. 5.10K).

dI^2

Compositional data for the dI^2 samples are plotted in Figure 5.11A-K. Mean values are shown in Table 5.1. As no neonatal line was present in this deciduous tusk, no postnatal samples are present. These samples were milled from the tusk, and are likely to average more time than the "peeled" dP^2 samples. A qualitative comparison of the dI^2 $\delta^{15}N_{col}$ series (Fig. 5.11B) to the dP^2 $\delta^{15}N_{col}$ series (Fig. 5.10B) suggests that the time included in the dI^2 samples is approximately equivalent to the time covered by dP^2 samples 4 to 12.

With such a short series of values, seasonal patterns are difficult to assess. However, it appears that $\delta^{15}N_{col}$ shows the same seasonal pattern exhibited in the dP^2 series. The $\delta^{13}C_{col}$ series increases with time (Fig. 5.11A) as seen in the dP^2 (Fig. 5.10A), although in this case, a regression is not significant. $\delta^{18}O_{carb}$ may show a seasonal pattern (though somewhat masked by an increasing trend) in which low $\delta^{18}O_{carb}$ is associated with low $\delta^{15}N_{col}$ (e.g. samples 1,2, and 6) (Figs. 5.11C, B). Mean $\delta^{13}C_{carb}$ is more enriched than might be expected given the $\delta^{13}C_{col}$ values, but may show seasonal variation (Fig. 5.11D).

Mg/Ca is low as in the dP^2 samples (Table 5.1), and has a significant positive trend ($p < 0.01$) (Fig. 5.11E). Zn/Ca and Sr/Ca (Figs. 5.11I, J) also have significant positive trends ($p < 0.01$). The general patterns in Zn/Ca and Sr/Ca are similar to those observed in dP^2 samples 4 through 12 (Figs. 5.10H, I).

Isotopic Composition of Bone, Tissues, and Gut Contents

The $\delta^{13}C_{col}$ of the bone sample falls within the range of values observed in the dentin samples, although the $\delta^{15}N$ is more depleted than any dentin sample (Fig. 5.12). The C/N of the bone collagen is also higher than observed in dentin samples from this and other juvenile mammoths (and modern elephant) (Table 5.1). Mg/Ca and P/Ca are slightly higher than mean values from Lyuba's dentin samples (Table 5.1). Mn/Ca, Fe/Ca, Sr/Ca, and Ba/Ca are higher in the bone sample than mean values of dentin samples from this individual and other juvenile mammoths (Table 5.1), although higher Mn/Ca and Fe/Ca were observed in pulp cavity samples from the 44-M juvenile

(this dissertation, chapter 4). Cu/Ca and Zn/Ca are similar in bone and dentin (Table 5.1).

$\delta^{13}C$ and and $\delta^{15}N$ for tissue samples, bulk gut contents, and fractions of gut contents are shown in Figure 5.12. In general, fatty tissues are more depleted in $\delta^{13}C$ than other tissues. Caecal tissue, intestinal tissue, and abdominal muscle are depleted in $\delta^{13}C$ relative to dentin collagen by about 2.7 ‰, and have $\delta^{15}N$ similar to dentin collagen (except abdominal muscle). Dentin collagen is enriched over bulk intestinal content by 5.5 and 1.8 ‰ in $\delta^{13}C$ and $\delta^{15}N$ respectively. The amber-colored masses from the intestine have the most depleted $\delta^{13}C$ of any sample analyzed, and sufficient quantities for analysis of $\delta^{15}N$ were not available. Plant material separated from the intestinal contents is similar in isotopic composition to bulk intestinal contents, though slightly enriched in ^{15}N and ^{13}C. The granules consisting largely of calcium stearate (interpreted as saponified milk fat) have the lightest $\delta^{15}N$ of any sample, and are also depleted in ^{13}C relative to bulk intestinal contents or plant material.

Discussion

Gut Contents

The dP^2 of Lyuba has a neonatal line, and based on a count of daily growth increments in the dentin, Lyuba died at an age of about 31 days. In African elephants, a calf of this age would be completely dependent on its mother's milk (Lee and Moss, 1986), and would remain very close to its mother at all times (Moss, 1988). Elephant

calves begin to feed on vegetation in about their fourth month of life, although nutritional self-sufficiency is not reached until about two years (Lee and Moss, 1986). Assuming that mammoth calves were similar to elephant calves, the presence of saponified milk fat in the intestine, which supports the hypothesis that Lyuba did not experience nutritional stress prior to death, seems reasonable. Its presence also indicates that Lyuba's death is probably not attributable to separation from her mother.

The presence of processed vegetation in Lyuba's alimentary tract is surprising. D. Fisher (pers. comm.) has suggested that the presence of the sheared and otherwise processed vegetation in the gut may indicate coprophagy. Young African elephants have been observed to ingest the feces of older elephants (Guy, 1977; Legget, 2004; D. Fisher, pers. obs.), and presumably this functions to either inoculate the calf with intestinal symbionts (e.g., as in rabbits, Ushakova et al., 2008), or to provide an additional source of protein or other nutrients.

Evidence of coprophagy also exists for adult mammoths. In an analysis of the intestinal contents of the Yukagir mammoth, van Geel et al. (2008) found fruit-bodies of a dung fungus suggesting that this adult male mammoth had ingested feces. If coprophagy was a common dietary strategy for mammoths, this could have implications for understanding the unusually enriched $\delta^{15}N$ values often measured in their remains (Bocherens et al., 1996). In cattle, feces are enriched in ^{15}N by about 2 ‰ over diet (Steele and Daniel, 1978). If this enrichment is a general phenomenon, and

mammoths ingested substantial amounts of feces, this could lead to ^{15}N enrichment in their tissues.

Diagenesis

The high Mn/Ca and Fe/Ca in the dP^2 and dI^2 samples (Table 5.1) indicates that substantial amounts of exogenous Mn and Fe are present in the tusk, likely as Fe- and Mn- oxides or oxyhydroxides (Kohn et al, 1999). This is also evidenced by the dark brown/orange color of the dentin (Fig. 5.8). Mn/Ca and Fe/Ca are higher in the porous bone (Table 5.1), suggesting a greater degree of alteration of this material. If one assumes that the bone is subject to more pervasive diagenetic alteration, the higher Ba/Ca and Sr/Ca of bone relative to the elevated (compared to other juvenile tusks from Siberia) levels in dentin suggest that Ba/Ca and Sr/Ca have also been altered (Table 5.1). Low Mg/Ca may indicate diagenetic loss of Mg (Hola et al., 2008).

$\delta^{13}C_{carb}$ may also be altered. The value of $\delta^{13}C_{carb} - \delta^{13}C_{col}$ ($\Delta^{13}C$) in modern herbivores is typically 7 to 9 ‰ (Koch et al., 1997). Koch et al., 1997, using fossil and sub-fossil materials, found that when the diagenetically-resistant enamel and collagen were compared, $\Delta^{13}C$ typically fell inside this range, but when dentin or bone and collagen were compared, $\Delta^{13}C$ was often greater than 9 ‰ indicating alteration of the dentin or bone carbonate values. The mean value of $\Delta^{13}C$ for dI^2 samples is 11.98 ± 0.25 ‰ (Table 5.1).

While mean Zn/Ca in dentin samples is higher than in other juvenile mammoth tusks (Table 5.1), most dP^2 samples are of the same order of magnitude as samples

from other tusks, with the mean being elevated by three high Zn/Ca samples near the pulp cavity (Fig. 5.10H). Zn/Ca in bone is higher than all dP^2 samples except these final three. If Zn concentration tends to increase during diagenesis, which is suggested by the lower values observed in modern elephant dentin (Table 5.1), and the bone sample represents a higher degree of alteration than dentin samples, the high Zn/Ca observed in the final three samples of dentin is difficult to explain. These high values may represent a primary signal.

Cu/Ca in dP^2 is of the same order of magnitude as the well-preserved Mol and Bolshoi Lyakhovskii tusks, suggesting minimal alteration (Table 5.1).

Seasonality

Seasonal variation appears to occur in the $\delta^{15}N_{col}$ of dP^2 and dI^2 (Figs. 5.10B, 5.11B). In dP^2 the depleted-enriched-depleted pattern that occurs from sample 4 to sample 10 is interpreted as variation over one year. Presumably, this corresponds to the same pattern that occurs in dI^2 from sample 2 to sample 5 or 6. Thus, based on the inclusion, in the dP^2 series, of an additional peak in samples 1,2, and 3, and the absence of this peak in dI^2, it seems that dP^2 mineralization was initiated prior to formation of dI^2, and that dP^2 records approximately 1.5 years of prenatal development.

Determination of the season represented by enriched or depleted $\delta^{15}N$ is problematic. Expression of seasonal $\delta^{15}N$ variation in fetal tissue composition has, to our knowledge, not been studied. While one might expect patterns to be similar to

patterns that would be found in the maternal tusk if it were present, the observations of Barboza and Parker (2006) indicate that body protein stores are preferentially utilized for fetal growth in reindeer. In addition to any seasonal variation caused by nutritional status or dietary changes in the mother, the relative contributions of maternal protein stores and dietary protein to the growth of the fetus might itself vary seasonally. It seems if this were the case, that high $\delta^{15}N$ (indicating use of maternal protein stores) would occur in winter or early spring when the availability of plant protein might be at a minimum. As winter/early spring is also the period in which maternal $\delta^{15}N$ might be elevated due to nutritional stress or feeding on dry, windblown ridges, it seems reasonable to assume that high fetal dentin $\delta^{15}N$ most likely represents winter/early spring.

In another juvenile mammoth (44-M), depleted $\delta^{15}N_{col}$ appears to represent early summer (this dissertation, chapter 4). In that individual, lows in the $\delta^{15}N_{col}$ series just follow lows in the $\delta^{18}O_{carb}$ series. The low $\delta^{18}O_{carb}$ is interpreted as late spring because this is the time of year during which snow melt is a major component of plant water and other surface water (this dissertation, chapter 4). The low $\delta^{15}N_{col}$ that occurs following this might result from decreased nutritional and/or water stress, a change from feeding on dry windblown ridges to wetter depressions, or, for a calf, a decrease in relative milk intake (this dissertation, chapter 4). In samples from Lyuba's dl[2], more depleted $\delta^{18}O_{carb}$ in samples 1,2, and 6 (Fig. 5.11C) is associated with more depleted $\delta^{15}N_{col}$ (Fig. 5.11B) supporting the hypothesis that higher $\delta^{15}N_{col}$ might represent winter or early spring.

As mentioned above, the dI^2 appears to have completed formation just before birth. Both $\delta^{15}N_{col}$ and $\delta^{18}O_{carb}$ become more enriched in the last two samples from dI^2 (Figs. 5.11B, C) and $\delta^{15}N_{col}$ in dP^2 also becomes more positive during this time (~samples 10-12) (Fig. 5.10B). In dI^2, the final $\delta^{15}N_{col}$ value is similar to that of the previous peak (sample 4) (Fig. 5.11B), perhaps indicating that birth occurred in early spring before decreasing $\delta^{18}O_{carb}$ or $\delta^{15}N_{col}$ would be recorded in the dentin. However, $\delta^{15}N_{col}$ in sample 12 from dP_2, though part of an increasing trend from sample 10 to 13, is more depleted than the previous peak (sample 6) (Fig. 5.10B). This might suggest birth earlier in the year, perhaps even in late winter. Oxygen isotope analyses of dP^2 samples might help to clarify the timing of birth.

Birth in late winter or early spring would seem dangerous as the quality of forage available for the lactating mother might be poor and the thermal stress on the calf might also be a problem. In African elephants, peak conception rates occur during the rainy season when high quality food is available (Williamson, 1976). With a 22-month gestation, births occur two months before this season of high food availability. If gestation was similar in mammoths, breeding during the productive summer would lead to births before this season (i.e., in spring). If, like elephants, mammoth calves began to feed on vegetation at about four months of age (Lee and Moss, 1986), birth prior to the start of the growing season would perhaps also permit calves to begin to feed on still-growing vegetation in late summer and early autumn

The lack of clear seasonal oscillations in $\delta^{13}C_{col}$ is surprising given that seasonal patterns are present in all juvenile mammoth tusks with sufficient temporal coverage

to exhibit these patterns (this dissertation, Chapter 4), and oscillations are also present in the tusks of adults (S. Gohman, D. Fox, D. Fisher, unpublished data). In dP^2, $\delta^{13}C_{col}$ generally increases through time (Fig 5.10A). Because the majority of this dentin was formed before Lyuba's birth, there may be some factor related to the pregnancy that is leading to this increase. In reindeer, neonatal blood cells are enriched in both ^{15}N and ^{13}C relative to maternal blood cells, and Barboza and Parker (2006) attribute this to preferential use of maternal protein stores to support fetal growth. This may be a factor in fetal $\delta^{15}N_{col}$ and $\delta^{13}C_{col}$, but the trends in these two variables are not similar. Thus, a hypothesis of increasing use of maternal protein stores through gestation, which might explain the increasing $\delta^{13}C_{col}$ trend, is not supported.

Postnatal Dentin

Only sample 13 from dP^2 represents postnatal dentin. $\delta^{13}C$ and $\delta^{15}N$ in this sample differ little from prenatal samples (Figs. 5.10A,B). However, the $\delta^{15}N$ of this sample is the highest observed in the series. This elevated value may be associated with ingestion of milk, but the value is only 0.15 ‰ more enriched than the prenatal peak $\delta^{15}N$ that occurred approximately one year before birth. Thus, enrichment may be due to the same seasonal factor that caused the previous peak. Because Lyuba died at such an early age, we cannot determine whether an increase in $\delta^{15}N$ associated with milk intake might mark the time of birth in mammoth dentin. In the tusk of another juvenile mammoth that contained a neonatal line, no marked increase in

$\delta^{15}N_{col}$ occurred near the transition from prenatal to postnatal dentin (this dissertation, chapter 4).

Zn/Ca and Cu/Ca

The elevated values of Zn/Ca in the last three samples from dP^2, and in samples representing late gestation in dI^2 (Figs. 5.10H, 5.11I) have several possible interpretations: 1) High Zn/Ca associated with late prenatal and early postnatal life; 2) Partial diagenetic alteration with areas near pulp cavities effected to a greater degree; 3) Preservation of a pattern of high Zn/Ca in dentin adjacent to the pulp cavity.

Partial diagenetic alteration near pulp cavity surfaces is a possibility as the open dentinal tubules might allow easier diffusion of Zn into this area. However, it is difficult to account for the Zn/Ca in dP^2 samples 11-13, which is higher than Zn/Ca in bone. Bone is higher in Mn/Ca, Fe/Ca, Ba/Ca, and Sr/Ca than dentin, suggesting it is more susceptible to alteration. Thus, alteration alone does not seem to be the cause of the high Zn/Ca values in late dentin samples.

Brudevold et al. (1963) observed that the concentration of Zn in human dentin was about three times greater near the pulp cavity surface than elsewhere. If this is a general phenomenon in teeth, it may explain the high Zn/Ca in samples of dentin from Lyuba's teeth taken near the pulp cavity surface. Due to the proximity of the neonatal line to the pulp surface, it is not possible to distinguish between this causative factor and a factor related to late gestation and early life. However, elevated Zn/Ca was not observed in dentin adjacent to the pulp cavity in any other juvenile

mammoths (this dissertation, Chapter 4), suggesting that Zn/Ca may not be generally elevated in dentin adjacent to the pulp cavity.

As mentioned in the introduction, elevated Zn/Ca has been observed in human enamel associated with the neonatal line (Kang et al., 2004), and also in juvenile mammoth dentin near an inferred neonatal line (this dissertation, chapter 4). Human serum Zn concentrations increase through gestation (Jeswani and Vani, 1982), and are highest in milk in the early stages of lactation (Vuori and Kuitunen, 1979). The high Zn/Ca of neonatal-line dentin or enamel may be related to these patterns. This hypothesis could be tested by analyzing dentin formed from late gestation to after birth in a modern elephant dP^2 or a tusk known to have begun mineralization prior to birth. Analyzing modern material allows diagenesis to be ruled out, and using a tooth from an animal that lived for some months after birth would allow evaluation of the perinatal Zn/Ca without the inclusion of dentin near the pulp cavity surface that might be elevated in Zn/Ca.

Lyuba died at such a young age, that detection of any postnatal trends in Cu/Ca that might be expected is not possible. It is of interest that both in Lyuba's dP^2 and in the tusk of another juvenile mammoth that contained a neonatal line, peak in Cu/Ca is observed during gestation (Fig. 5.10G; this dissertation, chapter 4). Peak Cu/Ca in Lyuba's dP^2 occurs in sample 7, which also is the location of a $\delta^{15}N_{col}$ peak that probably represents dentin accreted about a year before birth. It seems unlikely that this is related to late gestation Cu accumulation as Cu/Ca actually decreases prior to the neonatal line. Seasonal variation in serum Cu/Ca has been observed in cattle

(Yokus and Cakir, 2006), and this might account for the pattern. However, seasonal variation in Cu/Ca was not observed in the tusks of any juvenile mammoths studied (this dissertation, chapter 4).

The possibility of a dentin recording Zn and Cu dynamics in a fetus/calf raises the question of whether measurement of Zn and Cu concentrations in the dentin of adult females might provide some indication of reproductive status. In cattle, serum Cu increases through pregnancy, and the trend is markedly different from that which occurs in unmated females (Yokus and Cakir, 2006). In addition, maternal plasma Zn levels in cattle decrease during late pregnancy (Dufty et al., 1977). Thus, high Cu/Ca and low Zn/Ca in maternal dentin might indicate late pregnancy. If so, these measures could be used to determine life history parameters such as interbirth interval in mammoths. A study to determine the utility of these measures is currently underway.

$\delta^{13}C$ and $\delta^{15}N$ of Tissues

In general, dentin collagen is heavier in both $\delta^{13}C$ and $\delta^{15}N$ than other sampled tissues (Fig. 5.12). The positive offsets in $\delta^{13}C$ of postnatal dentin collagen over diet (+5.8 ‰ over bulk intestinal contents) and mean dentin collagen over lean tissues (average +2.7 ‰ over caecum, intestine, and abdominal muscle) are generally consistent with the offsets observed in modern animals. In samples from modern animals, the diet to collagen enrichment in ^{13}C is 4.5 to 5 ‰ (Lee-Thorp et al.,1989), and "meat" is 2-3 ‰ more depleted than collagen (DeNiro and Epstein, 1978; Vogel, 1978; Sealy, 1986; cited by Lee-Thorp et al.,1989). The slightly higher enrichment of

dentin collagen over diet in Lyuba might be due to the high lipid content of her diet. The presence of substantial quantities of isotopically light lipids in the bulk intestinal contents, little carbon from which is incorporated into collagen (Ambrose and Norr, 1993), tends to increase the offset by producing more negative $\delta^{13}C$ values for this material. Additional analyses of lipid-extracted intestinal contents are warrented.

Fatty tissues (abdominal fat, hump fat, and eye fat) are depleted in ^{13}C relative to mean dentin collagen by 5.9 ‰. This is close to the offset of 7 ‰ for modern herbivores proposed by Lee-Thorp et al. (1989).

Postnatal dentin collagen is enriched in ^{15}N over diet (bulk intestinal contents) by 2.2 ‰. This is somewhat less than the widely cited +3 ‰ per trophic level enrichment (Schoeninger and DeNiro, 1984). However, enrichment (diet-plasma) tends to be lower when animals are fed on diets of high protein quality such as milk (Robbins et al., 2005).

The depleted (relative to dentin collagen) $\delta^{15}N$ of abdominal and hump fat is difficult to interpret. In pigs, the diet-tissue fractionations for nails, hair, cartilage, muscle, liver, and fat are similar (between +2.2 and +3.0 ‰) (Nardoto et al., 2006). This suggests that $\delta^{15}N$ differences among tissues should be minimal. It is possible that the $\delta^{15}N$ has been altered by decomposition, but bacterially degraded collagen has been observed to be enriched rather than depleted in ^{15}N (Balzer et al., 1997).

Conclusions

Lyuba offers a unique glimpse into the paleobiology of mammoths. Having apparently died suddenly (i.e., without experiencing nutritional stress) at an age of about one month, she represents an individual likely following a normal path of development up to the point of her death. As such, the information gained from the study of her teeth and tissues should be applicable to arctic mammoths in general.

Analyses of Lyuba's teeth indicate that formation of dP^2 is initiated early in gestation and that analyses of dentin in dP2s can yield information on more than a year of prenatal development in mammoths. Similar analyses of dP2s from modern elephants may shed additional light on the factors affecting prenatal dentin composition and provide a much needed reference for studies of young mammoths. Furthermore, the lack of development of the permanent tusk in Lyuba, and the presence of a neonatal line in the permanent tusk of a male juvenile mammoth suggests that the timing of permanent tusk development in mammoths was variable. It is possible that sex differences in the timing of tusk development exist.

Lyuba's intestine contains both remnants of milk (saponified fats) and sheared/processed vegetation. Based on observations of modern elephants, it is unlikely that Lyuba was ingesting significant quantities of plant material as part of her diet. Furthermore, the state of eruption of her teeth suggests that her ability to process vegetation may have been minimal. Thus, the presence of the processed vegetation may indicate coprophagy. There is also evidence of coprophagy in an adult mammoth, suggesting that this may have been a typical behavior for both juvenile and adult mammoths. This would have implications for understanding the

nutrition of mammoths, as their ability to extract nutrients from vegetation using this system might be greater than previously thought. However, analyses of gut contents from other adult mammoths are needed to confirm that this activity was part of normal adult mammoth behavior.

Evidence from $\delta^{15}N_{col}$ and $\delta^{18}O_{carb}$ series indicates that Lyuba was probably born in early spring. Assuming a 22-month gestation, this implies a breeding season of late spring or early summer. If, like elephants, mammoth calves began to feed on vegetation at about four months of age, birth in early spring would allow calves to begin to feed on vegetation in late summer before the onset of possibly difficult winter foraging. This timing is analogous to that of modern elephants for which the peak in conceptions occurs when high quality forage is available, and births occur just before this season.

Elemental analyses of dentin samples imply alteration of primary Mg/Ca, Mn/Ca, Fe/Ca, and probably Sr/Ca and Ba/Ca. Evidence suggests that Zn/Ca and Cu/Ca may retain primary signals. Zn/Ca is elevated around the time of birth, which has been observed in human enamel. This is also consistent with what is known of serum Zn dynamics in late gestation. Therefore, Zn/Ca in dentin might be used as an indicator of late gestation or birth.

The possibility that dentin Zn/Ca records information regarding changes in Zn status has interesting implications. Zn (and Cu) status change in specific ways during pregnancy. Thus, high-resolution, serial analyses of dentin might allow the determination of the timing of parturition in mammals with evergrowing teeth. This

could be used to determine interbirth intervals or parity in mammals with teeth that record many years of growth such as elephants, dugongs, and sperm whales. Currently, the relationship between serum Zn or Cu levels and dentin Zn/Ca and Cu/Ca is not known. Furthermore, overprinting of seasonal patterns in these variables might limit the ability to identify patterns caused by pregnancy. Studies to clarify these issues are currently underway.

Isotope analyses of Lyuba's tissues and the contents of her intestine and caecum generally indicate differences among samples consistent with observations of modern animals. However, some values are difficult to interpret. Additional analyses on separated components (e.g. lipids and proteins) might help to clarify the patterns observed in these data.

Lyuba is truly a remarkable specimen. Her age at death and unparalleled preservation allows analyses that would not be possible on any other mammoth fossil. This work has led to characterization of aspects of juvenile mammoth paleobiology such as probable season of birth, the timing of tooth development, and early feeding patterns, but has also highlighted areas for further research. It is hoped that through continued work of this kind on both modern and fossil materials, that the ability to extract relevant life history information from compositional patterns in recording structures such as teeth will be enhanced.

Table 5.1. Mean compositional values for the dP2, dI2, and bone (single value) samples from Lyuba with mean values from dentin samples from five other juvenile mammoths and a modern African elephant (this dissertation, chapters 3,4). Standard deviations are listed below means. n.d. = not detected.

Specimen		$\delta^{13}C_{col}$	$\delta^{15}N_{col}$	$\delta^{18}O_{carb}$	$\delta^{13}C_{carb}$	C/N_{col}	$\delta^{13}C_{carb}$ - $\delta^{13}C_{col}$	Mg/Ca	P/Ca	Mn/Ca	Fe/Ca	Cu/Ca	Zn/Ca	Sr/Ca	Ba/Ca	Pb/Ca
Lyuba dP[2]	**mean**	**-21.50**	**9.19**	**-**	**-**	**3.23**	**-**	**15.20**	**603.71**	**2.285**	**85.54**	**0.058**	**1.160**	**2.127**	**1.067**	**0.004**
	s.d.	0.31	0.21	-	-	0.02	-	0.74	15.72	0.084	5.91	0.034	1.259	0.075	0.092	0.002
Lyuba dI[2]	**mean**	**-21.83**	**9.27**	**-10.29**	**-9.85**	**3.28**	**11.98**	**14.70**	**637.68**	**2.238**	**89.79**	**-**	**1.473**	**2.254**	**1.283**	**n.d.**
	s.d.	0.26	0.13	0.54	0.13	0.03	0.25	1.17	67.59	0.080	1.25	-	0.820	0.056	0.088	-
Lyuba bone (rib)	**value**	**-22.10**	**8.57**	**-**	**-**	**3.41**	**-**	**18.40**	**682.10**	**3.068**	**126.51**	**0.019**	**1.061**	**3.686**	**3.010**	**n.d.**
	-	-	-	-	-	-	-	-	-	-	-	-	-	-	-	-
44-M	**mean**	**-21.93**	**9.50**	**-8.05**	**-10.32**	**3.10**	**11.60**	**90.78**	**655.67**	**0.331**	**2.06**	**0.158**	**0.202**	**0.537**	**0.099**	**0.002**
	s.d.	0.47	0.83	0.56	0.98	0.03	1.02	63.12	59.59	0.918	3.82	0.131	0.293	0.029	0.056	0.002
Mol	**mean**	**-22.55**	**11.51**	**-**	**-**	**3.15**	**-**	**91.59**	**699.43**	**0.554**	**9.13**	**0.097**	**0.174**	**0.630**	**0.068**	**0.007**
	s.d.	0.49	1.61	-	-	0.02	-	19.18	39.93	1.530	18.23	0.076	0.096	0.088	0.023	0.009
Bolshoi Lyakhovskii	**mean**	**-22.10**	**11.16**	**-15.86**	**-15.40**	**3.14**	**6.51**	**125.51**	**721.17**	**0.262**	**3.38**	**0.084**	**0.215**	**0.748**	**0.046**	**0.002**
	s.d.	0.50	1.15	1.07	0.55	0.01	1.13	12.44	32.06	0.417	6.27	0.039	0.303	0.180	0.013	0.003
Allen	**mean**	**-22.13**	**9.28**	**-**	**-**	**3.25**	**-**	**18.39**	**636.63**	**0.937**	**85.27**	**0.390**	**0.285**	**1.680**	**0.564**	**0.002**
	s.d.	0.51	1.17	-	-	0.01	-	2.30	34.75	0.515	5.56	0.368	0.204	0.060	0.136	0.002
Oimyakon	**mean**	**-21.81**	**9.23**	**-14.22**	**-14.76**	**3.23**	**7.20**	**4.11**	**710.66**	**0.641**	**100.28**	**0.156**	**1.051**	**1.020**	**0.106**	**0.001**
	s.d.	0.22	0.74	0.94	0.24	0.01	0.51	0.91	27.54	0.034	4.59	0.240	0.435	0.080	0.013	0.001
ShabiShabi (Loxodonta africana)	**mean**	**-19.45**	**12.11**	**1.43**	**-12.28**	**3.18**	**6.97**	**194.78**	**795.76**	**0.052**	**0.64**	**-**	**0.144**	**1.710**	**0.158**	**0.001**
	s.d.	1.29	0.83	2.13	2.19	0.01	1.73	44.32	58.57	0.204	0.38	-	0.041	0.370	0.141	0.000

Figure 5.1. Map showing location at which Lyuba was discovered.


Arctic Ocean
Legend
Lyuba
Cities
Rivers
Lakes
Kolyma
Tiksi
Verkhoyvensk
Aldan
Lena
Yakutsk
Vilyuy
Noril`sk
Igarka
Lyuba
Salekhard
Neva
Suir
Pechora
Ob
Yenisey
Angara
Chita
Chatanga
Irkutsk
Dnieper
Volga
Don
Kama
Yekaterinburg
Irtysh
Tobol
Novosibirsk
Novokuznetsk
Ulaanbaatar
-10°
0°
10°
30°
70°
110°
130°
140°
150°
60°
50°
40°
50°
60°
70°
80°
90°
100°
1,000 Kilometers
Lambert Azimuthal Equal Area Projection

Figure 5.2. Right lateral aspect of Lyuba. Preservation is remarkable, with the only missing elements of the original anatomy being much of the hair, the nails, a portion of the tail, and a portion of the right pinna.

10 cm

Figure 5.3. The deciduous tusk (dI^2). Note the constricted apical margin indicating that formation of this tooth was complete at the time of death. There are small areas of resorption on the occlusal/distal and lateral surfaces.

Dorsal

Occlusal-
Distal

Lateral

Apical-
Proximal

Medial

Ventral

1 cm

Figure 5.4. The left dP^2. The crown consists of five fully-formed lophs with little or no cementum filling gaps between lophs. Very slight wear is evident on the occlusal surfaces of the mesial three lophs. The constriction near the apical margin, which is the surface expression of the neonatal line is difficult to see in this tooth due to some decay along the apical margin.

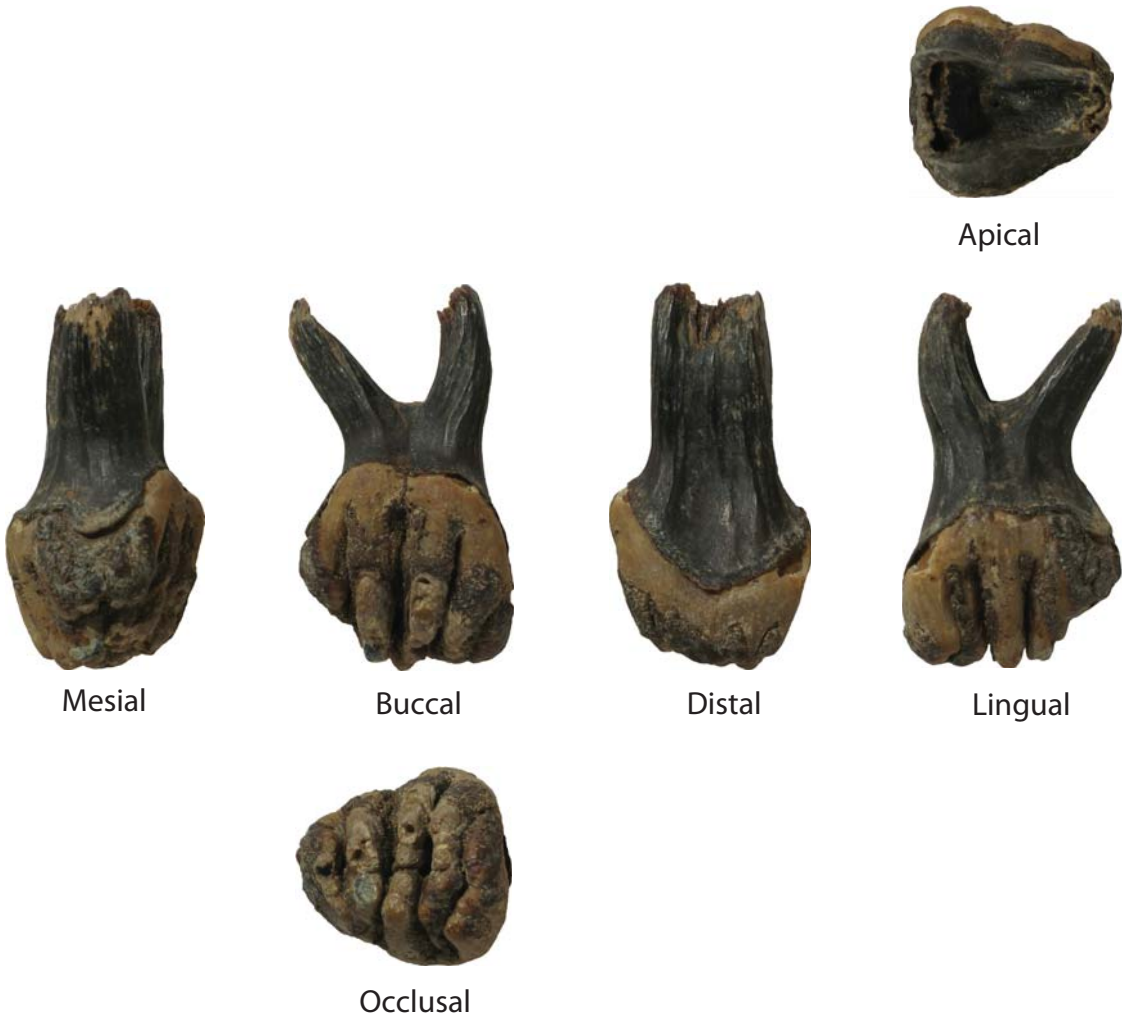

Figure 5.5. The left dP_2. The crown consists of four full lophs and an additional partial loph distally. Little or no cementum fills gaps between lophs. Wear is present on the mesial three lophs. Arrows indicate position of the a constriction in the root, which is the surface expression of the neonatal line.

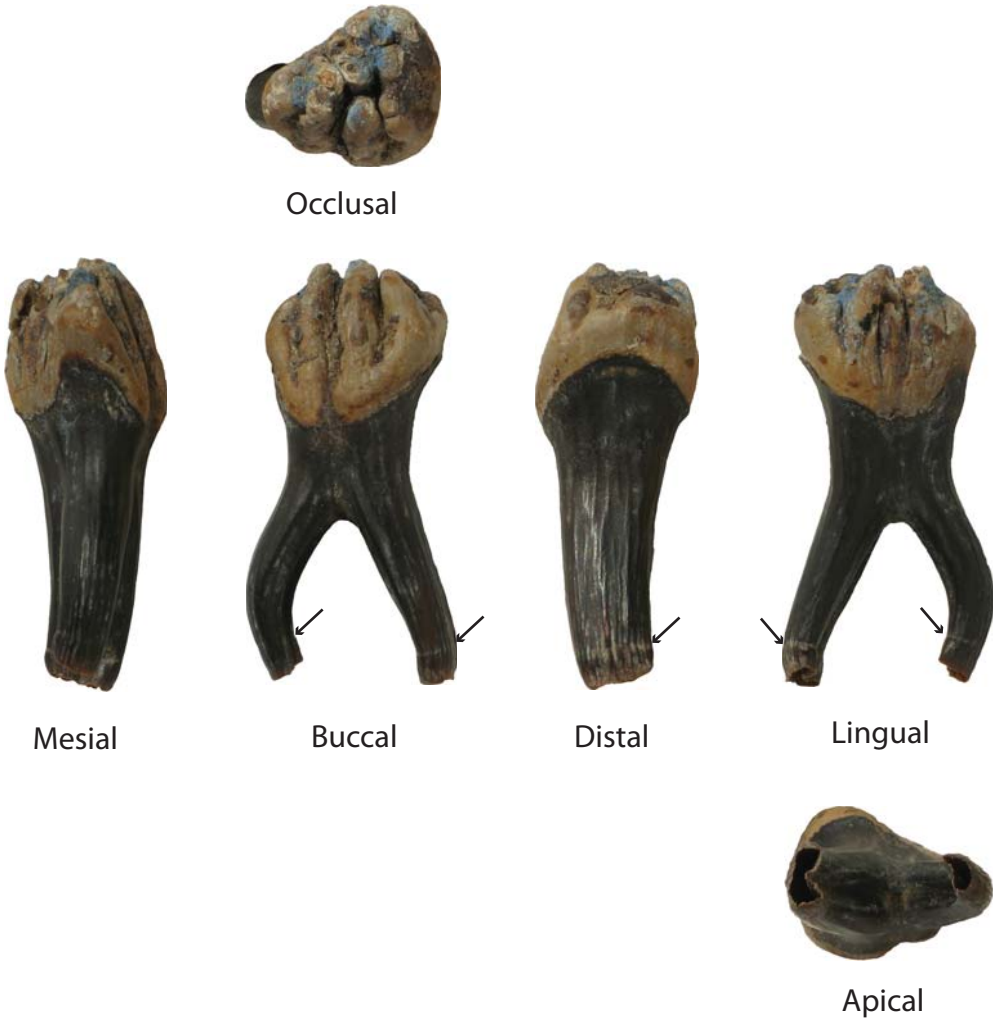

Figure 5.6. The left dP^3. The crown consists of nine lophs, and no cementum fills gaps between the lophs. Root formation is in an early stage. No wear is present.

Apical

Mesial

Buccal

Distal

Lingual

Occlusal

1 cm

Figure 5.7. The left dP_3. Crown formation is incomplete. Ten lophs are present, but the distal three lophs are incompletely formed and not joined to the remainder of the tooth. Cementum does not fill gaps between lophs, and no wear is present.

Occlusal

Mesial

Buccal

Distal

Lingual

Apical

1 cm

Figure 5.8. Left dP_2 after initial cut. While results from this tooth are not reported in this study, the cutting process for dP^2 was similar. This image was chosen as it allows illustration of both the cutting procedure and the internal and external expressions of the neonatal line, which are more easily seen in this tooth. Lines show the orientations of the second and third cuts made before samples were collected. Dentin was collected from the distal portion remaining after these cuts.

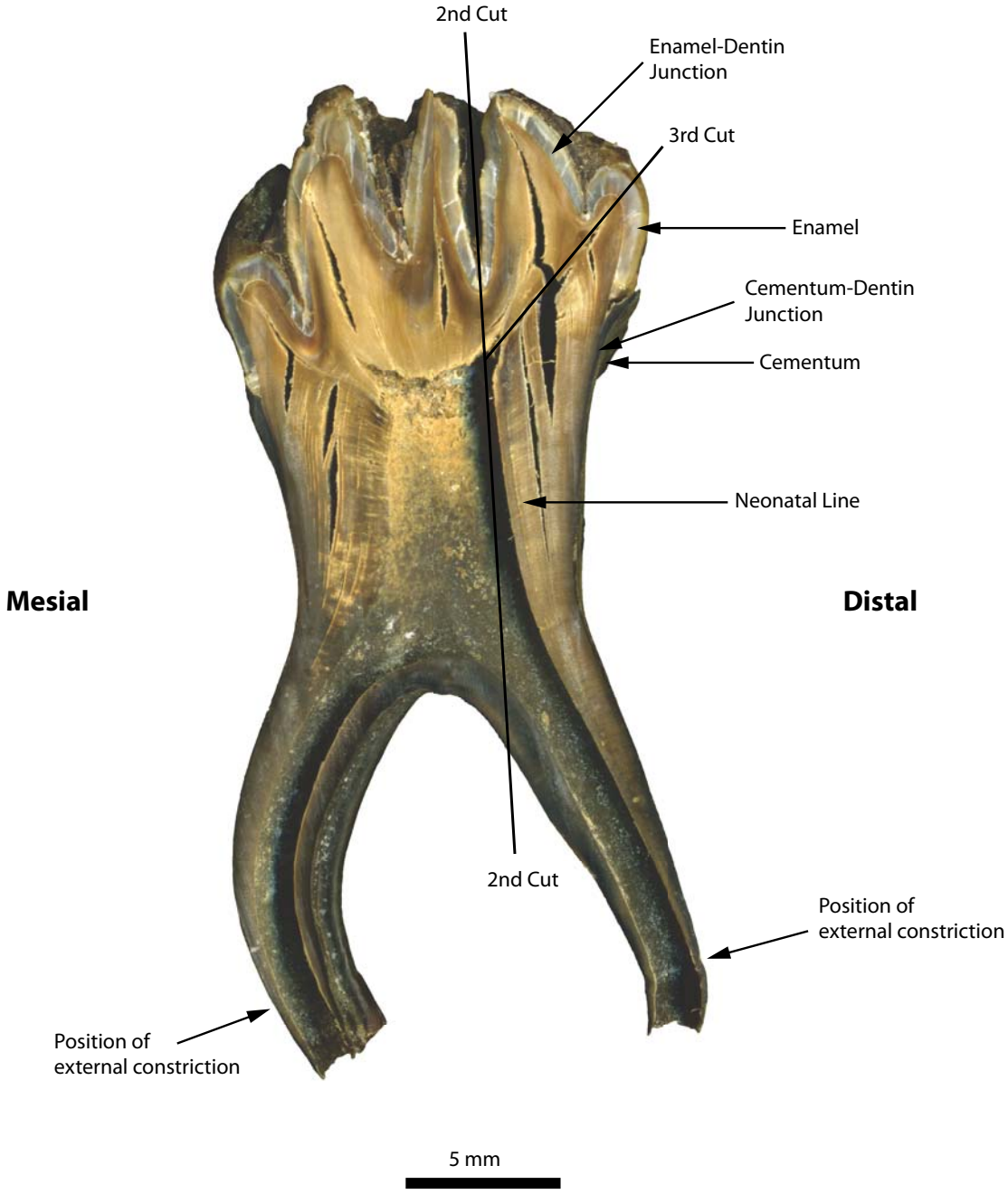

Figure 5.9. Separated fractions of the intestinal contents. A) Friable, fatty granules; B) Sheared/processed vegetation; C) Amber-colored masses.

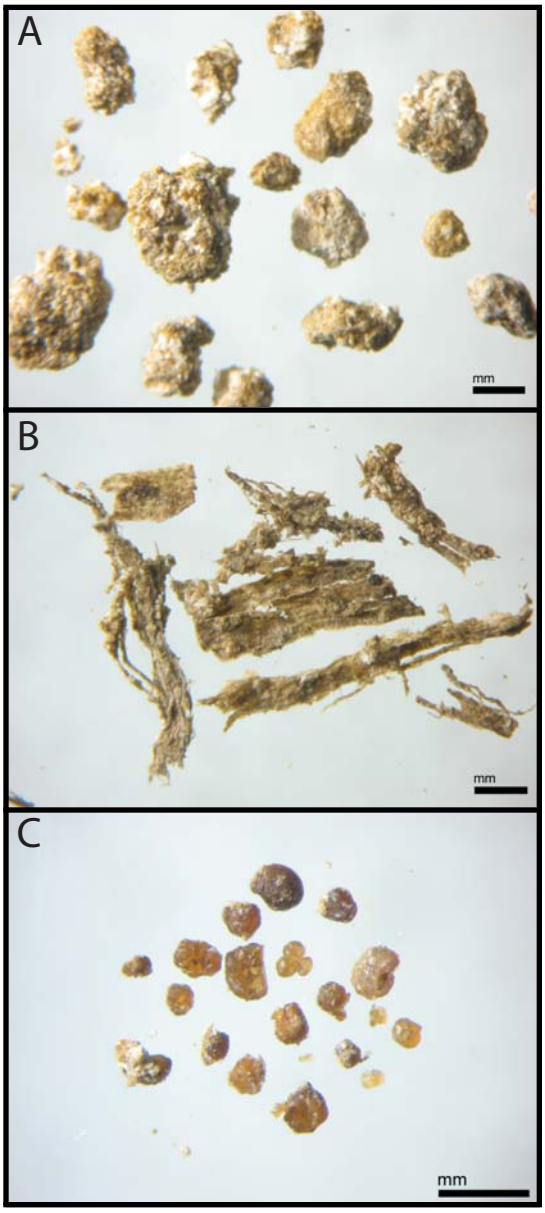

Figure 5.10, A-F. Compositional series for the dP^2. A) $\delta^{13}C_{col}$ relative to VPDB, B) $\delta^{15}N_{col}$ relative to AIR, C) Mg/Ca (mmol/mol), D) P/Ca (mmol/mol), E) Mn/Ca (mmol/mol), F) Fe/Ca (mmol/mol). Sample 13 represents postnatal dentin. Note the seasonal-scale pattern in $\delta^{15}N_{col}$ indicating that about 1.5 years of prenatal development are recorded in this tooth. Values in C and D are relatively low (see Table 5.1 for comparison), while values in E and F are relatively high (see Table 5.1). The pattern in A is difficult to interpret.

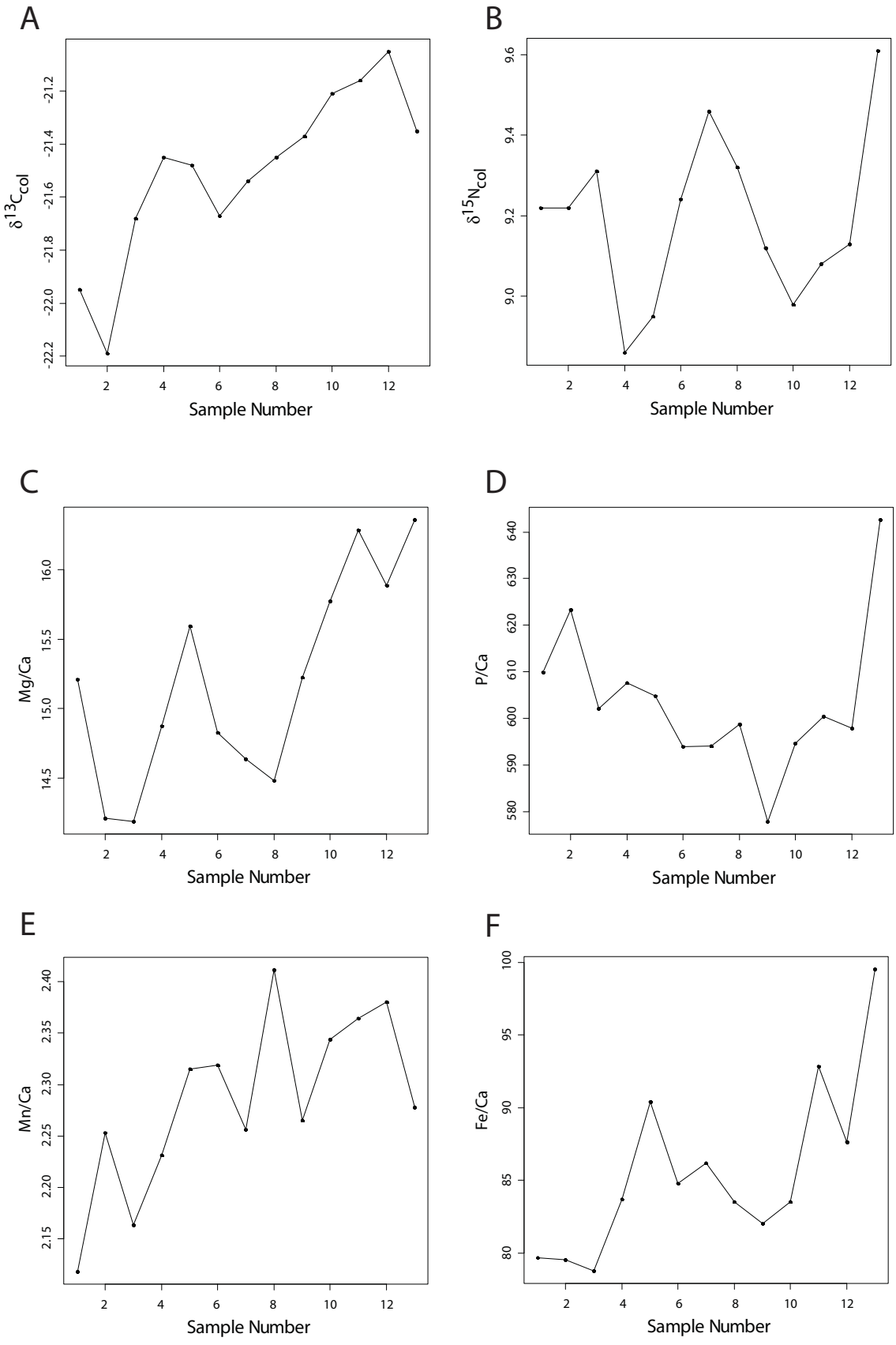
A
$\delta^{13}C_{col}$
-22.2
-22.0
-21.8
-21.6
-21.4
-21.2
2
4
6
8
10
12
Sample Number
B
$\delta^{15}N_{col}$
9.0
9.2
9.4
9.6
2
4
6
8
10
12
Sample Number
C
Mg/Ca
14.5
15.0
15.5
16.0
2
4
6
8
10
12
Sample Number
D
P/Ca
580
590
600
610
620
630
640
2
4
6
8
10
12
Sample Number
E
Mn/Ca
2.15
2.20
2.25
2.30
2.35
2.40
2
4
6
8
10
12
Sample Number
F
Fe/Ca
80
85
90
95
100
2
4
6
8
10
12
Sample Number

Figure 5.10, G-K. Compositional series for the dP^2. G) Cu/Ca (mmol/mol), H) Zn/Ca (mmol/mol), I) Sr/Ca (mmol/mol), J) Ba/Ca (mmol/mol), K) Pb/Ca (mmol/mol). Missing points occur in the elemental ratio series when concentration was below detection. Sample 13 represents postnatal dentin. Of particular interest are the prenatal peak in Cu/Ca and the elevated Zn/Ca around the time of birth (see text for discussion and Fig. 4.21I and J for similar patterns in another mammoth).

G

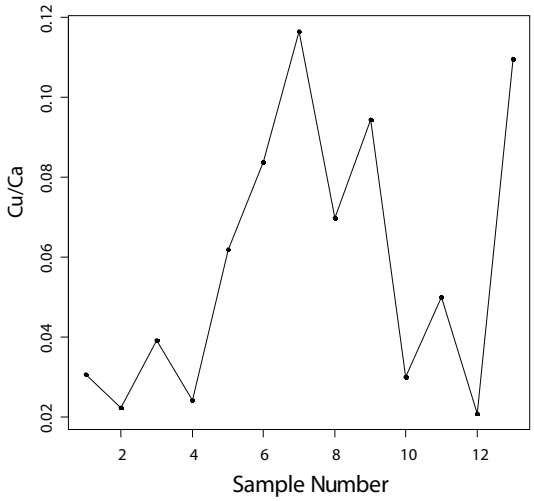
Cu/Ca
0.02
0.04
0.06
0.08
0.10
0.12
2
4
6
8
10
12
Sample Number

H

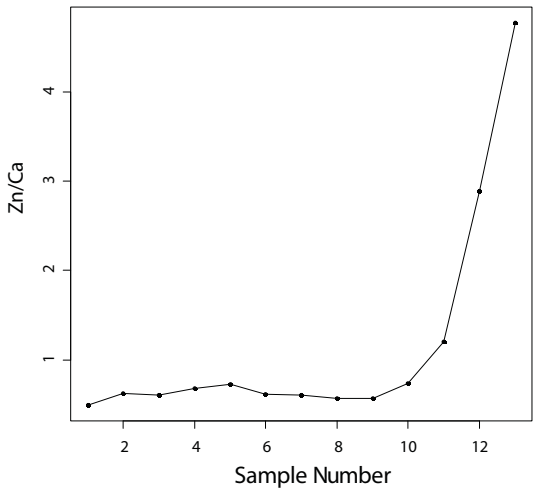
Zn/Ca
1
2
3
4
2
4
6
8
10
12
Sample Number

I

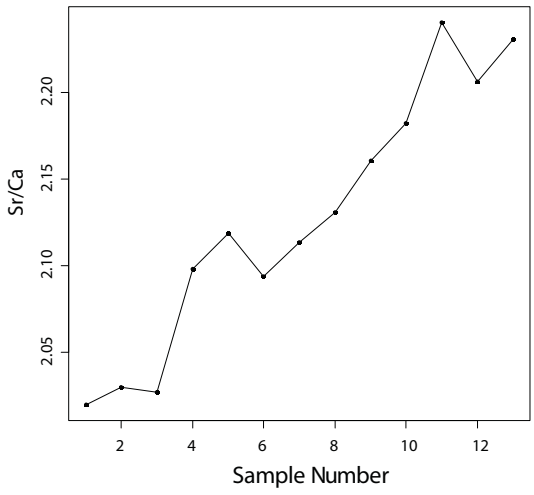
Sr/Ca
2.05
2.10
2.15
2.20
2
4
6
8
10
12
Sample Number

J

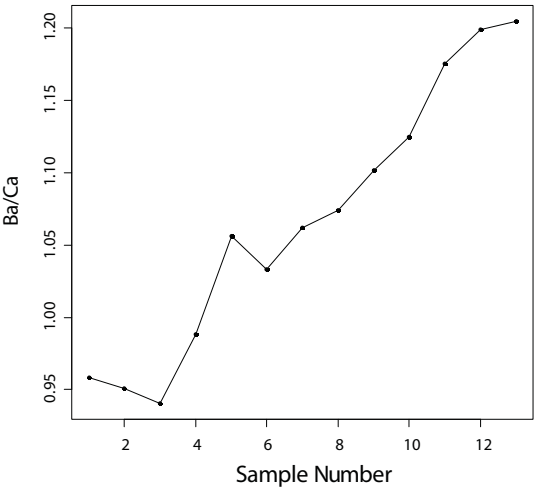
Ba/Ca
0.95
1.00
1.05
1.10
1.15
1.20
2
4
6
8
10
12
Sample Number

K

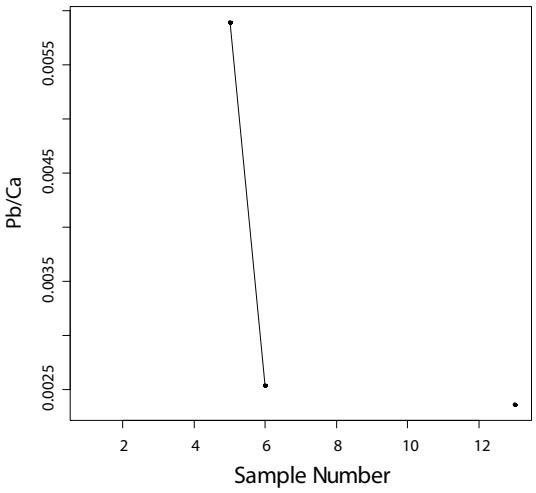
Pb/Ca
0.0025
0.0035
0.0045
0.0055
2
4
6
8
10
12
Sample Number

Figure 5.11, A-F. Compositional series for the dI^2. A) $\delta^{13}C_{col}$ relative to VPDB, B) $\delta^{15}N_{col}$ relative to AIR, C) $\delta^{18}O_{carb}$ relative to VPDB, D) $\delta^{13}C_{carb}$ relative to VPDB, E) Mg/Ca (mmol/mol), F) P/Ca (mmol/mol). Time covered in this series is roughly equivalent to that covered by samples 4-12 in dP^2. Of particular interest is the seasonal-scale variation in $\delta^{15}N_{col}$ which suggests that initiation of dI^2 development began after initiation of dP^2 (compare with Fig. 5.10B). $\delta^{18}O_{carb}$ and $\delta^{13}C_{carb}$ also show seasonal-scale variation. Mean values for E and F are similar to those observed in dP^2 (Table 5.1), but the patterns differ (Fig. 5.10C and D).

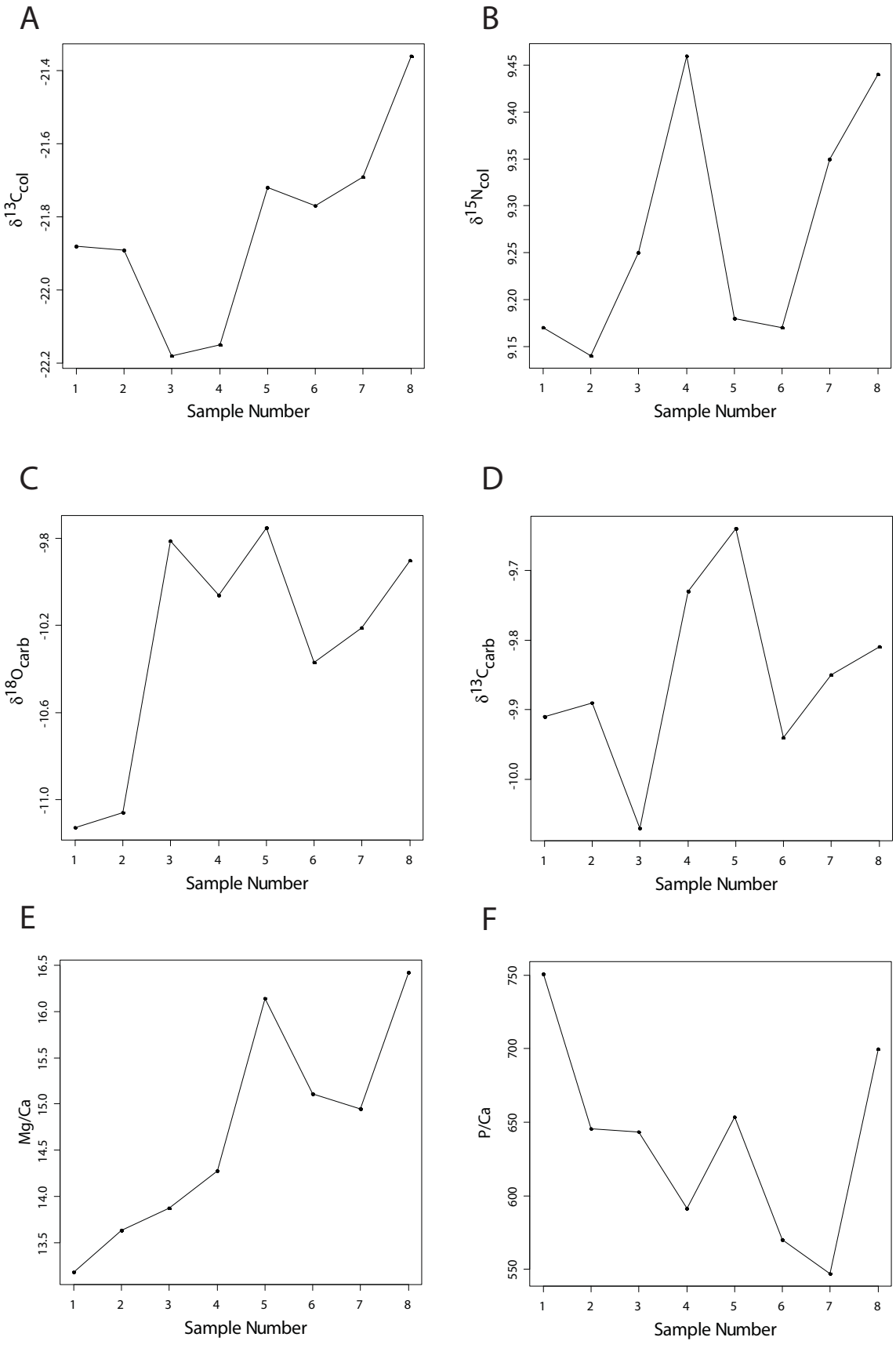
A
$\delta^{13}C_{col}$
-21.4
-21.6
-21.8
-22.0
-22.2
1 2 3 4 5 6 7 8
Sample Number
B
$\delta^{15}N_{col}$
9.45
9.40
9.35
9.30
9.25
9.20
9.15
1 2 3 4 5 6 7 8
Sample Number
C
$\delta^{18}O_{carb}$
-9.8
-10.2
-10.6
-11.0
1 2 3 4 5 6 7 8
Sample Number
D
$\delta^{13}C_{carb}$
-9.7
-9.8
-9.9
-10.0
1 2 3 4 5 6 7 8
Sample Number
E
Mg/Ca
16.5
16.0
15.5
15.0
14.5
14.0
13.5
1 2 3 4 5 6 7 8
Sample Number
F
P/Ca
750
700
650
600
550
1 2 3 4 5 6 7 8
Sample Number

Figure 5.11, G-K. Compositional series for the dI^2. G) Mn/Ca (mmol/mol) , H) Fe/Ca (mmol/mol), I) Zn/Ca (mmol/mol), J) Sr/Ca (mmol/mol), K) Ba/Ca (mmol/mol). Pb was below detection in all samples. Time covered in this series is roughly equivalent to that covered by samples 4-12 in dP^2. Note the elevated Zn/Ca in dentin formed during late gestation (samples 6-8). The pattern in J is similar to that seen in the dp^2, but the pattern in K differs (see Figs. 5.10J and K)

G

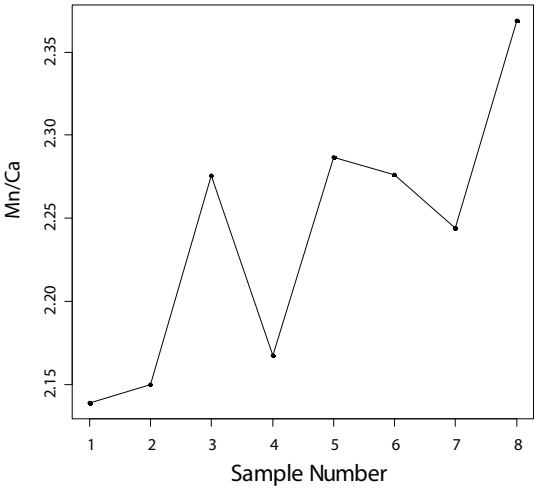
Mn/Ca
2.15
2.20
2.25
2.30
2.35
1
2
3
4
5
6
7
8
Sample Number

H

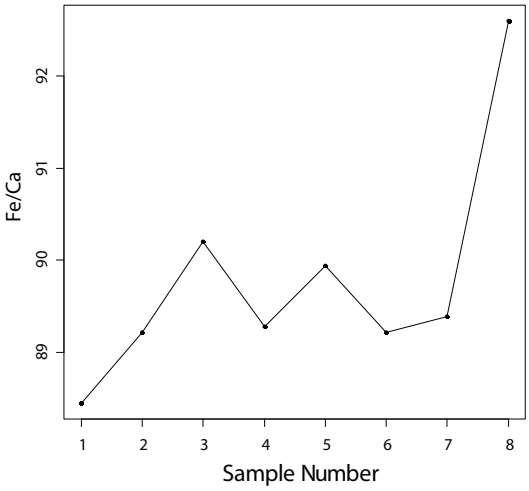
Fe/Ca
89
90
91
92
1
2
3
4
5
6
7
8
Sample Number

I

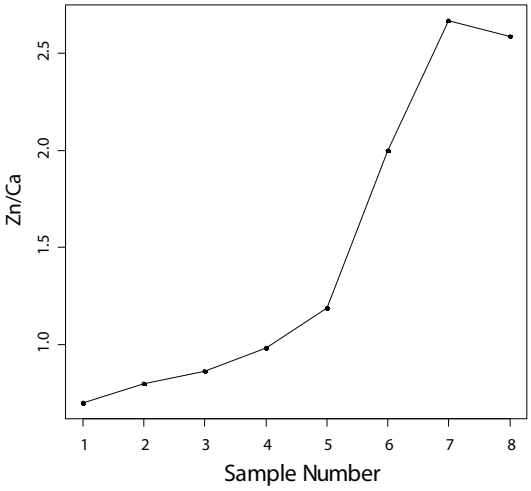
Zn/Ca
1.0
1.5
2.0
2.5
1
2
3
4
5
6
7
8
Sample Number

J

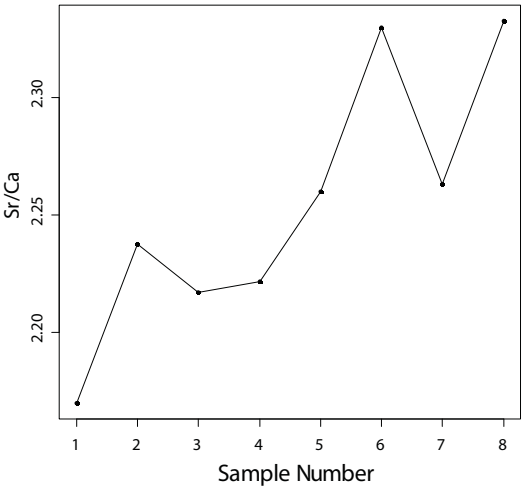
Sr/Ca
2.20
2.25
2.30
1
2
3
4
5
6
7
8
Sample Number

K

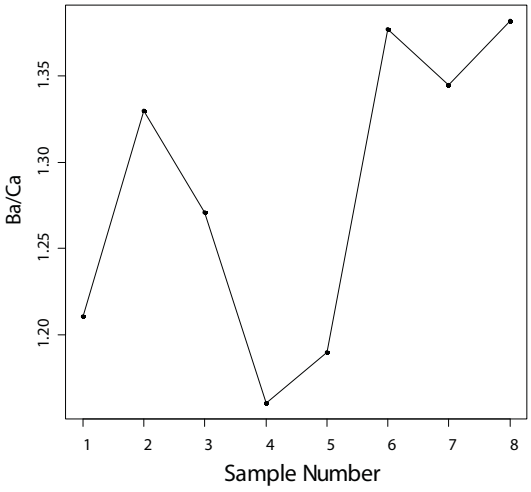
Ba/Ca
1.20
1.25
1.30
1.35
1
2
3
4
5
6
7
8
Sample Number

Figure 5.12. $\delta^{13}C$ and $\delta^{15}N$ of tissues and gut contents. Arrows mark $\delta^{13}C$ values for tissues without $\delta^{15}N$ values. "Peritoneum" had a high C/N and was not analyzed for $\delta^{15}N$. Sufficient mass was not available to analyze the $\delta^{15}N$ of the amber masses. Fatty tissues (and intestinal fat granules) are depleted in ^{13}C relative to lean tissues, and dentin collagen is enriched over bulk intestinal content by about 5.5 and 1.8 ‰ in $\delta^{13}C$ and $\delta^{15}N$ respectively.

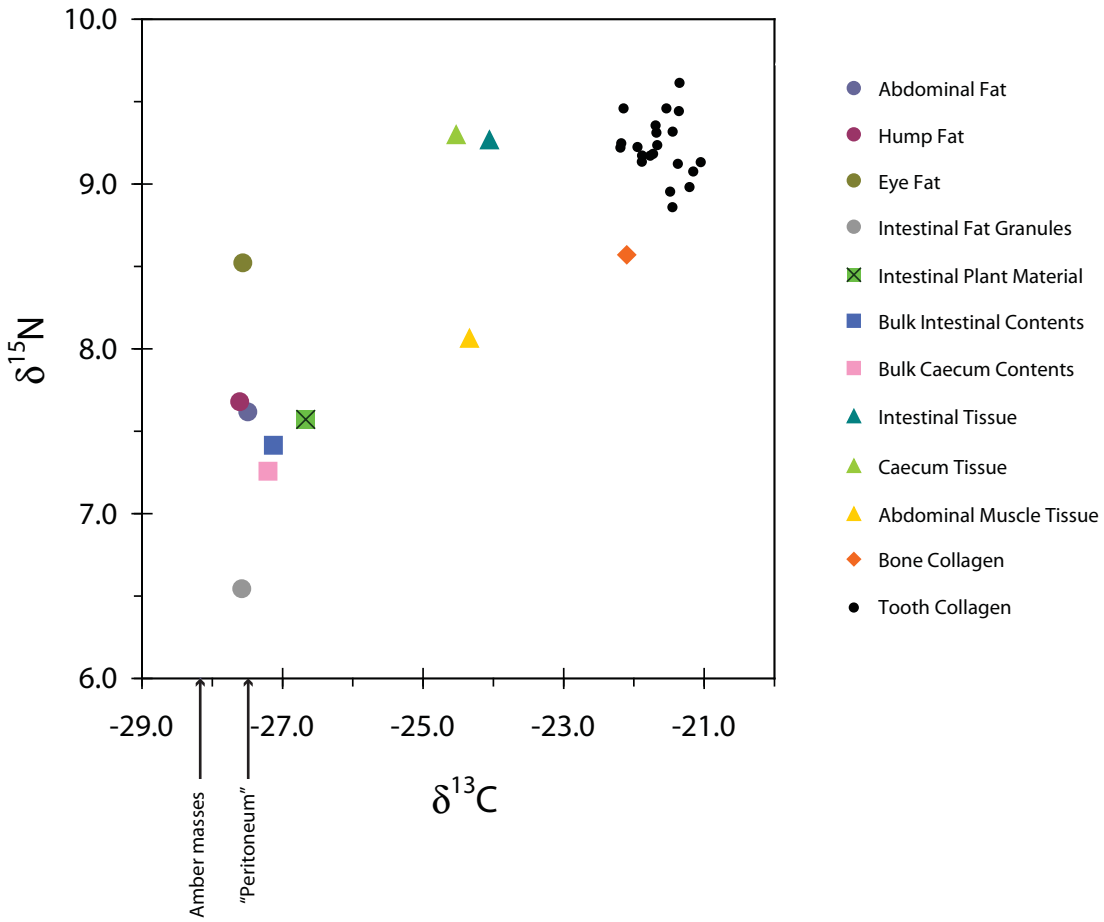

Appendix 5A. Compositional values for dP^2 and dI^2 samples.

Sample	$\delta^{13}C_{col}$	$\delta^{15}N_{col}$	$\delta^{18}O_{carb}$	$\delta^{13}C_{carb}$	C/N_{col}	$\delta^{13}C_{carb} - \delta^{13}C_{col}$	Mg/Ca	Sr/Ca	Ba/Ca	Pb/Ca	P/Ca	Mn/Ca	Fe/Ca	Cu/Ca	Zn/Ca
dP^2-1	-21.95	9.22	-	-	3.26	-	15.21 ± 0.26	2.02 ± 0.11	0.958 ± 0.050	n.d. -	609.85 ± 24.36	2.118 ± 0.069	79.67 ± 11.88	0.031 ± 0.001	0.492 ± 0.017
dP^2-2	-22.19	9.22	-	-	3.23	-	14.21 ± 0.24	2.03 ± 0.11	0.951 ± 0.049	n.d. -	623.36 ± 24.90	2.253 ± 0.074	79.52 ± 11.86	0.022 ± 0.001	0.620 ± 0.022
dP^2-3	-21.68	9.31	-	-	3.25	-	14.18 ± 0.24	2.03 ± 0.11	0.940 ± 0.049	n.d. -	602.09 ± 24.05	2.164 ± 0.071	78.76 ± 11.74	0.039 ± 0.001	0.608 ± 0.022
dP^2-4	-21.45	8.86	-	-	3.24	-	14.87 ± 0.25	2.10 ± 0.11	0.988 ± 0.051	n.d. -	607.63 ± 24.28	2.231 ± 0.073	83.68 ± 12.48	0.024 ± 0.001	0.677 ± 0.024
dP^2-5	-21.48	8.95	-	-	3.22	-	15.59 ± 0.27	2.12 ± 0.11	1.056 ± 0.055	0.0059 ± 0.0003	604.88 ± 24.17	2.315 ± 0.076	90.38 ± 13.48	0.062 ± 0.002	0.724 ± 0.026
dP^2-6	-21.67	9.24	-	-	3.21	-	14.82 ± 0.25	2.09 ± 0.11	1.033 ± 0.054	0.0025 ± 0.0001	593.97 ± 23.73	2.319 ± 0.076	84.81 ± 12.65	0.084 ± 0.003	0.611 ± 0.022
dP^2-7	-21.54	9.46	-	-	3.21	-	14.63 ± 0.25	2.11 ± 0.11	1.062 ± 0.055	n.d. -	594.10 ± 23.73	2.256 ± 0.074	86.20 ± 12.85	0.116 ± 0.004	0.605 ± 0.021
dP^2-8	-21.45	9.32	-	-	3.21	-	14.48 ± 0.25	2.13 ± 0.11	1.074 ± 0.056	n.d. -	598.83 ± 23.92	2.412 ± 0.079	83.52 ± 12.45	0.070 ± 0.003	0.565 ± 0.020
dP^2-9	-21.37	9.12	-	-	3.23	-	15.22 ± 0.26	2.16 ± 0.11	1.102 ± 0.057	n.d. -	577.87 ± 23.09	2.265 ± 0.074	82.00 ± 12.23	0.094 ± 0.004	0.569 ± 0.020
dP^2-10	-21.21	8.98	-	-	3.24	-	15.77 ± 0.27	2.18 ± 0.11	1.125 ± 0.058	n.d. -	594.61 ± 23.76	2.344 ± 0.077	83.51 ± 12.45	0.030 ± 0.001	0.732 ± 0.026
dP^2-11	-21.16	9.08	-	-	3.22	-	16.29 ± 0.28	2.24 ± 0.12	1.175 ± 0.061	n.d. -	600.39 ± 23.99	2.364 ± 0.078	92.86 ± 13.85	0.050 ± 0.002	1.205 ± 0.043
dP^2-12	-21.05	9.13	-	-	3.24	-	15.89 ± 0.27	2.21 ± 0.11	1.199 ± 0.062	n.d. -	597.94 ± 23.89	2.380 ± 0.078	87.62 ± 13.07	0.021 ± 0.001	2.887 ± 0.102
dP^2-13	-21.35	9.61	-	-	3.25	-	16.36 ± 0.28	2.23 ± 0.12	1.205 ± 0.062	0.0024 ± 0.0001	642.67 ± 25.68	2.278 ± 0.075	99.55 ± 14.84	0.109 ± 0.004	4.777 ± 0.169
dI^2-1	-21.88	9.17	-11.13	-9.91	3.31	11.98	13.18 ± 0.12	2.17 ± 0.05	1.211 ± 0.019	n.d. -	750.98 ± 45.72	2.139 ± 0.067	88.45 ± 16.01	- -	0.697 ± 0.018
dI^2-2	-21.89	9.14	-11.06	-9.89	3.33	12.00	13.63 ± 0.13	2.24 ± 0.05	1.330 ± 0.021	n.d. -	645.67 ± 39.31	2.150 ± 0.067	89.22 ± 16.15	- -	0.798 ± 0.020
dI^2-3	-22.18	9.25	-9.81	-10.07	3.30	12.11	13.87 ± 0.13	2.22 ± 0.05	1.271 ± 0.020	n.d. -	643.13 ± 39.15	2.276 ± 0.071	90.20 ± 16.32	- -	0.862 ± 0.022
dI^2-4	-22.15	9.46	-10.06	-9.73	3.28	12.42	14.27 ± 0.13	2.22 ± 0.05	1.160 ± 0.018	n.d. -	591.34 ± 36.00	2.167 ± 0.068	89.28 ± 16.16	- -	0.981 ± 0.025
dI^2-5	-21.72	9.18	-9.75	-9.64	3.28	12.08	16.14 ± 0.15	2.26 ± 0.05	1.190 ± 0.018	n.d. -	653.62 ± 39.79	2.287 ± 0.071	89.94 ± 16.28	- -	1.189 ± 0.030
dI^2-6	-21.77	9.17	-10.37	-9.94	3.24	11.83	15.11 ± 0.14	2.33 ± 0.05	1.377 ± 0.021	n.d. -	570.15 ± 34.71	2.276 ± 0.071	89.22 ± 16.15	- -	2.001 ± 0.050
dI^2-7	-21.69	9.35	-10.21	-9.85	3.26	11.83	14.94 ± 0.14	2.26 ± 0.05	1.345 ± 0.021	n.d. -	546.90 ± 33.29	2.244 ± 0.070	89.39 ± 16.18	- -	2.671 ± 0.067
dI^2-8	-21.36	9.44	-9.90	-9.81	3.24	11.55	16.43 ± 0.15	2.33 ± 0.05	1.382 ± 0.021	n.d. -	699.69 ± 42.59	2.369 ± 0.074	92.61 ± 16.76	- -	2.587 ± 0.065

References

Ambrose, S.H., Norr, L., 1993. Experimental evidence for the relationship of the carbon isotope ratios of whole diet and dietary protein to those of bone collagen and carbonate. In: Lambert, J.B., Groupe, G. (Eds.), Prehistoric Human Bone: Archaeology at the Molecular Level. Springer, Berlin, pp. 1–37.

Barboza, P.S., Parker, K.L., 2006. Body protein stores and isotopic indicators of N balance in female reindeer (*Rangifer tarandus*) during winter. Physiological and Biochemical Zoology 79(3), 628–644.

Balzer, A., Gleixner, G., Grupe, G., Schmidt, H.-L., Schramm, S., Turban-Just, S., 1997. *In vitro* decomposition of bone collagen by soil bacteria: The implications for stable isotope analysis in archaeometry. Archaeometry 39(2), 415–429.

Boeskorov, G.G., Tikhonov, A.N., Lazarev, P.A., 2007. A new find of a mammoth calf. Doklady Biological Sciences 417, 480–483.

Bocherens, H., 2003. Isotopic biogeochemistry and the paleoecology of the mammoth steppe fauna. DEINSEA 9, 57–76.

Bocherens, H., Pacaud, G., Lazarev, P.A., Mariotti, A., 1996. Stable isotope abundances (^{13}C, ^{15}N) in collagen and soft tissues from Pleistocene mammals from Yakutia: Implications for the palaeobiology of the Mammoth Steppe. Palaeogeography, Palaeoclimatology, Palaeoecology 126, 31–44.

Brudevold, F., Steadman, L.T., Spinelli, M.A., Amdur, B.H., Grøn, A, Grøn, P., 1963. A study of zinc in human teeth. Archives of Oral Biology 8, 135–144.

Cerling, T.E., Harris, J.M., 1999. Carbon isotope fractionation between diet and bioapatite in ungulate mammals and implications for ecological and paleoecological studies. Oecologia 120, 347–363.

Clark, M.A., Worrell, M.B, Pless, J.E., 1997. Postmortem changes in soft tissues. In: Haglund, W.D, Sorg, M.H. (Eds.), Forensic Taphonomy: The Postmortem Fate of Human Remains. CRC Press, Boca Raton, pp. 151–164.

DeNiro, M.J., Epstein, S., 1977. Mechanism of carbon isotope fractionation associated with lipid synthesis. Science 197(4300), 261–263.

Dolphin, A.E., Goodman, A.H., Amarasiriwardena, D.D., 2005. Variation in elemental intensities among teeth and between pre- and postnatal regions of enamel. American Journal of Physical Anthropology 128, 878–888.

Dufty, J.H., Bingley, J.B., Cove, L.Y., 1977. The plasma zinc concentration of nonpregnant, pregnant, and parturient Hereford cattle. Australian Veterinary Journal 53, 519–522.

Fisher, D.C., 2001. Season of Death, Growth Rates, and Life History of North American Mammoths. In: West, D. (Ed.), Proceedings of the International Conference on Mammoth Site Studies, Publications in Anthropology 22. University of Kansas, Lawrence, pp. 121–135.

Fisher, D.C., 1996. Extinction of proboscideans in North America. In: Shoshani, J., Tassy, P. (Eds.), The Proboscidea: Evolution and Paleoecology of Elephants and Their Relatives. Oxford University Press, Oxford, pp. 296–315.

Fisher, D.C., Fox, D.L., 2003. Season of death and terminal growth histories of Hiscock mastodons. In: Laub, R.S. (Ed.), The Hiscock Site: Late Pleistocene and Holocene Paleoecology and Archaeology of Western New York State, Bulletin of the Buffalo Society of Natural Sciences, 37, pp. 83–101.

Fox, D.L., Fisher, D.C., Vartanyan, S., Tikhonov, A.N., Mol, D., Buigues, B. 2007. Paleoclimatic implications of oxygen isotopic variation in late Pleistocene and Holocene tusks of *Mammuthus primigenius* from northern Eurasia. Quaternary International 169–170, 154–165.

Gat, J.R., 1996. Oxygen and hydrogen isotopes in the hydrologic cycle. Annual Review of Earth and Planetary Sciences 24, 225–262.

Guy, P.R., 1977. Coprophagy in the African elephant (*Loxodonta africana* Blumenbach). East African Wildlife Journal 15, 174.

Hartsook, E.W., Hershberger, T.V., 1973. Strontium-calcium discrimination during placental transfer and fetal uptake in rats: Effect of gestation duration. Proceedings of the Society for Experimental Biology and Medicine 143(2), 343–349.

Hobson, K.A., Sease, J.L., 1998. Stable isotope analyses of tooth annuli reveal temporal dietary records: an example using Stellar sea lions. Marine Mammal Science 14, 116–129.

Holá, M., Kalvoda, J., Bábek, O., Brzobohatý, R., Holoubek, I., Kanický, V., Skoda, R., 2008. LA-ICP-MS heavy metal analyses of fish scales from sediments of the Oxbow Lake Certak of the Morava River (Czech Republic). Environmental Geology DOI: 10.1007/s00254-008-1501-z.

Jeswani, R.M., Vani, S.N., 1991. A study of serum zinc levels in cord blood of neonates and their mothers. Indian Journal of pediatrics 58(5), 683–686.

Kang, D., Amarasiriwardena, D., Goodman, A.H., 2004. Application of laser ablation-inductively coupled plasma-mass spectrometry (LA-ICP-MS) to investigate trace metal spatial distributions in human tooth enamel and dentine growth layers and pulp. Analytical and Bioanalytical Chemistry 378, 1608–1615.

Koch, P.L., Tuross, N., Fogel, M.L., 1997. The effects of sample treatment and diagenesis on the isotopic integrity of carbonate in biogenic hydroxylapatite. Journal of Archaeological Science 24, 417–429.

Kohn, M., 1996. Predicting animal $\delta^{18}O$: Accounting for diet and physiological adaptation. Geochimica et Cosmochimica Acta 60(23) 4811–4829.

Kohn, M.J., Schoeninger, M.J., Barker, W.W., 1999. Altered states: Effects of diagenesis on fossil tooth chemistry. Geochimica et Cosmochimica Acta 63(18), 2737–2747.

Kurita, N., Yoshida, N., Inoue, G., Chayanova, E.A., 2004. Modern isotope climatology of Russia: A first assessment. Journal of Geophysical Research 109(D03102), 1–15.

Lee, P.C., Moss, C.J., 1986. Early maternal investment in male and female African elephant calves. Behavioral Ecology and Sociobiology 18, 353–361.

Lee-Thorp, J.A., Sealy, J.C., van der Merwe, N.J., 1989. Stable carbon isotope ratio differences between bone collagen and bone apatite, and their relationship to diet. Journal of Archaeological Science 16, 585–599.

Leggett, K., 2004. Coprophagy and unusual thermoregulatory behaviour in desert-dwelling elephants of north-western Namibia. Pachyderm 36, 113–115.

Moss, C.J., 1988. Elephant memories : Thirteen years in the life of an elephant family. University of Chicago Press, Chicago, 364 pp.

Nardoto, G.B., de Godoy, P.B., Ferraz, E.S.d.B., Ometto, J.P.H.B., Martinelli, L.A., 2006. Stable carbon and nitrogen isotopic fractionation between diet and swine tissues. Scientia Agricola 63, 579–582.

Newsome, S.D., Koch, P.L., Etnier, M.A., Aurioles-Gamboa, D., 2006. Using carbon and nitrogen isotope values to investigate maternal strategies in northeast Pacific otariids. Marine Mammal Science 22(3), 556–572.

Sullivan, C.H., Krueger, H.W., 1981. Carbon isotope analysis of separate chemical phases in modern and fossil bone. Nature 292, 333–335.

Pate, F.D., 1994. Bone chemistry and paleodiet. Journal of Archaeological Method and Theory 1(2), 161–209.

Robbins, C.T., Felicetti, L.A., Sponheimer, M., 2005. The effect of dietary protein quality on nitrogen isotope discrimination in mammals and birds. Oecologia 144, 534–540.

Rombach, E.P., Barboza, P.S., Blake, J.E., 2003. Costs of gestation in an Arctic ruminant: copper reserves in muskoxen. Comparative Biochemistry and Physiology Part C 134, 157–168.

Roth, V.L., Shoshani, J., 1988. Dental identification and age determination in *Elephas maximus*. Journal of Zoology 214(4), 567–588.

Schoeninger M.J., DeNiro, M.J., 1984. Nitrogen and carbon isotopic composition of bone collagen from marine and terrestrial animals. Geochimica et Cosmochimica Acta 48, 625–639.

Shaw, J.C.L., 1980. Trace elements in the fetus and young infant: II. Copper, Manganese, Selenium, and Chromium. American Journal of Diseases of Children 134, 74–81.

Sillen, A., Kavanagh, M., 1982. Strontium and paleodietary research: A review. Yearbook of Physical Anthropology 25, 67–90.

Steele, K.W., Daniel, R.M., 1978. Fractionation of nitrogen isotopes by animals: a further complication to the use of variations in the natural abundance of ^{15}N for tracer studies. Journal of Agricultural Science 90, 7–9.

Sugimoto, A., Yanagisawa, N., Naito, D., Fujita, N., Maximov, T.C., 2002. Importance of permafrost as a source of water for plants in east Siberian taiga. Ecological Research 17, 493–503.

Ullrey, D.E., Miller, E.R., Brent, B.E., Bradley, B.L., Hoefer, J.A., 1967. Swine hematology from birth to maturity IV. Serum calcium, magnesium, sodium, potassium, copper, zinc, and inorganic phosphorus. Journal of Animal Science 26, 1024–1029.

Ushakova, N.A., Fedosov, E.V., Kozlova, A.A., Kotenkova, E.V., 2008. Stimulation of development of rabbit offspring by probiotic bacteria of the mother's soft faeces. Doklady Biological Sciences 423, 406–408.

van Geel, B., Aptroot, A., Baittinger, C., Birks, H.H., Bull, I.D., Cross, H.B., Evershed, R.P., Gravendeel, B., Kompanje, E.J.O., Kuperus, P., Mol, D., Nierop, K.G.J., Pals, J.P., Tikhonov, A.N., van Reenen, G., van Tienderen, P.H., 2008. The ecological implications of a Yakutian mammoth's last meal. Quaternary Research 69, 361–376.

Vuori, E., Kuitunen, P., 1979. The concentrations of copper and zinc in human milk. Acta Paediatrica Scandinavica 68, 33–37.

Williamson, B.R., 1976. Reproduction in female African elephant in the Wankie National Park, Rhodesia. South African Journal of Wildlife Research 6, 89–93.

Wuthier, R.E., 1984. Lipids in dentinogenesis. In: Linde, A. (Ed.), Dentin and Dentinogenesis vol. II. CRC Press, Boca Raton, pp.93–106.

Yokus, B., Cakir, U.D., 2006. Seasonal and physiological variations in serum chemistry and mineral concentrations in cattle. Biological Trace Element Research 109, 255–266.

Chapter 6

Conclusions

So, what were mammoths "doing up there"? In this study, I have attempted to develop methods and perform analyses on the tooth dentin of juvenile mammoths to expand our knowledge of mammoth life history and paleobiology with a particular focus on early life. While I cannot completely answer the question regarding the behavior and activities of mammoths in Siberia, some aspects of their paleobiology can be addressed.

Regarding methods, experimentation with pretreatment procedures suggested that, for modern dentin, a procedure utilizing H_2O_2 and an acetic acid/calcium acetate buffer solution is preferable to treatments involving NaOCl. Use of H_2O_2 rather than NaOCl avoids conditions under which carbonate or bicarbonate might contaminate the sample during the pretreatment process. I have also developed a system for imaging polished dentin surfaces that allows digital enhancement of second-order features, mapping of sampling locations, and the transfer of sampling plans to the original dentin surfaces. This method permits high-resolution dentin sampling of specimens in which second-order features would not be visible during the sample milling process. This is usually the case for modern dentin

and well-preserved Siberian material. Development of this process adds to our ability to construct compositional time series from mammoth tusks.

These methods were utilized in the analysis of the tusk of a juvenile African elephant as well as some of the tusks from juvenile mammoths. The analysis of the elephant tusk revealed patterns in $\delta^{15}N_{col}$ consistent with higher milk intake in the first year of life, followed by seasonal oscillations. $\delta^{13}C_{col}$ also shows seasonal oscillation, which is largely due to changes in the ratio of C_3 to C_4 plants in the diet. This factor is probably not important for understanding patterns of variation in arctic mammoths because C_4 vegetation is rare or absent in the arctic. However, it does show that compositional variation in tusks records known shifts in diet.

There is also evidence from isotope and elemental ratio patterns that the relative importance of milk in the diet may have fluctuated seasonally. This has important implications for the interpretation of seasonal-scale compositional oscillations in the tusks of juvenile mammoths.

The elemental ratios determined in the elephant tusk can also serve as a reference for detection of diagenetic alteration in mammoth tusks. Some patterns, such as increased Fe/Ca and Mn/Ca in stained areas, meet expectations. However, it was also noted that Mg/Ca was low in the samples from the tip of the tusk and the pulp cavity. This is evidence of the rapid loss of Mg that can occur in tusks with postmortem exposure of only a few months. In one of the juvenile mammoth tusks, low, apparently-altered, Mg/Ca is associated with high $\delta^{13}C_{carb}$ suggesting that Mg/Ca

might be used as an indicator of the degree to which carbonate values have been altered by diagenesis.

The three juvenile mammoth tusks with sufficient time recorded show decreasing $\delta^{15}N_{col}$ consistent with decreasing milk intake. This suggests that it is possible to determine the weaning ages of mammoths. However, as all of these individuals died young, it is difficult to assess whether or not weaning was completed at the time of death.

$\delta^{13}C_{col}$ in these tusks and a tusk fragment from an older individual varies seasonally. As the periodicity of second-order increments appears variable in these tusks, the seasonal oscillations in $\delta^{13}C_{col}$ (and $\delta^{18}O_{carb}$) may serve as indicators of the scale at which seasonal oscillations in other compositional variables occur. The current hypotheses regarding the seasonal oscillation in $\delta^{13}C_{col}$ are: 1) increased plant protein intake in early summer leads to more depleted values; 2) feeding in lower, wetter areas during summer and on higher, drier, windblown ridges in the winters leads to depleted values in the summer and enriched values in the winter. Both hypotheses are supported by the seasonal oscillation in $\delta^{15}N_{col}$ present in one of the juvenile tusks, which varies in-phase with $\delta^{13}C_{col}$.

In a tusk fragment from an older, apparently weaned individual, seasonal $\delta^{13}C_{col}$ and $\delta^{15}N_{col}$ vary roughly anti-phase, and similar patterns have been observed in the tusk of an adult. Whether this anti-phase association is characteristic of weaned individuals or if the phase relationship is regionally or temporally variable is not known. Further analyses of adult and juvenile tusks are necessary to determine this.

Analyses of dentin samples from individuals that died before reaching one year of age have provided information on the prenatal and perinatal periods. Two individuals included in this study possessed neonatal lines marking the time of birth in dentin. To our knownledge, this is the first report of neonatal lines in proboscidean tusk dentin. In both individuals, birth occurred during a time when $\delta^{15}N_{col}$ was increasing. Prenatally, increasing $\delta^{15}N_{col}$ might indicate increasing maternal nutritional stress prior to the onset of new summer plant growth. It could also indicate that the mother was feeding on high, dry, windblown areas (due to the presence of snow cover in low areas). Both of these factors would be more likely to occur in winter. Thus, the season of birth would be spring. This is consistent with patterns of reproduction in elephants, which tend to give birth before the start of the season of higher food availability.

Interpretation of variations in $\delta^{18}O_{carb}$, which has been used to determine season in dentin, may be slightly complicated in arctic mammoths. The $\delta^{18}O$ of precipitation in Siberia varies seasonally, with winter precipitation being depleted relative to summer precipitation. However, plant water $\delta^{18}O$ is lowest in early summer due to contributions from snowmelt. It then increases through summer and retains summer values through until the following late spring. Generally, lakes also follow this pattern, though the amplitude of seasonal variation is itself variable. Based on these patterns, one might expect low $\delta^{18}O_{carb}$ to represent late spring/early summer.

If the pattern in $\delta^{18}O_{carb}$ is dominated by drinking water rather than food water, the season represented by low $\delta^{18}O_{carb}$ values it might depend on what the winter

source of water actually is. If mammoths ingested significant amounts of isotopically light snow, this might lead to low values during the winter. If they obtained water from thin ice at the edges of lakes during the winter, this would have enriched, late summer $\delta^{18}O$ leading to enriched $\delta^{18}O_{carb}$ values during the winter.

It seems that plant water and/or ice may be the relevant water sources during the winter. The coincidence of lows in the $\delta^{13}C_{col}$, $\delta^{15}N_{col}$, and $\delta^{18}O_{carb}$ series for the juvenile with the longest record in this set suggests that the lows in $\delta^{18}O_{carb}$ represent late spring or early summer.

In both of the individuals with neonatal lines, Zn/Ca is elevated near the time of birth. Evidence from this and other studies indicates that elevated Zn/Ca in dentin or enamel may mark the time of birth. Thus, Zn/Ca might be used to detect the timing of birth in dentin or enamel in which neonatal lines are difficult to see or differentiate from other growth lines. Furthermore, the fact that dentin Zn/Ca seems to be related to serum Zn/Ca suggests an interesting possible application in adult females. As serum Zn tends to be low in mothers around the time of birth, it is possible that low Zn/Ca in dentin might identify late gestation/parturition. If this can be corroborated in studies of modern mammals, measurements of Zn/Ca in dentin might be a means of determining parity and interbirth interval in mammals with evergrowing teeth.

In addition to contributing to the results discussed above, the study of Lyuba, a remarkably well-preserved mummified calf, has offered additional insights into juvenile mammoth paleobiology. The identification of milk residues as well as processed vegetation in her intestine suggests that, while feeding on milk, as would

be expected for a calf about one month old, she also was engaging in coprophagy. There is also evidence of coprophagy in an adult mammoth. This suggests that this may have been a typical behavior for mammoths. If so, we may need to reevaluate our ideas of how, and to what degree, mammoths were able to extract nutrients from the available vegetation.

The lack of prenatal permanent tusk development in Lyuba and its presence in another juvenile mammoth suggests that the timing of tusk development may have been variable in mammoths. As Lyuba is female, and the other individual mentioned is male, this hints that sex differences in tusk development may exist. This variation has implications regarding the attempt to define the relationship between tusk size and age in mammoths.

Additional tusks are in various states of preparation, and I intend to continue to expand the study of juvenile tusks. Furthermore, this work has shown that, in order to assess weaning ages in juvenile mammoths, tusks or other teeth from individuals that lived for more than five years are required. The tusks in this study do not contain sufficient post-weaning dentin to enable characterization of post-weaning compositional patterns. It is only by documenting compositional variation for at least two years following weaning that a post-weaning state can be confidently identified.

I conclude this work with an account of the early life history of a mammoth based on my results and filling in gaps with what is known of early elephant life history. While some of what follows is necessarily speculative, it is based on the

available data. This narrative should serve as a guide for developing studies to further test these hypotheses.

Conception likely occurred in early summer when food was plentiful. Gestation length was similar to modern elephants with the mother carrying her offspring for about 22 months. Development of the dP^2 was initiated early in gestation, with dentin formation beginning at perhaps only a few months gestational age. Dentin formation in the deciduous tusk began after dentin formation in the dP^2. During gestation, maternal protein stores were likely important for the growth of the fetus, perhaps more so during winters when available forage was of reduced quality.

Birth probably occurred in spring before the onset of new plant growth and the calf would have fed primarily on milk during its first months of life. This diet was supplemented through ingestion of feces. This coprophagy may have served to establish the intestinal symbionts necessary for the transition to a diet of vegetation, and/or it may have been a source of additional nutrients. In mid to late summer, the calf would have begun to feed on available vegetation. Through autumn, winter, and spring the relative importance of milk to meet the calf's nutritional needs may have increased, although vegetation and perhaps feces contributed to the diet as well. The following summer the calf would have been less dependent on its mother's milk. Weaning may have been completed when the calf was somewhere between about two years and six years of age, possibly coinciding with the birth of a sibling.

What next? Given that the oldest individual included in these studies was not much more than five years old, it is difficult to say. As was the case for juvenile woolly

mammoths prior to these studies, very little is known of sub-adult and adult mammoth life history in northern Asia. However, analyses of tusks from older individuals are ongoing. This work on juvenile proboscideans will likely aid in deciphering patterns that emerge in that work, and in a more general sense, patterns that emerge in other compositional studies of animal recording structures.